

Investigation and Mitigation of Moisture- and Potential-Induced Degradation Mechanisms of Silicon Heterojunction Solar Cells and Modules

Présentée le 26 juillet 2023

Faculté des sciences et techniques de l'ingénieur
Laboratoire de photovoltaïque et couches minces électroniques
Programme doctoral en énergie

pour l'obtention du grade de Docteur ès Sciences

par

Olatz ARRIAGA ARRUTI

Acceptée sur proposition du jury

Prof. J. A. Schiffmann, président du jury
Prof. C. Ballif, Dr A. F. A. Virtuani, directeurs de thèse
Dr P. Hacke, rapporteur
Dr K.-A. Weiss, rapporteur
Dr F. Fu, rapporteur

Ai ama...

Acknowledgements

First of all, I would like to extend my gratitude towards Prof. Christophe Ballif for giving me the opportunity to do my PhD at PV-Lab. Your continuous support, encouragement and trust in my research have been a motivating force that has guided me through these years. I would also like to thank you for extending your knowledge of PV and motivating me to continue working in the field. I would also like to thank my co-supervisor, Dr. Alessandro Virtuani, also known as the *Gurú*, for supervising me during these four years of lows and highs, always eager to help and provide feedback. You have pushed me when I needed it and supported me in the most difficult parts. Conversations outside the lab are also always interesting with you, thank you for the fun outings with the group and for being a good sport. On behalf of PV-Lab, I also thank you for showing us the three most important rules of life (if you know, you know). Also, thank you to Dr. Antonin Faes, who joined us as the group leader during the last year of my thesis and has provided advice, feedback and research ideas, always with a smile.

Next, I wish to thank the president of the jury, Prof. Jürg Schiffmann, and the experts of the jury, Dr. Fan Fu, Dr. Peter Hacke and Dr. Karl-Anders Weiss, for accepting to be part of the thesis committee. In particular, I would like to make a special mention to Peter for always being ready to talk about our corresponding results on PID.

A big big thanks goes to the best group ever, the Reliability Group: Luca G., Fabiana, Alejandro, Ebrar, Hugo, Andrew and Umang. I cannot imagine the last four years without you, our chats in the office, the coffee breaks, the times on the terrace and, especially, the moments outside the lab. Work-related or personal topics, it doesn't matter, you have always been there to motivate and cheer me up. Also, I wish to thank Eleonora for initially proposing me to join PV-Lab and start a new stage of my life here.

I would also like to thank Xavier for always helping around in the lab for whatever reason and having the infinite patience of teaching me and speaking with me in French. Big thanks to the other technicians as well for your support in the lab: Aymeric, Cedric, Sylvain, Joël and Nicolas.

Then, to my fellow Brunch Club founders, Ezgi and Sofia, and VIP member, Alejandro a.k.a. *el Señor*, thank you for always giving your time for a coffee and a chat, for providing gossip material and knowing how to cheer me up. It has been some intense four years, and you have walked with me all the way. You guys will be next!

Acknowledgements

To my office mates who put up with my constant chatting over the last three years, Peter and Mario, thank you for always taking things with good humour and being ready to talk about anything and everything when we needed to relax.

Huge thank you to all the colleagues at PV-Lab, Julien, Quentin, Kerem, Deniz, Jonathan, Marion, Samira, Austin, Noemie, Alejandro, Mostafa, Mohammed, Hilal, Daniel, Annaël... for making sure there is always a great environment in the lab and for all the coffee breaks in the open space, the karaokes, apéros and outings. A big thank you to Luca Massimiliano for always being ready to help, for being my teacher in all things SHJ and for your patience with all my incessant questions. I cannot forget Karine and Aïcha, who always make sure that the lab is up and running (and that we have enough coffee to survive). I also wish to thank our colleagues at CSEM, particularly Gianluca, Jordi, Leo, Florent, Adriana, Jan-Willem, Sylvain, Matthieu, Jacques, Jonathan...

También quería dar gracias a aquellas personas que han estado en distintas etapas de mi vida y que han contribuido al hecho de que esté hoy aquí: Cristina, Marta, Yolanda, Lidia, Ivet, Sanji, Selim, Seba... qué lejos quedan los años en la UAB y cómo han cambiado las cosas. A los que llegaron más tarde, sobre todo Uruguaxo y Andrés, gracias por estar ahí y por vivir conmigo momentos increíbles.

Nere kuadrilliei, Reytxu, Lorena, Larra, Nerea, Leire eta Aiora, eskerrik asko nahiz ta hilabetiek elkar ikusi gabe eon, beti besuk zabalik jasotzeatik ta beti hor eoteatik.

Ze esangoiot munduko famili onenai... zuek danok gabe ez nitzeke hau dana iteko gai izengo. Aitor ta Maialen, eta bereziki Aita ta Ama, jun naizen toki daneta nerekin etortzeatiken eta nere atzetik nere heguei beti haizie emateatik, mila esker. Ze ingo nuke zuek gabe...

And to you, who has been there for the last year of craziness, for putting up with my mood changes, for being the best ski teacher ever, for feeding me with energy to keep going (quite literally), for always being ready to cheer me up and motivate me, thank you.

Neuchâtel, 2023

Olatz

Abstract

Photovoltaic (PV) technology - due to its availability and cost-competitiveness - is one of the most promising renewable energy sources. The PV market is dominated by crystalline silicon (c-Si) based technologies, thus ensuring their long-term performance is of paramount importance for manufacturers, investors and customers. In this thesis, we focus on investigating the reliability, especially the sensitivity to moisture and high voltages, of silicon heterojunction (SHJ) technology. It is expected to be one of the main players in the near future, particularly in Europe. We not only study the root cause of these two degradation mechanisms but also provide strategies to prevent them at the module and cell levels.

First, we performed a literature review on the reported performance loss rates (PLR) of SHJ modules installed in the field. The data of all analyzed works indicates a median PLR of 0.56%/year, which falls in line with conventional c-Si technologies. The arbitrary filtering of "high-accuracy" data sets we applied increases the median PLR to 0.80%/year. We note that these data mainly refer to Sanyo/Panasonic technology, and the observed mechanisms will most probably change with the new developments. We then researched the indoor data referring to accelerated ageing tests and determined that SHJ technology is sensitive to three factors: moisture (i.e. damp heat (DH)-induced degradation), high voltages (i.e. potential-induced degradation (PID)) and UV exposure. We nonetheless established that with the right module configuration, SHJ solar cells can reach service lifetimes of 35+ years.

Next, we focused on two of the conditions SHJ is sensitive to: moisture and PID. We discovered that the two phenomena are interlinked in SHJ cells encapsulated in a glass/glass (G/G) configuration with ethylene vinyl acetate (EVA) as an encapsulating material. The laminates are prone to degradation when exposed to high-water contents, and this is enhanced when the cells are negatively biased. Conversely, a positive bias prevents all degradation from occurring. We propose, for the first time, a multi-factorial microscopic model unique to SHJ cells, in which degradation occurs at two different levels. First, the high moisture in the module corrodes the glass, creating sodium hydroxide (NaOH) molecules that can diffuse through the encapsulant (i.e. EVA) and reach the SHJ cell. The sodium (Na^+) ions and hydroxyl (OH^-) groups can then get adsorbed in the grain boundaries of the transparent conductive oxide (TCO), and increase grain boundary scattering. Second, the application of a high negative bias (i.e. -1 kV), in addition to amplifying the previous mechanism by increasing the availability of Na^+ in the

Acknowledgements

encapsulant, enhances the conventional drift of Na^+ through the EVA to the cell and into the passivating layers. The diffusion of such ions can create recombination centres, destroying the passivation of the solar cell. We propose three mitigation strategies at the module level: 1) the use of high-volume resistivity and low water vapour transmission rate (WVTR) encapsulants (e.g. polyolefin elastomers (POE) and ionomer); 2) the use of an edge seal in G/G laminates encapsulated with EVA to prevent moisture ingress; and 3) the combination of front-side POE with a rear-side EVA along with a (transparent) backsheet with low permeability.

We then investigated approaches to prevent PID (and DH-induced degradation as a consequence) at the cell level. We determined that nanocrystalline Si/indium tin oxide (nc-Si:H/ITO) layer stacks, which exhibit larger grain sizes, deter PID more effectively. We show that PID can be diminished to a certain point when capping layers - acting as barriers against diffusion of ionic species - are deposited on top of the ITO. The deposition of capping layers demonstrated that PID can be mitigated to some extent and, DH-induced degradation, completely prevented.

Finally, we compared the stability of SHJ technology to that of its main competitors in the PV market: passivated rear emitter and contact (PERC) and tunnel-oxide passivating contact (TOPCon) solar cell technologies. These showed more stability in DH conditions, but a higher sensitivity to PID at the same time (PERC in particular). We showed that, unlike SHJ, PERC and TOPCon technologies are prone to PID in G/G module configurations with EVA even when moisture ingress is prevented with the use of an edge seal. We would therefore dissuade the usage of EVA with these technologies and to employ polyolefin encapsulants to ensure their long-term stability.

Key words: reliability, solar module, silicon heterojunction (SHJ), degradation, damp heat (DH), potential-induced degradation (PID), ethylene vinyl acetate (EVA), mitigation, transparent conductive oxide (TCO), high efficiency

Résumé

La technologie photovoltaïque (PV) - en raison de sa disponibilité et de son coût compétitif - est l'une des sources d'énergie renouvelable les plus prometteuses. Le marché du photovoltaïque est dominé par les cellules solaires basées sur le silicium cristallin (c-Si). Il est donc primordial pour les fabricants, les investisseurs et les clients de s'assurer de leur performance à long terme. Dans cette thèse, nous nous concentrons sur l'étude de la fiabilité, en particulier la sensibilité à l'humidité et aux hautes tensions, de la technologie de l'hétérojonction au silicium (SHJ). On s'attend à ce qu'elle devienne l'un des principaux acteurs dans un avenir proche, en particulier en Europe. Nous étudions non seulement les causes profondes de ces deux mécanismes de dégradation, mais nous proposons également des stratégies pour les prévenir au niveau des modules et des cellules.

Tout d'abord, nous avons effectué une revue de la littérature sur les taux de perte de performance (PLR) des modules SHJ installés sur le terrain. Les données de tous les travaux analysés indiquent un PLR médian de 0,56 %/an, ce qui correspond aux technologies c-Si conventionnelles. Le filtrage arbitraire des ensembles de données de "haute qualité" que nous avons appliqué augmente le PLR médian à 0,80 %/an. Nous notons que ces données se réfèrent principalement à la technologie Sanyo/Panasonic, et que les mécanismes observés changeront très probablement avec les nouveaux développements. Nous avons ensuite recherché les données relatives aux tests de vieillissement accéléré et déterminé que la technologie SHJ est sensible à trois facteurs : l'humidité, les hautes tensions (c'est-à-dire la dégradation induite par le potentiel (PID)) et l'exposition aux UV. Nous avons néanmoins établi qu'avec la bonne configuration de module, les cellules solaires SHJ peuvent atteindre des durées de vie de plus de 35 ans.

Ensuite, nous nous sommes concentrés sur deux des conditions auxquelles le SHJ est sensible : l'humidité et la dégradation induite par le potentiel. Nous avons découvert que ces deux phénomènes sont liés dans les cellules SHJ encapsulées dans une configuration verre/verre (G/G) avec de l'éthylène-acétate de vinyle (EVA) comme matériau d'encapsulation. Les modules ont tendance à se dégrader lorsqu'ils sont exposés à des concentrations d'eau élevée, et ce phénomène est accentué lorsque les cellules sont polarisées négativement. Inversement, une polarisation positive empêche toute dégradation. Nous proposons, pour la première fois, un modèle microscopique multifactoriel propre aux cellules SHJ, dans lequel la dégradation se produit à deux niveaux différents. Tout d'abord, l'humidité élevée dans le module corrode le

Acknowledgements

verre, créant des molécules d'hydroxyde de sodium (NaOH) qui peuvent diffuser à travers l'encapsulant (c'est-à-dire l'EVA) et atteindre la cellule SHJ. Les ions sodium (Na^+) et les groupes hydroxyles (OH^-) peuvent alors être adsorbés dans les joints de grains de l'oxyde conducteur transparent (TCO) et augmenter la diffusion aux joints de grains. Deuxièmement, l'application d'une forte polarisation négative (c'est-à-dire -1 kV), en plus d'amplifier le mécanisme précédent en augmentant la disponibilité du Na^+ dans l'encapsulant, renforce la migration conventionnelle du Na^+ à travers l'EVA vers la cellule et dans les couches de passivation. La diffusion de ces ions peut créer des centres de recombinaison, réduisant la passivation de la cellule solaire. Nous proposons trois stratégies d'atténuation au niveau du module : 1) l'utilisation d'encapsulants à haute résistivité et à faible taux de transmission de la vapeur d'eau (WVTR) (par exemple, élastomères de polyoléfine (POE) et ionomères) ; 2) l'utilisation d'un joint hermétique pour les modules encapsulés G/G avec de l'EVA pour empêcher la pénétration de l'humidité ; et 3) la combinaison de POE sur la face avant avec de l'EVA sur la face arrière et une feuille arrière (transparente) à faible perméabilité.

Nous avons ensuite étudié des approches visant à prévenir le PID (et la dégradation induite par le test de "chaleur humide" (DH)) au niveau des cellules. Nous avons déterminé que les empilements de couches de silicium nanocristallin et d'oxyde d'indium dopés à l'étain (nc-Si :H/ITO), qui présentent des grains plus gros, empêchent plus efficacement le PID. Nous montrons que le PID peut être réduit jusqu'à un certain point lorsque des couches de recouvrement - agissant comme barrières contre la diffusion des espèces ioniques - sont déposées sur l'ITO. Le dépôt de couches de recouvrement a démontré que le PID peut être atténué dans une certaine mesure et que la dégradation induite par le DH peut être complètement évitée. Enfin, nous avons comparé la stabilité de la technologie SHJ à celle de ses principaux concurrents sur le marché photovoltaïque : les technologies de cellules solaires à émetteur et contact arrière passivé (PERC) et à contact passivant à oxyde tunnel (TOPCon). Ces dernières ont montré une plus grande stabilité dans les conditions DH, mais aussi une plus grande sensibilité au PID (PERC en particulier). Nous avons montré que, contrairement au SHJ, les technologies PERC et TOPCon sont sujettes au PID dans une configuration G/G avec un encapsulant EVA même lorsqu'un joint hermétique est utilisé. Ainsi, nous dissuadons l'utilisation d'EVA pour ces technologies et proposons l'usage de POE comme alternative pour garantir la stabilité sur la durée.

Mots clefs : fiabilité, module solaire, hétérojonction de silicium (SHJ), dégradation, chaleur humide (DH), dégradation induite par le potentiel (PID), éthylène-acétate de vinyle (EVA), atténuation, oxyde conducteur transparent (TCO), haute efficacité.

Contents

Acknowledgements	i
Abstract (English/Français)	iii
List of acronyms and symbols	xi
1 Introduction	1
1.1 Energy transition	1
1.1.1 Solar PV electricity: cost reduction	2
1.2 PV technology, market and projections	4
1.2.1 Solar cell technologies	5
1.2.2 Solar cell interconnections	8
1.2.3 PV module technology	9
1.3 Reliability in Photovoltaics	14
1.3.1 PV module reliability and concepts	14
1.3.2 Failure modes	16
1.3.3 Qualification Tests	20
1.4 Potential-Induced Degradation (PID)	23
1.4.1 Physical degradation mechanism	25
1.4.2 Role of the module materials	28
1.5 Structure of this thesis	29
1.6 Contribution to the field	30
2 Experimental Methods	33
2.1 Manufacturing of PV modules	33
2.1.1 Module design and material choice	33
2.1.2 Lamination procedure	36
2.2 Characterization of PV modules	37
2.2.1 Current-Voltage (I-V) measurements	37
2.2.2 Electroluminescence	40
2.2.3 External quantum efficiency	41
2.2.4 Photoluminescence	42
2.3 Characterization of module materials	42
2.3.1 Microstructural characterization of degraded solar cells	42

CONTENTS

2.3.2	Fourier-transform infrared spectroscopy	44
2.3.3	Electrical resistivity measurements	44
2.3.4	X-ray diffraction	45
2.3.5	Atomic force microscopy	45
2.3.6	Hall effect	45
2.4	Indoor accelerated ageing tests of PV modules	45
2.4.1	Damp Heat testing	45
2.4.2	Potential-induced degradation testing	46
3	Reliability and Long-term Performance of SHJ Solar Modules	49
3.1	Introduction	50
3.2	Method and approach	53
3.2.1	Overview of studies reporting on SHJ technology	54
3.2.2	Caveats	56
3.3	Literature survey	58
3.3.1	All data-sets	58
3.3.2	High-accuracy data-sets	59
3.3.3	The effect of climate	60
3.4	Failure modes and potential weaknesses reported for SHJ cells/modules	63
3.4.1	Outdoor exposure (this survey)	64
3.4.2	Indoor accelerated ageing testing	65
3.5	Discussion: targeting service lifetimes of 35+ years for SHJ modules	67
3.6	Conclusions	70
4	Sensitivity of SHJ Solar Cells and Modules to Moisture Ingress	73
4.1	Introduction	74
4.2	Experimental methods	74
4.2.1	Sample design and fabrication	74
4.2.2	Module characterization	76
4.2.3	Cells and materials characterization	76
4.3	Results	76
4.3.1	Module electrical characterization	76
4.3.2	The role of module components in degradation mechanism	79
4.4	Sensitivity to water: a multi-factorial degradation model	85
4.5	Conclusions	86
5	Degradation Model and Mitigation Strategies for PID in Bifacial SHJ Solar Cells and Modules	89
5.1	Introduction	90
5.2	Experimental methods	91
5.2.1	PID-stress testing	91
5.2.2	Scanning and transmission electron microscopies	92
5.3	PID mechanism in bifacial rear-emitter SHJ solar cells	93

5.3.1	Influence on voltage	93
5.3.2	Contribution of front and rear sides to the total degradation	94
5.3.3	Scanning and transmission electron microscopies	97
5.4	PID in SHJ solar cells and modules: a microscopic model	100
5.5	PID mitigation strategies for SHJ modules	102
5.5.1	Choice of encapsulant	102
5.5.2	Prevention of moisture ingress	104
5.5.3	Combination front-POE and rear-EVA encapsulation schemes	105
5.6	Conclusions	107
6	Development of PID-resistant SHJ Solar Cells	109
6.1	Introduction	109
6.2	Experimental methods	111
6.2.1	Sample design and fabrication	111
6.2.2	Material and module characterization	112
6.3	Improved PID and DH resistance: the role of different cell structures and TCOs	113
6.3.1	Industrial- vs. lab-scale SHJ cells	113
6.3.2	The role of surface texturization	116
6.3.3	The role of different TCO compositions and of substrate layers	118
6.4	The role of capping layers deposited by PECVD	121
6.4.1	Single capping layer	122
6.4.2	Double and triple capping layers	126
6.5	The role of capping layers deposited by ALD	130
6.6	Conclusions	132
7	Sensitivity to Moisture and High Voltages of High-efficiency c-Si Technologies	135
7.1	Introduction	135
7.2	Experimental methods	137
7.3	Degradation mechanism on G/G module configuration	138
7.3.1	Comparison of cell technologies	138
7.3.2	DH-induced degradation	140
7.3.3	Negative PID	142
7.3.4	Positive PID	146
7.4	Investigation of sensitivity to moisture	148
7.4.1	PERC technology	148
7.4.2	TOPCon technology	150
7.5	Conclusions	152
8	Conclusions and Perspectives	155
8.1	Summary of the main results	155
8.2	Perspectives	157
8.2.1	Update on reliability of SHJ technology	157
8.2.2	Microscopic model on DH-induced degradation	157

CONTENTS

8.2.3	Updates on PID with increased bias	157
8.2.4	Improvements in the development of PID-free SHJ cells	157
8.2.5	Understanding of PID mechanism in PERC and TOPCon technologies .	158
A	Appendix on PID in bifacial large-area SHJ cells and modules	159
A.1	Appendix on the front and rear-side contributions to PID in SHJ modules . . .	159
A.2	Appendix on the role of the emitter position on the PID mechanism	162
B	Appendix on development of PID-free SHJ cells	163
B.1	The role of AZO in the degradation mechanism	163
B.2	The role of TCO thickness on degradation rates	164
	Bibliography	191
	Curriculum Vitae	195

List of acronyms and symbols

Solar Cell Technologies

Al-BSF	Aluminum back-surface field
IBC	Interdigitated back-contact
PERC	Passivated emitter and rear contact
poly-Si	Polycrystalline silicon
SHJ	Silicon heterojunction
TOPCon	Tunnel oxide passivated contact

Solar Cell Materials

a-Si:H	Hydrogenated amorphous silicon
(i)a-Si:H	Intrinsic hydrogenated amorphous silicon
(n)a-Si:H	n-doped hydrogenated amorphous silicon
(p)a-Si:H	p-doped hydrogenated amorphous silicon
c-Si	Crystalline silicon
FZ	Float-Zone
nc-Si:H	Hydrogenated nanocrystalline silicon
Ag	Silver
Al	Aluminum
Al ₂ O ₃	Aluminum oxide
AZO	Aluminum-doped zinc oxide
ITO	Indium tin oxide
IWO	Indium tungsten oxide
IZrO	Indium zirconium oxide
SiN _x	Silicon nitride
SiO _x	Silicon oxide
TCO	Transparent conductive oxide
ARC	Anti-reflective coating
DARC	Double anti-reflective coating

Chapter 0. List of acronyms and symbols

Deposition Processes

ALD	Atomic layer deposition
PECVD	Plasma enhanced chemical vapor deposition

Module Configurations

G/Al-BS	Glass/aluminium backsheet
G/BS	Glass/backsheet
G/G	Glass/glass
G/G-ES	Glass/glass with an edge seal
G/T-BS	Glass/transparent backsheet

Module Materials

BS	Backsheet
EVA	Ethylene vinyl acetate
POE	Polyolefin elastomer
TPO	Thermoplastic polyolefin
ρ	Electrical volume resistivity
WVTR	Water vapour transmission rate
Na	Sodium
Na^+	Positively charged sodium ion
NaOH	Sodium hydroxide molecule
OH^-	Negative charged hydroxyl group

Characterizations

η	Energy conversion efficiency
FF	Fill factor
I_{SC}	Short-circuit current
P_{max}	Maximum power
V_{OC}	Open-circuit voltage
R_s	Series resistance
R_{sh}	Shunt resistance
$I - V$	Current-voltage
$J - V$	Current density-voltage
EL	Electroluminescence
EQE	External quantum efficiency
PL	Photoluminence imaging

AFM	Atomic force microscopy
EDX	Energy-dispersive X-ray spectroscopy
FTIR	Fourier-transform infrared spectroscopy
SEM	Scanning electron microscopy
STEM	Scanning transmission electron microscopy
TEM	Transmission electron microscopy
XRD	X-ray diffraction

Accelerated Ageing Tests

DH	Damp heat
HF	Humidity freeze
PID	Potential-induced degradation
TC	Thermal cycling

1 Introduction

1.1 Energy transition

Anthropogenic activities of recent decades have resulted into an exacerbated emission of greenhouse gases (GHG) - carbon dioxide (CO₂) in particular - to the atmosphere, increasing the average temperature on Earth as a consequence [1]. In 2015, the countries participating in the Paris Agreement agreed to establish protocols to limit the global temperature to a maximum of 1.5°C above pre-industrial levels [2]. In 2020, **CO₂ emissions** experienced a decline compared to previous years due to the COVID-19 pandemic, but they **reached a record peak in 2021** after the rebound of energy production based on the combustion of fossil fuels [3]. Conversely, the rapid implementation of renewable energies and the use of electric vehicles is expected to reduce CO₂ emission growth by the end of 2022. Nevertheless, data shows that atmospheric levels of GHG continued to increase in 2022, and the global temperature is estimated to be about 1.15°C above pre-industrial levels [4].

Because the measures established as a result of the Paris Agreement aim to reach the peak of GHG emissions as soon as possible, a swift energy transition (among other factors) is required. Such a transition is defined in the report published by the International Energy Agency (IEA) *Net Zero by 2050: A Roadmap for the Global Energy Sector* in 2021 [5], where they describe pathways to reach net zero emissions by mid-century. Additionally, the global energy and socio-economic crisis we face today shows an imperative need to provide large-scale clean cost-effective energy: countries with low GHG emissions do not have access to enough energy to meet their needs and, those who do, source it - mainly - from combustion of fossil fuels [6].

The urgency to **provide worldwide energy** - mainly electricity - **from sustainable and reliable sources** was made even more apparent after the invasion of Russia on Ukraine. The war and the European Union (EU) bans on Russia caused an increase of natural gas prices and the demand for coal [7]. The crisis also highlighted the EU's energy dependency on other countries.

In 2021, renewable energies provided for 28.3% of the world electricity production, compared

to the 62% pertaining to fossil fuel combustion [8]. From the reported 3146 GW global installed capacity from renewable sources, 10% came from wind and solar power. In fact, wind and solar are the renewable energy sources that have developed most in the last decade (2% of the global production in 2011), and have the largest potential for growth of all renewable energy technologies. They are thus leading the aforementioned energy transition.

Having added 175 GW to the global capacity in 2021 (accounting for the 56% of the total renewable-energy capacity added that same year) [8], [9] and reaching a record 1000 TWh of electricity generation [10], **solar photovoltaic (PV) is considered to be one of the safest, cleanest and most competitive renewable energy sources**. The technology has experienced exponential growth over the last decades and the landmark of **1 TW of installed cumulative capacity** was reached in 2022. It took ten years to increase the capacity tenfold (from 100 GW in 2012), but it is projected that it will double to 2.3 TW by the end of 2025 [9]. Although PV alone installed more capacity than all the other renewable energy sources combined, it only meets 4% of the global electricity demand [9], [10]. It is projected that an annual growth of 25% is needed in the period 2022-2030 to reach the Net Zero Emissions by 2050 Scenario [10]. Therefore, more efforts - in the field of policy making, regulations, investments, and technology development and integration - need to be made to increase the prominence of PV in the energy transition.

In 2021, **31.8 GW were added to the solar capacity in Europe**, representing an increase of 33% year-on-year. The Russian war on Ukraine, along with energy security challenges and climate goals, is pushing the energy transition in Europe and, in particular, the growth of PV.

In Switzerland, 683.7 MW were added to the installed PV capacity in 2021, bringing the total capacity to 3.7 GW and supplying 6% of the energy demand [11]. In order to meet the goals of 30-40 GW established in *Energy Strategy 2050* [12], the annual increase should triple to achieve 2000 MW by 2030. To facilitate the rapid transition, the Energy Commission of the Swiss Council of States is setting a series of legal procedures to gradually phase out nuclear energy and boost the development of large-scale PV systems.

1.1.1 Solar PV electricity: cost reduction

Cost-competitiveness is an indispensable requisite for both public and private investors as well as for stakeholders in order to endorse the expansion and implementation of PV. The reduction in price that the PV market has experienced in recent years has been promoted by advancements in solar cell and module technology, a rise in production volume and a dedicated supply chain. As shown in Figure 1.1, prices decreased by 24% - with a consequent learning curve of 24% - for each doubling of cumulative power capacity over the last 40 years. In 2020, an all-time low in the PV market was reported for c-Si module prices: **0.17 to 0.25 €/W_p**.

In addition to the initial costs of a PV system, the energy yield is a factor that is considered

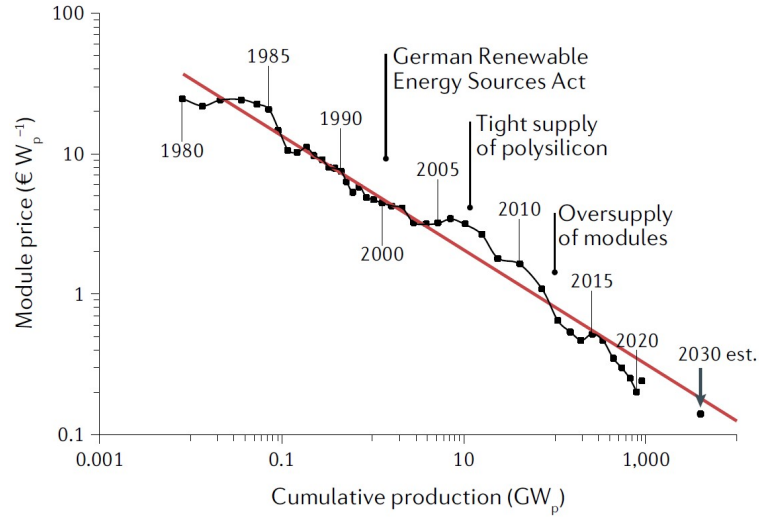


Figure 1.1: Diagram of cost reduction in module prices over the years with respect to the increase in cumulative production. Taken from [13].

when deciding whether to invest in a PV installation or not. This can be defined as the amount of electricity - in kWh - that a PV system can generate over a given duration. The energy yield has a strong impact on the cost and, thus, its accurate assessment is particularly relevant to PV plant owners. The viability of different technologies is often analyzed by estimating the **levelized cost of electricity (LCOE)**. There are several ways LCOE can be calculated, but the most common - and straightforward - is to divide the total lifecycle cost (from the initial investment to the operation, maintenance and decommissioning costs) by the total energy yield over the lifetime of the system (see Equation 1.1).

$$\text{LCOE} = \frac{\text{Lifecycle Cost}}{\text{Lifetime Energy Yield}} \quad (1.1)$$

LCOE is thus expressed in **€/Wh**. A more detailed explanation of parameters affecting the LCOE is given in [14]. LCOE can also be described as in the formula given in Equation 1.2:

$$\text{LCOE} = \frac{\text{CAPEX} + \sum_{n=1}^N \frac{\text{OPEX} - \text{RV}}{(1+r)^n}}{\sum_{n=1}^N \frac{Y_0 \cdot (1-D)^n}{(1+r)^n}} \quad (1.2)$$

where:

N is the number of years in operation [years];

CAPEX is the total initial investment [€];

$OPEX$ is the sum of the annual operation and maintenance expenses [€];

RV is the residual value [€];

r is the discount rate [%];

Y_0 is the initial energy yield [kWh];

D is the system annual degradation rate [%].

In addition to scaling up manufacturing processes and production lines (thus reducing the CAPEX value), LCOE can be further reduced in different ways. One is to increase the PV cell and module efficiency to maximize the conversion of sunlight to electricity: the higher the efficiency, the higher the nominal energy yield, Y_0 . The second is to ensure long service lifetimes with the aim of maintaining high energy yields for longer. A low annual degradation rate D , as well as a long lifetime N , reduces the LCOE, thus making a PV system financially competitive. Currently, PV is reportedly the cheapest source of electricity, accounting for **0.03 to 0.06 €/kWh** in utility-scale PV plants in Europe.

This thesis focuses on studying the **reliability** of novel high-efficiency solar cell technologies - **silicon heterojunction (SHJ)** in particular. The most vulnerable aspects of SHJ technology will be assessed from outdoor exposure and indoor testing data. Accelerated stress testings will then be performed in the laboratory environment with the objective of providing better insights into the most critical failure mechanisms of SHJ. Finally, we will focus on developing mitigation strategies at the solar cell and module level to ensure high performance for long service lifetimes.

In the following sections, we describe the high-efficiency solar cell technologies on the market, the interconnection technologies and PV packaging components, as well as the innovations and novelties adopted in each of them to enhance their performance. We then describe the concepts of reliability and durability of PV modules, and give a brief overview of the main failure modes found in PV modules installed in the field. Finally, we describe indoor accelerated stress testing to assess the stability of PV modules in a reasonable time frame.

1.2 PV technology, market and projections

The PV market has been through a significant upheaval in the last decades. Climate change, the energy crisis and the increase in electricity prices have pushed the exponential development of PV technology. Every component of PV modules - from solar cells to electrical interconnections and module structure - has evolved to reach better performance and stability. In this section, PV modules and their components will be described, along with innovation strategies and future projections in the PV market.

1.2.1 Solar cell technologies

Solar cells are the **active element** of a PV module, having the function of directly converting sunlight into electricity. The first silicon (Si) solar cell, developed in 1954 at Bell Laboratories, was initially used for space applications in 1958. Crystalline Si (c-Si) solar cells were industrialized for terrestrial applications in the 1970s, and the PV market has grown exponentially since then. Other technologies besides c-Si have had a significant role over the years (i.e. thin films and III-V cells such as GaAs) but currently, their application is limited to a niche market [15]. Instead, c-Si solar cells are dominating the PV industry (in 2021, 95% of the worldwide production was dedicated to c-Si technology) [16], [17], and are expected to continue doing so in the future [15]. In the present section, PV solar cell technologies based on c-Si will therefore be described.

Technologies based on c-Si have gone through a series of improvements over the last 50 years. Aluminium back surface field (Al-BSF) was the mainstream technology for decades, until 2015-2016 (see Figure 1.2(a)), when the industry started turning towards more novel high-efficiency technologies, such as passivated emitter and rear contact (PERC) (Figure 1.2(b)). In addition to PERC, other high-efficiency technologies are entering the market now, tunnel oxide passivated contact (TOPCon) (Figure 1.2(c)) and SHJ (Figure 1.2(d)) solar cells, for instance.

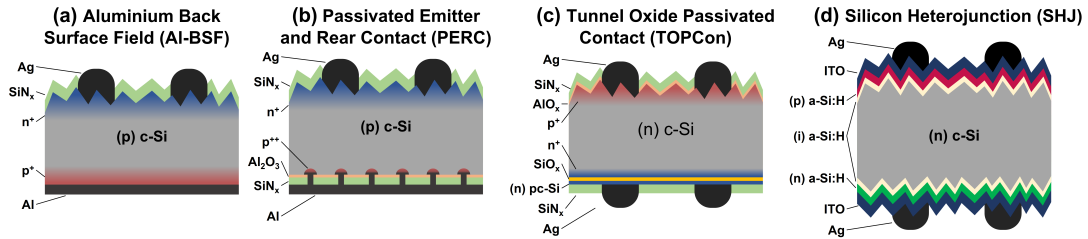


Figure 1.2: Schematics of solar cell technologies in the market: (a) aluminium back surface field (Al-BSF), (b) passivated emitter and rear contact (PERC), (c) tunnel oxide passivated contact (TOPCon) and (d) bifacial silicon heterojunction (SHJ). The solar cells are not drawn to scale.

Al-BSF solar cells, represented in Figure 1.2(a), consist of a p-doped c-Si wafer, with a phosphorus-doped emitter - creating the p-n junction - at the front, followed by a silicon nitride (SiN_x) layer acting as anti-reflective coating (ARC) and screen-printed silver (Ag) contacts. At the rear side, a highly p-doped region creates the back surface field and the electrical connection is made by depositing a full-area Al metallization layer. The technology initially presented **efficiencies of around 15% that rapidly increased to 18%** [18]. However, they soon **stagnated at 20%** due to the limited operational voltage caused by the direct contact between the Al layer and c-Si wafer [19]. The implementation of this technology was nevertheless promoted due to the simple structure and manufacturing process that led to a good performance/cost ratio.

In 1989, Blakers et al. introduced **PERC solar cells** for the first time [20]. It took 25 years for this technology to be adopted by the industry, mainly due to the complication of the

manufacturing processes [21]. Nowadays, PERC solar cells account for around **80% of the market share** [15]. They were originally developed as a **solution for the high recombination rates** reported for Al-BSF solar cells by chemically passivating the rear surface of the Si wafer and localizing the Al-Si contact. The passivation consists of depositing thin aluminium oxide $\text{AlO}_x/\text{SiN}_x$ layer stacks, as shown in Figure 1.2(b). The Al contacts are then deposited as line-shaped local rear contacts. The local p^+ doping surrounds the contact, suppressing most of the recombination of charge carriers. This configuration can therefore offer a good solution to the carrier recombination sites created by the Al/c-Si interface in conventional Al-BSF solar cells, and increased open-circuit voltage (V_{OC}) and fill factor (FF) values can be achieved as a consequence [22] (the maximum V_{OC} reported is 706 mV [23]). Moreover, PERC solar cells present decreased optical losses and thus increased short-circuit current densities (J_{SC}). The addition of the passivating $\text{AlO}_x/\text{SiN}_x$ layer stacks at the rear side, with a low refractive index, improves the optical reflectivity at the rear surface, enhancing light trapping and increasing the absorption of infrared light in the solar cell [24].

Because the direct contact of the Si wafer with the localized metallization (i.e. Al contacts) at the rear side limits the V_{OC} on PERC solar cells, in 2013, Fraunhofer ISE developed a new cell technology named **TOPCon** (see Figure 1.2(c)) [25], [26]. It consists of an ultra-thin (a few nanometers thick) silicon oxide (SiO_x) layer and a heavily-doped poly-silicon (pc-Si) layer. The former chemically passivates dangling bonds while the latter provides passivation by field effect and carrier selectivity [25]–[27]. The metallic contact is deposited as a full-area Ag layer following the $\text{SiO}_x/\text{pc-Si}$ stack. This stack is so thin that the collection of charge carriers is not compromised. It is usually used at the rear side of the cells in commercialized cell structures to avoid parasitic absorption in the pc-Si layer at the front, the front side resembling those of conventional Al-BSF and PERC solar cells (i.e. diffused emitter). Consequently, the direct contact between the front metallization and the Si wafer limits the V_{OC} to around 720 mV [28], [29]. The most efficient approach for obtaining higher V_{OC} values and, thus, higher efficiencies, would be to develop **double-side TOPCon cells** (i.e. by applying the passivated contact technology on both sides). However, several factors in the manufacturing process of such cells currently hinder this development [30], [31]. One of the main advantages of the TOPCon technology is that the manufacturing processes do not require patterning, and can have a significantly straightforward integration into existing production lines for Al-BSF or PERC cells [32]. TOPCon technology is expected to increase its market share from 10% in 2022 to up to 58% by 2032; it is thus a **direct competitor of PERC technology**.

The development of **SHJ technology**, available on the market since the early 1990s [33], was motivated as a means to solve the passivation and recombination problems in the c-Si technologies previously described. SHJ offers **high surface passivation and carrier selectivity on both sides** of the solar cell [34]. This is achieved by combining highly hydrogenated amorphous Si (a-Si:H) and c-Si layers. The basic device structure of such cells, shown in Figure 1.2(d), is based on the deposition of intrinsic a-Si:H layers ((i)a-Si:H) on both sides of n-type c-Si wafers, followed by p/n-doped a-Si:H for hole/electron selectivity, a transparent conductive oxide (TCO) - acting as ARC with very low resistance - and the metallic (i.e. Ag)

electrodes. In standard c-Si cells (e.g. Al-BSF and PERC), the metal contacts are deposited in such a way that they penetrate the dielectric $\text{SiN}_x/\text{SiO}_x$ layer stack, and they make contact with the active layer of the cell, that is, the bulk. This creates a high recombination site in the cell and hinders the efficiency. In Al-BSF solar cells and, to a lower extent PERC cells, a similar process takes place at the rear side, where the metallization has direct contact with the c-Si. This limitation was overcome in SHJ by depositing the intrinsic and doped a-Si:H layer stacks, that provide surface passivation, carrier selectivity, light trapping and charge extraction [29], [34], [35].

Additionally, the processing temperature also differs from that of conventional c-Si cells. The p-n junction in SHJ cells is formed by the deposition of doped a-Si:H layers on top of the c-Si by using temperatures below 200°C , whereas the formation of the p-n junction in conventional c-Si cells depends on thermal diffusion of dopants at around 900°C . This factor limits the thermal degradation of SHJ cells, but also complicates the formation of low-resistivity contacts. The **thickness and, consequently, the cost are also reduced** due to the intrinsic structure of SHJ solar cells. Last, due to the **higher V_{OC}** (751 mV for the commercial record cell [36]), the temperature coefficient is lower for SHJ cells, meaning that temperature-dependent loss of performance is slower than for other c-Si cells. This feature makes SHJ cells particularly suitable for applications in hot climates.

One of the main limitations in SHJ solar cells derives from the relatively low transparency of the a-Si:H and the TCO layers, limiting the cell J_{SC} [37], [38]. Consequently, the PV industry developed a technology derived from SHJ called **interdigitated back contact (IBC)** with the goal of reducing the shadowing from the front metallic contacts [39]. The improved light absorption is achieved by placing all the metallic contacts at the rear side of the solar cell and depositing a SiN_x ARC at the front. This technology had the highest efficiencies among c-Si solar cells until November 2022, when LONGi published their **record-breaking SHJ solar cells with an efficiency of 26.81%** [36]. Currently, standard SHJ technology has a **market share of around 3%** and is expected to gain up to 19% in 10 years [15]. The growth of production lines is limited to China, but it is also significant in European countries, helping to boost the implementation of PV.

However, the efficiencies of all c-Si single-junction technologies mentioned above (i.e. one p-n junction, at the front or rear side) are physically limited at 29.4 to 29.6% by what is called the **Shockley-Queisser limit** [40]. Considerable efforts are devoted to the development of **tandem** technologies to overcome the 30% limit. Tandem solar cells combine two junctions with different band gaps in order to make maximum use of the incident light and can reach efficiencies of 47% (without concentration). Different materials and cells are being postulated to be applied in tandems, but SHJ in particular poses as a good candidate to be the bottom cell. Consequently, the growth of SHJ is even more interesting.

At the beginning of this section, the importance of achieving high-efficiency solar cells to reduce LCOE was mentioned. However, the parameters of these sophisticated structures -

leading to higher efficiencies - have been optimized to such an extent that they may portray a higher sensitivity to a series of new degradation and failure modes. Preventing the formation of defects in high-efficiency technologies is thus critical to ensure their long-term stability.

1.2.2 Solar cell interconnections

Solar cells need to be electrically connected to increase current or voltage to match load requirements. Usually, the cells are **connected in series** with each other and, then, the strings are interconnected to the junction box to ensure optimal extraction of current. Conventional c-Si modules consist of **60 or 72 series-connected solar cells**.

With the aim of extracting current from the solar cells while reducing the ohmic resistances, thin rectangular-shaped strips called **busbars** are printed at the front and rear sides of a cell (see Figure 1.3). **Ag fingers**, of around $100\ \mu\text{m}$, are screen-printed perpendicular and connected to the busbars to help collect the current and to minimize contact resistance when soldering the ribbons. The **cell interconnections**, mentioned above, are implemented by soldering thin wires to the busbars at high temperatures (usually around 350°C is enough for the soldering process), as shown in Figure 1.3 at the right. The solar cells are connected in series by soldering the front-side busbars to the rear side of the next - and so on. The strings are then interconnected by soldering the thin busbar wires to thicker wider wires that are then connected to the junction box of the PV modules.

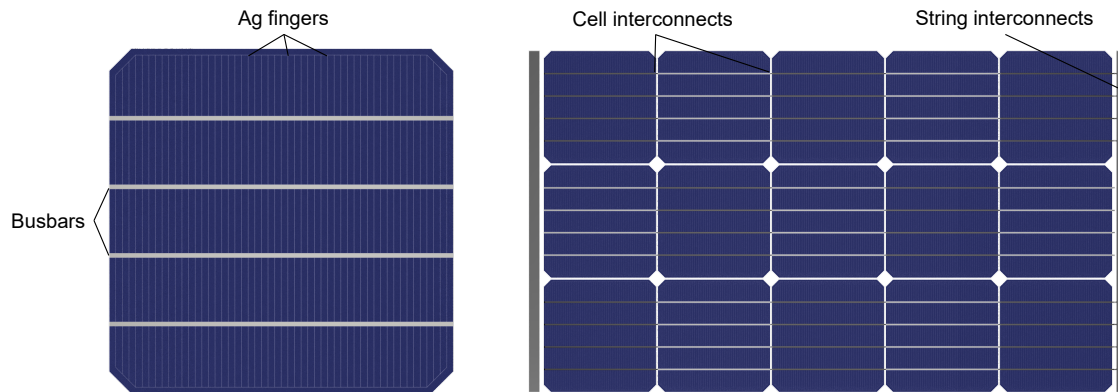


Figure 1.3: Schematics of a conventional 4-busbar solar cell (left) and 3-string interconnections (right).

Similarly to the evolution experienced in solar cell technologies, the interconnection concepts and methodologies have also evolved over the years to optimize PV module performances [41]. Conventionally, solar cells used to have 2 to 3 busbars, but the major trend in recent years in module and busbar technology has been to **increase the amount of busbars** (even up to 9) and to **reduce the thickness** [15]. The former aims to reduce resistive losses by placing the busbars closer together and the latter to decrease wire shadowing and, thus, improve light

absorption.

Another trend related to busbar technology is the use of **IBC solar cells**, for which no busbars are laced on the front side, and the collection of carriers takes place only on the rear side. These solar cells not only optimize photo-generated current (as was explained in Section 1.2.1), but they are also more aesthetically pleasing and can be good candidates for building integrated PV (BIPV) [41]. The main downside however is production costs.

The sensitivity of SHJ technology to higher temperatures (over 200 to 220°C) was mentioned in the previous section. The cell interconnections in this technology cannot therefore be done with the standard high-temperature soldering processes, but the procedure needs to be adapted. One strategy is to adapt the temperature to match the thermal budget of SHJ technology while applying conventional busbar soldering processes [42]. It is not the mainstream process, but it has been gaining more weight recently. Another strategy and the one utilized most for SHJ, is the use of an **electrically conductive adhesive (ECA)** to "paste" the ribbons to the busbars at low temperatures [41]. ECAs are usually alloys of different metals, with high content in Ag, in order to ensure a good conductivity and low resistive losses. The drawbacks of the ECA technology are the need to adapt stringers in commercial production lines and the increased use of Ag and thus the cost.

MultiWire (MWT) and **SmartWire (SWT)** technology, further developed by Meyer Burger, can also pose as an alternative to the standard soldering process [43]. Conventional 3 to 6 ribbons/busbars are replaced by 20+ round wires with a small diameter. The main objective of utilizing this technology is to reduce the current distribution by increasing the number of ribbons and, thus, we can use wires with lower conductance. This also implies a reduction in silver consumption. Additionally, it decreases the sensitivity of the cells and modules to cracks/breakages, so enhances the durability of the PV modules.

One of the main concerns in PV is the large amount of Ag needed for the production of solar cells and modules. Currently, efforts are being made in finding solutions to that problem, especially on SHJ technology. In the field of interconnections, the development of **copper-plated (Cu-plated)** contacts to replace Ag is reportedly being pursued [44].

Ensuring good cell and string interconnections is key to extracting current in the most efficient way by minimizing resistive losses. As with any developments and introduction of new concepts, research is crucial to provide stable interconnections in PV modules.

1.2.3 PV module technology

PV modules are **exposed to a variety of stressors** when installed in the field: **temperature variations** due to performance and environment, **high humidity** conditions, **mechanical stress** (e.g. wind, snow and hail) and **light and UV irradiance**. Consequently, solar cells and interconnections - due to their fragility - need to be packaged in sturdy module configurations to last more than 25 years in the field. The objective of PV module packaging is to:

- protect the electrical circuitry from weathering;
- provide structural stability and protect mechanical integrity;
- isolate electrical circuits from the environment (e.g. to protect operators from electrical shocks).

A representative glass/backsheet (G/BS) PV module structure is shown in Figure 1.4 [41]. The front-side cover of standard PV modules in most cases consists of a 3.2 mm-thick **glass**. The rear-side cover is traditionally a **polymeric backsheet** (BS) - consisting of several layers - that would ideally have similar properties as the front cover. One of the major differences in requirements between the front and rear covers is the transparency, which the latter does not need (unless a bifacial technology is employed). Then, enveloping the solar cell and interconnections, two layers of **encapsulant** are placed (one layer at each side of the cells). Last, an **Al frame** is placed around the PV module to ground it and provide structural support, and a **junction box** is glued at the rear side (through connectors) to enable the extraction of the generated power.

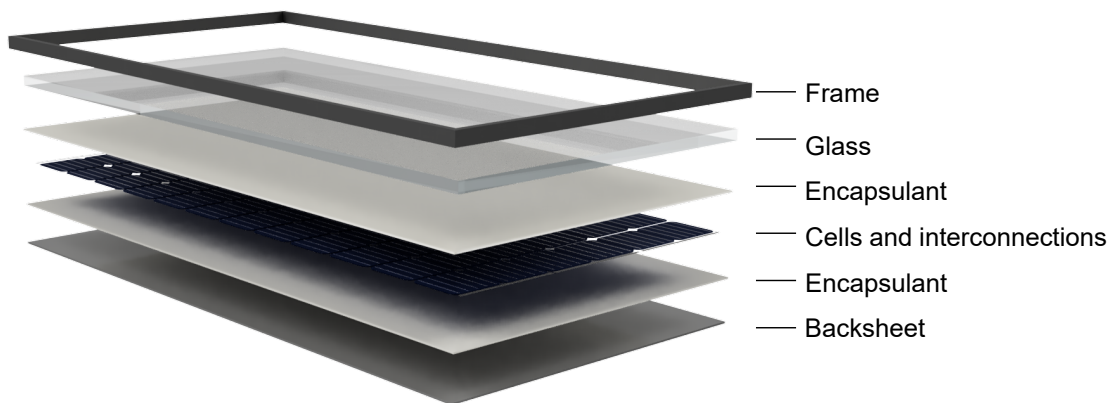


Figure 1.4: Schematics of a conventional glass/backsheet PV module structure.

The **front cover** is usually a **soda-lime glass** sheet; the typical composition of such glasses is defined in Table 1.1. The main goal is to provide physical insulation (against moisture ingress to protect internal circuitry) and mechanical stability against external aggressors (e.g. wind, snow and hail), thus tempered glass - strengthened by thermal or chemical treatments - is often favored. Moreover, it needs to have good optical properties (i.e. high transmittance) to allow the sunlight to pass through to the solar cells to generate the maximum current. Innovative concepts regarding optical improvements on the glass will be mentioned in the following section.

As mentioned, most PV modules use a composite polymer sheet as BS. An example of a commercially available BS is presented in Figure 1.5. Usually, these types of BS are composed of multi-stack structures of three layers - **Tedlar-PET-Tedlar** or **T-P-T** - with an overall thickness

Table 1.1: Standard composition of soda-lime glass used for PV applications.

Chemical component	Percentage [%]
SiO ₂	70-74
Na ₂ O	12-16
CaO	5-11
MgO	1-3
Al ₂ O ₃	1-3
Others	1

of 280 to 400 μm (see). The commercial name *Tedlar* stands for polyvinyl-fluoride (PVF) and protects the internal circuit from weathering agents. Conversely, polyethylene terephthalate (PET) isolates the module electrically and provides mechanical stability.

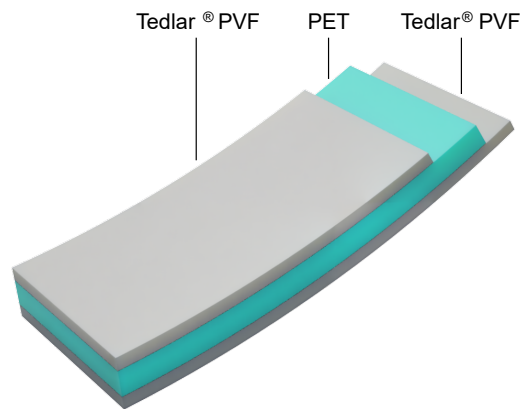


Figure 1.5: Cross-section of a conventional Tedlar-PET-Tedlar backsheet.

Encapsulants play a significant role in the long-term performance of PV modules. The main functions of encapsulants are to provide:

- **adhesion between components** - cells-front glass, cells-backsheet and front glass-backsheet;
- **physical insulation** - protecting cells from weathering agents (e.g. UV and rain);
- **electrical insulation** - keep high voltages away from people and the current from flowing out of the array circuit to the ground (although they are not considered as insulating components, according to the International Electrotechnical Commission (IEC));
- **optical transparency** - couple as much incoming light as possible into the cells (same as the front glass).

Encapsulants can be divided into two categories depending on the type of cross-linking they go through: chemically cross-linked elastomers and physically cross-linked (also defined

as "non-cross-linking") thermoplastic elastomers [45]. The former require the formation of covalent bonds between the polymer chains to cross-link during the lamination process at high temperatures (explained in detail in Chapter 2). The latter melt during the manufacturing process without the formation of these bonds.

The most common of encapsulants - mainly due to its cost-effectiveness - is **ethylene vinyl acetate (EVA)**. EVA, which pertains to the family of encapsulants that chemically cross-link during the encapsulation process, has been the main player on the market for more than 20 years [15]. However, the durability of PV modules encapsulated with EVA has always been questioned owing to the several degradation modes attributed to it. The main failure found initially in EVA encapsulants was discoloration or yellowing, most likely due to the degradation of the additives used [45]. Although newer EVA formulations seem to have solved those issues and show higher stability, the production of by-products (i.e. acetic acid) characteristic of this copolymer can still cause degradation related to corrosion.

This led to the development of other copolymers that do not have the vinyl acetate group, hence preventing the formation of acetic acid. The most common cross-linking polymers are **polyolefin elastomers (POE)**, whereas the non-cross-linking polymers most often found in the industry are **thermoplastic polyolefin elastomers (TPO) and ionomers**. Other new formulations, such as EPE (i.e. an EVA-POE-EVA tri-layer) have also been developed, in which the multiple materials are co-extruded into one single polymer foil [46]. These types of multi-layer structures present an attractive alternative since they combine the best properties of EVA and PO-based materials, and in particular for bifacial applications. Nevertheless, EVA is expected to remain the dominant encapsulant in the market for the near future [15].

Innovative concepts

The main innovative concepts in the field of module technology target: (1) increased module performance by reducing cell-to-module losses, (2) increased energy yield and (3) increased reliability.

There are several methods to **increase module performance**. One of them, which has gained strength in the industry lately, is to use half-cells instead of full-area-cell modules, for which resistive losses are lessened due to the lower currents. The cell interconnection losses are consequently diminished. Production of half-cell modules has already taken over full-cell modules, and is projected to keep doing so in the future [15]. Similar to this strategy but with a twist, is the use of shingled solar cells to reduce the inactive area of the module [41], [47]. Cells are cut down into smaller sizes and then interconnected in a way that they slightly superpose each other (the interconnection is usually done with an ECA), as shown in Figure 1.6. This strategy is aimed at optimizing cell density in the module to increase efficiency. Finally, the module's performance can also be increased by using light-capturing ribbons to reduce shading losses [48].

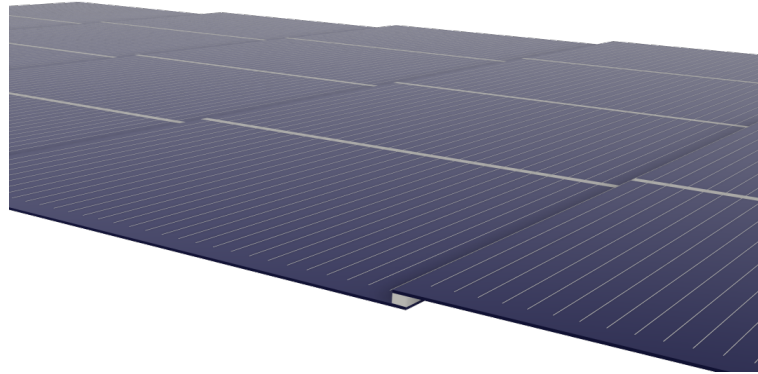


Figure 1.6: Schematics of interconnected shingled solar cells.

Strategies to **increase energy yield** are based on maximizing light absorption into the PV modules. The first strategy is to add an ARC on the front surface of the glass to reduce the reflection at the air/glass interface; the second is to texturize the glass to increase light absorption at low angles [49]. Last, the use of bifacial cells/modules is currently one of the most cost-effective methods to increase electricity production. Depending on the characteristics of each installation site (e.g. ground albedo, design of the mounting structures, etc.) energy-yield gains in the range of 10 to 20% can be achieved [50], [51]. The conventional G/BS module structure requires the rear cover to be changed to glass so light can be absorbed from the rear side (see Figure 1.7). Production of glass/glass (G/G) modules has gained strength in recent years and is expected to become the dominant module technology in the future [15]. SHJ technology, which is "naturally" bifacial owing to having a TCO layer on both sides, may become a major asset in the development of bifacial technologies.

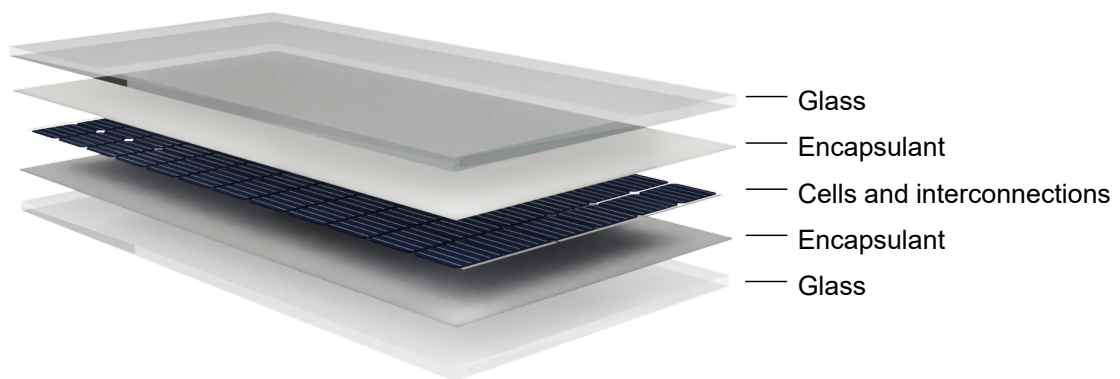


Figure 1.7: Schematics of a glass/glass PV module structure.

G/G modules can also grant additional protection in harsh environments (e.g. snow, hail or wind loads), thus potentially **increasing the reliability** of PV systems. The double glass layer - which does not need the Al frame used in standard G/BS modules - can add more rigidity to the system, as well as high insulation to external stressors. Transparent BS (T-BS) - instead of

glass - could also be used as a rear cover. However, it is still a technology in development, and its reliability has not been thoroughly studied yet.

1.3 Reliability in Photovoltaics

1.3.1 PV module reliability and concepts

In Section 1.1.1 we explained how maximizing a module's long-time performance is essential to minimize risks and reduce the LCOE of a PV system and therefore make it more attractive for investors and stakeholders. PV modules, once installed in the field, are expected to have an optimal performance to meet users' requirements for as many years as possible. They are nevertheless exposed to a variety of environmental stresses such as high humidity and temperature, snow, hail and rain, which may invariably put the long-term stability of the modules (and their components) at risk.

The stability of PV modules is often defined by quantifying the **performance degradation**. Performance degradation can be described as the loss in **maximum power** (P_{max}) with respect to the initial or nominal power (i.e. the nameplate value), as described in Equation 1.3.

$$P_{loss}(t)[\%] = \frac{P_{max}(0) - P_{max}(t)}{P_{max}(0)} \cdot 100 \quad (1.3)$$

where:

$P_{max}(0)$ is the initial maximum power measured before the installation [W];

$P_{max}(t)$ is the maximum power at an operating time t [W].

The module P_{max} provided by manufacturers is measured at standard test conditions (STC), which entail irradiance of 1000 W/m^2 , solar spectrum of AM 1.5G and temperature of 25°C . The procedure to perform electrical characterization of modules is described in detail in Chapter 2.

Conventionally, most PV module manufacturers have offered **warranties of 25 years** ensuring a **nominal maximum power of 80%** (i.e. a maximum power loss (P_{loss}) of 20%). Nowadays, top-tier manufacturers (e.g. Trina Solar) tend to offer a double warranty: a P_{loss} of 2% in the first year of use and a linear degradation rate of a maximum 0.55%/year for the remaining 25 years. Sunpower has even announced warranties of 40 years for their Maxeon products. Such warranty curves are presented in Figure 1.8.

It is very rare, with the exception of extreme catastrophic events, for the module performance to drastically drop to very low values. There is however a certain P_{max} threshold that may indicate whether modules are economically viable anymore. Median annual degradation rates

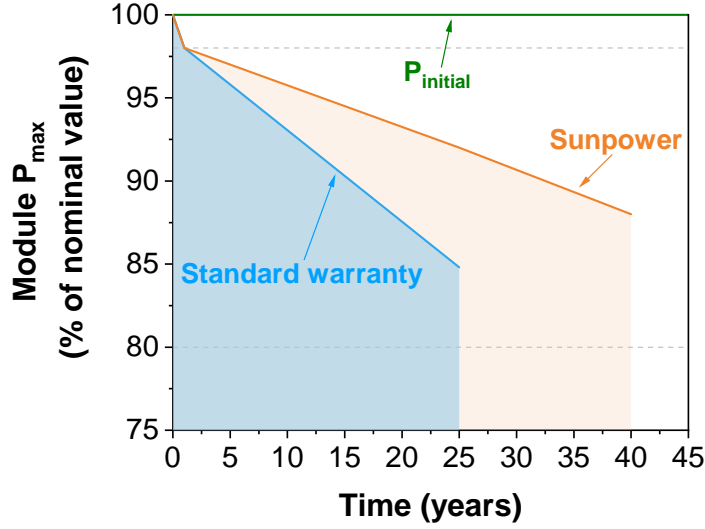


Figure 1.8: Typical power warranties of c-Si modules given by top-tier manufacturers (blue line) and Sunpower (orange line). The module P_{max} is defined as the percentage with respect to the initial maximum power rated by the manufacturer (green line).

of 0.5 %/year have been reported for conventional c-Si modules installed in the field [52]. A large distribution is often found in these types of analysis, where some PV modules exceed the warranties of 80% of nominal P_{max} after 20 or 30 years in operation, whereas others have reportedly shown high degradation rates after a few years in operation.

The terminology employed in the field of PV module reliability can sometimes be confusing. The remaining of this section focuses on clarifying the terms **lifetime**, **failure**, **reliability** and **durability**, and how we will use them in this thesis.

The 25-year span given in PV-module warranties is often described as the module **lifetime**. In reliability, the term lifetime or useful time is however defined as "*the time interval from first use until user requirements are no longer met, due to economics operation and maintenance, or obsolescence*" (from [53]). Therefore, calling lifetime to the duration of 25 year after which the P_{max} is 80% with respect to the nominal power may not be accurate, as long as the PV installation supplies enough energy to meet the users' requirements.

The lifetime of modules is tightly related to the **failure modes** that might occur in the field. A failure can be defined as the "*the loss of ability to perform as required*". In this work, we use the term failure to refer to any occurrence that has a detrimental effect on the module performance and that takes place under normal module operating conditions.

Reliability is a relevant topic of research in many fields. In [53], it is defined as "*the ability [of a system or component] to perform as required, without failure, for a given time interval, under given conditions*". Reliability can also be described by the probability function $R(t)$, which

expresses the probability of a component to function properly by a given time t : $R(t) = 1 - F(t)$, where $F(t)$ is the probability of failure by time t .

Durability is another term often used, diverging from reliability by defining it as the "*ability to perform as required, under given conditions of use and maintenance, until the end of useful life*". Durability can also be considered as the expected value of useful life and can thus be measured in years or cycles. A durability test is usually performed to quantify the duration for a failure-free time frame, whereas a reliability test focuses on replicating failure or degradation mechanisms with the objective of solving them [54].

Thorough and systematic long-term data collection is vital for an accurate assessment of performance degradation. Owing to its complexity, the industry employs the analysis of outdoor data and indoor tests that replicate degradation mechanisms to account for the long-term performance of each module design. In the next sections, we will provide an overview of the most common failure modes reported by studies analyzing PV systems installed in the field. Additionally, we describe the main accelerated ageing tests and the qualification standards employed in the PV industry to assess the reliability/durability of PV modules.

1.3.2 Failure modes

Usually, the failure rate of systems or components is described by a **bathtub curve** [55], [56] (see Figure 1.9). The so-called bathtub curve classifies the failure modes by their occurrence time during the lifetime of the component and their severity regarding safety.

1. **Infant mortality phase.** This occurs at the initial stages of system deployment and showcases the highest failure rates. It is often due to defective components and can cause the end-of-life of the product.
2. **Midlife failure phase.** It refers to random failures that occur during the normal operation of the system.
3. **Wearout phase.** It takes place towards the end-of-life of the system, where the failure rate increases again.

Infant-life failures should be mitigated or prevented by strong quality-control procedures during production. Conversely, midlife and wearout failures are strongly dependent on the usage of the system and on the climatic conditions of the installation site.

The most common failure modes affecting PV modules during the aforementioned three phases are presented in Figure 1.10. In this thesis, we focus mostly on one specific failure mode: **potential-induced degradation (PID)**. Although sometimes it can be considered an infant-life failure, PID mostly falls in the category of midlife failure.

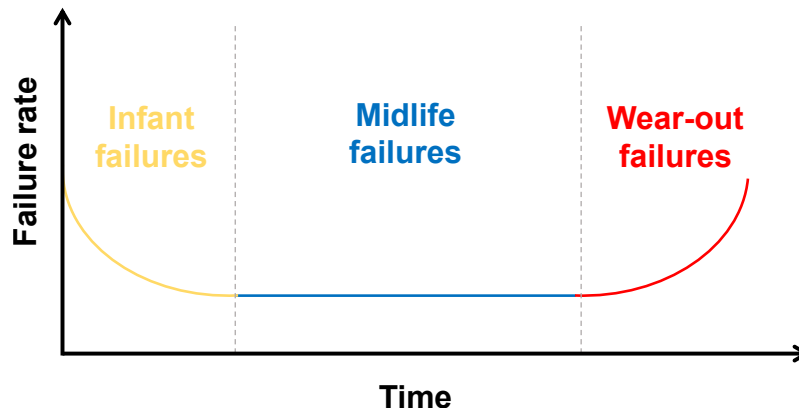


Figure 1.9: The bathtub curve.

1. Infant failures occur at the early stages of a PV module, just after being installed. Infant failures usually may originate from a defective manufacturing and installation process. Light-induced degradation (LID) is one of these degradation modes that take place right after the installation, and is often excluded from reliability analyses.
2. Most failures take place during the active life of the modules (i.e. around 10 years after installation). Midlife failures are often due to a non-optimal choice of module design. In a study performed by DeGraff et al. [57], it was observed that the failures range from degradation due to encapsulant discoloration to interconnection breakage and PID (among others). Other recent works also described crack formation in polyamide backsheets.
3. Wearout failures occur at the end of the working lifetime of PV modules, determining their useful active life. These failure modes accelerate during the last years of the installation; for instance, the corrosion of the cells and the interconnections can be aggravated until the safety of the PV modules is at risk.

Failure modes, midlife and wearout failures in particular, and the consequential performance degradation are processes that are heavily affected by a combination of factors, as described below.

- **Climatic conditions of the installation site.** Various studies reported that the long-term stability of PV modules can be heavily impacted by climatic conditions [59]. In an extensive survey performed by Jordan et al. from the National Renewable Energy Laboratory (NREL), the authors addressed the link between encapsulant discoloration and hot climates [52]. Similarly, common degradation mechanisms such as delamination of the BS from the encapsulant due to moisture are reportedly dominant in tropical regions [60]. Often, degradation modes can be caused by more than one environmental stressor.

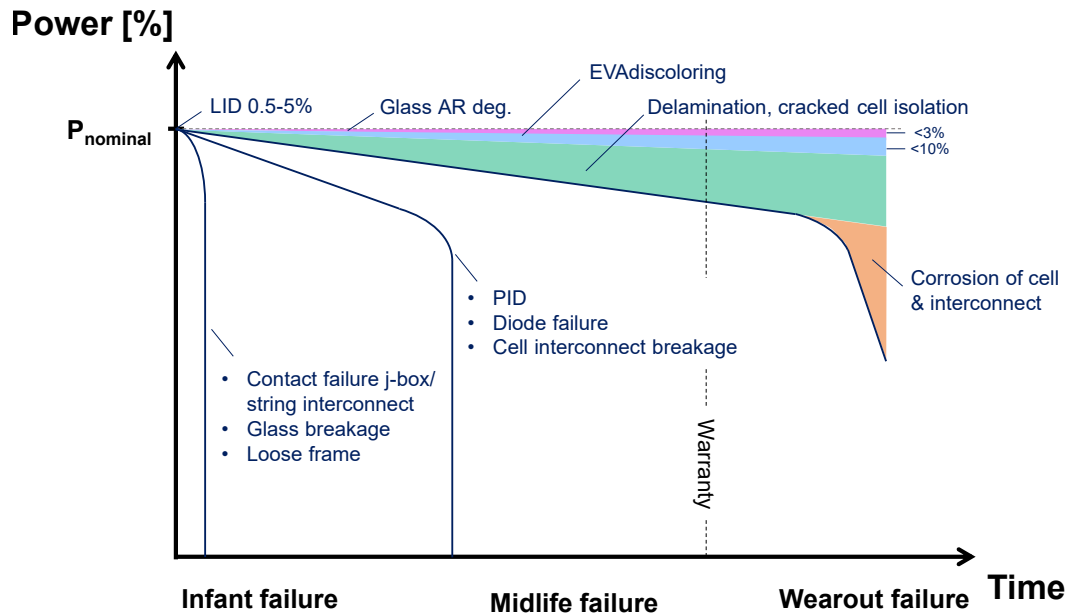


Figure 1.10: Failure scenarios most commonly found in c-Si modules installed in the field. Adapted from source [58].

For instance, PID can be enhanced by a combination of high temperature and high relative humidity [61].

- **Bill of materials (BOM) and module design.** The module materials play a key role in mitigating the risk of a variety of degradation mechanisms: encapsulants with different mechanical and electrical properties can prevent certain types of degradation, a module with an edge seal can prevent degradation caused by water ingress... For instance, as explained in Chapter 5, high-volume resistivity encapsulants can prevent PID from occurring in SHJ modules. It is therefore recommended to design a module based on the climatic conditions of the installation site.
- **Module mounting system.** Mounting structures with a reduced airflow at the rear side (e.g. building integrated compared to open-rack mounted) have higher risks for increased performance degradation due to the higher-temperature operating conditions.
- **Manufacturing process and quality control.** A good quality control process during the manufacturing stage is essential to ensure good module performance over time. Seemingly minor mistakes, such as bad interconnection soldering, may precede a variety of failure modes in the future.

Considering all of this evidence, it is imperative to understand the failure modes that can occur on the field in order to ascertain how they can impact the power output of PV modules.

Common failure modes in the field

Some of the most significant failure modes (and their corresponding severity) were analyzed in the aforementioned field survey performed by Jordan et al. [52]. The authors observed different degradation mechanisms depending on the installation date of the PV modules, as represented in Figure 1.11. Throughout the past years, both cell and module designs have changed and improved. In particular, it has been noted that the module configuration scheme has a significant impact on the reliability of PV modules. Out of all the analyzed modules, it was observed that 48% of them presented **encapsulant discoloration**, followed by **delamination**. The most dominant failures for modules installed in the **last 10 years** were **hot spots** and **internal circuitry degradation**. The latter presented a lower degradation rate than those installed in previous years, but the main failure mode itself was more severe.

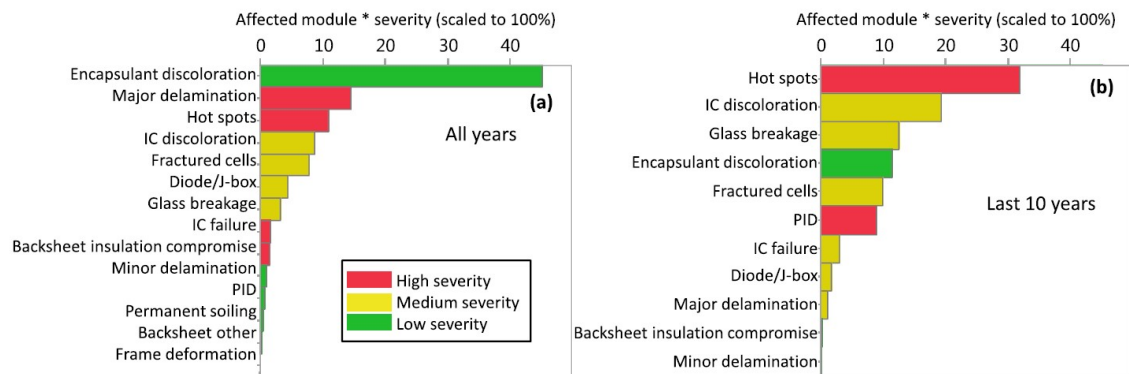


Figure 1.11: Classification of several degradation mechanisms of affected modules (in percentage, %) of c-Si cells installed during (a) all years and (b) the last 10 years of analysis. The severity of each degradation mechanism is classified as high (red), medium (yellow) and low (green). Adapted from source [52].

Nowadays however manufacturers target 35 to 40 years of PV module lifetimes, yet a very limited amount of PV systems have been monitored for such durations. Most reliability studies have been performed in younger installations for shorter periods of time [62], [63]. Conversely, the TISO-10-kW solar plant has been monitored for the last 40 years [64], [65]. The plant is located in Lugano (Switzerland), and it was the first grid-connected PV plant in Europe. The modules were measured in regular intervals over the years. Researchers observed that the degradation rate increased during the last 7 years of use compared to previous years. It was also discovered that this was not homogeneous through all the modules, but they degraded in two different rates, thus two groups of modules were considered (Group 1 and Group 2).

Modules from Group 1, 21.5% of all, presented a moderate degradation with a yearly power degradation of $-0.2\%/y$. The rest of the modules, 72.9% of them, pertaining to Group 2, had a higher mean power degradation of $-0.69\%/y$. Nonetheless, 70% of the modules had a performance higher than 80% of their initial one after 35 years in a temperate climate [64]. Therefore, the modules would satisfy the warranty given by manufacturers. The long-

term degradation rates could be correlated to the quality of the encapsulant, highlighting the significance of the BOM. The results indicate that changes of individual components in the system and module configuration can have an effect on the degradation rates and their durability.

Collectively, these studies lead to the classification of PV module field degradation into five categories [66].

- **Degradation of module materials**, for instance, encapsulant discoloration, glass breakage and BS cracking.
- **Delamination** or loss in adhesion strength. Field data has highlighted the propensity for front-side delamination (i.e. between glass and front encapsulant), causing absorption losses due to optical decoupling and degradation due to ineffective heat dissipation. Since module reliability is inevitably linked to a good adhesion of all packaging materials, its loss can put the module's performance at risk.
- **Degradation of cell and module interconnections**. Thermomechanical stresses can cause the interconnections (including the junction box) of a module to degrade, increasing losses in a system due to poor current extraction.
- **Water ingress** can reduce the performance of a module by, for instance, corroding the metallic parts, increasing the leakage current and enhancing delamination.
- **Degradation of the semiconductor devices** are particular to each solar cell technology, such as LID in conventional c-Si solar cells.

Until today, the majority of field studies involved conventional c-Si (Al-BSF) solar cells, and thin films to a lesser extent. However, new challenges can arise from the installation of new high-efficiency technologies in the field. In Chapter 3, we perform a study of the performance loss rates and degradation modes of SHJ PV modules installed in the field to address the question of their long-term stability.

1.3.3 Qualification Tests

In the previous section, we mentioned the need to collect field data for long time series (ideally longer than 10 years) in order to accurately assess the degradation rates and failure modes of PV modules. It is however evident that procedures with a shorter time frame are needed to develop reliable products in a feasible time interval - without having to wait for 30 years for outdoor monitoring data. The PV industry has therefore developed a series of indoor tests called **accelerated ageing tests**. The tests aim to reproduce, in an accelerated manner, the failure modes observed in the field by subjecting the PV modules to a combination of stresses (e.g. high temperature and humidity, high voltages and temperature variations). The main

objectives of the indoor accelerated tests are thus to identify the relationship between different failure modes and the stress factors causing them.

Similarly to other industries, specific test series (**Qualification Tests**) have been developed and approved by the **International Electrotechnical Commission (IEC)**. The tests provide requirements for minimum product quality and are globally adopted by PV module manufacturers. The series of tests developed for c-Si PV modules are defined on the International Standard **IEC 61215: Terrestrial photovoltaic (PV) modules - design qualification and type approval** [67]. The *pass/fail* criteria per test are determined by established requirements on output power, visual appearance and safety.

The work carried out in this thesis focuses mainly on two of the tests described in IEC 61215.

- **Damp heat (DH) test.** Modules are exposed to a temperature (T) of 85°C and 85% of relative humidity (RH) for 1000 hours. The main goal of the DH test is to examine whether modules can withstand penetration of moisture for long time periods. Modules are considered to pass when they display a power loss lower than 5% with respect to the initial P_{max} .
- **PID test.** The test suggests the exposure of modules to high voltages (typically -1000 V) between the cell's circuit and the grounded frame at DH-like conditions (i.e. 85°C, 85% RH) for 96 hours. This test is performed with the objective of analyzing the propensity of particular module designs to PID. Modules are considered to pass the PID test when they display a P_{max} of 95% with respect to their $P_{initial}$. The development and methodology of the PID testing procedure is explained in detail in Chapter 2.

The main tests from the IEC 61215 standard and their most common failure modes are described in Table 1.2.

Qualification tests can be effective procedures to identify potential material failures and assess the quality of PV modules. Although sometimes mistakenly considered predictive lifetime tests, the goal of the tests is to determine the capability of the modules to withstand prolonged exposure in general outdoor conditions. However, the actual service lifetime expectancy will be defined by the module design, the environment and the operating conditions. The main limitations of such tests are the following.

- **They are not climate specific.** Modules might pass the unique IEC 61215 test sequence but, ultimately, their long-term behaviour will depend on the climatic conditions of the installation site (i.e. temperature and humidity, UV dose, soiling...).
- **The correlation between the test parameters (e.g. duration and stress levels) and real stress conditions is not clear.** That is, the tests cannot predict the module lifetime.

Chapter 1. Introduction

Table 1.2: Summary of the main accelerated ageing tests defined in IEC 61215 and their prominent failure modes. Adapted from [67].

Accelerated stress test	Failure mode
Damp heat (DH)	Delamination Encapsulant discoloration Corrosion Junction box adhesion
PID test	Solar cell degradation Delamination
Thermal cycling (TC)	Delamination Interconnection breakage Solder bond failure Junction box failure
Humidity freeze (HF)	Delamination Interconnection breakage Solder bond failure
Mechanical load	Glass breakage Interconnection breakage Cell breakage Solder bond failure
Hail test	Glass breakage Cell breakage
UV exposure	Delamination Encapsulant discoloration Backsheet discoloration

- The increase or prolongation of one (or more) accelerating factors can cause the **occurrence of unrealistic failure modes**. For example, too high temperatures can lead to degradation modes that are not realistic in normal operating conditions on the field.
- The tests are **one size fits all** for all cell and module technologies. For instance, DH tests after just some hundreds of hours can degrade PET backsheets enough for 25 years in a humid environment [68], [69], but cells encapsulated in a module encapsulation with an edge seal may require 2000 to 3000 hours to exhibit degradation.

Lately, new testing sequences and protocols have been developed to tackle the limitations mentioned above. DuPont has implemented a module-accelerated stress test (MAST) to replicate backsheet failure modes previously observed in the field [70]. More recently, researchers at NREL proposed the combined accelerated stress test (C-AST) to simulate stresses found in realistic environmental conditions by applying combined and/or sequential stress procedures [71], [72]. These procedures are valuable to the reliability/durability research field to improve the prediction of PV module lifetimes. They are however more difficult to be applied in commercial climatic chambers owned by most institutes, and there is still a long way before their

validation and adoption.

This thesis focuses on one degradation mechanism that was recently standardized in the IEC 61215 as a qualification test: **PID**. PID testing combines the application of high voltages and high temperature and humidity conditions (explained in detail in Chapter 2). The next section describes in detail the intricacies of studying and understanding PID on different cell technologies and module designs and highlights the relevance of this subject in the PV field.

1.4 Potential-Induced Degradation (PID)

The first accounts for voltage- and current-induced degradation on c-Si and a-Si solar cells were reported by the Jet Propulsion Laboratory (JPL) in the 1980s [73]. In the early 2000s, the effect of leakage currents under high-voltage stresses in PV modules was further researched by NREL [74]–[76]. Swanson et al. reported a certain type of degradation on Sunpower n-type c-Si solar cells when these were subjected to very high voltages, termed *surface polarization* [77]. It was not until 2010 that some works from Pingel and Hacke introduced the term PID and started investigating the degradation mechanism in **p-type c-Si solar cells** [78], [79]. Although the dissolution of the ARC and the corrosion of the fingers may occur [80], the main mechanism often found in conventional p-type c-Si solar cells (i.e. Al-BSF) is of the *shunting* type, also denoted as PID-s [79].

PID occurs when there is a high potential difference between the solar cells and the grounded frame, generating a leakage current through the module. The effect generally varies linearly with applied voltage and was first observed on PV systems, where modules are connected in series, with system voltages of a maximum of 1000 V [78]. Today the system voltage of larger PV systems is increasing to 1500 V with targets of extending these limits further, as a means of cost control [81], [82].

Research on PID has gained significant attention in the last decade due to its severe detrimental effects on module performance, hence putting a PV plant's long-term reliability at risk. It is a tricky mechanism to detect due to its lack of visual evidence and the complexity of its occurrence. Some of the first accounts of PID in field installations reported P_{max} losses of up to 27% in Spain after only 4 months [83], while a performance loss of 60% was noted in a PV plant in southern Italy after 1 year [84]. Annigoni reported on P_{max} losses of up to 66% and 85% of modules installed in PV plants operating for less than 3 years in central Italy and Greece, respectively [85].

As it was mentioned above, PID is an intricate degradation mechanism and it can heavily depend on several factors (a detailed description is given in [86]):

- **Climatic conditions** in which PV modules operate can strongly affect the occurrence (and level of severity) of PID. High temperatures have been shown to accelerate degradation by, for instance, reducing the resistivity of the encapsulating material [61]. Humidity

(e.g. rain and morning dew) is also a known factor that can exacerbate the occurrence of PID by creating an equipotential between the surface of the glass and the module frame [84]. Soiling can also increase PID effects by increasing the conductivity of the glass covers.

- **Grounding and polarity of the PV array.** The electrical layout of PV modules in a string or array can have a determining impact on PID. The modules are usually connected in series to achieve high voltages of 1000 V, with the current trend being to increase the maximum system voltage to 1500 V [81], [82]. The high cell-to-frame voltage differences can cause increased leakage currents within the module materials (i.e. encapsulant), affecting the module performance over time. Moreover, the grounding scheme (i.e. positive or negative pole grounding or no grounding) determines how the voltage polarity is distributed, thus causing more damage to modules located at certain positions in a string than to others [78].
- **Inverter choice.** Transformer-based inverters could prevent PID by grounding the negative or positive pole (depending on the solar cell technology employed). The industry is however moving towards transformer-less inverters, leaving a floating potential where modules in a string are biased with both polarities.
- **Module design, with respect to the mounting solution.** The presence or lack of an Al frame can determine the occurrence (or lack thereof) of PID. Cells closest to the frame (at the perimeter of the module) are usually the ones that suffer the highest degradation rates. Modules with a conventional four-edge frame have been shown to degrade faster than newer designs with clamps at only two points [87].
- **Module configuration, related to the choice of encapsulants, glass and backsheets.** Several works have highlighted the importance of the right choice of BOM in order to prevent degradation from occurring. A more detailed description is given in Section 1.4.2.
- **Solar cell technology.** Depending on the solar cell technology, the factors causing PID and, consequently, the underlying physical mechanism change (see Section 1.4.1). It is therefore critical to understand the degradation mechanism for each technology in order to prevent it with the appropriate module and system designs.

This thesis mostly focuses on investigating PID in SHJ solar cells and modules (but other high-efficiency c-Si technologies are considered at the end of the work), in combination with exposure to high temperature and humidity conditions. In the next subsections, we will give a detailed overview of the physical degradation mechanism found in historically relevant and mainstream c-Si technologies and the role the BOM can play in mitigating or accelerating PID.

1.4.1 Physical degradation mechanism

At the beginning of this section, we mentioned that PID at the early stages was identified for n-type c-Si solar cells from Sunpower, conventional p-type c-Si (i.e. Al-BSF) and thin-film solar cells [73], [77], [78]. Because the mainstream PV technology was Al-BSF until some years ago, most research efforts were focused on understanding the degradation mechanism of this type of solar cell. The study of PID in high-efficiency c-Si cells is however in the early stages. The particularity of this mechanism makes it very difficult to estimate the degradation for all technologies. Case-by-case studies are thus needed to evaluate its impact on PV modules based on novel solar cell technologies.

Due to the current mainstream technology being PERC, followed by SHJ and TOPCon (all based on c-Si), we will make an initial introduction to the degradation mechanisms found in Al-BSF and Sunpower solar cells (i.e. p-type and n-type c-Si technologies, respectively). We then provide an overview of the research performed on the other PV solar cells described in Section 1.2.1 so far.

Al-BSF solar cells

PID in Al-BSF solar cells occurs when these operate at a **high negative potential** with respect to the ground (see e.g. [78], [79], [83], [84]). The high voltages can induce the migration of ions between the cells and the other materials of the module, thus leading to leakage currents (see Figure 1.12).

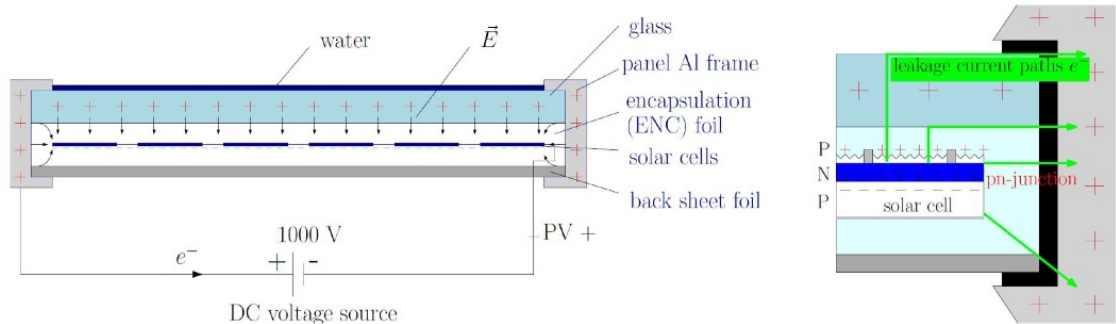


Figure 1.12: Representative illustration of PID mechanism at the module level. Image is taken from [78].

The most accepted explanation is that sodium ions (Na^+) play a critical role in the physical mechanism behind PID [79], [88], [89]. Naumann et al. at Fraunhofer CSP performed a thorough study on this topic and, in 2012, they reported the underlying physical mechanism of PID in p-type c-Si solar cells [90]. The authors demonstrated that the Na^+ ions migrate towards the cell and, later on, the c-Si bulk, where they can create shunts [91], [92].

It is considered to be a two-stage process. First, the voltage difference between the cell and the

frame creates an electrical field across the SiN_x ARC on the surface of the cell. This electrical field is the driving force for PID. Indeed, it creates the drift of Na^+ ions towards the interface with the bulk Si, where it accumulates in the SiO_x layer, as shown in Figure 1.13 [86], [90]. Second, they might diffuse into the bulk Si through the stacking faults (defects in the crystal). If the stacking faults intersect the p-n junction, and there is a sufficient concentration of Na^+ , shunts are created and the cell efficiency is therefore reduced. PID on p-type c-Si cells is sometimes referred to as PID of the shunting type, *PID-s*.

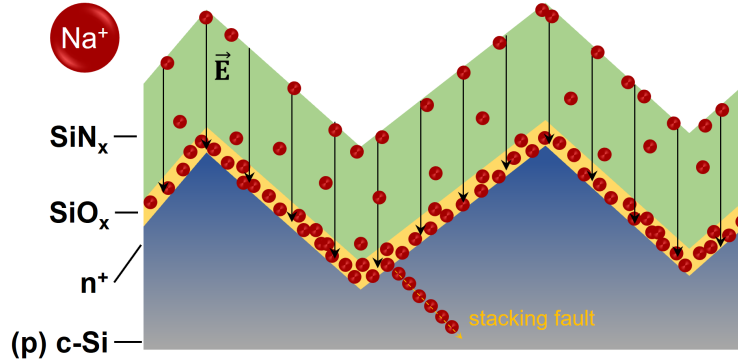


Figure 1.13: Schematic illustration of the PID root mechanism in p-type c-Si cells. Na^+ ions are drifted by the electric field from the external surface of the ARC and accumulate at the interface between the ARC and the bulk Si. From there, they might diffuse following favoured paths, mainly stacking faults. The SiO_x was later added to Al-BSF cells because it was empirically found to partially mitigate PID-s.

PID-s was proven to be a (partly) reversible mechanism: the cell performance can recover when a reverse bias is applied. The direction of the electric field through the SiN_x is thus the opposite, and Na^+ ions drift from the bulk Si and onto the surface of the cell. This phenomenon reduces the ion concentration at the SiO_x interface, hence accelerating this out-diffusion due to a change in gradient concentration of the Na^+ ions between the interface and the bulk [93].

n-type c-Si solar cells

The first reports of PID on n-type c-Si technology were published on Sunpower back-contact solar cells by Swanson et al. [77]. Unlike conventional p-type c-Si cells, this technology exhibits PID when subjected to high positive biases with respect to the ground. The authors found that negative charge, coming from the leakage current, accumulated at the SiN_x layer, can recombine with the light-generated holes and increase front-surface recombination. This phenomenon was denoted as *surface polarization effect* or PID-p. The authors also reported this effect to be reversible.

In 2014, Naumann et al. investigated PID under negative and positive biases in IBC solar cells [94]. They also reported the sensitivity of these cells to high positive biases and a similar degradation mechanism to that described by Swanson et al. was reported.

Hara et al. tested the effect of PID on front- and rear-emitter n-type c-Si solar cells under negative and positive voltage polarities [95]. In both cases, the solar cells exhibited enhanced front-surface recombination between the charge carriers. The authors explained however that the polarity causing degradation depends strongly on the cell structure. Indeed, rear-emitter cells showed degradation when subjected to high positive biases (with respect to ground) whereas front-junction cells degrade under high negative voltages. Further studies on rear-emitter n-type cells however revealed that these are heavily degraded when biased negatively (i.e. -1000 V) [96]. The mechanism is characterized by a large drop in V_{OC} , followed by decreases in J_{SC} and FF, and an increase in j_{01} . The authors attributed it to the accumulation of Na in the surface region, causing increased surface recombination of minority carriers. Conversely, the cells experience a much more moderate degradation rate when positively biased with respect to the frame. Hara and co-authors hypothesized that the degradation behaviour could be caused by the polarization effect similar to IBC cells but to a lower extent.

PERC solar cells

Considering the structure of PERC cells is similar to that of Al-BSF technology (see Figure 1.2), it is reasonable to expect the former to experience PID as well. Several studies were published in recent years confirming the occurrence of PID in PERC solar cells (and its variations). However, there is no consensus regarding the mechanism itself. In this subsection, we strictly focus on the standard PERC cell configuration, which is the workhorse of the PV industry.

In 2017, Luo et al. reported PID in bifacial PERC solar cells, both at the front and rear sides [97]. The test was performed on G/G modules and applying an Al foil to the rear surface, creating a high bias of -1000 V with respect to it. The modules were tested at 50°C and 30% RH. The results focused on the PID mechanism at the rear side of the cell. They observed a large degradation in J_{SC} and V_{OC} after 40 hours of testing, and they attributed it to a surface polarization effect. They suggested that positive charges accumulate in the passivation stack in the rear side of the cell, generating a carrier recombination site, similar to what was reported in conventional n-type c-Si cells [86]. Carolus et al. supported this supposition and added that the degradation at the front differs in its mechanism [98]. They proposed that PID at the front side is of the shunting type, the same as in conventional Al-BSF solar cells.

Studies from Sporleder et al. propose that if the stress levels are increased, the rear side of the silicon wafer oxidizes and a SiO_2 layer is formed as a consequence, causing local passivation failure [99], [100].

More recently, Sulas-Kern and co-authors published a thorough investigation on bifacial PERC solar cells encapsulated in G/G and G/T-BS module structures and compared the impact of employing EVA or POE encapsulants [101]. The PID testing was performed at standard DH-like conditions for 96 hours, with an extended duration of 1000 hours. The authors investigated both the effect of negative and positive polarities (i.e. -1 kV and +1 kV, respectively). The results demonstrated that using POE as an encapsulant material is a good method to manufacture

PERC modules resistant to PID (under both polarities), while mini-modules with EVA exhibited performance losses both in G/G and G/T-BE configurations when subjected to -1 kV. The mechanism in G/G laminates was consistent with the previous reports in the literature, and the authors assumed PID-s and PID-p to be the main degradation mechanisms at the front and rear sides, respectively. They also observed some corrosion at the edges of the mini-modules. G/T-BE modules however exhibited lower degradation rates, due to the lack of a rear-cover glass that would act as an additional Na reservoir. Moreover, for the first time, the authors showed that PERC solar cells can be sensitive to high positive voltages, mainly at the rear side. Although the mechanism is not clear yet, decreased rear-surface passivation was observed in G/G structures.

Our contribution to this topic is developed in Chapter 7.

SHJ solar cells

As shown in Figure 1.2, SHJ solar cells have a conductive layer (i.e. TCO) at the top and bottom that enables the collection of charge carriers. It was initially supposed that the TCO could avoid any charge accumulation typical to the PID behaviour experienced by the aforementioned technologies and, thus, prevent any leakage current. In fact, some initial studies performed on Sanyo/Panasonic modules exhibited a lack of sensitivity to PID [102]. The cells were most probably encapsulated with high-volume resistivity encapsulants, thus rendering the modules PID-free, but not the SHJ cells necessarily. Nevertheless, due to the apparent lack of degradation and Sanyo/Panasonic's patent on SHJ solar cells, the topic was not researched to its full potential.

However, more recently, Yamaguchi et al. investigated PID in commercial bifacial SHJ solar cells and reported their propensity to degradation when subjected to high negative voltages [103], [104]. The experimental work was performed on module configurations with EVA as the encapsulating material. The reported degradation mechanism and behaviour are described in detail in Chapter 3 and our research work on this topic is developed in Chapter 5.

1.4.2 Role of the module materials

As discussed in Section 1.4, the materials chosen to manufacture the modules can play a critical role in the propensity to suffer from PID (or lack thereof) and the degradation mechanism.

The solar cell technology employed and the quality of the materials in the manufacturing process can be determining factors. In conventional Al-BSF solar cells, the leakage current through the SiN_x ARC can determine the degree of degradation that can occur. In fact, the impact of the layer composition has been well studied and results have shown that materials with higher refractive indexes can increase stability to PID [80]. Higher refractive indexes are more conductive, which can lead to the precipitation of Na^+ ions at the SiN_x layer and reduce the electromotive force for their diffusion into the c-Si. Although it should be studied on a

case-by-case basis, choosing cells resistant to PID (or *PID-free*) could be potentially an option to prevent its occurrence.

The diffusion of Na^+ (and potentially other ions) through the encapsulant to the solar cells is the main mechanism - and arguably the most relevant - observed for PID in the field. Efforts to identify the origin of Na have been made in the past. It was initially presumed that Na originated exclusively from the solar-grade soda-lime glass used in PV (see Table 1.1). Some studies showed however that PID can occur on bare cells without the presence of glass [105]. Indeed, the presence of Na on the surface of the solar cell as a consequence of contamination during the manufacturing process can be enough to cause PID. Nevertheless, the front (and rear) glass cover can act as an additional Na reservoir and exacerbate the occurrence of PID. The employment of glass-free or Na-free materials can thus be a potential solution to minimize this problem.

Polymeric encapsulants also have a fundamental impact on PID. The use of high-volume resistivity encapsulants to minimize the leakage current and, thus, the electric field through the module, has shown to prevent PID in a variety of cell structures and module configurations [61], [106], [107]. This topic will be further addressed in Chapter 5, where we study the effect of various encapsulants on the sensitivity of SHJ cells and modules to PID.

PID has exhibited to somehow be dependent on the humidity or water/moisture ingress. High contents of water ingress in the module can also reduce the resistivity of the materials and, by enhancing the leakage current, cause higher diffusion of ions and, thus, degradation [61]. Therefore, manufacturing modules with low permeability properties against moisture ingress (e.g. G/G with an edge seal or an aluminium foil in the BS) can reduce and, in some cases prevent, PID from occurring.

Although measures to prevent PID might be well-known within the industry and module manufacturers, the final choice of materials is often reduced to a trade-off between their performance and cost. Consequently, and particularly in recent years, the aim to reduce costs can result in PV modules that are more sensitive or prone to certain degradation mechanisms.

1.5 Structure of this thesis

Chapter 2 describes the module preparation procedure as well as the electrical and material characterization techniques employed throughout the thesis to assess the degradation mechanism of our samples.

Chapter 3 provides a thorough meta-analysis of the long-term performance and reliability of SHJ technology. This has been done by collecting published literature inputs. We highlight the main failure modes found in the field, assess the sensitivities from both outdoor and indoor testing data and present suggestions on how to ensure the long-term stability of the technology.

Chapter 4 explains the degradation mechanism of SHJ encapsulated in a G/G module configuration with EVA when subjected to DH testing. We develop a model (particular to the technology), that describes the root cause for degradation when SHJ cells, encapsulated with EVA, are exposed to high moisture content.

Chapter 5 assesses the behaviour of SHJ technology to PID under high voltage bias and polarities in DH-like testing conditions. We investigate the contributions of the front and rear sides of bifacial SHJ solar cells to degradation when encapsulated in a G/G module structure with EVA, and provide an explanation for the underlying physical degradation mechanism. We propose a microscopic model that explains the degradation mechanism of these cells. We finally demonstrate how to manufacture more robust SHJ modules by reinforcing the packaging schemes.

Chapter 6 investigates how to make SHJ cells more resistant to DH-induced degradation and PID. The role of the TCO properties in the degradation mechanisms and the influence of different capping layers on the improvement of PID resistance are studied.

Chapter 7 studies different high-efficiency c-Si technologies' (i.e. PERC and TOPCon) behaviour to PID compared to SHJ, and the influence of moisture in the degradation mechanism.

Chapter 8 summarizes the main results obtained in this work and provides an outlook for future activities.

1.6 Contribution to the field

The work presented in this thesis led to the following contributions to the field of PV module reliability and long-term performance.

1. We perform, for the first time in the field, a meta-analysis of the long-term performance of SHJ technology. Besides performing a literature review of the reported degradation rates of this particular technology, we identify the main failure modes observed from outdoor and indoor monitoring. The understanding of the degradation modes of SHJ will provide the knowledge to resolve them at the R&D and manufacturing stages. We present strategies to ensure their performance for 35+ years in the field.
2. We are the first to develop a model explaining the sensitivity of SHJ cells/modules to DH testing and water ingress. We highlight that this sensitivity is not only dependent on moisture ingress but on a reaction of the Na contained in the glass of the module covers with water. This degradation mechanism is particular to SHJ cells and is not observed for other cell technologies.
3. For the first time, we report the PID mechanism in SHJ solar cells under the influence of different bias polarities in combination with high humidity conditions. We also develop a microscopic model describing PID for SHJ technology, which is a multi-factorial

mechanism that is caused by the combination of the glass corrosion due to moisture ingress and the drift of Na^+ ions towards the solar cell as a consequence of the high negative bias. Strategies to overcome the degradation caused by DH and PID exposure are described in detail.

4. We aimed at understanding how to directly manufacture SHJ cells more resistant to PID. In previous chapters, we developed strategies to mitigate PID at the module level. Here however we study the significance of the ARC and capping layers in the degradation mechanism and develop strategies to prevent PID at the cell level.
5. We compare the behaviour of other prominent high-efficiency technologies (i.e. PERC and TOPCon) with SHJ cells/modules under high moisture and voltage conditions when these are encapsulated with EVA. We are among the first to report PID and DH studies on TOPCon solar cells, and to investigate the impact of water ingress in the PID mechanism of the three technologies.

At the time of writing, one paper was published in *Progress in Photovoltaics: Research and Applications*, one publication was submitted to *Cell Reports* and another paper was submitted to *Progress in Photovoltaics: Research and Applications* (see [108], [109], [110], respectively). The outcomes of the research presented in this thesis that led to contributions to conferences and workshops are listed at the end of this manuscript.

2 Experimental Methods

2.1 Manufacturing of PV modules

2.1.1 Module design and material choice

The research work of this thesis was performed by manufacturing and testing several types of mini-modules and samples, as depicted in Figure 2.1.

- Industrial-size solar cells were packaged in $20 \times 20 \text{ cm}^2$ 1-cell mini-modules with a front-cover glass/encapsulant/cell/encapsulant/rear cover configuration. Several types of rear-cover materials, which will be defined later on in this section, with varying properties were employed.
- Lab-scale cells were encapsulated in $6 \times 6 \text{ cm}^2$ 1-cell mini-modules with front-cover glass/encapsulant/cell/encapsulant/rear-cover polymeric sheet schemes.

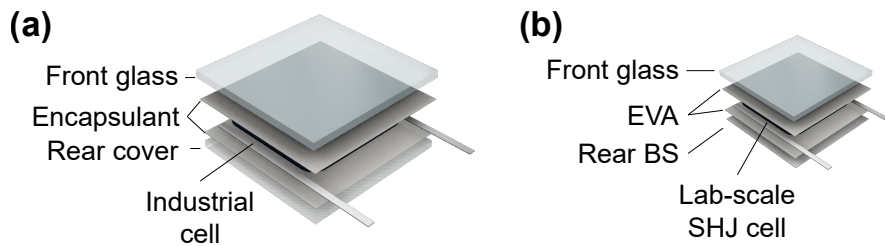


Figure 2.1: Schematics of the module and sample schemes manufactured in this thesis: (a) $20 \times 20 \text{ cm}^2$ 1-cell mini-module with industrial-size cells, (b) $6 \times 6 \text{ cm}^2$ 1-cell G/BS mini-module with lab-scale cell.

In the following sections, we define the exact materials used for each layer of the module stack.

Cover glass

The front (and sometimes rear) cover glass used in this thesis is a commercially-available glass from the German provider Petraglas. The specifications of the glass are the following.

- Dimensions of 600 mm x 600 mm x 3.2 mm.
- Solar-float extra-clear soda-lime glass.
- Non-tempered, raw glass.

The lack of tempering enabled us to cut the glass into pieces with the desired dimensions with a glass diamond cutter.

Edge sealant

With the aim of understanding the effect of moisture on the degradation mechanism of different solar cell technologies, G/G modules highly resistant to water ingress were manufactured. To do so, strips of edge sealant (ES) were placed along the edges of one of the glass plates and on top of the cell interconnecting ribbons. The ES employed in this work was a 1.2 mm x 8 mm PVPS 101 desiccated solar edge sealant from HelioSeal.

Encapsulant

Most of the experimental work in this thesis has been carried out using EVA as the encapsulating material unless differently indicated. The EVA used was a commercially available EVA 406S from Chinese manufacturer Hangzhou First. The main specifications of this EVA are the following:

- a thickness of 550 μm ;
- UV transparent, it does not have a UV absorber added;
- a relatively low-volume resistivity of $< 10^{16} \Omega\text{cm}$ (for the cured sheet) to facilitate the occurrence of PID;
- transmittance of $> 80\%$ and $> 91\%$ for the wavelength ranges of 290 nm to 380 nm and 380 nm to 1100 nm, respectively.

Solar cells and interconnections

In most chapters (Chapters 4, 5 and 7), industrial-size bifacial high-efficiency technologies were employed.

- Bifacial M2 rear-emitter SHJ solar cells with 4 and 5 busbars, manufactured by CEA INES.
- Bifacial M6 p-type PERC solar cells with 9 busbars, from Trina Solar.
- Bifacial M3 front-emitter n-type TOPCon solar cells with 9 busbars, from DAS Solar.

The work in Chapter 6 was performed on $2 \times 2 \text{ cm}^2$ monofacial front-emitter SHJ solar cells, manufactured at PV-Lab. We gratefully acknowledge the contribution of Luca Antognini, Vincent Paratte, Deniz Türkay, Joël Spitznagel and Sylvain Dunand to the manufacturing of these cells.

The soldering processes for the cell interconnects were adapted to each technology:

- PERC and TOPCon solar cells were soldered manually at 360°C to 370°C with $1.5 \text{ mm} \times 0.2 \text{ mm}$ copper (Cu) ribbons coated with SnAg.
- The soldering process for SHJ technology needs to be adapted. In order to avoid damaging the passivating layers (i.e. a-Si:H), an electrically conductive adhesive (ECA) was employed to "paste" the ribbons to the busbars.
 - The industrial-size SHJ cells from CEA were provided with the cell interconnections already done. The ECA used for these cells was a formulation developed at CEA INES.
 - The lab-scale SHJ cells were soldered by using a commercially available ECA from Henkel, Ablestik 3556HF, with a fast-curing process (i.e. 2 min at 100°C).

The string interconnections, equal to all technologies, were manually soldered at 370°C using SnAg-coated Cu ribbons. The thickness of the ribbons depended on the module schemes: 0.2 mm- and 0.4 mm-thick ribbons for G/G and G/BS laminates, respectively.

Polymeric backsheets

Although most of the experimental work was performed on G/G - and G/G-ES - modules, other module configurations with different rear covers were manufactured and tested. In particular, three types of commercially available polymeric backsheets were employed:

- a permeable conventional polymeric backsheet was used in Chapters 5, 6 and 7 to investigate the impact of moisture ingress into the laminates;
- a polymeric backsheet with an Al foil was employed in Chapter 5, to prevent moisture ingress from the rear side;
- a transparent polymeric backsheet (i.e. NovaFlex XBF) with a very low water vapor transmission rate of $10^{-3} \text{ g/m}^2/\text{d}$ from BASF was also used in Chapter 5 to investigate the possibility of developing modules resistant to PID.

2.1.2 Lamination procedure

The lamination or encapsulation process is that which melts the polymeric encapsulants and activates the curing agents to enhance the adhesion of the module components. A good lamination procedure is key to ensuring the manufacturing of high-quality and long-performing PV modules. This process is performed in what is called a flat-bed vacuum-bag laminator, with two chambers (i.e. upper and lower chambers) separated by a membrane. The lower chamber consists of a heating plate and pins that can slide up/down to adapt the heating rate to the modules. During the encapsulation procedure, the temperature, pressure and time are controlled to match the conditions required for the particular polymeric encapsulant to be well cross-linked.

Once the module components are stacked face down on a metallic plate, silicone strips are placed around it to prevent mechanical stresses at the edges of the module, as shown in Figure 2.2. The height of the silicone frame usually matches the total thickness of the "sandwich" stack.

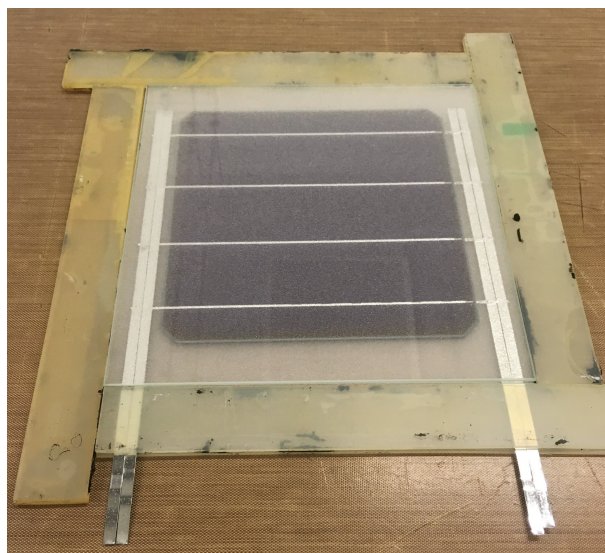


Figure 2.2: Representative image of a "sandwich" module stack before lamination.

The lamination procedure usually takes around 20 minutes, with temperatures in the range of 145°C to 160°C, depending on the encapsulant. The process can be divided into the following three steps.

1. **Degassing and pre-heating step.** The metallic plate with the module stack is placed in the laminator with the pins up to avoid thermal shocks. A short degassing step takes place in which the air within the module components is evacuated to avoid bubbles, while the module temperature increases to ~60°C and softens the encapsulant. Then, the pins are retracted so the stack is directly placed on top of the heating plate and pressure is applied through the membrane into the module.

2. **Curing step.** The module starts heating up to reach the set temperature (around 150°C), and the polymeric chains of the encapsulants cross-link. This process ensures the thermal and mechanical stability of the encapsulant, as well as makes it transparent for optimal light absorption. In order to manufacture reliable modules, a gel content of > 80 % is advised. This step usually takes between 300 and 900 seconds.
3. **Cooling step.** The plate is moved to another chamber - or to a table - set at a certain cooling temperature. At the same time, a pressure of 1 atm is applied to the plate to prevent bending and hence, delamination at the edges.

2.2 Characterization of PV modules

2.2.1 Current-Voltage (I-V) measurements

I-V characteristics of solar cells

The operation of a solar cell can be described as one of a diode: when the voltage across it is negative, then the current is not allowed to flow, and the resistance is very low to it with positive voltages. In fact, a solar cell in the dark behaves like a diode, and the current density [mA/cm²] is defined by the following equation:

$$J = J_0 \left[\exp\left(\frac{qV}{nkT}\right) - 1 \right] \quad (2.1)$$

where J_0 is the recombination current density [mA/cm²], q is the elementary charge ($q = 1.602 \times 10^{-19}$ C), V is the voltage through the diode, n is the ideality factor, k is the Boltzmann constant ($k = 1.38 \times 10^{-23}$ J/K), and T is the temperature of the cell [K].

When illuminated, the current flowing through the solar cell is the superposition of the curve of the solar cell in the dark (J_D) and the photo-generated current density (J_L).

$$J = J_L - J_D \quad (2.2)$$

Equation 2.2 describes the behaviour of an ideal solar cell. In practice, however, photo-generated carriers might follow alternate paths within the cell due to recombination processes (e.g. cracks, shunting at edges and particles) during manufacturing steps. This behaviour can be represented as a resistance in parallel to the diode: shunt resistance, R_{sh} . Ideally, we look for the highest shunt resistances, in the order of 10^3 - $10^6 \Omega \text{ cm}^2$. Moreover, we can also find resistance in series (R_s) with the other components in the circuit as a consequence of, for instance, contact resistances between the c-Si and the busbars and resistances of the metal contacts. Therefore, the voltage measured between the cell's terminals is reduced. The ideal R_s should be in the range of 0.1-3 $\Omega \text{ cm}^2$. The equation describing the equivalent circuit of the

solar cell is then adapted as follows.

$$J = J_L - J_{01} \left[\exp \left(\frac{q(V + JR_s)}{nkT} \right) - 1 \right] - \frac{V + JR_s}{R_{sh}} \quad (2.3)$$

Equation 2.3 is also termed the **one-diode model**.

Solar cells are reportedly more accurately described if a second diode is included in parallel with the first one. Then, the equation is adapted to what is called the **two-diode model**. The equivalent circuit is depicted in Figure 2.3.

$$J = J_L - J_{01} \left[\exp \left(\frac{q(V + JR_s)}{n_1 kT} \right) - 1 \right] - J_{02} \left[\exp \left(\frac{q(V + JR_s)}{n_2 kT} \right) - 1 \right] - \frac{V + JR_s}{R_{sh}} \quad (2.4)$$

where:

J_{01} is the saturation current density of the first diode [mA/cm²]. It depends on lifetimes in the emitter and bulk, as well as on surface passivation;

n_1 is the ideality factor for the first diode ($n \sim 1$);

J_{02} is the saturation current density for the second diode [mA/cm²]. It is defined by defects in the depletion region (i.e. p-n junction);

n_2 is the ideality factor for the second diode ($n \sim 2$).

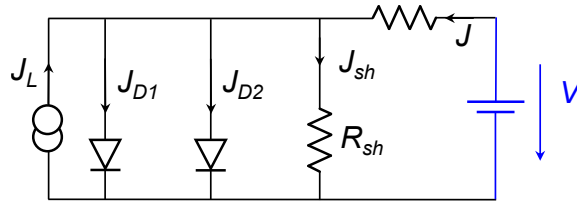


Figure 2.3: Characteristic I-V curve of a PV cell or module.

Low values of J_{01} and J_{02} are desired to develop high-efficiency technologies (e.g. SHJ and TOPCon). Minimal changes in these parameters will have a great impact on the performance of the solar cells, as can be deduced from Equation 2.4, and thus in the measured I-V curves.

Measurement of I-V curves

The I-V measurements provide fundamental information on the electrical characteristics of solar cells and modules. The standard test conditions (STC) to perform I-V measurements on PV modules are defined by the IEC 60904-3:2016 norm [111]: the device is at 25°C, illuminated

by a light with an intensity of 1000 W/m^2 and a solar spectrum of AM1.5G as reference. The measurement is performed by scanning the voltage in a specific interval and recording the photo-generated current per voltage point. The product of the voltage-current gives the corresponding power-voltage (P-V) curve (see Figure 2.4).

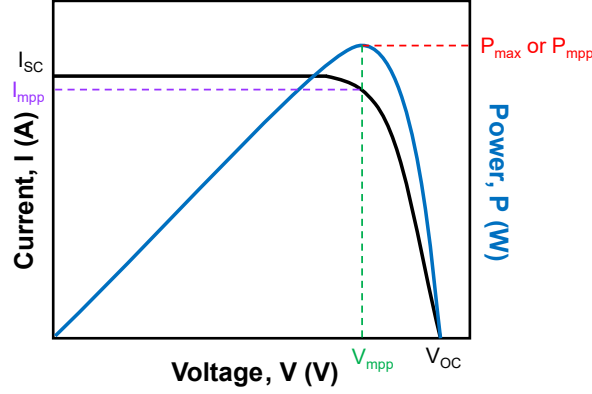


Figure 2.4: Characteristic I-V and P-V curves of a PV cell or module.

As illustrated in Figure 2.4, the following electrical parameters can be extracted from the I-V curves.

- Open-circuit voltage (V_{OC}): the maximum voltage of a PV device, when the current is zero.
- Short-circuit (I_{SC}): the maximum current a device can generate when the voltage is zero.
- I_{mpp} and V_{mpp} , the current and voltage values when the device is operating at the maximum power point.
- Maximum power point power (P_{mpp} or P_{max}): the maximum power a PV module can generate. It can be calculated by: $P_{max} = I_{mpp} \times V_{mpp}$.
- Fill factor FF : it indicates the percentage of how the real device approaches the performance of that of an ideal cell. FF is given by:

$$FF = \frac{I_{mpp} \times V_{mpp}}{I_{SC} \times V_{OC}} \quad (2.5)$$

- Power conversion efficiency (PCE), η : the ratio of the power output with respect to the incident light.

Depending on the solar cell dimensions (i.e. industrial-size vs. lab scale), different tools were utilized to perform illuminated I-V measurements.

- Mini-modules encapsulated with industrial-size solar cells were measured with a solar simulator developed in a collaboration between PV-Lab and Pasan. The modules are

placed horizontally facing downwards on a glass table. The simulator consists of a combination of halogen and LED light sources that simulate the AM1.5G spectrum. The temperature at the rear side of the modules is controlled by a thermocouple and the deviation from STC conditions (i.e. 25°C) is used to correct the I-V curve. The tool is estimated to have an uncertainty of $\pm 3\%$. Each side of the bifacial modules was measured separately and the non-measured side was covered with a black cloth to avoid undesired absorption.

- The I-V curves of lab-scale laminates were measured using a class AAA WXS-90S-L2 solar simulator from Wacom. The light source is composed of a 400 W halogen lamp and a 500 W Xenon lamp, homogeneously illuminating an area of 90 x 90 mm². A reference cell was systematically measured to correct the current and respect the 1000 W/m² illumination in the AM1.5G solar spectrum.

In parallel to the one-sun I-V curves, dark I-V measurements were performed on both types of mini-modules using the same instrument, built in-house. Similarly to standard illuminated I-V measurements, the current generated at each voltage point was recorded. In this case, however, the lamps were not activated and the laminates were covered with a black cloth to avoid any incoming illumination. This characterization technique was employed in combination with the light I-V measurements, to detect whether the performance loss was caused by optical defects or material degradation.

The laminates were measured consistently before, during and after indoor testing. Besides extracting the electrical parameters, we monitored the change in the I-V curves to understand the cause of degradation. Figure 2.5 illustrates some of the deviations of the I-V curve when the device has sustained some type of degradation. A reduction in V_{OC} can be caused by the loss of passivation in the solar cell, whereas a I_{SC} reduction is often due to optical defects (e.g. encapsulant discolouration and ARC degradation) decreasing the light absorption in the device. The degradation (i.e. corrosion) of cell and string interconnects usually results in a decreased FF. Increased slopes near the V_{OC} (higher R_s) and I_{SC} (reduced R_{sh}) can be induced by corrosion of the metallization and the formation of shunts in the solar cell, respectively.

We usually do not find just one type of effect, but a combination of several due to different degradation mechanisms occurring simultaneously in our devices. Therefore, it is essential to complement the I-V curve measurements with other techniques to understand the degradation mechanisms in our solar cells and modules.

2.2.2 Electroluminescence

Electroluminescence (EL) is a commonly-used characterization technique for PV modules, and is useful to assess degradation in combination with I-V measurements. A DC current is injected into the module (usually the applied current is the I_{SC} of the module), and the radiative recombination of charge carriers (i.e. electrons and holes) stimulates a response in

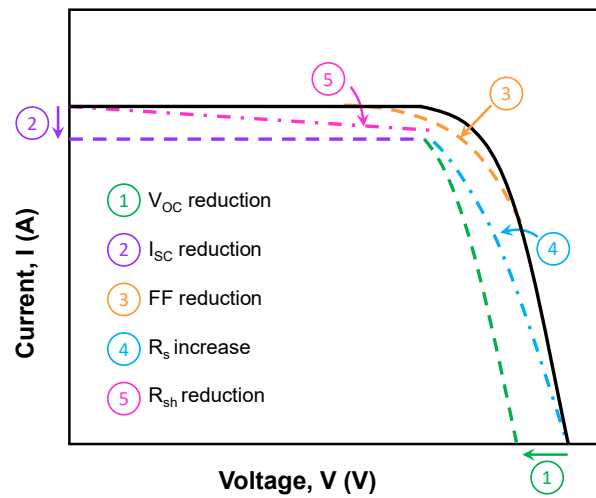


Figure 2.5: Illustration of possible changes that I-V curves can exhibit when the devices experience degradation.

the form of photon emission in the near-infrared (NIR). This technique enables the qualitative and visual detection of defects such as cracks, degraded areas of cells, and corrosion of the metallization.

The tool employed to detect the modules' responses was a charge-coupled device (CCD) camera equipped with a Nikon lens, with a fixed focal length and a pixel resolution of 1660 x 1252. The measurements were performed in the dark to remove background noise. Mini-modules were measured throughout the ageing tests to keep track of the progress of the module performance.

2.2.3 External quantum efficiency

External quantum efficiency (EQE) is another non-destructive measurement technique that can measure material degradation at the cell level. The technique is based on the concept of the generated electrons with respect to the incident photons. The quantum efficiency is most often given as a function of wavelength (i.e. 320 nm to 1200 nm, usually), and it can indicate whether the increased recombination occurs near the measured surface or the bulk. For instance, front-surface recombination will affect charge carriers generated near the surface, thus the generated response will be impacted in short wavelengths.

The tool used for the EQE measurements was an IQE-SCAN system from PV-Tools GmbH. Spectral response measurements were performed on 2 cm x 2 cm square areas of the laminates, before and after accelerated ageing tests. For bifacial modules, the front and rear sides were measured separately.

2.2.4 Photoluminescence

Photoluminescence (PL) is a tool that measures cell performance and can qualitatively (and quantitatively) indicate the level of passivation of the solar cell (or areas of the same). Unlike EL, where cells are injected with a current, PL measurements are performed by irradiating the cells with a laser. Our PL measurements were performed by employing a laser with a central wavelength of 808 nm and a CCD camera to detect photons emitted as a consequence of the radiative recombination of charge carriers. Areas with good passivation will emit more IR light than poorly passivated ones, thus they will appear brighter in the acquired image.

We performed PL images as a complementary analysis to EL. If both techniques show a lack of response in the same areas, then we assume that the solar cell itself is degraded. If however, we observe dark regions in EL measurements and not in PL, it is not due to material degradation, but it is a problem regarding the injection of current and thus, the metallization in the solar cell.

2.3 Characterization of module materials

2.3.1 Microstructural characterization of degraded solar cells

Extraction and sample preparation procedure

Once solar cells have been laminated in a module scheme and the polymeric encapsulant has been cured, it is not possible to separate the module components. The solar cells need to be extracted somehow to enable their micro-structural characterization. Therefore, we developed an extraction and sample preparation procedure for microscopic measurements.

The process is divided into the following steps (examples of the process are shown in Figure 2.6).

1. **Extraction.** An area of interest - with a maximum dimension of 2 cm x 2 cm - is cut from the module using a 6500 Well diamond wire saw. A coil with the diamond wire goes back and forth, while the module is fixed to a slightly tilted table, so the gravitational force pushes the module downward and enables the cut through the laminate.
2. **Embedding.** The extracted piece is placed face down in a 2 cm-diameter mould, which is then filled up with epoxy resin. The epoxy resin employed is a mix of two commercially available components from Struers: EpoFix Resin and EpoFix Hardener. The moulds with the pieces and the epoxy are then put in a vacuum desiccator for a minimum of 12-24 hours to harden the resin.
3. **Grinding.** Once the resin is hardened, the surface of the embedded sample needs to be ground. This step is done to remove the epoxy that has potentially hardened at the surface and to polish off the first layers of the device that may exhibit some roughness

due to the extraction procedure. The grinding is performed manually in an ESC 300 GTL system with a rotating disc and a water supply. The direction and speed rotation can be adapted to match the materials. Silicon carbide (SiC) grinding papers with different grain sizes are used. The order of use for the grinding papers is from largest grain size (58.5 μm) to smallest (10 μm). The grinding is complete when the surface of the sample looks flat in the optical microscope.

4. **Polishing.** The purpose of the polishing process is to smoothen the surface at the micro- to nano-scale. An ATA SAPHIR 520 system was used to polish the samples, which automatically presses, holds and rotates them. The polishing time, pressure and speed are also controlled. Different materials are used for the polishing step, first white silk and then FD6, FD3 and FD1. At each polishing step, a solution of water and diamond particles is used to optimize the process. The size of the particles (from 6 μm to 1 μm) depends on the paper used, and the samples need to be cleaned in an ultrasonic bath with water when changing from one solution to the other. The polishing step is complete when the surface seems mirror-like and no scratches are visible in the optical microscope.

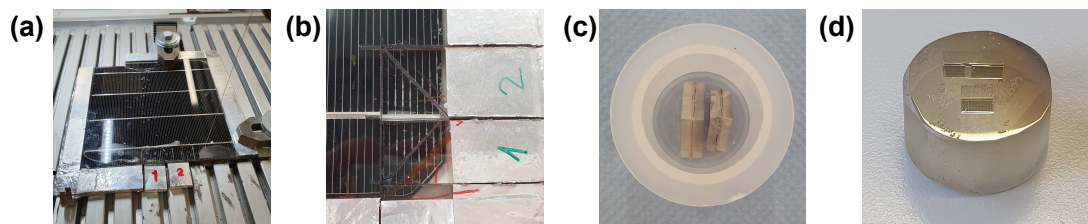


Figure 2.6: Pictures of the sample preparation process: (a) mini-module being cut using a diamond wire saw, (b) already cut mini-module cut, (c) wire-cut pieces in the mould ready to embed and (d) resin-embedded samples after grinding and polishing processes.

Scanning electron microscopy

Scanning electron microscopy (SEM) was performed to investigate the stability of the solar cell layers (mainly the TCO) and the metallization. SEM images were taken on JEOL JSM-7500 TFE and Zeiss Gemini 2 microscopes, usually operated with a 5 kV electron beam.

In Chapters 4 and 5, SEM analysis was used on the polished samples to check the adhesion (or lack thereof) of the metallic fingers, busbars and ribbons to the solar cells. The measurements performed in Chapter 4 were performed by Quentin Jeangros. In Chapter 6, top-view and cross-section SEM images were taken on un-encapsulated and un-tested solar cells, by Julien Hurni.

Transmission electron microscopy and energy-dispersive X-ray spectroscopy

Transmission electron microscopy (TEM), scanning TEM and energy-dispersive X-ray spectroscopy (EDX) analyses were carried out in Chapter 5 on mechanically polished devices to investigate microstructural damages and chemical changes in the solar cell layers caused by degradation.

First, the cross-sections of the resin-embedded devices were analyzed by SEM and then thin lamellae containing the desired interfaces were extracted with a conventional focused ion beam (FIB) lift-out method. This was performed in a Zeiss NVision 40 FIB/SEM. Next, a gallium ion polishing was performed at 5 kV to diminish surface damage. Finally, the FIB lamellae were transferred to a Thermo Fisher Osiris TEM operating at 200 kV, where the TEM, STEM and EDX measurements were performed. For comparison purposes, resin-embedded reference devices (from pristine modules) were analyzed alongside the tested and degraded ones.

2.3.2 Fourier-transform infrared spectroscopy

Fourier-transform infrared (FTIR) spectroscopy is a useful technique to characterize changes in the chemical composition of materials. A beam with several frequencies of light is directed to the sample and the system measures how much of it is absorbed. This process is repeated with many ranges of frequencies and then the software processes the data to calculate the absorption at each wavelength.

The measurements were carried out on a Bruker Tensor 27-Spectrometer and the data were treated using the Opus software. The analysis of each sample consisted of 32 scans with a resolution of 4 cm^{-1} . Non-encapsulated solar cells were characterized in transmission mode and continuous scanning from 650 cm^{-1} to 4000 cm^{-1} .

2.3.3 Electrical resistivity measurements

The electrical resistivity of polymeric encapsulants for PV applications is characterized following the method established in the standard *IEC 62788-1-2: Measurement procedures for materials used in in photovoltaic modules - Part 1-2: Encapsulants - Measurement of volume resistivity of photovoltaic encapsulants and other polymeric materials* [111].

The measurements were performed with a Keithley 8009 resistivity test fixture and a Keithley 6571B electrometer. Two layers of $55 \times 55\text{ mm}^2$ encapsulant were laminated following the standard lamination recipe for the particular material. Once cured, the average thickness was measured and the samples were pre-conditioned for a minimum of 48 hours. The volume resistivity was then measured in three different conditions: (1) ambient ($23^\circ\text{C}/50\%\text{ RH}$), (2) hot dry ($85^\circ\text{C}/15\%\text{ RH}$) and (3) damp heat ($85^\circ\text{C}/85\%\text{ RH}$). Five replicates per condition - and encapsulant - were prepared and characterized for reproducibility and statistics.

2.3.4 X-ray diffraction

X-ray diffraction (XRD) is an analytical technique that can determine the crystallographic structure of materials. The characterization is based on irradiating the surface of the sample with incident X-rays and measuring the preferential scattered angles and intensities.

The XRD measurements were performed in a PanAnalytical X'Pert Pro Diffractometer at CSEM, at a 2θ angle range between 20° and 60° . We gratefully acknowledge Julien Hurni's contribution to performing the measurements. In this work, the XRD analysis was done on a-Si:H/TCO and nc-Si:H/TCO layer stacks to investigate the impact of the sub-TCO layer on the crystallite size of the TCO. These layer stacks, deposited on single-side textured (SST) wafers, were deposited by Joël Spitznagel and Sylvain Dunand. The peaks were treated by using *Match!* software and by fitting them with an In_2O_3 10.425 Å lattice constant reference.

2.3.5 Atomic force microscopy

Atomic force microscopy (AFM) is a non-destructive imaging technique that can provide topographic information about the analyzed sample. For imaging and morphology analysis, a piezoelectric scanning the surface of the sample is used in "tapping" mode, and the height of this movement is recorded, providing information about the topology.

The AFM measurements were done by Mostafa Othman in a Bruker Dimension Edge with ScanAsyst system. We performed the topographic characterization on a-Si:H/TCO and nc-Si:H/TCO layer stacks (same samples as the ones analyzed by XRD) to obtain the root mean square (RMS) roughness values for the TCOs with different substrates.

2.3.6 Hall effect

Hall effect measurements are employed to characterize Hall mobility and carrier concentration - among other electrical properties - of thin film materials. To measure the Hall effect, a magnetic field perpendicular to the carrier flow is applied.

In this work, we measured the Hall effect on a-Si:H/TCO and nc-Si:H/TCO layer stacks deposited on glass and cut into $1 \times 1 \text{ cm}^2$ pieces that were then placed on a dedicated printed circuit board holder. We used an HMS-500 system from Ecopia with an applied magnetic field of 0.56 T.

2.4 Indoor accelerated ageing tests of PV modules

2.4.1 Damp Heat testing

As mentioned in Chapter 1 Section 1.3.3, DH testing was developed to test the modules' resilience to sustained exposure to high relative humidity (RH) and temperature conditions.

The DH tests are performed based on the standard described in IEC 61215-2:2021, which states that modules should be subjected to 85°C and 85% RH for 1000 hours. In order to pass the test, the loss in P_{max} should be below the 5% threshold with respect to the initial value.

In the present work, we extended the DH tests to 2000 hours - with the aim of studying their behaviour over time - and systematically measured the performance of the PV modules (with the described characterization techniques described in the previous sections) every 500 hours. The tests were performed in three different climatic chambers, depending on space availability and usage: a Weiss C180/-40, an ACS ATT DY250 and an ACS ATT DM1200.

2.4.2 Potential-induced degradation testing

PID tests were developed as a method to simulate the occurrence of this phenomenon and to test PV modules' sensitivity to it. Initially, two test procedures were proposed for the provisional IEC Technical Specification 62804 and, in 2021, one of them was accepted and adapted to the IEC 61215 standard. This standard is the one we base our testing procedure on.

First, a conductive metallic tape is placed around the edges of the mini-modules to simulate the Al frame of commercial products. Then, the module leads (i.e. string interconnects) are short-circuited and a voltage is applied to the cell by an Iseg ECH 224 high-voltage supply, while the frame is grounded as defined in [88] (see Figure 2.7). The cells can be either negatively or positively biased with respect to the frame. The mini-modules are then placed in a climatic chamber (the same systems as the ones used for the DH testing) at DH-like conditions (i.e. 85°C/85% RH) for 96 hours. The voltage applied should correspond to the V_{OC} of the nameplate rating. Similarly to the DH testing, the pass/fail criteria are defined by the P_{max} loss limit of 5%.

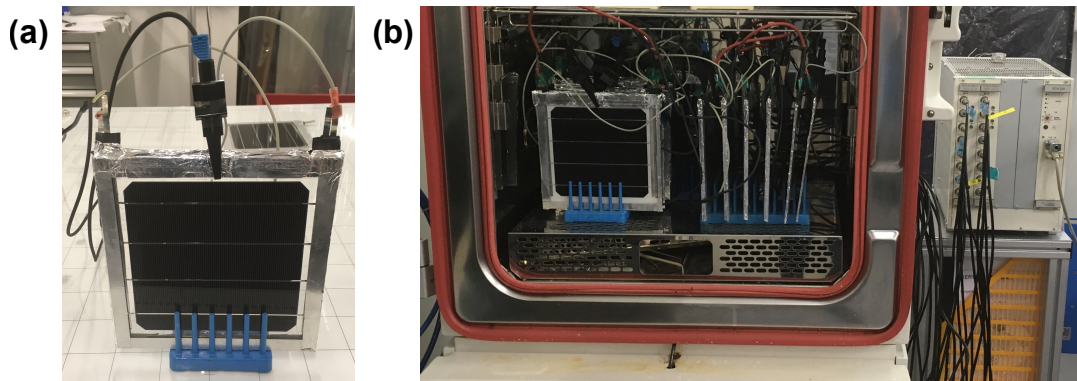


Figure 2.7: Pictures of (a) one-cell mini-module with the metallic frame and the connectors and (b) a set of mini-modules placed vertically in racks in a climatic chamber and connected to the high-voltage supply.

The initial test procedure suggested by Hacke and co-authors differs from the current standard in the chamber temperature [87]. In the first proposal, a temperature of 60°C combined with

2.4. Indoor accelerated ageing tests of PV modules

85% RH were proposed as the PID testing conditions. The authors determined that subjecting the modules to those indoor conditions for 96 hours, along with a negative -600 V, replicated the performance loss observed on modules installed in Florida, USA, after 28 months. Not only the IEC 61215 standard has adopted the higher temperature stress conditions, but the reliability field, in general trends, has chosen to stress the modules with voltages higher than their nameplate rating. This is done with the goal of simulating the worst-case scenario that cells can be exposed to when installed in large-scale systems in the field.

In the present work, the cells are biased with a voltage of 1 kV and the PID tests are further accelerated in terms of testing duration: we usually extend the tests to 500 hours (or more in some cases). The modules are systematically measured every 48 hours to 96 hours to keep track of the performance loss.

3 Reliability and Long-term Performance of SHJ Solar Modules

The work in this chapter is based on the following publication, which was also presented at the WCPEC-8 in Milan, 2022:

- O. Arriaga Arruti, A. Virtuani and C. Ballif, *Long-term Performance and Reliability of Silicon Heterojunction Solar Modules*, Progress in Photovoltaics: Research and Applications, 2023 [108].

Abstract

The high-efficiency silicon heterojunction (SHJ) technology is now perceived mature enough to enter the Giga-Watt manufacturing scale with several players around the globe. The growth of the SHJ technology requires confidence from manufacturers, investors and system developers about its reliability and long-term performance. In this chapter, we perform a literature survey collecting performance data (and performance loss rates (PLR)) published for SHJ modules. Publications on this specific subject are still limited, however enough available data exist to drive some preliminary conclusions. Despite a long list of caveats specific to this type of meta-analysis, when considering all published data-sets, we obtain for SHJ modules median and average PLR values of 0.56 %/year and 0.70 %/year, respectively. These numbers are in line with PLR generally reported for field-deployed crystalline silicon (c-Si modules). We then apply a filtering procedure to distinguish what we perceive to be high-accuracy data-sets from less accurate ones. This methodology is understandably arbitrary, but it helps increasing the robustness of the present analysis. Our refined analysis leads us to slightly higher PLR for SHJ modules: 0.80 %/year and 0.83 %/year for median and average values, respectively. These values fall between previously reported PLR of c-Si and thin-film modules. Additionally, we observe some mild correlations between the PLRs and the climatic conditions of the installation sites, even if we need to stress that for each climate we find a large variability, including a PLR value as low as 0.29 %/year. We complement the survey with information about the main failure modes reported in the literature for this technology and an analysis

of the limits and caveats for this type of study. The most significant one is that the reported numbers refer - for the vast majority - to modules from just one manufacturer (i.e. the first company manufacturing and commercializing the SHJ technology). We finally point out that a deep understanding of the potential weaknesses of the technology – collected over the years – has led to several improvements in terms of reliability. A careful material choice and module design may in fact allow the SHJ technology targeting extended service lifetimes of 35+ years

3.1 Introduction

The global solar photovoltaic (PV) industry has been growing exponentially over the last two decades. With a newly installed capacity of 183 GW last year, the cumulative capacity has approached almost 1 TW worldwide by the first quarter of 2022 [112].

With a market share of approximately 95%, the dominant PV module technology is that based on crystalline silicon (c-Si) cells (with the remaining share covered by thin-film based technologies). Due to several factors, which include efficiency, costs, technology track-record, availability of materials and stability, the dominant role of c-Si solar cells and modules is deemed to continue [15].

As a result of the relatively young age of existing PV installations, experience about their long-term performance is key to investors, project developers and plant owners. Nowadays, most PV manufacturers guarantee a linear power reduction, with a maximum loss of 16 to 20% after 25 years of operation. Nevertheless, studies have shown that PV modules can suffer from non-linear degradation losses or early life failure modes, such as potential induced degradation (PID) [58] or other degradation modes. Therefore, a close monitoring of the performance of modules installed in the field is essential in studying their failure modes and, thus, in developing stable modules that can target 35+ years of active service lifetime.

Modules made with conventional c-Si PV cells (i.e. aluminium back surface field, Al-BSF) have been in the market for the longest time and have the longest track-record. They are currently by far the leading solar cell technology, in terms of cumulative installations, but are about to be completely replaced by more sophisticated technologies, still based on c-Si wafer, that allow targeting higher efficiencies. This is the case of the PERC (passivated rear-emitter cell), which has become in the last 3-4 years the workhorse of the industry (see Figure 3.1). Other high-efficiency technologies, including silicon heterojunction (SHJ) and tunnel oxide passivated contact (TOPCon) solar cells, will compete in the coming years for increasing their market share. Noticeably with increased efficiency and reliance on surface passivation and higher bulk lifetime, these advanced cell technologies can easily become more prone to degradation.

Developed by Japanese manufacturers in the 1970s, SHJ solar cells are based on an n-type c-Si wafer, with doped amorphous silicon (a-Si:H) layers deposited on the top and bottom surfaces. A transparent conductive oxide (TCO) is used as a transparent electrode [34]. With record

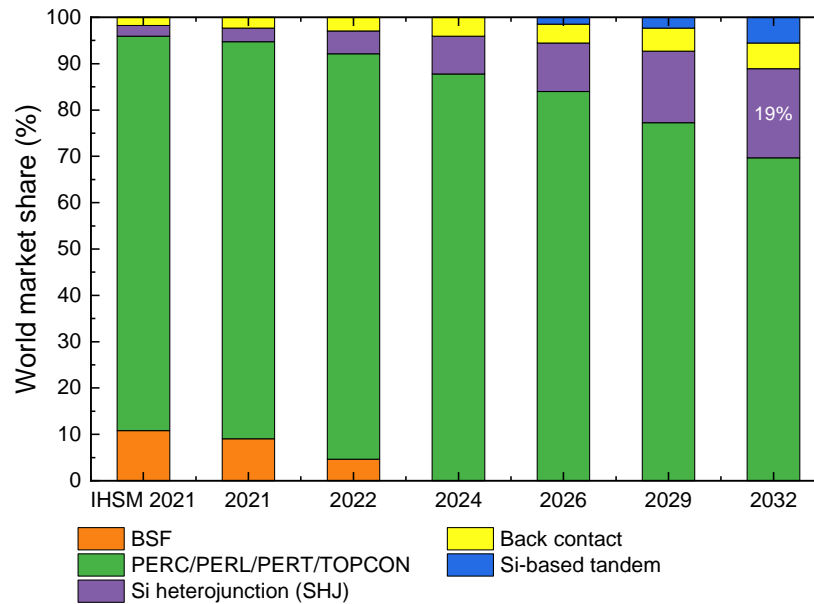


Figure 3.1: Projection of the world market share of different solar cell technologies over the next decade [source: ITRPV2022]: back-surface field (BSF), passivated rear-emitter cell (PERC), passivated rear-emitter locally diffused (PERL), passivated rear-emitter totally diffused (PERT) and tunnel oxide passivated contact (TOPCon).

efficiencies of large 6" cells of 26.5% [36], they offer several advantages over conventional Al-BSF and high efficiency (e.g. PERC) cells. The main benefits of the industrialization of SHJ solar cells are the shorter processing times and the reduction in the number of manufacturing steps, as well as the possibility to use a lower wafer thickness thanks to the ideally passivated surfaces, thus potentially lowering production costs and material consumption. Additionally, the passivating properties of the a-Si layer allow the achievement of higher open-circuit voltages (V_{OC}) (i.e. 751 mV for the SHJ record cell compared to 650 mV and 700 mV for Al-BSF and PERC solar cells, respectively [113]), and consequently, lower temperature coefficients of the power, which leads to increased energy yields, particularly in hot climates. An additional advantage of using a TCO on both faces, is that the cells are "naturally" bifacial, with potential bifaciality factor over 90% (compared to 70% of that of PERC solar cells) [114].

Besides the several advantages, some drawbacks are also associated to the SHJ technology. One of them is related to the string and cell's interconnection processes. The passivating a-Si layer should usually not be heated at temperatures exceeding 200-220°C. Thus, SHJ cells can usually not be stringed using conventional high-temperature soldering, unless the process and soldering materials are adapted. One possible easier approach is to use electrically conductive adhesives (ECA), which have a high silver (Ag) content, to "glue" the ribbons to the cell's busbars. Moreover, the symmetrical stack structure implies printing a Ag grid on

both sides of the cell. The consumption of Ag is, thus, higher for SHJ cells than for PERC or other technologies. The industry has been working on finding solutions to reduce Ag consumption by creating alternative interconnecting processes. These include using multi-wire (MWT) or SmartWire technologies (SWCT) or using copper-plated grids [44]. Another potential bottleneck towards a massive deployment of this solar cell technology in the coming decades is related to the availability of some key elements, such as indium (In) [115]. Indium tin oxide (ITO) is, in fact, the most widely used and reliable material for TCOs. It is commonly used in the electronic industry, particularly for touch screens and large-area displays. Thus, efforts are also being made to overcome this potential constraint. Some groups use alternative TCOs, such as aluminium-doped zinc oxide (AZO) [116], and transparent conductive layers such as copper or carbon nanotube networks [117], [118]. Alternative solutions aim to reduce the thickness of the ITO layer (using some capping layers based on silicon nitride (SiN_x)) or completely get rid of it [119], [120].

Presently, SHJ modules cover ~3% global market share but, thanks to their several advantages, and the number of players entering the market, this number could increase considerably in the coming years (19% by 2032 (see Figure 3.1) according to ref. [15]). The SHJ solar cell/module technology is not a new one. The first SHJ cell (called HIT: heterojunction with intrinsic thin-layer) was patented by Sanyo (later Panasonic) in 1997 [33]. This patent prevented other manufacturers from producing this solar cell structure; hence, its commercialization and deployment was limited to Sanyo/Panasonic for more than a decade. However, the patent that protected the HIT technology expired in 2010, allowing other players to potentially enter the market and with different manufacturing processes. Consequently, R&D activities for this technology have experienced a significant growth over the last decade, leading to several initiatives of industrial players deciding to invest in it and announcements in 2021 and 2022 of capacity expansions targeting the Giga-Watt scale.

SHJ technology is key to boost the European PV market, and several companies in Europe have decided to proceed on to mass production. With a production capacity of 600 MW in Singapore, the REC Group has announced the addition of 600 MW more to their SHJ production line by the end of 2022 [121]. Maxwell is their main equipment supplier for cell lines. Hevel Solar, one of the first companies to enter mass production, currently runs a 340 MW manufacturing line in Russia [122]. Additionally, Meyer Burger, who delivered several production lines, has now moved to solar cells and module production, focusing on SHJ with the SWCT technology in Germany [123]. Production of SHJ modules has started with a capacity of 400 MW per year, now in ramp up to 1.4 GW (with plans to expand to over 5 GW in the coming years). Similarly, 3SUN from Enel Green Power (EGP) has ramped a manufacturing line of SHJ cells/modules in Italy (200 MW) and targets capacity expansion plans to 3 GW of production in the coming years [124].

Many manufacturers in Asia, particularly in China, have also taken steps to increase their production capacities. Companies such as GS-Solar, Huasun New Energy and Akcome, with installed capacities of 500-600 MW, have announced expansion plants for the Giga-Watt scale

[125]–[127]. Talesun also announced plans of building a 5 GW factory [128].

The surge of the SHJ technology in the PV industry requires confidence from manufacturers, investors and system developers about its reliability and long-term performance. With this aim in mind, in this chapter, we have been collecting data published over the last two decades (literature reporting degradation rates and performance indicators for SHJ modules). We have also gathered information about failure modes specific to this technology and ways of mitigating/preventing their occurrence.

3.2 Method and approach

Recent evidence suggests that properly designed modules can reach service lifetimes of 25-30+ years [64], [65], [129]. A frequently used definition of lifetime for modules/systems refers to a threshold (power loss beyond a defined limit) corresponding to 80% of the initial nominal power of the device.

However, the lifetime is expected to depend on the operating conditions. In particular, it is strongly influenced by the general climatic conditions and the type of installation (e.g. open-rack mounting versus full building integration) that may affect the module ventilation and consequently impact the module's operating temperature.

Typical long-term annual degradation rates have been reported (from statistical analyses of data given in the literature) to be in the order of 0.5 to 1 %/year for conventional c-Si modules and somewhat higher for thin-film modules [130], [131]. Additionally, for simplicity, performance losses are generally assumed to follow a linear trajectory, even if this is not the case, particularly when the modules approach their end of life [64], [65]. The most relevant ageing and failure mechanisms for c-Si modules that may arise in the early period (so-called "infant-life" failures), during the middle of the operating life, and at the wear out (end-of-life) include: module delamination, glass breakage, encapsulant discoloration (or browning), corrosion of cell interconnects (and of anti-reflective layers), cell or ribbon breakage, and many others.

In addition to impacting the module performance, these failures can, in the worst cases, lead to safety hazards such as the loss of electrical insulation.

Unfortunately, inferring the service lifetime of PV modules exclusively based on stress tests performed in the laboratory is a complex task and often leads to unrealistic estimations. Monitoring and performance data of field-deployed modules (of the same make/typology) extending over a reasonable time horizon (understandably, the longer the extension of the time-series, the better) should complement this information in order to get a realistic estimation of the service lifetime of these devices and increase market acceptance of a specific technology.

3.2.1 Overview of studies reporting on SHJ technology

In this survey, we collected 54 data points originating from 14 different studies and various climates (see Table 3.1). Understandably, most entries are relative to the Sanyo/Panasonic's HIT technology, the first company to manufacture and commercialize the technology, and the only one for which a relatively long time series of field-deployed modules have been published. In Table I, we can observe that most of the installations are less than ten years old.

Several works have been published comparing the performance and performance loss rates (PLR) of c-Si and thin-film technologies, highlighting the relevance of several factors in this kind of analysis [52], [131], [132]. A sound methodology is, in fact, a critical aspect in order to obtain reliable results in these types of studies. Each institute/group uses different set-ups and methodologies (including data processing, aggregation and filtering) to assess the long-term performance of modules or strings. These factors can all play a significant role in the assessment of PLR. As a general rule, we consider current-voltage (I-V) measurements of individual modules performed regularly over time indoors as a more accurate method for this kind of analysis, compared to data obtained by outdoor monitoring systems (e.g. the performance ratio, PR). However, for various reasons, including practicality, most of these data are usually obtained by analyzing time series of PR data. Conversely, several methods can be applied to improve the data accuracy and improve the accuracy of outdoor data. In this work, we label as high-accuracy data-sets the ones that meet the following criteria:

- Indoor laboratory measurements of modules at Standard Test Conditions (STC);
 - Measurement of modules at STC conditions taken before their installation, rather than using the nameplate rating (i.e. the value provided by the manufacturer) as the initial value, to avoid the underrating or overrating of initial power values [133].
- In the case of outdoor performance measurements (when reported):
 - Available information on the periodic service and maintenance of the monitoring system (regular calibration and cleaning of radiometric and other sensors);
 - Available information on proper data treatment and filtering (generally on the irradiance and module power and removal of outliers);
 - The adoption of additional inspection methods, besides the determination of electrical parameters, e.g. visual inspection and thermal imaging;
 - A well-explained and thorough data treatment methodology.

Table 3.1: Description of the data sets investigated in the survey: location, climate, installation year, years in operation, manufacturer, module structure (G/BS = glass/backsheet, G/G = glass/glass) and type of structure (BIPV = building integrated PV). Where the symbol (-) is present, the module were installed in several different locations and no direct information is available. Marked with an asterisk (*) are the works considered more accurate.

Institute	Location	Köppen climate classification	Installation year	Years in operation	Manufacturer	Module structure	Type of structure
AIST	Tsukuba, Japan* [134]	Cfa - Humid subtropical	2004	3	Sanyo/Panasonic	G/BS	Ground
	Kyushu, Japan* [135]		2012	4			
ASU	Arizona, USA [136]	Bwh - Hot desert	2010	6	Unknown	-	-
EURAC	Bolzano, Italy* [137]	Cfb - Temperate oceanic	2010	6	Sanyo/Panasonic	G/BS	Ground
	Nicosia, Cyprus* [137]	Bsh - Hot semi-arid	2006	8			
	Alice Springs, Australia* [137]	Bwh - Hot desert	2008	7			
	Milan, Italy* [137]	Cfa - Humid subtropical	2009	6			
	Catania, Italy* [137]	Csa - Hot-summer Mediterranean	2009	6			
HEVEL Solar	Novosibirsk, Russia* [138]	Dfb - Warm-summer humid continental	2017	4.5	Hevel Solar	G/BS, G/G	Ground
NISE	Gurgaon, India* [139]	Bsh - Hot semi-arid	2009	2	Sanyo/Panasonic	G/BS	Ground
	India (multiple locations) [140]	-	-	-	-	-	-
NREL	Colorado, USA* [141]	Bsk - Cold semi-arid	2006	10	Sanyo/Panasonic	G/BS	Ground
SERIS	Singapore* [143]	-	-	6 (mean)	-	-	-
SERT	Thailand* [144]	Af - Tropical rainforest	2010	9	Sanyo/Panasonic	G/BS	Rooftop
SUPSI	Lugano, Switzerland* [145]	Aw - Tropical savanna	2012	4	Unknown	Unknown	Ground
	Tempe, USA* [146]	Cfb - Temperate oceanic	2016	4	Prototype	G/G	Ground, BIPV
TÜV Rheinland	Chennai, India* [146]	Bwh - Hot desert	2016	2	Unknown	Unknown	Ground
	Ancona, Italy* [146]	Aw - Tropical savanna					
	Cologne, Italy* [146]	Cfa - Humid subtropical					
	Dietikon, Zurich, Switzerland* [147]	Cfb - Temperate oceanic					
ZHAW		Cfb - Temperate oceanic	2009	10	Sanyo/Panasonic	G/BS	Rooftop

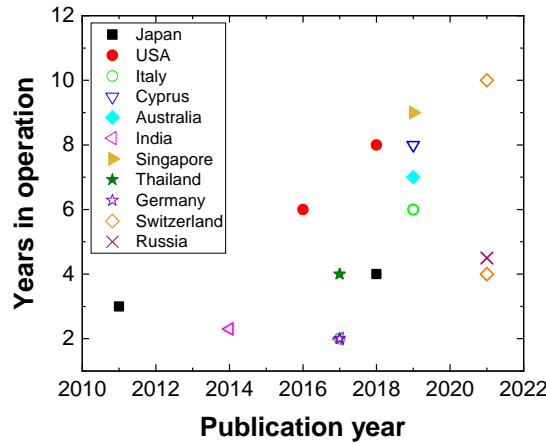


Figure 3.2: Overview of the publications considered in this survey, providing information about field exposure time, publication year and color-coded according to the country of installation.

Jordan et al. reported that degradation rates of modules could vary depending on location and mounting configurations [131]. They showed that modules installed in hotter climates, such as deserts, and those in array configurations leading to higher operating temperatures can suffer higher degradation rates. Temperate climates are generally characterized by more moderate temperature variations, with PV modules not suffering from extreme weather variations, thus subjecting them to lower stress conditions. Figure 3.2 provides an overview of the publications considered in this survey, granting information about field exposure time, publication year, and the installation location. In this work, the vast majority of the reported degradation rates refer to modules deployed in different countries worldwide (mainly in temperate and arid climates) for more than 4-5 years.

A more exhaustive discussion of the caveats of these types of surveys is performed in the following section.

3.2.2 Caveats

As mentioned above, in general, surveys of degradation rates come with some limitations and caveats, which we briefly recall here.

1. High-accuracy (few) vs low-accuracy (for which no clear information about the methodologies or monitoring systems used is available) data-sets are mixed.
2. Usually, module data (i.e. indoor laboratory measurements) are mixed with degradation rates of arrays/systems, for which the reported PLR may be partly due to performance degradation of other non-module components (e.g. inverter, cables and connectors). Therefore, focusing on the arrays/system level (rather than just on module level) may introduce more significant uncertainty in the analysis, associated with resistive losses in

the cables/connections or inverter losses.

3. Climatic conditions may have a substantial impact on PLRs, when the data-sets are mixed together.
4. PLRs for the latest technologies are (understandably) not available, as a minimum temporal horizon of at least a few years is required for this kind of analysis.
5. Longer time-series, for which it is possible to obtain more accurate and reliable information, may be obtained for older modules/technologies, not necessarily representative of the technologies available on the market today.
6. A linear degradation rate is generally assumed, which may be a good approximation in several cases, but not always. This kind of analysis generally assumes, for simplicity and sometimes as a reasonable approximation, constant degradation rates, corresponding to a linear loss in performance over time. In reality, particularly during the first months of field exposure and approaching end-of-life, or in the case of modules with serious performance issues due to specific failure modes, performance curves can follow non-linear trajectories [64], [132].

Additional caveats are specific to the technology investigated in this work (SHJ cells/modules). These include:

1. The vast majority of the PLR data reported in the literature for SHJ are relative to Sanyo/Panasonic's technology, which may differ in many respects from the technology developed/manufactured today by other SHJ players. These differences may be relative to the cells or the module structure.
 - Many SHJ modules entering the market today have a glass/glass (G/G) structure to benefit from the intrinsic bifaciality of SHJ cells. However, Sanyo/Panasonic modules have a more conventional glass/backsheet (G/BS) structure, even if it is highly probable that this manufacturer adopted – at least for a reasonable timespan – a backsheet containing a metal foil, used as a barrier to water/moisture ingress. Thus, this structure somehow resembles more that of a G/G module rather than that of a conventional G/BS one. Only recently, Panasonic has disclosed the module structure of their later products that are reportedly manufactured with a conventional and breathable backsheet as a rear cover using polyolefin (PO) and ethylene vinyl acetate (EVA), respectively, as the front- and rear-side encapsulants [148].
 - Additionally, Sanyo/Panasonic has introduced several technological advancements for their cells over the years. Initially, their HIT cells had a front-emitter structure (with the p-doped a-Si:H layer at the front), but they reportedly changed their technology to rear-emitter around 2009 [148]. Therefore, the performance of a ten to fifteen-year-old module may not be necessarily representative of a module

manufactured today. The advantages of a rear- vs front-emitter structure are briefly recalled in Section 3.4.1.

2. Statistics (i.e. number of published works) and the temporal horizon (maximum 10-15 years) for SHJ devices are still limited. Therefore, the SHJ modules from other players presently entering the market may exhibit different long-term performances (and degradation modes) compared to the Sanyo/Panasonic technology for which most information is available today.

Despite these potential limitations, we believe that this analysis is strongly beneficial to better understand this technology's potential. In parallel, focusing on potential weaknesses and specific failure modes of SHJ modules and understanding the root-causes behind, should promote overcoming these potential reliability issues.

3.3 Literature survey

3.3.1 All data-sets

It would be meaningless to assess the degradation rates of SHJ modules without comparing them to technologies with a longer track-record in the field. These would correspond to conventional c-Si as well as thin-film technologies. In 2013, Jordan et al. reported degradation rates of 2000 c-Si modules installed worldwide [130]. They observed a median degradation rate of 0.5 %/year for c-Si modules compared to 1.0 %/year for thin-film modules. The reported PLRs on thin-film technologies are a mix of several of them (e.g. cadmium telluride (CdTe) and copper indium gallium selenide (CIGS)). Conversely, due to the age of the modules, the PLR for c-Si refer to mainly modules manufactured with conventional c-Si based on Al-BSF. In 2016, this work was further expanded by reporting more than 11000 data-sets on PV modules/systems in different countries [131]. Here, more mainstream technologies, such as PERC solar cells, were considered, SHJ solar cells included. Nevertheless, the mean PLRs for c-Si and thin-film technologies were very similar to the previous ones.

As previously mentioned, in this survey, we analyze 54 data-sets from 14 different publications. Figure 3.3 shows: (a) a histogram distribution of PLR (%/year) together with a Lorentz distribution curve, and (b) a corresponding Pareto chart for the reviewed degradation rates. These charts provide an overview of all data points, including all climates and levels of data-set accuracy and entries from single modules or string/arrays. The median PLR for all the investigated modules is of 0.56 %/year, with an average of 0.70 %/year (please note that in our analysis, a positive value corresponds to performance degradation over time).

However, the "reliability" of the different works surveyed may sometimes be questionable. The direct comparison of PLR can be problematic because, as previously pointed out, monitoring equipment and practices and data analysis methodologies may vary considerably between research groups. In Section 3.2.2, we discuss the issues of considering constant degradation

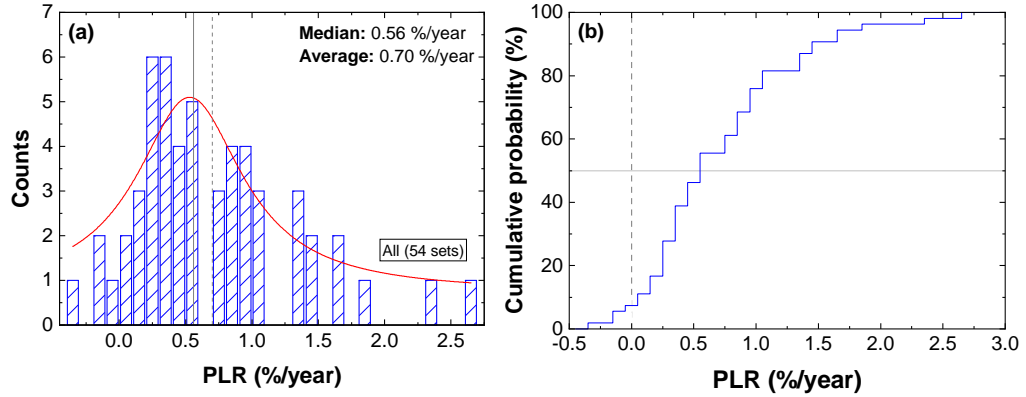


Figure 3.3: (a) Histogram of all 54 data-sets investigated in this survey reporting the PLR for SHJ modules, fitted with a Lorentz distribution curve. Solid and dashed lines indicate the median and average values, respectively. (b) The corresponding Pareto chart, with the median PLR defined as 50% of the cumulative probability. In our analysis, a positive PLR corresponds to performance degradation over time.

rates. In this literature survey, all analyzed contributions assumed a linear degradation trend. In a paper reporting about a 10-year-old SHJ system in Colorado, USA, the authors observed a non-linear performance loss trend [141]. Nonetheless, they also adopted a linear model to describe the degradation rate of the corresponding modules.

3.3.2 High-accuracy data-sets

In the following, we apply some filters to our analysis, preserving only the data-sets that we perceive as more accurate or for which more information is made available by the authors. The applied filtering procedure is understandably arbitrary, but in our view, it helps in increasing the accuracy of the present analysis. The conditions that we apply to filter out what we perceive to be lower accuracy data-sets are recalled in Section 3.2. For example, Raupp et al. reported degradation rates of PV systems installed in Arizona and Colorado [136]. However, no clear information about the individual PV systems or the corresponding operation and maintenance (O&M) practices are given. An additional data-set in this review pertains to a PV module reliability survey published in 2016 covering multiple installations in India [140]. Similarly, several degradation rates were reported in 2020 for plants distributed around the USA [142]. A clear description of the monitoring systems and the exact locations of the PV modules/systems studied are lacking in both reports, as well as specific information about the climatic conditions of the installations. Removing these data sets from the survey leads to an increased median and average degradation rates of 0.80 and 0.83 %/year, respectively, for the SHJ technology. In the US survey, Jordan et al. stated that the low degradation rates with a median of 0.34 %/year observed might be correlated to installations in colder climates. Thus,

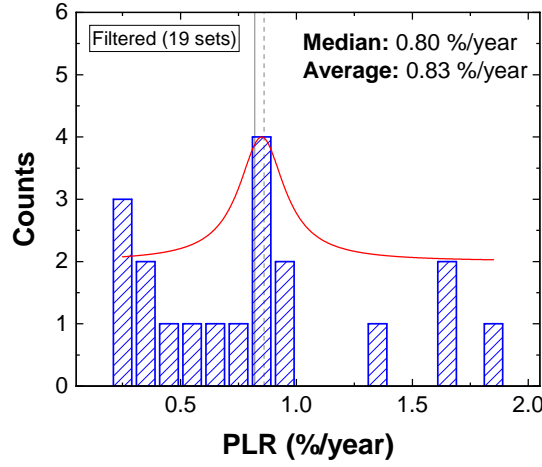


Figure 3.4: Histogram of 19 filtered "high-accuracy" data sets reporting PLR for SHJ solar modules. The filtered data-sets discarded did not meet the conditions listed in Section 3.2. A Lorentz distribution curve has been applied to the histogram. Solid and dashed lines indicate the median and average values, respectively.

the median and average PLR reported in Figure 3.3 increase by removing these data-sets. As observed in Figure 3.4, most PLR data-sets are distributed in the 0.5-1.0 %/year range.

In the following, focusing on the 19 filtered data-sets, we attempt at observing if any particular correlation can be noticed between the absolute values of the PLR and the site-specific climatic conditions.

3.3.3 The effect of climate

Several works reported the impact of climate on PLR, with – in general – systems installed in hotter climates experiencing higher degradation rates compared to those installed in temperate climates [131]. Moreover, humid climates may also impact modules' long-term performance by triggering specific degradation modes (e.g. delamination and acetic acid generation if EVA is used as an encapsulant or PID [61]). The studies analysed in this meta-analysis report data from a variety of climates. Here we divide them according to the Köppen-Geiger classification (see 3.5). A basic Köppen classification is applied in Figure 3.5 (a), classifying the different locations as dry, temperate and tropical (i.e. hot and humid) climates. In Figure 3.5 (b), more specific Köppen-Geiger sub-classifications are applied. Additionally, due to the specificity of the Mediterranean climate, we add it as a sub-class of the temperate climate.

A large variability is observed for all data groups, regardless of the climate. This may be possibly explained by two factors: the limited amount of data and, in some cases, the relatively short times of operation of the investigated systems. As a first approximation, and surprisingly, modules operating in temperate climates show the most significant median degradation rates

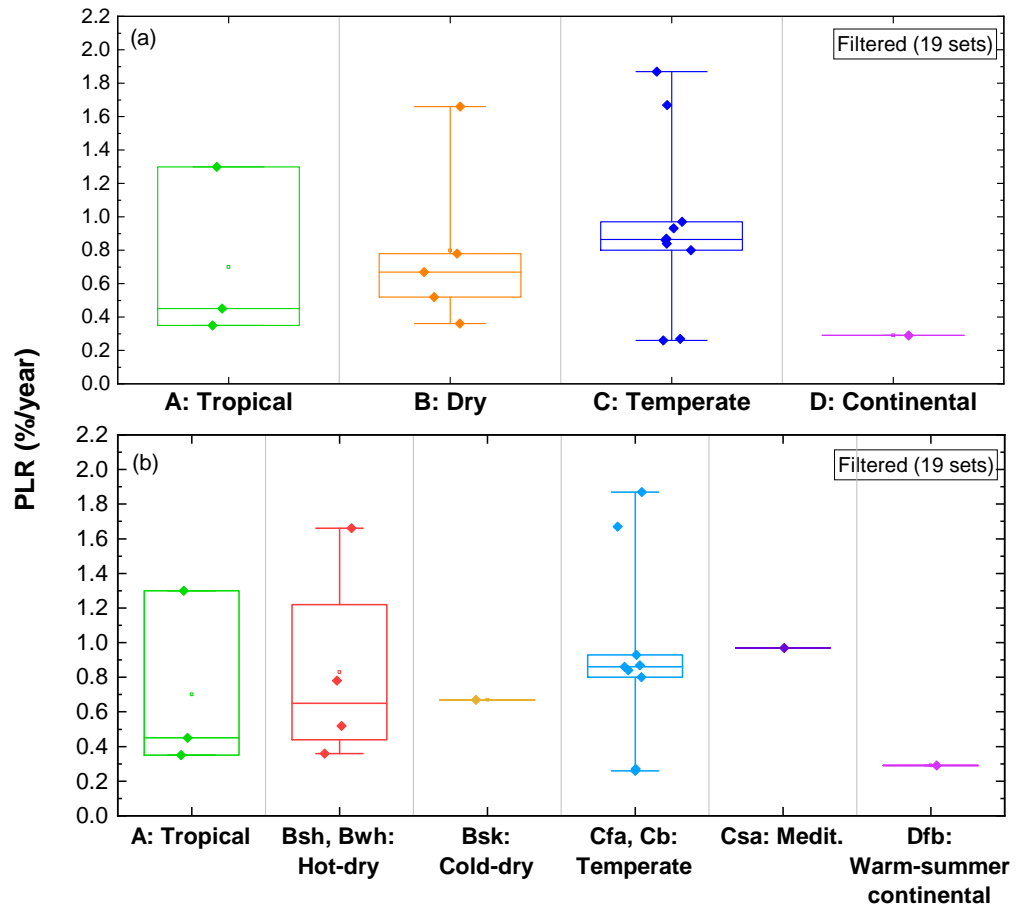


Figure 3.5: Distribution of the degradation rates (from the filtered data-sets) by type of climate according to: (a) the basic Köppen-Geiger classification (arid, temperate, tropical and continental climates); and (b) more specific Köppen-Geiger sub-classifications dividing arid climates into hot-dry and cold-dry and general temperate into temperate and Mediterranean.

of 0.87 %/year, followed by arid (0.78 %/year) and tropical climates (0.45 %/year) and, finally, continental climates with the lowest median PLR of 0.29 %/year.

With a median degradation rate of 0.78 %/year, arid climates present a lower variability when sub-classified into hot-dry and cold-dry categories. PV systems/modules installed in cold-dry climates have a median degradation rate of 0.91 %/year, higher than those in hot-dry climates, with 0.52 %/year. Instead, the variability of the former is significantly lower. The performance monitoring of PV modules reported by Schweiger et al. in the dry-hot climate of Tempe (USA) shows a slight reduction in the power of the PV modules in the first 2 years (similarly to the ones observed in other locations), with a degradation rate of 0.35 %/year [146]. In agreement with these findings, Sharma et al. reported a 0.36 %/year loss for their PV array in India [139]. No visual defects were detected. Conversely, a performance loss of 1.66 %/year, attributed

to a significant encapsulant browning, was identified in modules installed in Alice Springs (Australia) [137].

Two publications report findings in dry-cold climates. Ingenhoven et al. reported 0.78 %/year performance loss in Nicosia (Cyprus), without any apparent defects [137]. Similarly, in 2018 Jordan et al. published an exhaustive work on performance monitoring of a 10-year-old SHJ array in Colorado (USA) [141]. A median degradation rate of 0.67 %/year was observed, with the authors concluding that the system showed a similar trend to that of conventional c-Si systems. The performance loss was non-linear, but a linear behaviour was assumed. In this latter work, the degradation was mainly attributed to a loss in V_{OC} , which may be compatible with a loss of the surface passivation properties of SHJ solar cells.

With a median degradation rate of 0.87 %/year, PLR data from modules installed in temperate climates are the more abundant but also affected by the most significant spread. This number barely changes (i.e. to 0.85 %/year) when removing the data points from Mediterranean climates. Ishii et al. reported performance monitoring data from SHJ modules installed in two different locations in Japan: Tsukuba [134] and Kyushu [135]. The performance degradation over 3 years of monitoring in the former was systematically lower than that reported for monocrystalline Si technologies, whereas a higher loss, i.e. 0.8 %/year, was observed in Kyushu compared to other c-Si technologies monitored in parallel. Also, in this work, the authors attributed the higher performance losses to a decrease in V_{OC} . In the survey published by Ingenhoven et al., the SHJ modules installed in temperate climates (Bolzano and Milan in Northern Italy) showed significantly different degradation trends [137]. Modules installed in Bolzano and monitored by EURAC suffered a performance loss of 0.86 %/year, more in line with what was reported in other works. However, the modules in Milan showed a significantly higher degradation of 1.67 %/year. Similarly to what was observed in Alice Springs, the high degradation rate was attributed to a considerable encapsulant browning. Conversely, performance monitoring of modules located in Cologne reported the same trend as those in Tempe, below 1 %/year [146]. The performance loss rates of two experimental G/G SHJ modules installed in Lugano (Switzerland) showed a large variability [145]. This work reported results about two different mounting configurations: an open-rack and a fully-integrated one, mimicking a building integrated PV (BIPV) installation. The performance loss rates for both G/G modules were significantly different. The module in the open-rack configuration degraded by 0.84 %/year, while the BIPV module exhibited a more significant degradation of 1.87 %/year over the 4 years of monitoring. Again, this high value was ascribed to a severe browning of the encapsulant material (likely worsened by the higher operating temperatures due to a reduced ventilation) rather than to degradation mechanisms specific to SHJ cells/modules. Finally, in 2021 Carigiet et al. published a study of degradation rates for SHJ modules installed in Zurich (Switzerland) [147]. In this case, a detailed methodology was followed where the authors compared indoor measurements of modules to outdoor PR of strings. They reported that the average degradation rate of SHJ modules from indoor laboratory measurements was 0.26 %/year, whereas PLR calculated from outdoor data were twice as high (0.52 %/year). They attributed this mismatch to resistive losses in the cabling of the modules connected in the

3.4. Failure modes and potential weaknesses reported for SHJ cells/modules

string. This showcases the importance of "high-accuracy" monitoring methodologies and the fact that degradation rates of modules or string/arrays may differ due to contributions in assessing the degradation rates from other non-module system components.

SHJ modules installed in hot-summer Mediterranean climates showed consistent degradation rates. In both publications, Ingenhoven and Schweiger et al. reported performance loss rates just below 1 %/year (i.e. 0.97 %/year and 0.93 %/year, respectively [137], [146]). In principle, these PLRs, though limited to just a few entries, position the Mediterranean climate as the statistically most detrimental for the long-term performance of the SHJ modules considered in the study.

Three reported data-sets were from modules installed in tropical (i.e. hot and humid) climates. PV modules installed in Thailand showed a degradation rate of 1.3 %/year through 4 years of monitoring [144]. Conversely, monitoring modules in Singapore over 9 years lead to observed PLR of 0.45 %/year [143]. In this latter case as well, a significant loss in V_{OC} was reported. Finally, Ingenhoven et al. reported a 0.35 %/year loss rate in the tropical climate of Chennai (India), driven by a loss in V_{OC} [137].

Only one data-set was present for a continental climate, coming from the region of Novocheboksarsk, Russia, and reported by Hevel Solar [138]. Two different set of module configurations were monitored: G/G and G/BS. Bifacial SHJ solar cells encapsulated in G/G module structure did not show any signs of degradation after 2 years of operation. Conversely, the same authors reported a median degradation rate of 0.29 %/year for the monofacial SHJ G/BS modules. Similarly to other PERC modules being monitored in parallel, the degradation in these SHJ modules was caused by a reduction in short-circuit current (I_{SC}) (not in V_{OC} or FF), showing that a good module design can prevent V_{OC} degradation.

Unfortunately, the limited data-sets for the different climatic conditions, often accompanied by the large spread in the data for a specific climate, make it difficult to drive any sharp conclusions looking at a correlation between PLR of SHJ modules and different climatic conditions. The following section further analyzes the failure modes of the PV modules/arrays studied in this survey.

3.4 Failure modes and potential weaknesses reported for SHJ cells/-modules

Identifying failure modes and weaknesses in the design of PV modules is critical in improving their reliability/durability and long-term performance. This can be done by carefully selecting the bill-of-material (BOM), reinforcing the packaging structure and optimizing the manufacturing processes and quality controls. Several authors have extensively researched the main failure modes of conventional c-Si modules, including Jordan et al. [132] and the 2015 IEA-PVPS Task 13 [58] report. The authors found that, in conventional c-Si modules, one of the main parameters affected in the degradation kinetics is the I_{SC} . The loss in I_{SC} can be

caused by several reasons, with one of the most common being a reduction of light absorption due to encapsulant discoloration. This is confirmed by Annigoni et al. reporting a significant encapsulant browning (and a striking correlation between the degree of browning and overall module performance) in a 35-year-old PV installation in Lugano, Switzerland [65].

3.4.1 Outdoor exposure (this survey)

Encapsulant discoloration

In the articles surveyed in our analysis, several failure modes (specific or not specific to the technology) have been reported for SHJ modules. Ingenhoven et al. observed significant degradation rates (i.e. above 1 %/year, higher than the median PLR reported) in SHJ modules installed in Alice Springs and Milan [137]. This was attributed to a significant encapsulant discoloration, causing I_{SC} losses. Similarly, modules installed in a BIPV system in Lugano also suffered from high degradation rates attributable - at least in part - to encapsulant browning. In these cases, the degradation mechanism is most likely related to a poor encapsulant selection rather than to a degradation mechanism peculiar to the SHJ technology. We similarly want to emphasize that the largest degradation rates reported in 3.3(a) and 3.4 are correlated to encapsulant browning.

The very high PLRs might also be related to other degradation mechanisms occurring in parallel to browning. As an example, Wohlgemuth et al. observed delamination between the encapsulant and aluminium backsheet on Sanyo modules installed in the hot dry climate of Tucson, Arizona [149]. These modules reportedly presented significant power losses, although it was unclear if directly linked to the delamination process.

Loss of passivation

Conversely, a different degradation mechanism – allegedly specific to the SHJ technology – is reported for other systems and locations. Some authors reported an apparent V_{OC} loss, compatible with a loss of the surface passivation properties in the SHJ cells, as the main cause of degradation in SHJ modules. Luo et al. documented a substantial loss in V_{OC} in modules installed in tropical Singapore [143], whereas Ishii et al. found similar behaviour in the location of Kyushu, Japan [135]. Moreover, Schweiger et al. consistently observed a performance loss in SHJ modules with a continuous degradation in V_{OC} in several different climates [146]. In addition, the authors reported that this decrease did not show any signs of saturation. Jordan et al., finding a non-linear degradation trend for the SHJ modules installed in Colorado, dwelt more into the analysis by performing electroluminescence (EL), photoluminescence (PL) and dark I-V measurements, followed by microscopic analysis [141], [142]. The authors found increased saturation currents at the module level, concluding that increased carrier recombination was the cause of the degradation. On the other hand, neither visual defects nor hot spots were observed. Microscopic analysis based on transmission

3.4. Failure modes and potential weaknesses reported for SHJ cells/modules

electron microscopy (TEM) and dynamic secondary ion mass spectroscopy (d-SIMS) led them formulate the hypothesis that the passivation loss indicated by the reduction in V_{OC} could be caused by a reduction of the hydrogen content in the a-Si:H layers. Simon et al. reported additional results obtained on the same samples [150], attributing the cell degradation to a loss in passivation and to an increased presence of bulk defects. Nevertheless, the authors did not observe any specific indication of a deterioration of the a-Si:H layers.

For older SHJ modules (thus a considerable portion of the modules surveyed here), part of the reported loss of cell passivation properties, however, may be attributed to the use of front-emitter cell structures, a structure which is not allegedly used any longer today by SHJ cell manufacturers. Alternatively transparent conductive oxides with lower density or active grain boundaries, which should be controlled during cell processing, can lead to enhance diffusion of ions.

In front-emitter cells, Cattin et al. reported the lack of stability (i.e. loss in V_{OC} and FF) when SHJ cells with very thin p-doped a-Si:H were exposed to light [151]. Using thicker (p) a-Si:H layers may overcome the problem, but increasing the absorption of light, thus reducing the overall efficiency of the cell. This p-layer problem is not critical for the rear-emitter cells, which have in fact demonstrated a higher stability in laboratory stress tests.

3.4.2 Indoor accelerated ageing testing

Literature on indoor accelerated ageing tests is still limited and in the early stages when referring to SHJ cells and modules. All reported studies highlight the importance of a robust encapsulation and packaging structure to protect the active components of the module against ageing and weathering.

Water/moisture ingress

In 2019, Park et al. reported the sensitivity to damp heat (DH) exposure of SHJ solar cells encapsulated in a G/G configuration [152]. This depended on the encapsulant used; they reported degradation on cells encapsulated with EVA and polyvinyl butyral (PVB). In both cases, the power loss was mainly driven by a loss in I_{SC} , with a less significant loss in FF and V_{OC} for modules encapsulated with PVB. Conversely, the adoption of polyolefin elastomer (POE) encapsulants, with a lower water vapour transmission rate (WVTR) and a lower water absorption, prevented this degradation from taking place. The observed degradation kinetics was much faster than the one observed in conventional c-Si solar cells encapsulated with EVA [153], [154]. Production of acetic acid in PV modules usually takes around 2000-3000 hours [155], [156]. Therefore, the degradation in these SHJ-based modules is not caused by acetic acid, but it must be rooted by some different degradation mechanism, potentially water ingress.

Recent publications have also reported on DH induced degradation on Cu-plated SHJ solar

cells [157]. As we mentioned previously, the availability and cost of Ag can constitute a bottleneck for the mainstream adoption of SHJ solar cells in the industry. Therefore, this type of technology can be an effective alternative and assist on the efforts of commercializing SHJ-based PV modules. Karas et al. performed DH testing on SHJ solar cells encapsulated with EVA and POE in G/G and G/BS configurations. Similarly to what reported by Park et al., G/G modules encapsulated with EVA degraded the most, whereas the ones encapsulated with POE showed slower degradation kinetics. The degradation was driven by losses in V_{OC} , I_{SC} and FF, caused by increased recombination and series resistance. The limited moisture ingress provided by the G/G configuration prevented part of the higher degradation observed in G/BS modules, driven by passivation losses. Thus, it emphasizes the sensitivity of SHJ solar cells to moisture ingress and to possible interaction with the encapsulant and other module/cell materials.

The effect of DH on industrial size SHJ solar cells was further studied by Liu et al. [158]. The degradation of unencapsulated bare SHJ solar cells exposed to a hot and humid environment was attributed to the susceptibility of the a-Si:H/c-Si interface to moisture. Fourier-transform infrared spectroscopy (FTIR) measurements indicated the formation of silicon-oxygen (Si-O) bonds, suggesting the oxidation of the a-Si:H layers, with an impact on the passivating properties of these layers. In the same work, the authors proposed the application of capping layers made of SiN_x and silicon oxide (SiO_x) to the surface and the edges of the TCO layer, demonstrating the possibility to fabricate unencapsulated damp-heat resistant solar cells.

We further investigate the mechanism of DH-induced degradation and its root mechanism in Chapter 4.

Potential-induced degradation

Analogously, whereas PID on conventional c-Si cells and thin-films is a relatively well-understood phenomenon, SHJ solar cells/modules have been believed for a long time not to suffer from exposure to high potential differences with respect to ground [61], [86]. This is because the TCO capping the a-Si layers – generally an ITO layer – does avoid charges to accumulate at the encapsulant/TCO interface; this is an effect generally observed for conventional ARC layers with charges accumulating at the SiN_x layer when this layer is highly resistive. Nevertheless, recent works have reported the possibility of SHJ cells/modules to similarly suffer from PID, despite the kinetics seeming to be slower. Yamaguchi et al. reported PID on SHJ solar cells exposed to dry conditions – differing from the test conditions defined in the IEC 61215 standard [67], i.e. 85°C and 85% RH – and very high voltages (i.e. -2 kV) encapsulated in a G/BS configuration [104]. A clear two-step degradation mechanism was reported. In the first step, a loss of current due to the degradation of the TCO layer (a tungsten-doped (W-doped) IWO layer) was observed. After 30 days of the test (i.e. more than 7 times the test duration defined in the IEC 61215), the reported mechanism changed, and a loss of passivation was also observed. They attributed this to the introduction of sodium ions (Na^+) into the solar cell, disrupting the a-Si:H/c-Si interface.

Our contribution to this topic is developed in Chapter 5.

UV exposure

Studies about the impact of UV on the long-term performance of PV modules, particularly on modules encapsulated with EVA, have increased in recent years [159]–[161]. However, much research needs to be done on the effect of sunlight on novel solar cell architectures, particularly the SHJ technology. In 2020, Sinha et al. reported a higher UV induced degradation (UV-ID) for high-efficiency technologies [162]. SHJ technologies, in particular, showed high sensitivity to UV-ID, with a higher susceptibility of the rear side. Losses in FF and V_{OC} drove the degradation. This was attributed to an increased recombination current due to defect generation at the a-Si:H/c-Si interface. In further studies, the previous results were completed by performing X-ray photoelectron spectroscopy (XPS) measurements on the rear side of the cell [163]. The authors reported a change in chemistry at the rear side by the diffusion of Si towards the cell's surface and the formation of Si-O_x bonds.

Other works have reportedly attributed this UV-ID to the use of an inappropriately chosen encapsulant. Witteck et al. reported that the use of UV-transparent polymers could result in a module power loss on PERC solar cells (not SHJ cells) after UV irradiation exposure [164]. The effect of this degradation was an increased surface recombination, with a loss of passivating properties. The authors indicated that encapsulants with a UV cut-off of lower than 353 nm could cause Si-H bond breakage, compromising the passivation. Photons below a wavelength of 353 nm would have a high enough energy to break the Si-H bonds of 3.5 eV. Therefore, the authors stressed the fact that encapsulants with a UV cut-off higher than 353 nm (or non-UV-transparent encapsulants) should be used to ensure a good UV stability. Similarly, to protect SHJ cells from UV-ID, we highly suggest avoiding the adoption of UV-transparent polymers to encapsulate these cells. The possible use of down-converters (UV to visible), as reported by CIC and Maxwell, would also be a mitigation strategy against such phenomena [165].

3.5 Discussion: targeting service lifetimes of 35+ years for SHJ modules

Currently, most manufacturers offer performance warranties of 25 years with a maximum power loss of 20% and a linear degradation over time. However, the industry, as a means of product differentiation, strives to increase the service lifetime of PV modules and systems. Thus, several companies are considering extending performance warranties to 30 or even 35+ years. This can prospectively be done by fully understanding the weaknesses of a specific module configuration and by taking steps towards improving them.

The comparison of the reported PLRs of the different solar cell technologies is presented in Figure 3.6. As mentioned above, for simplicity, studies reporting degradation rates often

assume linear degradation curves. The degradation kinetics of SHJ technology, with median PLRs of 0.56 %/year and 0.80 %/year for all and for the high-accuracy data-sets, respectively, position itself between previously reported degradation rates of conventional c-Si (i.e. 0.5 %/year) and that of thin-film (i.e. 1.0 %/year) technologies [130].

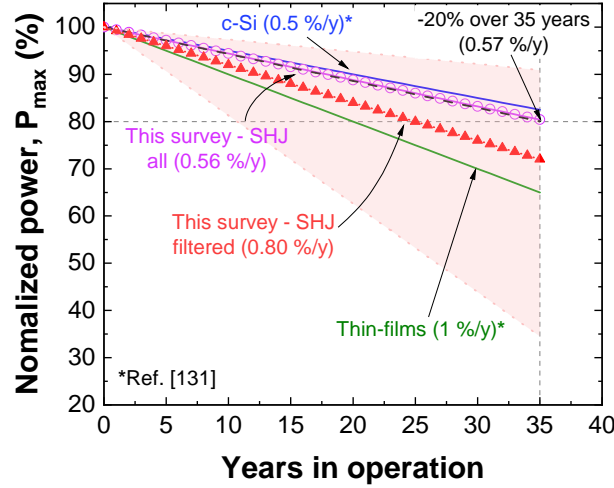


Figure 3.6: Performance loss curves – assuming a linear degradation at constant degradation rate – using the PLRs obtained in the survey for: median degradation rates analyzed in this survey, for all data-sets (purple) and for the selected ones (red). These trajectories fall in-between the boundaries reported in the literature for more mature solar cell technologies, i.e. conventional c-Si (blue solid line) and thin-films (green solid line) [130]. The performance loss curves corresponding to the maximum and minimum PLRs reported in this survey are indicated in dashed red lines, and the area between them (light red) indicates the variability in degradation rates observed in this meta-analysis. A black dashed line has been added to the chart: this trajectory corresponds to a PLR of 0.57 %/year, consistent to a 20% module power loss after 35 years in operation.

A definition of lifetime is arbitrary, depending on the end application and the system used. A frequently used definition of lifetime for modules/systems refers to a threshold (power loss beyond a definite limit) corresponding to 80% of the initial nominal power of the device. Therefore, if we stick to this definition assuming a linear degradation rate and targeting an operational lifetime of 35 years, this would correspond to a maximum allowed degradation rate of 0.57 %/year. This trajectory is shown in Figure 6 - together with the trajectories for the degradation rates reported above. The mean PLR obtained for SHJ modules in our analysis (all data) is in line with this trajectory, consistent with a lifetime set at 35 years. Conversely, the PLR values (i.e. 0.80 %/year) that we obtain when filtering out data-sets that we do not perceive as highly accurate are slightly higher. All efforts for an improved SHJ cell and module reliability should be directed to target this goal, which seems to be within reach (particularly if we understand well the root causes of technology-specific failure modes). Understandably, in order to do this, further investigations and R&D activities are needed.

3.5. Discussion: targeting service lifetimes of 35+ years for SHJ modules

In this work, we have reported the main failure modes observed for SHJ modules. These include, for field-deployed modules, V_{OC} losses ascribed to a loss of the passivating properties of the a-Si layers and I_{SC} degradation from absorption losses due to encapsulant browning [137], [141]. On the other hand, indoor accelerated ageing tests highlight the sensitivity of SHJ solar cells to water/moisture ingress, high voltages and UV exposure. The former can realistically be associated to losses in passivation properties observed in several studies [157], [166]. Additionally, we discussed the effect of UV irradiation on the encapsulants and SHJ solar cells. A poor encapsulant selection may result in both polymer discoloration, such as the browning reported in this survey, and on a degradation of the passivating properties of the SHJ cells if an encapsulant with a low UV cut-off is used.

However, most of these studies suggest ways to reinforce the module structure making SHJ prospectively more reliable, and highlighting the importance of understanding the physics behind the observed degradation mode. These strategies include:

1. The adoption of encapsulants with a low WVTR and water absorption (e.g. POs) to minimize water ingress. Alternatively, in G/G structures, the use of an edge seal in combination with a mainstream encapsulant such as EVA has been demonstrated to protect the modules from moisture, and to degradation modes associated to water ingress.
2. The adoption of high-volume resistivity encapsulants (such as POs) to prevent diffusion of Na^+ ions (and leakage currents) when a high voltage potential is applied between the SHJ solar cells and the grounded module frame, preventing PID. Additionally, as we have seen that Na^+ migration can also impact the passivation, we also expect that the nature of the front and back TCOs plays a role in promoting or slowing some of the degradation mechanisms. This can be strongly linked to the materials and processing parameters used in the cell fabrication.
3. UV-ID can be prevented by using encapsulants that are not transparent to UV or polymers with a UV cut-off higher than 353 nm to prevent Si-H bond breakage. The use of down-converters to convert UV to blue/visible light would also be a potentially effective approach to prevent UV-ID.
4. The approach of using a rear-emitter solar cell architecture in place of a front-emitter one, to prevent losses in the cell passivation properties upon exposure to light (when an insufficiently thick front (p) a-Si:H is used).

In conclusion, a deep understanding of the root cause specific to the failure modes of SHJ cells/modules is required to find solutions. Apparently, strategies to overcome these limitations exist and may transform a service lifetime of 35 years for SHJ modules into a realistic target.

3.6 Conclusions

We have performed a literature survey on the reliability and long-term performance of SHJ modules installed in the field. Understandably, most (but not all) of the data-sets reviewed in this survey refer to the HIT technology from Sanyo/Panasonic, the first company to manufacture and commercialize this technology. However, accessing statistically reliable data can be a point of concern. We therefore analyse the caveats particular to this type of survey, such as the mix of high- and low-accuracy data-sets, the combination of degradation rates for both modules and array/systems others. Further, we highlight the limits of the transferability of the observed results to SHJ modules of other manufacturers with different cell types and module structures (e.g. glass/foil vs glass/glass).

From this survey (54 data-sets from 14 publications), we obtain for SHJ modules median and average PLR of 0.56 %/year and 0.70 %/year, respectively. These numbers are absolutely in line with PLR generally reported for field-deployed c-Si modules.

We then filter out data-sets that we perceive as less accurate (because of the lack of clear information about the monitoring systems, practices, or methodology used) and obtain slightly higher PLR values for SHJ modules: 0.80 %/year and 0.83 %/year for median and average values, respectively. As reported by several authors, these numbers fall between PLR of c-Si and thin-film modules.

In addition, some mild correlations of PLR to the different climates of the installations have been noticed, but current available data on outdoor performance of SHJ based modules is still scarce. We find a considerable variability for each climate, particularly in temperate climates. Not without surprise, we observe that statistically, the highest median PLR corresponds to modules installed in these climates. Surprisingly, data points reported from arid and tropical climates, subjected to harsher environmental conditions, show lower PLR values. Still, these preliminary correlations may be due to the limited number of studies surveyed in this work. Further investigations are therefore required to obtain a higher degree of confidence in the observed correlations.

Moreover, we also report that, conversely to what generally happens to more conventional c-Si technologies deployed in the field for several years, many SHJ modules present performance losses caused by the degradation of the V_{OC} , which can be attributed to a loss in passivating properties of the a-Si layers. Furthermore, the literature survey points out that most of the modules experiencing higher degradation rates (>1 %/year) suffered (possibly in combination with other degradation modes) from encapsulant discoloration. Although this failure mode is not intrinsic to the SHJ technology, a correct selection of the encapsulant and its resistance against long-term photo-degradation (induced by combined exposure to UV, humidity and heat) is critical in guaranteeing the performance of the module over time.

In this thesis, we mainly focus on the sensitivity of SHJ to moisture and high voltages. In Chapter 4, we investigate the degradation mechanism on DH conditions, isolate the cell

and module components' roles and propose a degradation model. Next, in Chapter 5, we complement the study by understanding the impact of high negative and positive voltages at the module and cell levels. We also present a multi-factorial microscopic model combining high humidity and voltage conditions. We then propose mitigation strategies - for both DH-induced degradation and PID - at the module level. Finally, in Chapter 6, we aim at developing PID-resistant SHJ technology at the cell level.

4 Sensitivity of SHJ Solar Cells and Modules to Moisture Ingress

The work in this chapter is based on the following article submitted to a journal, and presented at the WCPEC-8 in Milan, 2022:

- L. Gnocchi, A. Virtuani, O. Arriaga Arruti and C. Ballif, *Insights into the sensitivity of Silicon Heterojunction (SHJ) solar photovoltaic modules to water ingress: a detailed microscopic model.*, submitted to Cell Reports, 2023 [109].

The experimental work reported in these publications was separated into two parts: the mini-module manufacturing, testing, characterization and data analysis, as well as the sample preparation for microscopic measurements, were performed by me, and the FTIR measurements and Na⁺ droplet test were done by Dr. Luca Gnocchi. The final tests on decoupling the role of the cover glass were done in conjunction. The brainstorming to conceptualize the degradation model was done with the other co-authors of the article submitted to *Cell Reports*. The manuscript was drafted by Dr. Luca Gnocchi and Dr. Alessandro Virtuani, and I provided inputs and corrections. We gratefully acknowledge Dr. Quentin Jeangros for the SEM measurements.

Abstract

With 268 GW of newly added capacity and global installations reaching the milestone of 1 TW of cumulative capacity in 2022, solar photovoltaic electricity continues its exponential growth, demonstrating its competitiveness and its pivotal role in the energy transition. With the primary goal of reducing further overall costs and solar's levelized cost of electricity, the technology is rapidly evolving focusing on two main drivers: i) increasing device efficiencies, and ii) extending service lifetimes. In this chapter, we focus on one of the most promising technologies (i.e. with the highest efficiencies and a strong market potential for the coming decade), the silicon heterojunction (SHJ) cell, and point out how to make it more reliable and durable in high-humidity conditions, overcoming a degradation mechanism that seems

specific to the technology.

4.1 Introduction

Novel high-efficiency photovoltaic (PV) technologies are required to demonstrate high stability in order to ensure their continuous deployment. In particular, silicon heterojunction (SHJ) solar cells, having demonstrated efficiencies up to 26.81% [36] and higher open-circuit voltage (V_{OC}) and fill factor (FF) values over other technologies [167], are key to further drive the growth of PV in Europe. Moreover, the natural symmetry of the SHJ architecture makes it possible to fabricate bifacial devices easily enabling the absorption of the reflected light from the rear side [168].

In past years, a mass-market entrance has been delayed though by some negative perceptions concerning the maturity of the technology. These include the difficulty in achieving homogeneous ultra-thin passivation layers, the relatively high cost of high-quality n-type silicon wafers, the adoption of a transparent conductive oxide (TCO), and the high silver (Ag) consumption [168]. However, as explained in Chapter 3, a market share of 20% is expected for this technology by 2030 [15]. Reflecting this target, in very recent years, several companies have launched pilot production or even mass production of SHJ solar cells and modules in Asia and Europe. Some companies have noticeably recycled equipment for the deposition of thin-film silicon solar cells for coating the passivating layers of SHJ structures [169], [170].

When considering SHJ PV modules we want to stress that generally, the industry uses polyolefin (PO)-based encapsulants rather than the widely employed, ethylene vinyl acetate (EVA) which is however less expensive and easier to process. As explained in Chapter 3, in the presence of humidity, SHJ performs better when a PO polymeric foil is used in both the glass/foil and glass/glass (G/G) configurations [157], [171]. Nevertheless, the root cause behind the high sensitivity of the SHJ technology to moisture is generally not understood. Here, we investigate in detail the degradation mechanism and propose a microscopic model highlighting the root causes behind the poor damp heat (DH) performance of SHJ G/G modules when EVA is used as an encapsulant. The degradation mechanism seems to be specific to SHJ cells and modules, as no sign of degradation can be observed when using main-stream passivated emitter rear cells (PERC) as a control technology [172].

4.2 Experimental methods

4.2.1 Sample design and fabrication

We manufactured single-cell G/G modules using standard 6" bifacial n-type rear emitter SHJ cells. A cross-section of the SHJ cell is presented in Figure 4.1. The module design comprised front and rear plates with a 3.2 mm-thick solar-grade soda-lime glass and a commercial EVA roll.

Modules were subjected to accelerated DH testing (i.e. 85°C and 85% RH), for up to 2000 hours, with the electrical performance of the module and physical characteristics of the materials monitored at regular intervals.

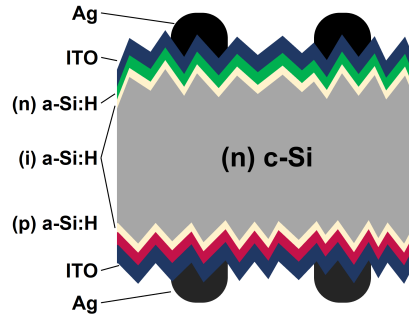


Figure 4.1: Schematic of the bifacial rear-emitter SHJ solar cells used. The cell is not drawn to scale.

Three different encapsulation structures were employed, as shown in Figure 4.2.

- a) Standard G/G module scheme.
- b) Glass-free modules in which the front and rear glass covers were replaced by two ethylene tetrafluoroethylene (ETFE) foils. The surface of the ETFE foil exposed to the external environment had the classical hydrophobic property of fluoro-based polymers. The inner surface (i.e. the one in contact with the EVA) was chemically treated to promote a good adhesion to the encapsulant. This configuration was used to compare degradation in the presence or absence of a potential sodium source (i.e. the soda-lime glass plate).
- c) SHJ cell encapsulated between two layers of EVA, without an external glass, backsheet or ETFE layer.

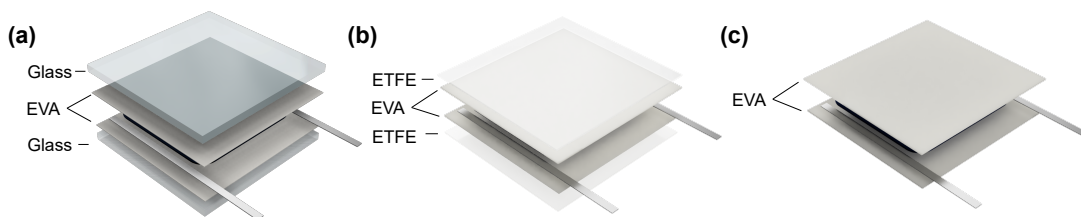


Figure 4.2: Schematic of the different samples design used: (a) standard G/G layout; (b) "glass-free" configuration in which the front and rear plates are replaced by a transparent hydrophobic ETFE foil; (c) SHJ cell sandwiched between two layers of EVA only.

Additional samples that we manufactured and tested include:

- bare cells to investigate the effect of moisture directly on the solar cell;

- double-side polished (DSP) (i.e. non-textured) wafers with different coatings (a-Si:H and a-Si:H/ITO) as seen in Figure 4.3 (a)-(d), to compare the effect of water exposure on the n-doped and p-doped sides of the cell and the presumed protective role of the external ITO layer.

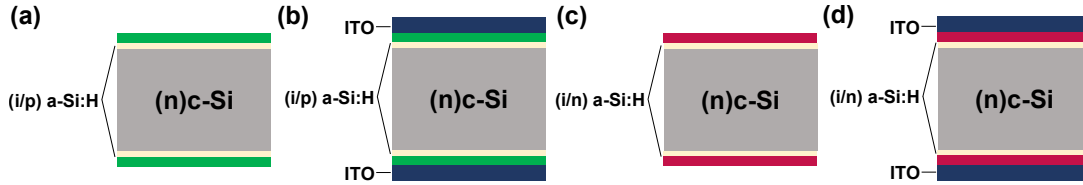


Figure 4.3: Schematic of the different layer stacks used on n-type double side polished wafers wafer: (a) (i/n) a-Si:H layer, (b) (i/n) a-Si:H layers with ITO, (c) (i/p) a-Si:H layer, (d) (i/p) a-Si:H layers with ITO. The layers are not drawn to scale.

4.2.2 Module characterization

During the ageing test, samples were periodically monitored to characterize both the front and rear sides. Single-cell modules were visually inspected, and light current-voltage (I-V) characteristics were measured at standard test conditions, STC (25°C and light intensity of 1000 W/m²). The main optoelectronic properties monitored included the power at maximum power point (P_{max}), short-circuit current (I_{SC}), V_{OC} , and FF. Electroluminescence (EL) imaging was performed by forward biasing the cells with a current close to 8.5 A (i.e. the cell's I_{MPP}). Additionally, we performed external quantum efficiency (EQE) measurements.

4.2.3 Cells and materials characterization

The stability of metallization lines (i.e. the fingers, busbars, and ribbons) and the electrically conductive adhesive (ECA) were analyzed by scanning electron microscopy (SEM). Double-side-polished Si wafers were characterized by Fourier transform infrared (FTIR) spectroscopy in order to collect information about the formation of new chemical bond groups on the different cell layers due to the presence of moisture. Additionally, photoluminescence (PL) images were taken to effectively and swiftly compare the evolution of the cell degradation for the different module structures.

4.3 Results

4.3.1 Module electrical characterization

The normalized values of the electrical parameters (i.e. P_{max} , I_{SC} , V_{OC} and FF) extracted from I-V measurements and EL images measured on standard G/G mini-modules (assembled with bifacial SHJ cells and encapsulate with EVA), exposed to DH-ageing conditions [67] are

presented in Figure 4.4. The measurements throughout the extended DH testing of 2000 hours of the front and rear sides of the laminates are shown in Figures 4.4 (a) and (b), respectively. We note that the loss in performance at the front side is more significant than at the rear side.

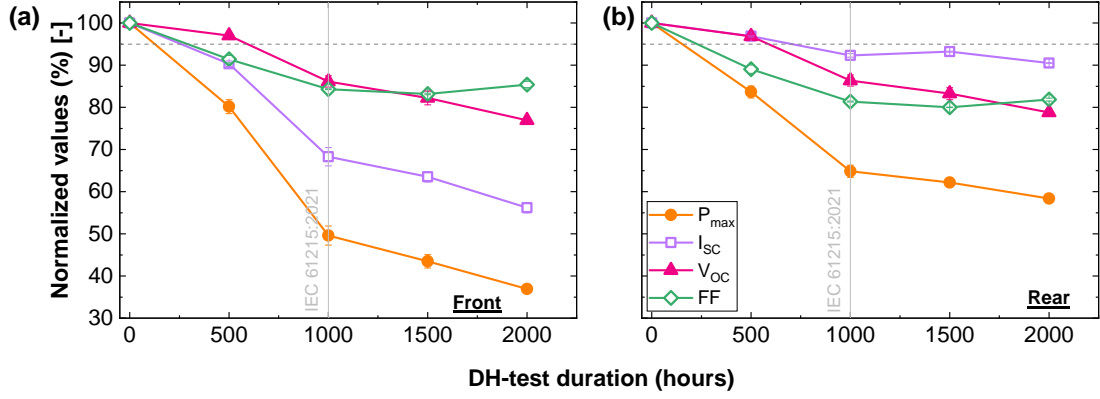


Figure 4.4: Normalized values of electrical parameters with respect to initial measurements standard 1-cell G/G modules measured from the (a) front and (b) rear sides of the module, throughout the extended 2000 hours of DH testing.

Besides the strong P_{max} degradation experienced after 2000 hours (i.e. 63% and 42% for the front and rear sides, respectively), what is even more surprising is the pronounced reduction in performance experienced by our samples just after 500 hours of testing (i.e. P_{max} losses at 20% and 16% at the front and rear). For most combinations of cells such as PERC and encapsulants (including EVA), devices are reportedly stable in DH – when using state-of-the-art materials – at least until the first 1000 hours of test duration [172] (or even much longer if the right bill of material (BOM) is used).

Therefore, what we observe here seems to be a degradation mechanism peculiar to SHJ solar cells, confirming the high sensitivity of this technology to moisture and water ingress, which consequently requires dedicated efforts to be prevented.

The degradation mechanisms on both sides are also different. While a significant loss in I_{sc} is observed for the front side, followed by losses in V_{oc} and FF, the degradation at the rear seems driven by a reduction in V_{oc} and FF (more or less equally). Figure 4.5 shows the comparison between I-V curves (Figure 4.5 (a)) and the EQE (Figure 4.5 (b)) from the illuminated front and rear sides of the mini-modules, before and after 2000 hours of exposure in DH. The reduction in EQE from the front side is more evident for short wavelengths (i.e. charge carriers generated close the illuminated surface), whereas the reduction is more significant for longer wavelengths (i.e. distant from the illuminated surface) when the laminates are measured from the rear side. We assume that this enhanced recombination at the front side is induced by a loss in passivation, hindering the collection of charge carriers generated at the front.

EL images, shown in Figure 4.5, indicate that the degradation is initiated at the edges and spreads over all the solar cell area as the testing is extended to 2000 hours. By the end of the test,

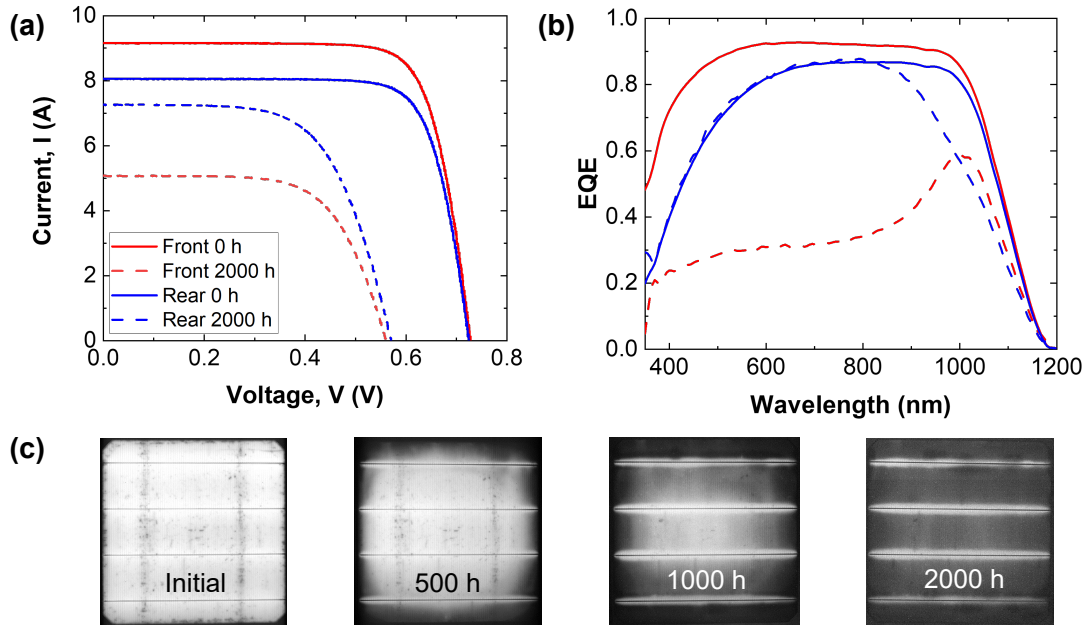


Figure 4.5: (a) I-V curves and (b) EQE curves of the front (red) and rear (blue) sides of our SHJ G/G modules before (solid lines) and after (dashed lines) 2000 hours of DH testing; (c) EL images taken periodically of the front side of the G/G mini-modules during DH testing.

the laminate exhibits an overall homogeneous degradation. We remark that the sandwiched encapsulant is exposed to the environment (i.e. high humidity conditions) from the sides of the module when packaged in a G/G scheme. Taking into consideration the observed edge effect and the progression of the degradation, as well as the pathways for moisture to enter the modules, we assume that these phenomena are induced by the moisture ingress in the laminates.

The assumption was confirmed by Gnocchi [172], who correlated the degradation rates with the moisture ingress within the mini-modules. Based on the water-ingress modelling described in previous works [61], [173], the water concentration profiles within the laminates were linked to the different stages of the DH-induced degradation process. It was demonstrated that darkened areas observed in the EL images in Figure 4.5 (c) correspond to a water concentration close to the saturation value. That is, in the case of the 500 hours of DH exposure, for which the laminates exhibit degradation on the outer part of the cell, the edges are saturated with moisture. The same correlation was observed for the measurements corresponding to 1000 hours, for which the center of the mini-module is saturated with water. Besides confirming the correlation between moisture ingress and degradation rates, it was established that the water content should be close to a saturation concentration in order to observe degradation. Here we want to stress the fact that mini-modules – due to their limited size - are expected to be more sensitive than large-area G/G modules, for which water ingress at the center of the module would be considerably delayed, as shown by Mittag et al. [174].

4.3.2 The role of module components in degradation mechanism

Once understood the direct correlation between water ingress and DH-induced degradation, we focused on investigating the root cause(s) of the degradation mechanism itself. In order to do that, we identify the contributing factors and the role of different module components in the degradation mechanism. In the next sections, the following cell and module materials are studied:

- passivating cell layers and interfaces;
- cell and module interconnections;
- EVA encapsulant;
- glass covers.

Passivating cell layers and interfaces

The results in the previous sections indicated that the performance degradation was partly due to a loss in passivation (i.e. reduced V_{OC}). To assess the influence of moisture on the surface properties of the Si wafers and, particularly, the passivating a-Si:H layers, we subjected a set of non-encapsulated Si wafers to DH and looked for modifications of the cell surface using FTIR spectroscopy. Samples were DSP (i.e. non-textured to avoid FTIR signal losses after the signal passed through the sample) Si wafers with a-Si:H films and a-Si:H/ITO layer stacks deposited on both sides.

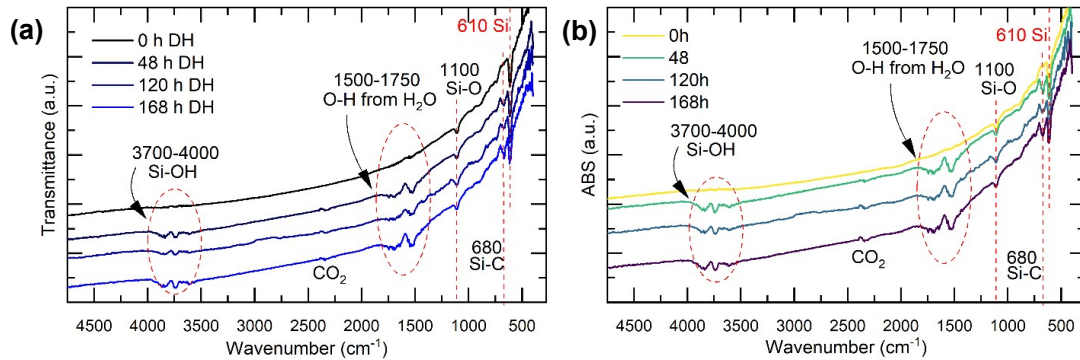


Figure 4.6: FTIR spectra performed on DSP Si wafers coated with (a) (i/n) a-Si:H layers and (p) (i/n) ITO layer stacks before and during DH ageing.

Figure 4.6 presents the transmittance spectra recorded at regular intervals during the ageing test of a-Si:H and a-Si:H/ITO double-coated samples (Figure 4.6 (a) and (b), respectively). The peaks at 610 cm⁻¹ and at 1100 cm⁻¹ were attributed to the phonon absorption of the silicon lattice [175] and the presence of Si-O bonds. We note that non-tested samples also displayed the latter peak, most probably due to the formation of a native oxide layer formed

after exposure to the air. During DH exposure, new peaks were detected at 680 cm^{-1} , in the $1500\text{--}1750\text{ cm}^{-1}$ range and from $3700\text{ to }4000\text{ cm}^{-1}$. Those peaks were assigned to Si-C [175], the O-H groups of water molecules, and the formation of Si-OH [176], respectively. Similar results were recently observed by Liu et al. [158], who noted the formation of Si-O bonds in SHJ cells upon exposure to a hot and humid environment. Conversely, Si-H bonds were never observed. The absence of Si-H bonds could be related to the thickness of the a-Si:H layer, which was probably too thin (i.e. 4-5 nm) to be detected experimentally. As the same spectra modifications and peak formations were obtained in both samples, with and without an ITO, we conclude that the ITO does not act as a protective layer for the underneath a-Si:H films.

Other TCO configurations such as aluminium zinc oxide (AZO) are reportedly very sensitive to DH-induced degradation [177]–[180]. Environmental molecules (e.g. water molecules) and hydroxyl (OH^-) groups can diffuse through the grain boundaries and react with the AZO [177], [180]. Moreover, OH^- can also be adsorbed or chemisorbed (i.e. create chemical bonds) in the grain boundaries, increasing grain-boundary scattering and, hence, acting as traps for charge carriers and reducing mobility [178], [179].

We speculate that due to the crystalline morphology of the ITO, hydroxyl groups - which have the highest diffusion rates [180] - can adsorb in the grain boundaries and diffuse through them, potentially reaching the passivating layers. The OH^- groups in the ITO, as has been reported for AZO films, can increase grain boundary scattering and, thus, hinder the collection of charge carriers, resulting in increased series resistance. We dismiss the degradation of the ITO being the root cause of degradation, due to the compositional stability shown in the FTIR spectra. Nonetheless, we conclude that this mechanism is not critical enough to explain the critical degradation experienced by SHJ cells in the G/G module schemes under DH exposure.

Cell and module interconnections

High water contents inside the laminates can potentially cause degradation of the cell metalization and string interconnections, increasing the series resistance of the module (R_s) and the FF, as a consequence. The screen-printing and the ribbon-soldering processes need to be adapted for SHJ technologies to prevent degradation of the a-Si:H layers, that is, they are performed at lower temperatures. In particular, the soldering of the ribbons to the cell was done using a low-temperature curing ECA. The potential deterioration of these materials, particular to SHJ technology, needs to be considered to have further insights into the degradation mechanisms.

In our particular case, the EL image after 2000 hours of DH testing - for which the laminate shows to be significantly degraded - shows that the ribbons attached to the busbars can still inject and thus, collect, the current effectively (see Figure 4.7 (a)). Consequently, we assume that the ECA employed to solder these SHJ cells is stable and does not in fact contribute to the degradation of the modules.

We then extracted a piece (through a coring and polishing procedure developed in-house, explained in detail in Chapter 2) of a very degraded area at the edge of the module, signalled by the green rectangle in Figure 4.7 (b). SEM measurements were performed on the polished sample to assess the stability of the screen-printed Ag metallization. SEM images on the polished cross-section of the G/G module are displayed in Figure 4.7 (c). The images also indicate that the adhesion between the EVA and Ag finger and, more importantly, between the Ag finger and the SHJ cell, is good even after significant degradation. Consequently, we conclude that the cell metallization and the interconnects are not contributing to the DH-induced degradation mechanism.

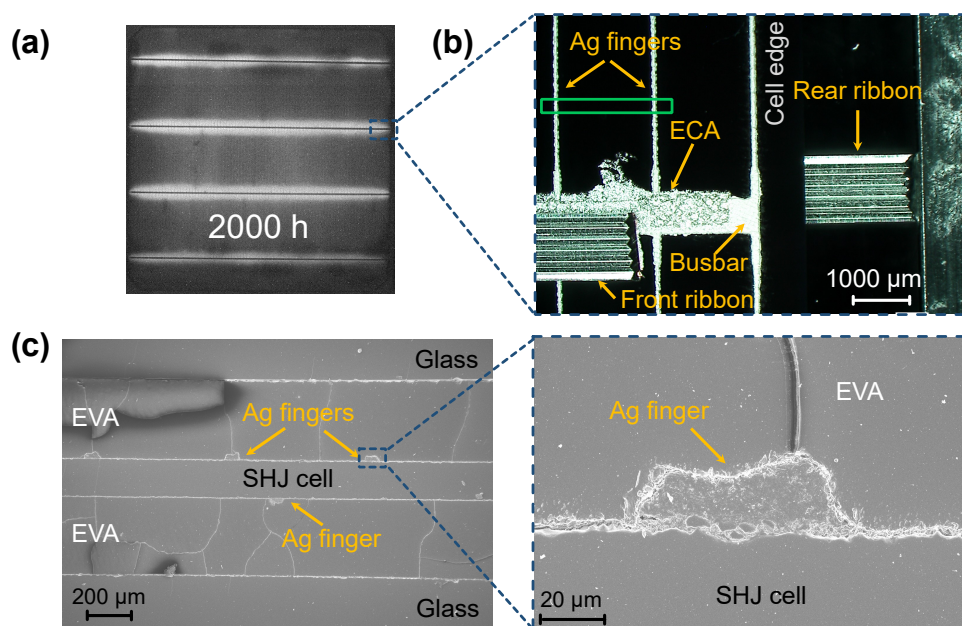


Figure 4.7: (a) EL image of a SHJ 1-cell G/G mini-module after 2000 hours of DH testing; (b) top view of the metallization of the mini-module taken by optical microscopy; (c) SEM images of a cross-section of a very degraded area of a bifacial SHJ cell encapsulated in G/G and EVA, after 2000 hours of DH exposure. The samples were prepared by a coring and polishing procedure developed in-house.

EVA encapsulant

The degradation mechanism of the EVA occurring in the presence of moisture and elevated temperature is well documented in the literature. Particularly, the hydrolysis reaction produces acetic acid [181], lowering the pH and potentially leading to corrosion of the metallic interconnections [182]. However, recent results published by Barretta et al. [159] on new encapsulant formulations (particularly EVA) indicate that these are more resistant to compositional changes when exposed to high humidity and temperature conditions.

Optical transmittance and FTIR measurements were performed on glass/EVA/glass sam-

ples exposed to DH-like conditions by Gnocchi [172]. The analyzed EVA was the same as the one employed in the mini-modules investigated throughout this work. The obtained results demonstrated that the selected EVA formulation is chemically stable in highly humid environments, and no chemical and optical changes could be detected after the extended testing.

The observed DH-induced degradation mode of SHJ modules cannot therefore be attributed to a degradation process of the EVA layer, such as the formation of acetic acid, which generally would take much longer (i.e. 3000 to 4000 hours) to form in a hot and humid environment in the absence of UV radiation (i.e. dark) like DH-test conditions.

Glass covers

To have further insight into the role of the glass covers, several different glass-free modules were manufactured and subjected to DH testing: (1) a bare SHJ cell with no protection; (2) a SHJ encapsulated within two layers of EVA only; (3) a SHJ cell encapsulated with EVA and an ETFE foil. PL images were performed on all samples prior to and after 500 hours and 1000 hours of DH testing and were compared to those of the G/G single-cell modules (see Figure 4.8).

In Section 4.3.1, we linked the strong degradation to the presence of high water concentrations (i.e. close to the saturation value). Thus, we expected the SHJ bare cell to degrade significantly (i.e. reduction of the PL signal) after a few hours of exposure – for which we assumed a condition of complete water saturation. Contrarily, as shown in Figure 4.8 (a), the PL images exhibited a good signal on a large portion of the cell surface after 500 hours of testing. We then extended the DH test to 1000 hours. Despite a significant reduction in the PL signal, the cell remarkably still exhibited some luminescence. Surprisingly, even better results were obtained on the SHJ encapsulated with EVA only, as shown in Figure 4.8 (b). The corresponding PL images performed after DH exposure to 500 hours and 1000 hours showed that the presence of only the encapsulant foils did not lead to a significant degradation in cell performance, even if we expected the polymeric encapsulant to reach full water saturation after being exposed to some dozens of hours only in a highly humid environment. Therefore, the exclusive role of water - as generally assumed - in explaining the observed degradation phenomenon should be dismissed. Additionally, the adsorption of hydroxyl groups in the ITO and the formation of Si-OH bonds, which can be expected in the a-Si:H layers or at the a-Si:H/c-Si interface, are not enough to explain the overall degradation mechanism. In other words, these results indicate that SHJ cells and modules are not sensitive to just the presence of water.

The loss in performance in the PL signal (and the EL signal, shown in Figure 4.5 (b)) is considerable and much higher for G/G modules than for any other sample. These results point out the role of the glass cover in the degradation process that is speculatively triggered by an interplay between the presence of water and glass.

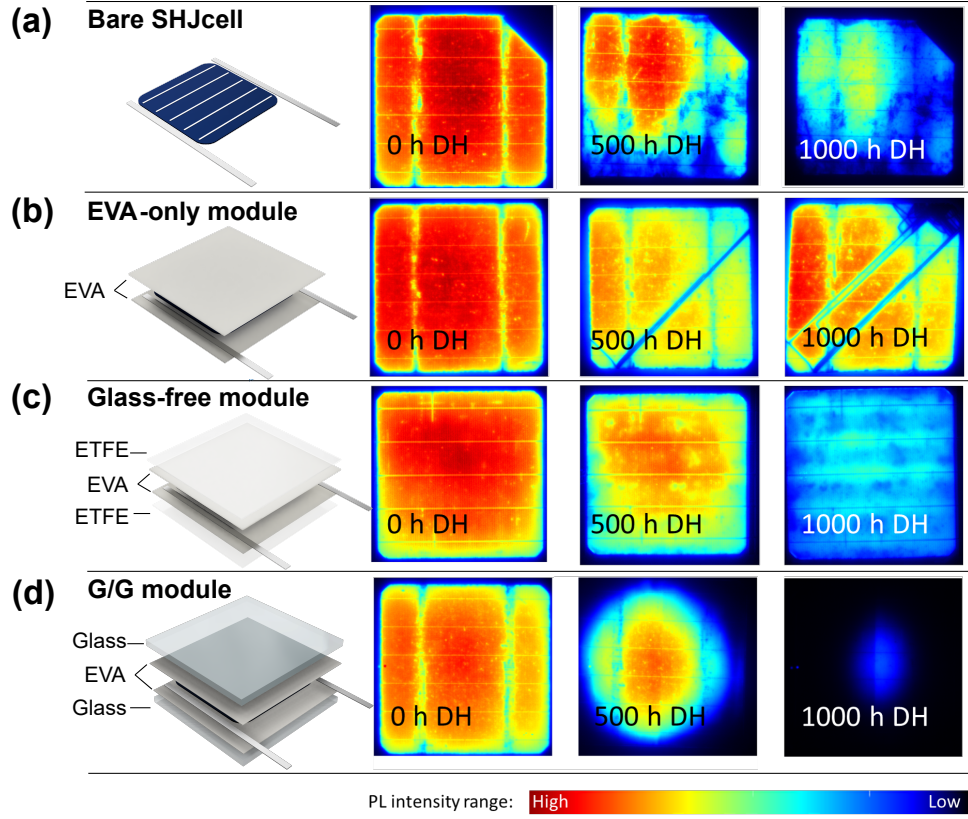


Figure 4.8: Photoluminescence images of the different module designs before and after 500 hours and 1000 hours of DH test: (a) bare SHJ cell, (b) EVA-only (i.e. EVA-SHJ cell-EVA), (c) glass-free module with the replacement of the front and rear glass plates with the polymeric film of ETFE, (d) standard SHJ G/G module encapsulated with EVA.

The sodium (Na) contained in standard solar-grade soda-lime glass is generally associated with the potential-induced degradation (PID) phenomena of PV cells. The application of a high-negative bias between the cell and the module frame can extract positively charged sodium ions (Na^+) - and other ions - out of the glass cover [61]. In the absence of a strong electric field, such as in DH conditions, however, Na is not expected to play a major role in any degradation mechanism. However, from our results, we observed that the worst degradation scenario occurs when using samples encapsulated in a G/G scheme and in presence of moisture. In fact, when the glass is replaced with another cover material, or simply not used, the modules experience a much lower degradation.

Therefore, we hypothesize that there must be a combined role of water and Na in describing the DH-induced degradation of SHJ cells. Two recent publications have pointed at the role of Na in the DH-induced degradation in the absence of an electric field [158], [183]. In fact, the high temperature and humidity of the DH test can *accelerate changes of surface and bulk chemistry representative of leaching process* as recently reported by Guiheneuf et al. [184]. The authors reported that high water contents induce the release of cations (i.e. Na, potassium and

calcium) and the hydrolysis of the Si-O-Si glass network, which can in turn cause a corrosion phenomenon at the glass surface. This corrosion mechanism (i.e. leaching process) can generate Na^+ ions bonded with OH^- groups.

We speculate that the diffused water inside the EVA triggers the leaching corrosion mechanism, leading to the formation of sodium hydroxide (NaOH) molecules at the glass/EVA interface. This aqueous solution (NaOH_{aq}), according to our hypothesis, can diffuse through the encapsulant and reach the EVA/cell interface. Then, as explained in Section 4.3.2, we speculate that the OH^- groups can diffuse through the ITO, along with the Na^+ ions.

In order to further investigate the role of the glass cover, $2 \times 2 \text{ cm}^2$ pieces of ETFE were placed between the glass and the EVA encapsulant at both sides to act as barrier layers (see Figure 4.9 (a)). The EL images shown in Figure 4.9 demonstrate that the areas below the ETFE layers do not degrade, thus the presence of ETFE between the glass and the EVA prevents DH-induced degradation. The results further confirm the hypothesis that even in DH-testing conditions, the performance loss is directly linked to the presence of the glass on top.

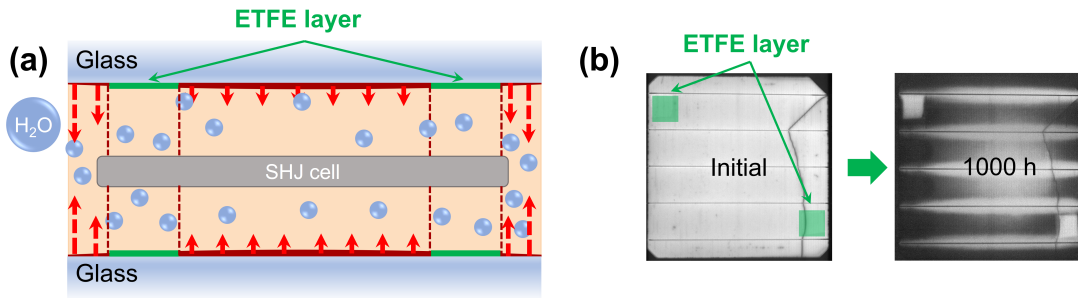


Figure 4.9: (a) Schematic section of the module (not drawn to scale) highlights that in presence of a moisture barrier the corrosion of the glass is stopped and in the corresponding area, the cell does not get damaged during DH ageing test. (b) The portion of the cell underneath the protected glass/EVA interface shows no sign of degradation after 1000 hours of exposure to DH, whereas the unprotected area shows the typical EL blackening pattern.

Na^+ droplet test

To test our hypothesis (the role of Na and the creation of an aqueous solution containing NaOH), we prepared water solutions with different NaOH concentrations (i.e. 0.01%, 0.05%, 0.1%, w/w), a test previously proposed by Adachi et al. [185]. We then placed two drops of each solution on top of the front side of an unencapsulated SHJ cell and let them dry before placing the cells in a DH chamber.

Figure 4.10 (a) presents the PL images taken before and after the DH testing. We performed the same test on a conventional PERC cell (i.e. stable in DH) (see [172]) as a reference. The results confirmed the poor stability of the SHJ cell in the presence of Na and water. The treated areas (i.e. where the drop was applied) degraded after only 4 hours of DH testing, regardless

4.4. Sensitivity to water: a multi-factorial degradation model

of the concentration of the NaOH solution. We note that the parts of the cell without this NaOH treatment did not exhibit losses in PL signal. Conversely, the PERC cell proved to be stable during the first 4 hours in DH, showing only a minor and well-localized reduction in PL intensity after 24 hours, corresponding to the higher concentrated NaOH droplet sites (i.e. 0.05%, 0.1%, w/w.) This can be attributed to the high pH value of the NaOH solution, which can eventually attack the silicon solar cell. These results additionally support the premise of encapsulated PERC cells being unstable in DH-testing conditions. This point is taken into consideration again in Chapter 7.

The results of the droplet tests reinforce these findings: (1) a combined role of Na (or NaOH) and water is needed to trigger the degradation mechanism in SHJ cells; (2) we are uncovering a degradation mechanism which is specific to the SHJ technology.

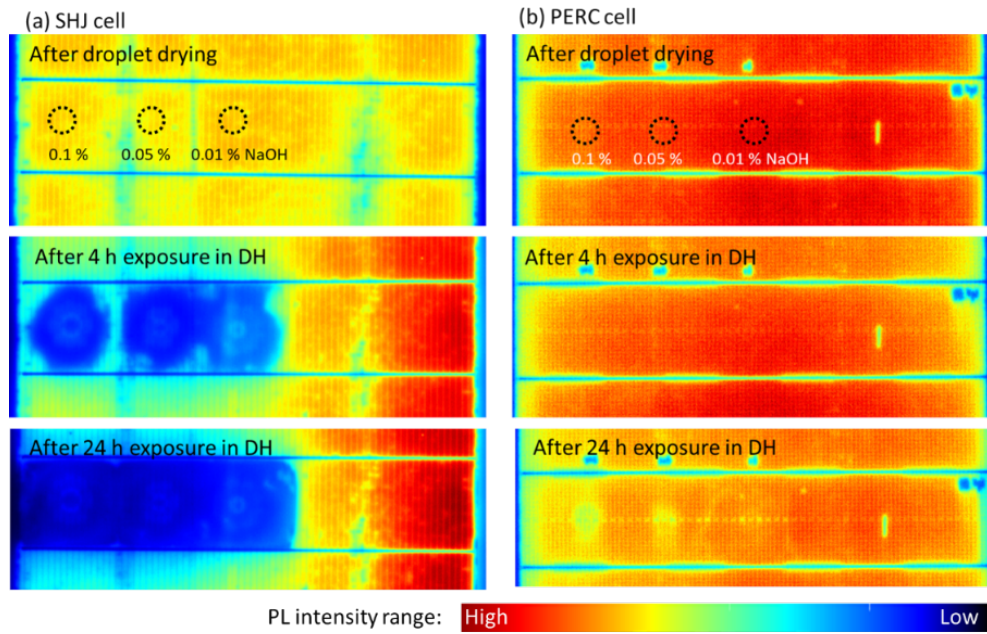


Figure 4.10: Droplet test performed with a NaOH aqueous solution. PL images of (a) SHJ and (b) PERC cells taken after having the droplets drying for different NaOH concentrations (i.e. 0.01%, 0.05%, 0.1% w/w.), and after 4 and 24 hours of exposure in damp heat conditions.

4.4 Sensitivity to water: a multi-factorial degradation model

To explain the experimental results, we propose here for the first time a detailed microscopic model which attempts to explain the root cause behind the observed degradation mechanism and the well-known extreme instability of SHJ cells/modules to moisture (even if water, as shown earlier, is only one of the ingredients of this complex degradation mechanism). The model is depicted in Figure 4.11.

1. In our model, the role of EVA (with a relatively high WVTR and water absorption, compared to other encapsulants such as POs) is instrumental in allowing a progressive ingress of water from the module's edges, which tends to reach a saturation level. This is confirmed by EL, PL imaging and the water diffusion model. In G/G module schemes, the EVA encapsulant reaches water saturation relatively fast at the edges (after only 500 hours of exposure to DH testing), progressing towards the module center, where saturation is nearly reached after ~1000 hours.
2. The contact of water with the inner face of the cover glass can promote a corrosion process, described by Guiheneuf et al. [184], in which the molecular water reacts with monovalent cations (like Na^+) present in soda-lime glass (the glass composition is given in detail in Chapter 1). The cationic atoms – in particular Na – are released from the glass network to the water film where they accumulate as a soluble precipitate with a mixture of molecular water and hydroxide ions (NaOH) [184].
3. The highly soluble NaOH molecules are able to diffuse through the polar matrix of the wet EVA polymer, reaching the SHJ cell surface.
4. Once on the cell surface, we speculate that the Na^+ ions and OH^- are able to diffuse through the crystal grains of the TCO layer. The diffusion process will depend on the morphology of the sputtered TCO film (more details on this are given in Chapter 6) [183]. These ionic species, which can be adsorbed in the grain boundaries of our ITO layer, can increase grain-boundary scattering, reducing the collection of charge carriers. Moreover, we hypothesize that these ions, Na^+ ions in particular, can reach the ITO/a-Si:H interface, create recombination centres and hence induce a loss in the passivation of the cell [186]. Simultaneously, but to a much lower extent, OH^- could also reach the aforementioned interface and displace Si-H bonds.

4.5 Conclusions

To our knowledge, we are the first to propose a detailed microscopic model explaining the sensitivity to water (and DH) of the SHJ technology. In reality, the presence of water (enabled when using EVA as an encapsulant) is only a contributing factor, as clearly indicated by the fact that both water and glass are needed to trigger the observed degradation mode. In the absence of a glass cover, the degradation is severely mitigated.

We propose that high water contents in the laminate leach the cover glass - glasses in the case of G/G module schemes - and create NaOH molecules. These can diffuse through the EVA polymer, due to its high polarity, and reach the cell surface. Then, Na^+ ions and OH^- groups can further percolate through grain boundaries of the TCO layer, hindering the collection of charge carriers. We hypothesize that these ionic species can potentially reach the ITO/a-Si:H interface and reduce the passivation of the solar cell.

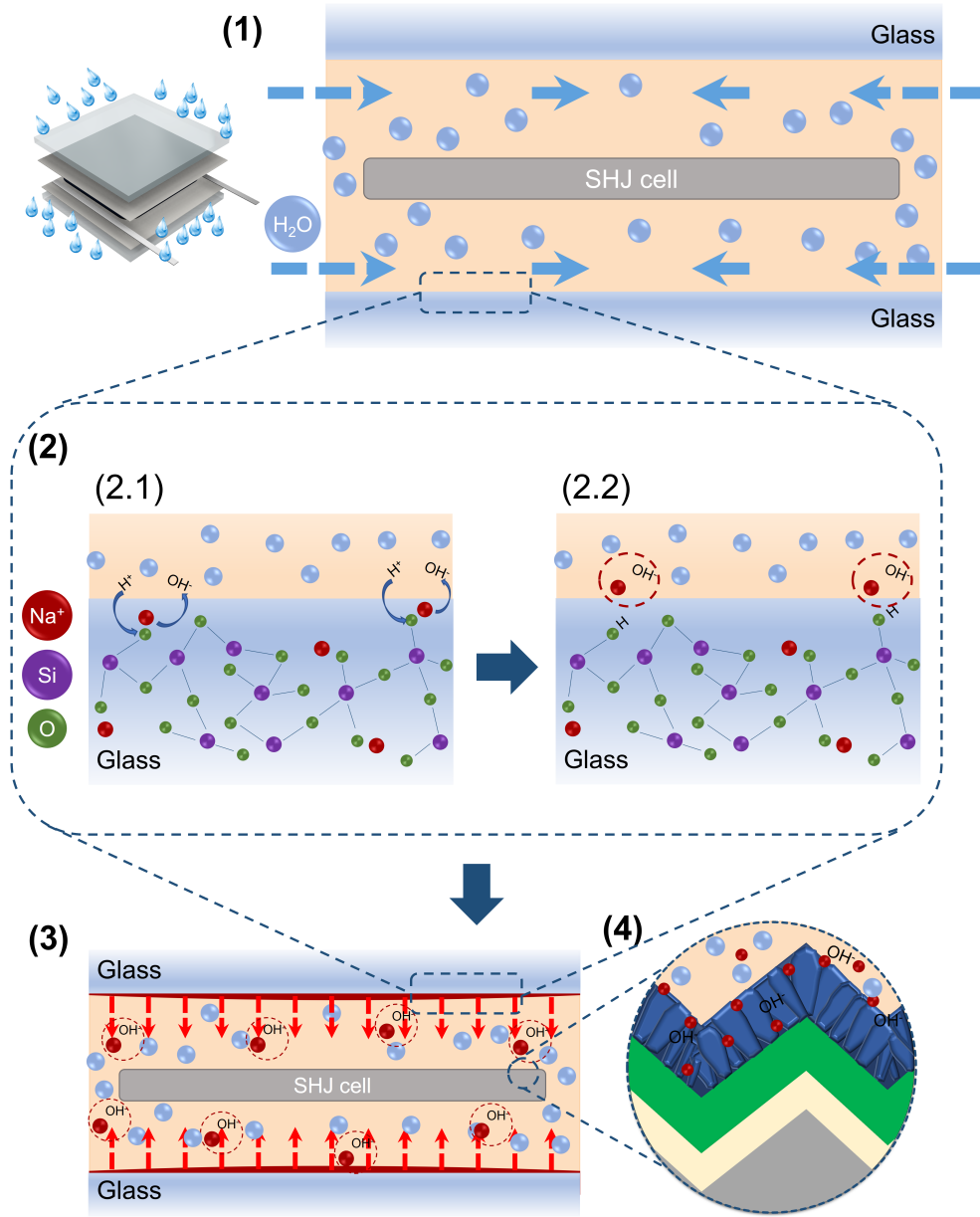


Figure 4.11: Schematic of the microscopic model proposed to explain the sensitivity to water of SHJ cells encapsulated in a glass/glass structure with EVA as an encapsulant. (1) Water ingress through the EVA from the module edge; (2) Glass corrosion process: leaching occurs in the presence of water at the EVA-glass interface with the release of Na^+ and OH^- ions which are dissolved in the encapsulant; (3) NaOH_{aq} solution diffuses through the EVA to the cell surface; (4) Na^+ and OH^- ions cross the ITO and degrade the passivation layer at the $a\text{-Si:H/c-Si}$ interface.

Furthermore, it is interesting to stress that the degradation method observed (and the explanation proposed) is specific to the SHJ technology. When using solar-grade EVA as an encapsulant material with mainstream PERC or Al-BSF solar cells, in fact, the performance of the cells in DH is quite stable, at least until the first 1000 hours (and often beyond) of

operation in a climatic chamber [172]. We assume that the different coatings and layers of more conventional solar cell structures are not impacted by the presence of dissolved NaOH and diffused through the EVA encapsulant, are This observation is reinforced by the results of the droplet test on a conventional PERC solar cell (see Figure 4.10).

Nevertheless, we cannot exclude that other sophisticated cell architectures, leading to high-efficiency devices and candidates for massive market deployment in the coming years, such as TOPCon or interdigitated back contact (IBC) cells will not be impacted by a similar degradation mechanism.

In the next chapter, we complement these results by researching the negative and positive PID mechanisms on the same bifacial rear-emitter SHJ cells encapsulated in G/G module schemes, using EVA as the encapsulating material. Moreover, we develop strategies to mitigate both DH-induced degradation and PID at the module level.

5 Degradation Model and Mitigation Strategies for PID in Bifacial SHJ Solar Cells and Modules

This chapter is based on the work submitted for publication in *Progress in Photovoltaics: Research and Applications*, which is a compilation of the works presented at various conference proceedings.

- O. Arriaga Arruti, A. Virtuani, L. Gnocchi, Q. Jeangros and C. Ballif, *Potential-Induced Degradation in Bifacial Silicon Heterojunction Solar Modules: Insights and Mitigation Strategies*, submitted to *Progress in Photovoltaics: Research and Applications*, 2023.
- O. Arriaga Arruti, L. Gnocchi, F. Lisco, A. Virtuani and C. Ballif, *Optimized Module Packaging for Silicon Heterojunction Solar Cells and Increased PID Resistance*, oral presentation and proceedings at the 37th European PV Solar Energy Conference and Exhibition (EU PVSEC), online, 2020.
- O. Arriaga Arruti, L. Gnocchi, A. Virtuani and C. Ballif, *Encapsulant Selection for Increased PID Resistance in Modules made with Silicon Heterojunction Solar Cells*, visual presentation and proceedings at the 37th European PV Solar Energy Conference and Exhibition (EU PVSEC), online, 2020.
- O. Arriaga Arruti, L. Gnocchi, Q. Jeangros, A. Virtuani and C. Ballif, *Potential-Induced Degradation Mechanism in Rear-Emitter Bifacial Silicon Heterojunction Solar Cells Encapsulated in Different Module Structures*, oral presentation and proceedings at the 48th IEEE Photovoltaic Specialists Conference (IEEE PVSC), online, 2021.

Abstract

Potential-induced degradation (PID) may be a serious concern in photovoltaic (PV) modules and plants, particularly when approaching high system voltages (1500+ V). Here, we investigate PID occurring in bifacial rear-emitter silicon heterojunction (SHJ) solar cells encapsulated in a glass/glass (G/G) module configuration with ethylene vinyl acetate (EVA)

Chapter 5. Degradation Model and Mitigation Strategies for PID in Bifacial SHJ Solar Cells and Modules

as an encapsulant. PID testing was performed at 85°C in 85% relative humidity (RH) and the solar cells were subjected to -1 kV and +1 kV for up to 800 hours. SHJ cells were found to degrade when subjected to -1 kV and, to a lesser extent when left unbiased in damp heat (DH) conditions, while the application of +1 kV prevented degradation. Although prone to PID after extended test durations, the SHJ mini-modules investigated in this study noticeably passed the industry standard (IEC 61215:2021) PID test of 96 hours. A cross-sectional microscopy analysis of the laminates subjected to -1 kV highlighted a transport of sodium (Na) through the transparent conductive oxide (TCO), reaching the amorphous Si/TCO. The samples tested in DH conditions and with positive PID test conditions did not exhibit such a migration of Na. To account for these observations, we updated a previously-proposed model describing the sensitivity of SHJ cells to water. In our degradation model, moisture in the module corrodes the glass, creating sodium hydroxide (NaOH) that then percolate through the EVA before reaching the SHJ cell. The application of a high negative bias amplifies the previous mechanism by increasing the availability of Na^+ and also enhances the drift of Na^+ through the EVA to the cell. Finally, we demonstrate that PID can be mitigated at the module level by using a high-volume resistivity encapsulant with a low water vapor transmission rate (WVTR) or by encapsulating SHJ solar cells in a configuration impermeable to water (e.g. using an edge sealant).

5.1 Introduction

Potential-induced degradation (PID) can significantly impact the performance of photovoltaic (PV) systems and modules. With power losses in the worst cases of 30% in the initial months and up to 70% to 85% for the most affected modules after a few years [83], [84], research on PID and its mitigation strategies has increased significantly in recent years. PID occurs when a high potential difference between the solar cells and the grounded frame exists, generating a leakage current through the module. The effect generally varies linearly with applied voltage and was first observed in PV systems, where modules are connected in series, with maximum system voltages of 1000 V [78]. Today the system voltage of larger PV systems is increasing to 1500 V with targets of extending these limits further, as a mean to save on balance of system (BOS) costs, such as on cabling, mounting structures, etc. Consequently, despite the considerable efforts in understanding and mitigating PID in recent years, the topic is likely to gain importance in the coming years.

PID mechanisms vary depending on the solar cell technology, as described in detail in 1. Although it was initially thoroughly investigated in conventional aluminum back-surface field (Al-BSF) cells, this is no longer the mainstream technology, since the market has moved rapidly in the last five years towards high-efficiency technologies such as passivated emitter and rear contact (PERC) solar cells [15]. These novel technologies may, however, be prone to degradation mechanisms never observed before. This is notably the case of light and elevated temperature-induced degradation (LeTID) for PERC cells [187], [188]. Similarly, the exposure to high string voltages of these new technologies may impact the cell's performance in ways that are different to that for Al-BSF cells [98]–[100]. Ensuring their long-term performance is

therefore key for investors and stakeholders.

Owing to silicon heterojunction (SHJ) experiencing a considerable increase in production in recent years, particularly in Europe and Asia [123], [124], efforts on ensuring its long-service lifetimes have recently increased. As explained in Chapters 1 and 3, SHJ solar cells were initially considered to be PID-free, due to the presence of the transparent conductive oxide (TCO) layer on both sides, which would supposedly avoid any charge (including sodium (Na^+) ions) accumulation at the interface between the encapsulant and the TCO. However, these initial tests performed by Ishiguro et al. were most probably performed on SHJ solar cells encapsulated with a high-volume resistivity encapsulant such as polyolefin elastomers (POE) [102], which is known to prevent PID.

More recently, Yamaguchi et al. have reported PID on commercial negatively-biased SHJ solar cells [103]. In their work, the authors were testing bifacial rear-emitter SHJ cells, with a tungsten-doped indium oxide (IWO) as TCO, encapsulated in a glass/backsheet (G/BS) structure using EVA as an encapsulant (more details on the referenced work are given in Chapter 3). In the initial stages of degradation, the authors reported a performance loss caused by the deterioration of the optical properties of the solar cell. Indeed, it was shown that the short-circuit current (I_{SC}) was the main electrical parameter affected by this high potential difference. The loss in current was attributed to the reduction of the IWO layer: with indium oxide reduced to metallic indium (In), parasitic absorption increased in the front TCO. The authors further investigated PID mechanisms by pre-conditioning the samples in damp heat (DH) conditions (i.e., at 85°C in 85% RH) and for varying durations [104]. In these conditions, a second degradation phenomenon was observed, with an increased degradation rate over longer periods of time.

In the present paper, we contribute to this research topic by investigating the PID of both the front and rear sides of bifacial SHJ solar cells when mini-modules are exposed to different voltage biases. The behavior and kinetics of the degradation under different bias conditions lead us to propose a microscopic model (supported by transmission electron microscopy data) describing the root causes of the observed degradation mode and highlighting a clear contribution from moisture ingress into the laminate. Finally, we complement our findings by investigating the impact of different BOMs and the permeability to moisture ingress.

5.2 Experimental methods

5.2.1 PID-stress testing

We investigated the effect of PID on bifacial rear-emitter SHJ solar cells (the same as in Chapter 4) by encapsulating them in one-cell glass/glass (G/G) module structures. As encapsulant material, we employed a 0.5 mm-thick EVA foil with a relatively high electrical resistivity ($\rho \sim 1 \cdot 10^{15} \Omega \cdot \text{cm}$), since it is known to enable the occurrence of PID. The SHJ cells were contacted by applying an electrically conductive adhesive (ECA) – with a low-temperature curing – to the

Chapter 5. Degradation Model and Mitigation Strategies for PID in Bifacial SHJ Solar Cells and Modules

busbars. The string interconnections were then soldered with a standard soldering process.

We simulated the PID conditions following the International Electrotechnical Commission (IEC) 61215-2:2021 PID test described in Table 5.1 [67]. An aluminum tape was placed at the four edges of the mini-module to simulate the presence of a metallic frame. Voltage biases of -1 kV and +1 kV were applied to the short-circuited module leads with respect to the grounded frame to analyze the effect of voltage polarization; two samples were kept unbiased as control (i.e. exposed to standard DH test conditions) (see Table 5.1).

Table 5.1: Summary of the configurations and test conditions on the PID test for the SHJ one-cell glass/glass mini-modules encapsulated with EVA.

Temperature / RH	Encapsulant	Module configuration	Voltage
85° C / 85%	EVA	G/G	-1 kV (x2)
			0 V (x2)
			+1 kV (x2)

The mini-modules were characterized during the PID testing by one-sun and dark current-voltage (I-V) curves, electroluminescence (EL) and external quantum efficiency (EQE) measurements.

We then further investigated strategies to mitigate PID at the module level focusing on the BOM. Two factors were considered: the choice of encapsulant and the effect of moisture ingress. The first one was investigated by preparing modules using six different encapsulants (i.e. ionomer, three POEs and thermoplastic polyolefin (TPO)) with various volume resistivities. The second was performed by employing encapsulation schemes with different permeability properties to water ingress: i.e., G/BS, glass with aluminum foil backsheets (G/Al-BS) and G/G with an edge seal (G/G-ES). For every module configuration, we tested two replicas with every voltage bias (i.e., -1 kV, 0 V or DH only and +1 kV).

5.2.2 Scanning and transmission electron microscopies

We investigated the underlying physical degradation mechanism of PID in SHJ solar cells by analyzing the cross-section of the devices under test by transmission electron microscopy (TEM). To do so, EL imaging was used to identify the most degraded regions of the mini modules after PID testing. These regions were cut into 1 cm² pieces using a diamond wire saw, before embedding them in an epoxy resin, and mechanically polishing the cross-section of the resin-embedded devices. The cross-sections were analyzed by scanning electron microscopy first. Then, the conventional focused ion beam (FIB) lift-out method was used to select and extract thin lamellae containing the interfaces of interest. The electron-transparent FIB lamellae were then transferred to a TEM, operated at 200 kV. Scanning TEM (STEM) and energy-dispersive X-ray spectroscopy (EDX) techniques were performed to assess microstructural and chemical changes induced by PID testing.

5.3 PID mechanism in bifacial rear-emitter SHJ solar cells

5.3.1 Influence on voltage

Six identical SHJ modules, encapsulated in a G/G configuration with a low-volume resistivity EVA were tested under -1 kV, 0 kV and +1 kV with respect to the grounded frame. The stress test conditions foreseen in IEC 61215:2021 (i.e. 85°C/85% RH for 96 hours) [67]), have been increased in terms of test duration (800 hours, almost 8 times the standard). The values plotted in the chart are the averages for each type of sample. The results summarized in Figure 5.1 show the evolution of maximum power losses over the PID-stress duration. Similarly to what was previously reported by Yamaguchi et al., our SHJ solar cells degrade when a negative bias – with respect to the grounded frame – is applied [103]. The degradation starts after 132 hours of testing and evolves linearly with time. Remarkably, the samples are stable up to a test duration of 96 hours, which would allow the samples to pass the conventional PID test defined by the IEC 61215 protocol.

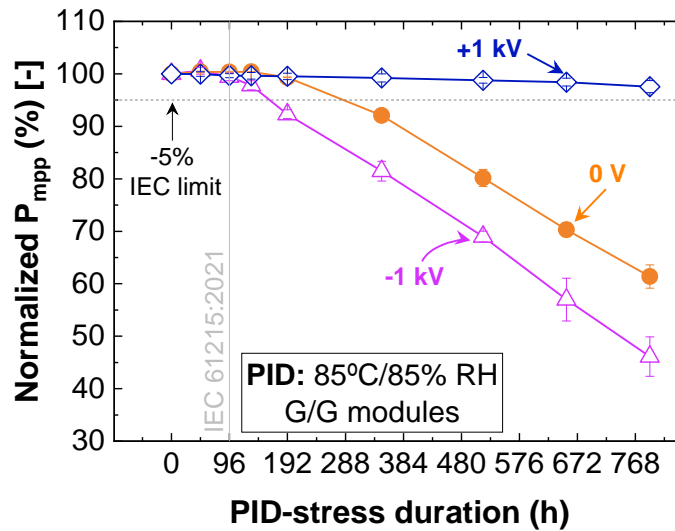


Figure 5.1: Normalized power of the front-side of SHJ 1-cell G/G laminates with EVA, after 800 hours of PID testing at 85°C/85% RH for different bias conditions: -1 kV, 0 V and +1 kV

In addition, we note that the unbiased samples (used as a control and exposed to DH-like test conditions), and for which no degradation was expected, show a comparable degradation, although with a slower kinetics. This was to some extent unexpected, because more conventional Al-BSF or PERC solar cells encapsulated with solar-grade EVA (in G/G or even G/BS structures) are generally stable at least during the first 1000 hours of exposure to DH test conditions. But what we observe here is already a considerable loss in performance (i.e. 20%) after only 500 hours in DH. This topic was investigated in Chapter 4 and a degradation model was proposed. We come back to this point in Section 5.3.3.

Conversely, no degradation is observed for the positively biased samples (i.e. +1 kV).

5.3.2 Contribution of front and rear sides to the total degradation

Having discussed the effect of different voltage polarities – or lack thereof – on SHJ G/G laminates, this next section investigates the impact of negative PID (i.e., -1 kV) on both the front and rear sides of the solar cell. The single-cell laminates were measured from both sides, by fully covering the untested side with a black cloth in order to avoid undesired light absorption.

The normalized values of the electrical parameters of the front and rear sides of the G/G mini-modules subjected to -1 kV for 800 hours are summarized in Figure 5.2. In these graphs, we focus on the maximum power (P_{max}), I_{SC} , open-circuit voltage (V_{OC}) and fill factor (FF). As a convention in indoor reliability/durability tests, P_{max} is the parameter that is considered when deciding whether a PV module passes or not the various IEC 61215 protocols [67]. In the case of the PID test, a module is considered to pass the test if the loss in P_{max} is lower than 5% after 96 hours of testing. Consequently, the SHJ mini-modules tested in this work (i.e., 1-cell G/G mini-modules encapsulated with EVA) pass contained in IEC 61215. The samples are nevertheless prone to degradation when the test is extended further. This degradation, however, is not linear. It accelerates when doubling the conventional 96-hour test duration, for both front and rear sides. Additionally, the degradation kinetics and mechanisms are different for both sides of the module. By the end of the extended PID test of 800 hours (i.e., ~8 times the IEC 61215), the P_{max} losses are 53.9% and 40.4% for the front and rear sides, respectively. We note that modules did not recover after storage in the dark.

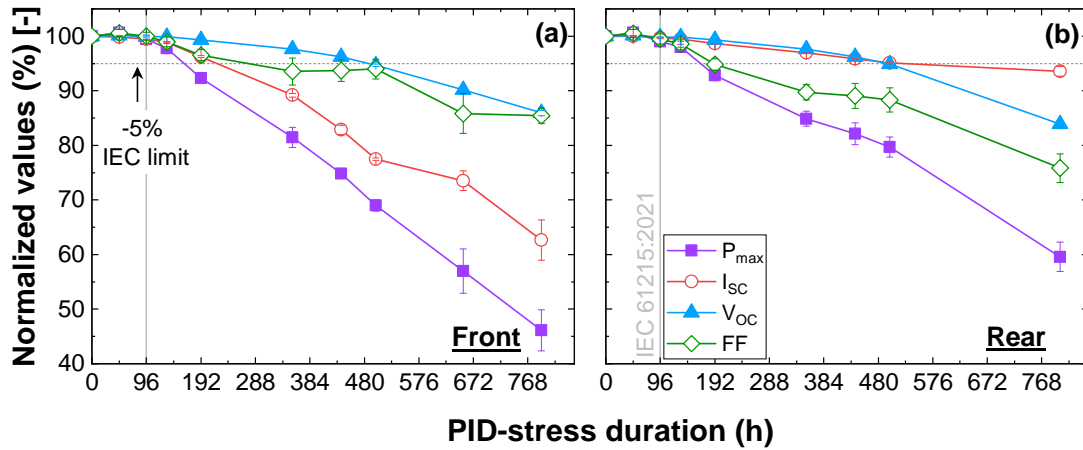


Figure 5.2: Normalized values of the electrical parameters of the (a) front and (b) rear sides of SHJ 1-cell mini-modules encapsulated in a G/G structure with EVA, after an extended 800 hours of testing at 85°C/85% RH and -1 kV conditions

Regarding the mechanism, the front-side degradation is driven by a large loss in I_{SC} that

follows the same degradation trend as the P_{max} . The V_{OC} and FF also degrade, but to a lower level and following a more lineal trend. Conversely, the degradation at the rear side is driven by a pronounced loss in FF. This loss, with the highest impact on the degradation of P_{max} , is accelerated after 192 hours of testing. Conversely, the V_{OC} and I_{SC} follow the same trend of degradation throughout the duration of the PID test.

It is worth mentioning that even though the extent of degradation in I_{SC} and FF is different for the front and rear sides, the V_{OC} trend is similar. We observe a comparable degradation of the V_{OC} on the one-sun I-V curves presented in Figure 5.3 (a), while a higher I_{SC} loss occurs for the front side of the SHJ solar cell. Therefore, besides the optical issues that may affect the cell differently at the front and rear sides, the losses in V_{OC} indicate degradation in the passivation layers that affect the SHJ cell as a whole.

For these G/G mini-modules, the dark J-V curves are also gradually affected (see Figure 5.3 (b)). This indicates that the losses in I_{SC} are not only a consequence of reduced absorption due to optical reasons, but also related to the diode itself. The semi-log J-V curve is presented as an inset in Figure 5.3 (b). The J-V curves exhibit an increase both in the recombination ($V < 0.35$ V) and diffusion ($V > 0.35$ V) currents [189]. These results imply an enhancement in the recombination rates at the p-n junction and in the bulk and/or interfaces, respectively.

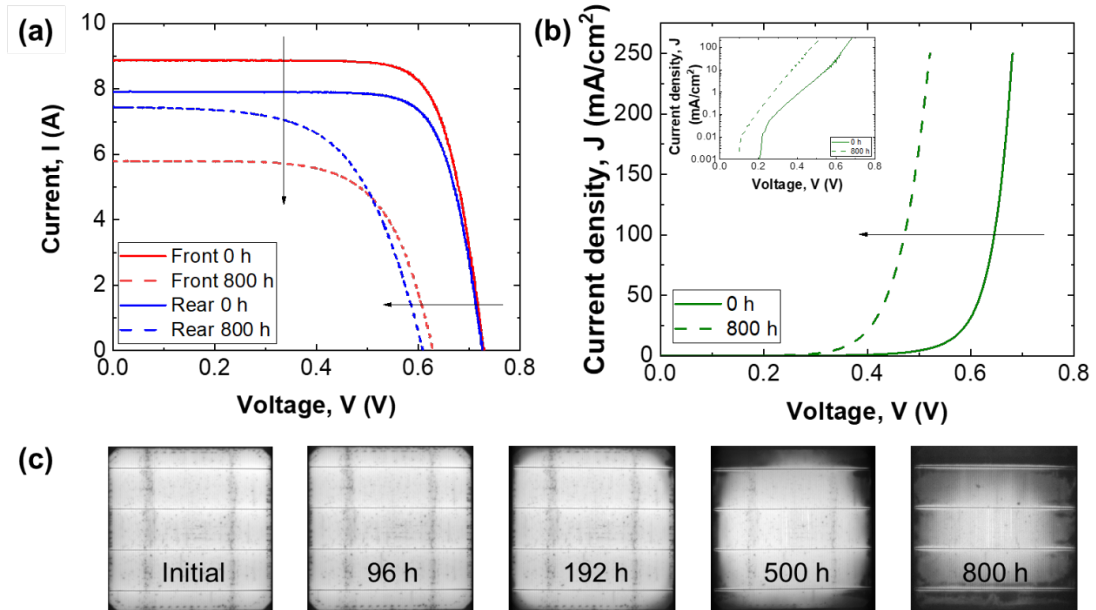


Figure 5.3: (a) One-sun and (b) dark I-V curves, and (c) EL images of G/G mini-modules with EVA subjected to PID testing at 85°C/85% RH and -1 kV for up to 800 hours. Dark I-V curves with the y-axis in semi-logarithmic scale are shown in the inset. We observe degradation on both the one-sun and dark I-V curves. EL images show that degradation starts at the edges of the module after 500 hours of testing, gradually expanding inwards.

EL images taken at several time intervals during PID testing are shown in Figure 5.3 (c). We can observe the contribution and progression of water ingress from the edges for test times

Chapter 5. Degradation Model and Mitigation Strategies for PID in Bifacial SHJ Solar Cells and Modules

higher than 500 hours. After 800 hours of testing, the current is injected mostly at the busbars and the center of the cell in the modules. On the one hand, these images validate the adverse effect of moisture ingress on the SHJ solar cells when combined with an EVA encapsulant and high negative biases. On the other, we can confirm that the use of the ECA does not contribute to the degradation of SHJ cells under PID tests (or DH).

These characterization techniques were complemented by EQE measurements to further comprehend the degradation mechanism. The EQE curves of the front and rear sides are shown in Figure 5.4. EQE measurements were performed both at the center and edges of the modules, which experience different degradation kinetics, as seen in Figure 5.3 (c). The curves shown here after 800 hours of testing correspond to the measurements taken at the edges of the laminates, where the degradation is much stronger. In addition, we modelled the EQE curves using PC1D and adopting the SHJ solar cell parameters proposed by Procel et al [190]. The basis parameters that we assumed were: intrinsic carrier density of $9.65 \times 10^9 \text{ cm}^{-3}$ bulk lifetime of 10 ms, surface recombination velocity of 0.1 cm/s and band gap of 1.7 eV for the amorphous silicon (a-Si:H) layers.

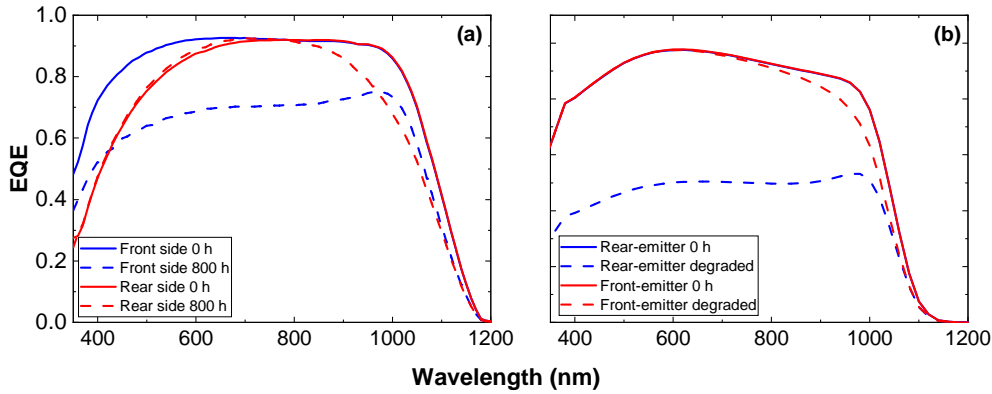


Figure 5.4: EQE curves of (a) measurements of the front and rear sides of a G/G mini-module subjected to PID testing at 85°C/85% RH and -1 kV for up to 800 hours; and (b) simulation performed with PC1D taking the model from [190]. Measurements shown in (a) were performed at the edges of the mini-module. For the front side the degradation is more pronounced at short wavelengths, whereas at the rear side the degradation is enhanced at longer wavelengths. Simulations confirmed that the observed curves are due to increased recombination rates at the front-side a-Si:H/c-Si interface.

The aim of our simulations was to qualitatively describe what occurs at the microscopic level. The EQE measured from the front side of the mini-modules highlights a decrease in collection of the short wavelength light (blue light). This type of curve is typical of front-surface recombination in solar cells. We simulated this curve by increasing the surface recombination rates at the (i)a-Si:H/(n)c-Si interface, while increasing the surface recombination at the rear-side did not affect the shape of the EQE curve. This explains the large decrease in I_{SC} observed in the 1-sun I-V curves – and the consequent loss in V_{OC} – due to the high recombination

of charge carriers, preventing them from being collected at the front contacts of the solar cells. The EQE measured from the rear-side of the cell confirms this interpretation. We do not observe an evident degradation at shorter wavelengths (i.e., close to the rear junction which is now sunwards). Instead, a pronounced degradation is observed at longer wavelengths, indicating a reduced photon collection at the back side in these illumination conditions (the front side of the device). Therefore, these two EQE spectra confirm that the cell degraded and exhibits an increased front-surface recombination, especially at the edges of the cell.

During PID testing however a high potential voltage difference was applied to both sides of the solar cells. In fact, the I-V measurements displayed increased recombination not only at the front side of the SHJ solar cell, but in proximity of the p-n junction (i.e. the rear side) as well. We hypothesize that we are not able to discern severe recombination at the rear side from EQE measurements because the minority carriers are collected as soon as they are generated. That is, electron-hole pairs that are generated at the p-n junction (rear side) are so close to the rear-side contact that holes can easily be collected, despite having a very defective interface. Therefore, the increased recombination does not affect the collection of these charge carriers. Conversely, the carriers generated close to the front (i.e., electrons) need to diffuse through the bulk and reach the front-side contact layer. Thus, a lower diffusion length (corresponding to a general loss in the EQE) combined with increased defects at the front surface greatly affect the collection of the electrons; this has an evident effect on the current that is extracted from the cell, in particular at the front side.

In order to further investigate the origin of this phenomenon, we performed a microscopic analysis of the degraded samples.

5.3.3 Scanning and transmission electron microscopies

The mini-modules were first studied by optical microscopy. This method, along with the visual inspection performed throughout the PID tests, is a useful tool to recognize visual defects. We observe, both macro- and microscopically, that there is delamination around the silver (Ag) fingers at the edges of the mini-module, where the degradation is the most substantial (see Figure 5.3). PID is usually considered a sneaky degradation mechanism, with no visual defects to the naked eye. However, Hacke et al. reported the occurrence of PID-delamination (PID-d) under similar conditions to the tests carried out in this report [191]. Thus, besides the degradation mechanisms described previously, PID-d also occurs in these SHJ G/G laminates. We note that, among the tested BOMs with different encapsulants, only the modules with EVA presented delamination.

The SEM images of such a cross-section are presented in Figure 5.6. Figure 5.6 (b) and (c) reveal two different areas of the same sample where there is a layer of epoxy resin between the encapsulant and the solar cell. The layer indicates the presence of delamination – or gap – previous to the grinding and polishing; it is not thus an artefact of such procedures. Additionally, as seen in the zoomed-in image in Figure 5.6 (d), the Ag finger is also delaminated

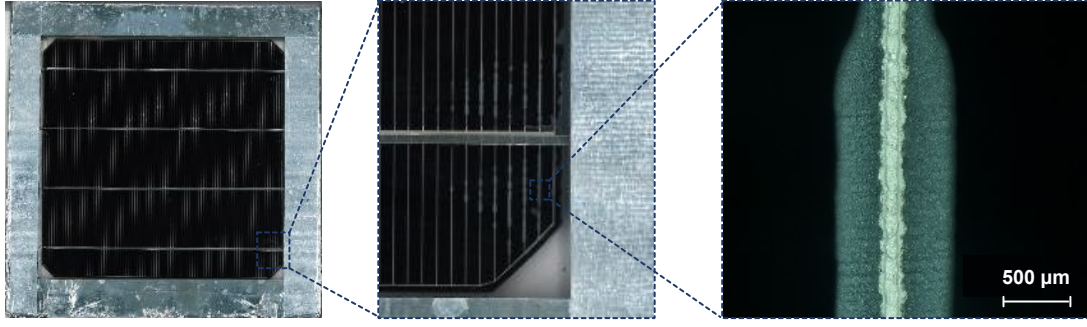


Figure 5.5: Visual inspection (left and center) of the front surface of a G/G mini-module subjected to -1 kV and 85° C/85% RH for 800 hours with a magnified image taken by an optical microscope (right). The images reveal delamination at the edges of the module and around the Ag fingers.

from the solar cell. This points to a loss in adhesion between the finger and the ITO layer of the SHJ cell after PID. Although this phenomenon may contribute to the degradation by decreasing the current due to the added interface, we assume it plays a small role in the total degradation mechanism. Firstly, the delamination only occurs in very small areas at the very edges of the mini-modules, whereas the EL images have exhibited degradation in larger areas. Secondly, the potential losses in absorption at the edges do not explain the significant loss in passivation experienced by the laminates.

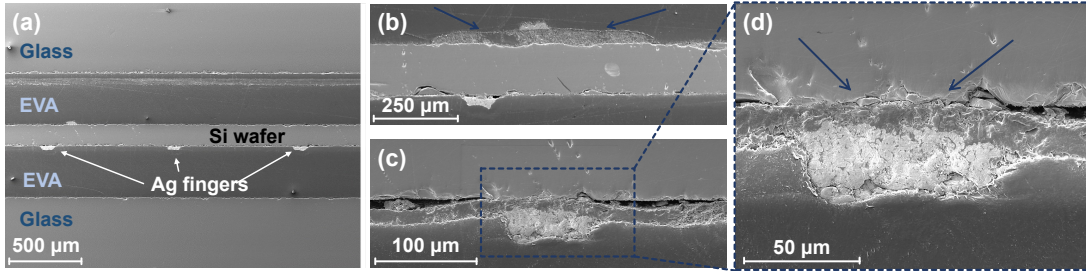


Figure 5.6: Representative SEM images of a cross-section of the front-side of a SHJ solar cell subjected to PID at -1 kV and 85° C/85% RH for 800 hours.

STEM imaging and EDX profiles of the front side of a G/G module subjected to PID for 800 hours are shown in Figure 5.7. We observe that the ITO is not visibly damaged from a structural and compositional point of view. In opposition to Yamaguchi et al. [103], we do not observe any precipitation of metallic indium (In) in the ITO. However, we observe an accumulation of Si and Na on the front surface of the ITO layer. Furthermore, some of the Na seems to have migrated through the TCO and to have accumulated on the surface of the a-Si:H layer at the interface with ITO (Figure 5.7 (d)-(f)). While no Na is detected into the a-Si:H layer likely as a result of the limited sensitivity of EDX, this observation of the migration of Na is consistent with the PC1D simulations. Indeed, the introduction of defects by Na at the a-Si:H interface may lead to additional recombination and hence explain the J-V trends observed here.

The same analysis was performed on the cross-section of modules subjected to DH and posi-

tive PID (+1 kV) test conditions. We did not observe any migration of Na (or other elements) in either sample.

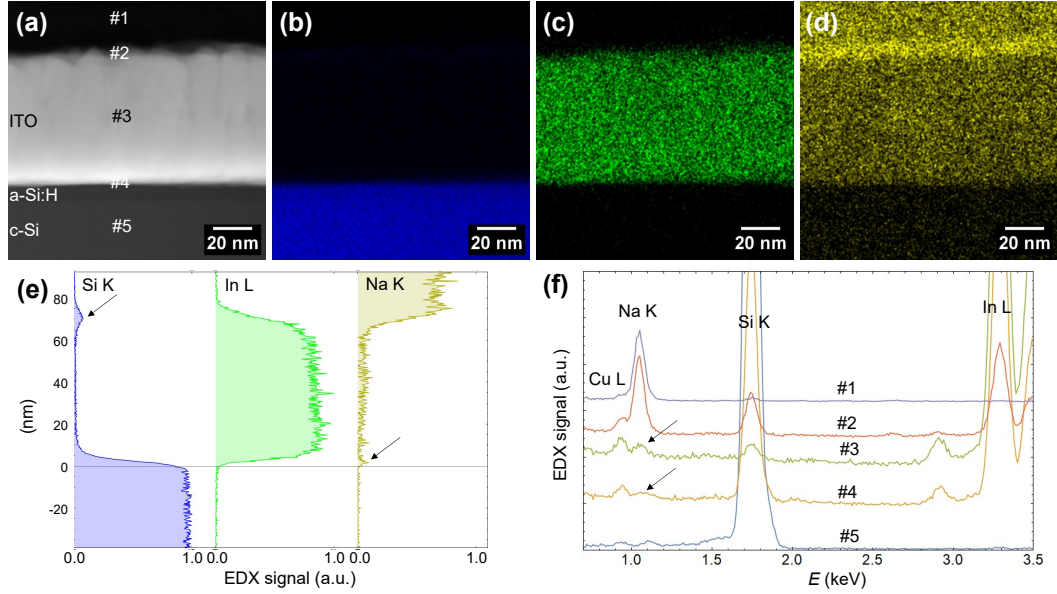


Figure 5.7: (a) STEM high-angle annular dark-field image and (b)-(d) EDX image of the cross-section of the front side of a SHJ 1-cell G/G mini-module subjected to PID at -1 kV and $85^{\circ}\text{C}/85\%$ RH for 800 hours; (e) EDX line profile taken across the stack, highlighting the accumulation of Si on the front TCO and the diffusion of Na into the ITO layer (arrowed); (f) EDX spectra taken from different positions in the stack (positions shown in (a)), with arrows showing the small Na peak detected inside the ITO layer and at the ITO/a-Si:H interface.

We also performed SEM top view analysis on SHJ solar cells prior to degradation to study the ITO surface roughness and morphology. Figure 5.8 showcases the highly textured surface of the ITO, and highlights large “wrinkles” or “nano-cracks” all over the pyramids. Closer inspection to the SEM measurements reveals increased rugosity and interfaces at the bottom of the pyramidal structure. It is worth mentioning that both the front and rear sides portrayed this surface morphology. The cross-section of the same sample – also analyzed by SEM – is presented as an inset at the right side of Figure 5.8. The figure clearly illustrates the grains and grain boundaries of the crystalline TCO, as well as one of such “nano-cracks” intersecting its surface area.

The importance and role of the density of ARC in the PID mechanism of conventional Al-BSF was already investigated by Koch et al. [80]. The authors highlighted the importance of the layer composition, and determined that ARC with higher densities mitigate the detrimental effects of PID. In the present case, we assume that the observed “nano-cracks” hinder the effectiveness of the ITO as a barrier and can further facilitate the diffusion of Na ions (and potentially other elements) into the SHJ solar cells.

We however note that the observed TCO morphology strictly belongs to our SHJ solar cells,

and that the degradation kinetics may vary from manufacturer to manufacturer.

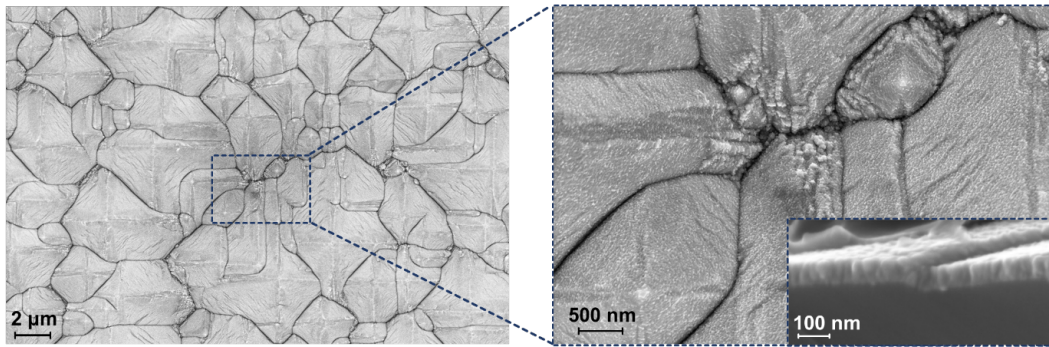


Figure 5.8: SEM top-view images of a SHJ solar cell front surface prior to encapsulation and PID testing; the cross-section of such solar cell is placed in an inset at the right.

5.4 PID in SHJ solar cells and modules: a microscopic model

As shown in Figure 5.1, our 1-cell G/G mini-modules encapsulated with EVA pass the 85°C/85% RH 96-hour long PID test. The extension of the test to 800 hours nevertheless reveals that PID starts impacting the cell performance after approximately 192 hours of test exposure (i.e. twice the duration foreseen in the IEC standard), which may not be representative of actual field conditions. However, discerning the root cause behind the observed degradation mode may be critical in understanding potential weaknesses of the technology, looking for solutions, eventually increasing the overall reliability – and market acceptance – of the technology. For this reason, we interpret the observed experimental findings presented in the previous section and propose a microscopical model describing the PID of the SHJ cells used in this study.

In Chapter 4, we investigated the degradation mechanism of SHJ solar cells and modules exposed to DH conditions, proposing a detailed microscopical model explaining the sensitivity of SHJ to water. In the referenced work we were able to demonstrate that this sensitivity to moisture depends on an interplay of factors, which include: (1) moisture ingress into the laminate; (2) the presence of a glass cover (on the front and/or rear side); and (3) the use of EVA as an encapsulant.

In the present chapter, we complement our previous findings with the inclusion of the effect of negative and positive biases in the degradation mechanisms. We thus propose a PID microscopic model – a multi-factorial degradation mode unique to SHJ solar cells – where degradation occurs at two different levels. The degradation model is presented in Figure 5.9.

- a) **Damp heat.** In DH conditions (i.e. no bias applied), moisture entering from the edges of the laminate corrodes the surface of the glass – by removing Na ions from the glass surface – creating sodium hydroxide (NaOH) molecules [184]. We then hypothesize that the polarity of EVA allows the NaOH molecules to diffuse through the encapsu-

lant. The cell's ITO layer should act as a barrier, but the presence of grain boundaries, “nano-cracks” and voids can further enable the diffusion of Na^+ ions and OH^- groups that can increase grain-boundary scattering in the ITO [183] and could eventually reach the passivating layers and cause the observed degradation. The role of EVA is thus instrumental in promoting water diffusion in the laminate, but it is not per se contributing to the performance decrease. The presence of Na could not be observed by EDX characterization (see Section 5.3.3) in the DH-degraded samples. We hypothesize that diffusion of elements or ions occurred in quantities below the sensitivity of the method.

- b) **Negative PID.** The degradation increases under negative PID conditions (i.e. -1 kV). In this case, we most likely have the superposition of two self-reinforcing mechanisms: i) the previously mentioned corrosion process, which is possibly amplified by a larger availability of Na^+ removed from the glass; ii) the conventional supply and drift of Na^+ from the glass through the EVA to the top of the cell. It is a well-known fact that positively charged Na^+ ions contained in the glass are attracted by negatively biased solar cells [61]. High temperature and humidity conditions such as those experienced in DH conditions can reduce the resistance to PID by increasing the conductivity of encapsulants and thus, enhancing the drift of Na^+ ions through the encapsulant.
- c) **Positive PID.** A high positive bias (i.e. +1 kV) prevents all degradation from occurring – even in DH-like conditions. We hypothesize that no Na^+ extraction can take place under +1 kV, due to the positive bias preventing the “glass corrosion” process. The observation that positively biased modules are stable for the full test duration reinforces our model for both DH and -1 kV samples.

We can thus conclude that the main factor affecting the SHJ solar cells under PID is not the water ingress per se, but a combination of the materials (mainly the encapsulant) used in the manufacturing process and the module polarity – with respect to grounding – in a string.

The findings in the present study led us to develop a microscopic model for the diffusion of Na^+ ions into the SHJ solar cell (see Figure 5.10). We hypothesize that the positively charged Na^+ ions and hydroxyl groups (due to the formation of NaOH and the drift caused by the high negative bias) can diffuse into the SHJ cell through the ITO, especially the enhanced interfaces generated by the aforementioned “wrinkles” or “nano-cracks” (see Figure 5.8), inducing increased grain-boundary scattering. The Na^+ ions can further diffuse into the a-Si:H layers – both at the front and rear sides – through the grain boundaries of the ITO, as shown in the right side of Figure 5.10, and reach the a-Si:H/c-Si interface creating recombination centers for charge carriers. We therefore propose that the accumulation of Na^+ can create recombination centers at these interfaces and be the cause for the loss in I_{SC} at the front side and in the general of the passivating properties (i.e. V_{OC}) of the solar cell.

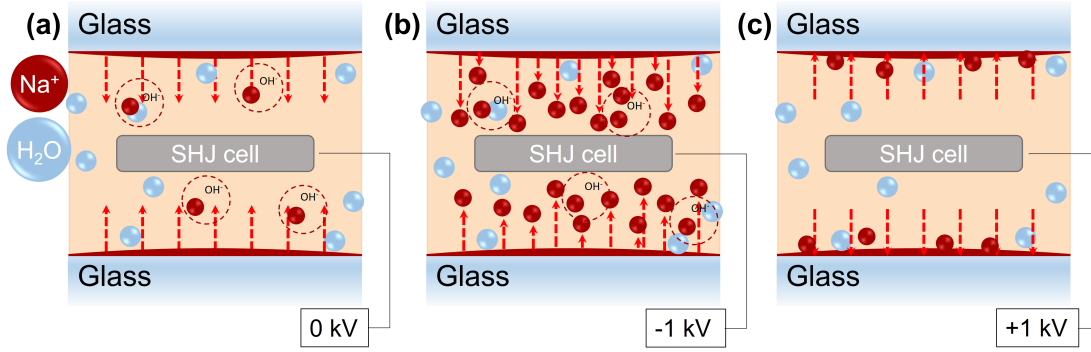


Figure 5.9: Degradation model of 1-cel SHJ G/G mini-modules subjected to (a) 0 V or DH only, (b) -1 kV and (c) +1 kV after an extended PID testing at 85° C/85% RH. High negative biases between the solar cell and the module surface cause Na⁺ ions, in combination with OH⁻ groups, to diffuse through the encapsulant into the solar cell. In DH, high moisture content corrodes the surface of the glass, creating NaOH molecules, that under high humidity conditions diffuse through the encapsulant and into the solar cell. In contrast, high positive biases repel the Na⁺ ions from the solar cells, preventing degradation.

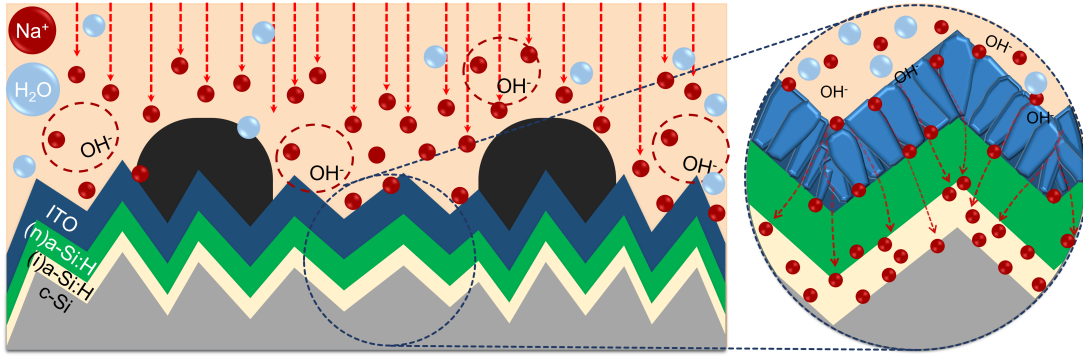


Figure 5.10: Proposed microscopic model of the PID degradation at the front side of SHJ solar cells. The figures are not drawn to scale.

5.5 PID mitigation strategies for SHJ modules

5.5.1 Choice of encapsulant

Figure 5.11 summarizes the relative variation of the electrical parameters at the end of the extended PID testing (500 hours) of G/G mini-modules for all six encapsulants. Modules with a voltage bias of -1 kV and +1 kV with respect to the grounded frame and no voltage (only DH) are considered here. The different degradation rates to the PID tests are evident among them. As expected, ionomer, three POEs and TPO do not show any kind of degradation even after 500 hours of testing, regardless of the voltage applied. Conversely, and as shown in the previous section, the modules encapsulated with EVA do degrade, both under -1 kV and in DH only. Therefore, the utilization of any of these encapsulants would be a good approach to prevent PID (and DH degradation) in SHJ solar cells. This is already a well-known strategy employed

in the industry.

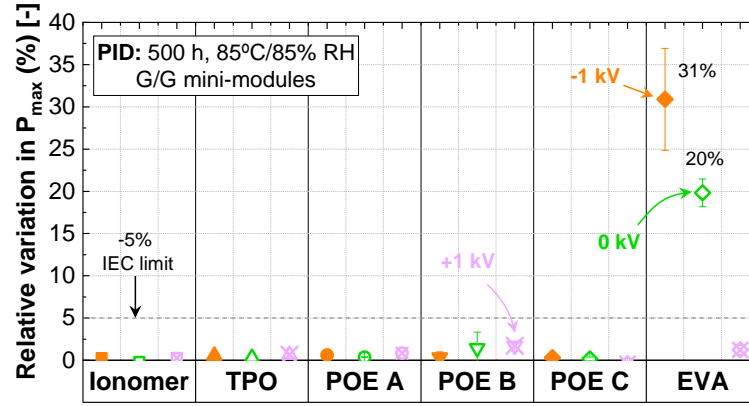


Figure 5.11: Relative variation of the maximum power (P_{max}) of SHJ cells with six different encapsulants after 500 hours of PID test at 85°C/85% RH. Comparison between applied voltages of -1 kV, 0 V (as reference) and +1 kV with respect to the frame and packaged in a G/G mini-module structure, to study the effect of voltage polarization in the degradation rate. Values are the averages of two samples.

We also aimed to understand the reasons behind this difference in degradation among the different encapsulants that were tested in the same conditions. The first approach was to measure the volume resistivity of each encapsulant, since it reportedly has an impact on PID mechanisms. Previous studies have demonstrated that the volume resistivity of encapsulants diminishes with increasing temperature and humidity (see [61], [106]). Consequently, all six encapsulants were “laminated” and the volume resistivity was measured at lab ambient (23°C/50% RH), hot dry (85°C/15% RH) and in DH (85°C/85% RH) conditions, as shown in Figure 5.12), following IEC 62788-1-2 standard [111].

We observe that ionomer, TPO and EVA present volume resistivities in the order of $10^{16} \Omega \cdot \text{cm}$ in lab ambient conditions. As reported in literature, the resistivity decreases when both the temperature and RH decrease, even more so for EVA, displaying losses of three orders of magnitude. Nonetheless, even in DH conditions the volume resistivity of the EVA used in this study is similar – or even higher – than some of the POEs tested (i.e., POE A and POE C). These results suggest that the volume resistivity is not the sole reason for the higher degradation rates of mini-modules encapsulated with EVA.

We have already mentioned that PID in SHJ solar cells/modules is a result of a multi-factorial degradation mode that combines high voltage differences with high-water content in the module. The diffusion rate of water through the encapsulants is therefore another key parameter. The permeability to moisture is commonly quantified by means of WVTR [41], [192]; the values pertaining to the family of encapsulants tested in this study are reported in Table 5.2. We see that the WVTR of EVA is one order of magnitude higher than those of ionomers and POs; thus, water molecules can penetrate and diffuse more easily inside the laminate encapsulated with

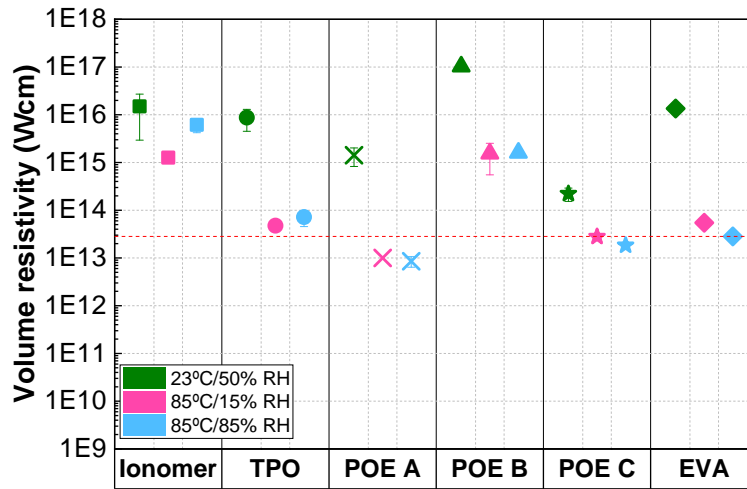


Figure 5.12: Volume resistivity values measured for all the six encapsulants (after the lamination process) at three different environmental conditions: lab environment (23° C/50% RH) in green, hot dry (85° C/15% RH) in pink and damp heat (85° C/85% RH) in blue. All values are averages of five different samples. The horizontal lines mark the volume resistivities of EVA used in the study, as reference.

EVA, potentially enhancing the corrosion of the glass in DH conditions and, PID, as a result.

Table 5.2: Water vapor transmission rates (WVTR) for the encapsulants used in the study, taken from [41].

Encapsulant	WVTR [g/m ² /day]
EVA	15-25
Ionomer	≤ 1
POE, TPO	≤ 5

The volume resistivity and WVTR values do not explain however the increased percolation of NaOH molecules and Na⁺ ions through the EVA compared to other encapsulants. Some works link the propensity to PID of EVA-encapsulated laminates to its intrinsic ionic conductivity, but this mechanism is not yet well understood [193]. Nevertheless, Habersberger et al. associated a higher ionic compatibility of EVA to its polarity and hydrolized acid species [194]. The authors suggested that the higher moisture intake of EVA (i.e. higher WVTR) could improve the solubility of ions such as Na⁺ and the formation of acetic acid could contribute to an increased compatibility.

5.5.2 Prevention of moisture ingress

Because we have established a relation between moisture ingress in the laminate and the observed degradation mechanism of SHJ solar modules and cells, preventing such an ingress from occurring should clearly benefit the long-term performance of such modules. In the

following, we have investigated four 1-cell mini-module structures, with different properties with regards to water permeability, as described in Table 5.3. In all cases, EVA was used as an encapsulant.

Table 5.3: Module structures with different water permeability properties to investigate the effect of moisture ingress in the degradation mechanism.

Module structure	Permeable from
G/BS	sides and full rear surface area
G/Al-BS	sides only
G/G	sides only
G/G-ES	Impermeable

Figure 5.13 summarizes the evolution of the module's P_{max} throughout the extended PID tests of 500 hours for all four mini-module configurations subjected to -1 kV. As expected, the G/BS mini-modules – with a high absorption of moisture in the encapsulant – show the largest degradation. The P_{max} of these modules is reduced by 70% after 500 hours of PID testing. G/Al-BS and G/G mini-modules, although similar with regards to their permeability properties, differ greatly in their degradation rates and kinetics. While the G/G mini-modules degrade 31% after 500 hours of extended test, the G/Al-BS do so by only 8%. Moreover, the degradation of the latter is accelerated after 350 hours of testing (i.e., more than 3 times the duration stated in the IEC 61215 protocol). The presence of glass at the rear side in G/G mini-modules (acting as a Na reservoir) accelerates the degradation of the solar cells. The rear side of these rear-emitter SHJ cells, along with the cover material used, thus plays an important role in the degradation mechanism. This means the use of the G/Al-BS module packaging would be a good option to delay PID in SHJ solar cells. Finally, it is clear that the best module configuration to encapsulate SHJ solar cells, even with EVA, is the one with an edge seal as it prevents effectively the ingress of moisture. As shown in Figure 5.13, this structure prevents any form of PID from occurring, even when extending the test to 500 hours. This observation clearly reinforces our conclusion (the instrumental role of water in order to trigger PID and DH degradation) and the proposed microscopic model.

5.5.3 Combination front-POE and rear-EVA encapsulation schemes

As mentioned in Chapter 3, Sanyo/Panasonic recently disclosed that their later SHJ products were manufactured in a conventional G/BS module scheme with a breathable backsheet, combining a front-side POE and rear-side EVA configuration [148]. This module configuration is reportedly able to ensure the long-term stability of SHJ technology. Here, we investigate whether such a scheme is indeed stable in PID conditions, and we complement it by testing other encapsulant combinations with different module configurations (see Table 5.4). Besides a conventional G/BS scheme, we also manufactured mini-modules with a G/transparent BS (G/T-BS) configuration. We expect the front-side POE to prevent the migration of Na^+ ions in both DH and PID testing conditions. The transparent BS (T-BS) employed as rear cover,

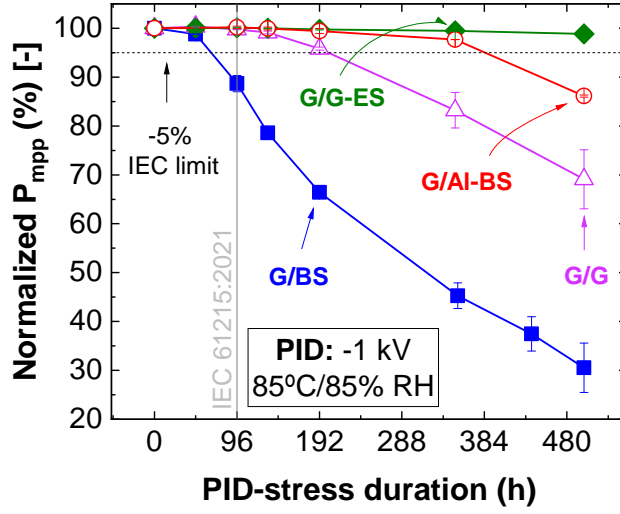


Figure 5.13: Normalized values of the maximum power SHJ 1-cell mini-modules in G/G-ES (green), G/G (lilac), G/Al-BS (red) and G/BS (blue) structures, after an extended 500 hours of testing at 85°C/85% RH and -1 kV conditions.

in addition to having a low WVTR (10^{-3} g/m²/d) similar to that of an Al-BSE, opens up the possibility to employ it in bifacial technologies, such as the one investigated here.

Table 5.4: Module structures with different water permeability properties to investigate the effect of moisture ingress in the degradation mechanism.

Front encapsulant	Rear encapsulant	Module scheme
POE	EVA	G/G
		G/BS
		G/T-BS

Figure 5.14 presents the variation of P_{max} with respect to the initial value over the PID-test duration for the three module configurations. Somewhat surprisingly, the G/BS modules, although passing the IEC 61215 standard of $P_{loss} < 5\%$, degrade almost 25% after 500 hours of PID testing. Despite mitigating degradation by ~45% (compared to the G/BS laminates with EVA/EVA encapsulation scheme), it does not display long-term stability in PID and DH testing conditions. The occurrence of PID is also somehow mitigated in G/G modules with the present encapsulation scheme but, as expected, not completely prevented due to the rear-cover glass acting as Na reservoir. These results reinforce our degradation model and highlight how critical it is to reduce moisture ingress into laminates with SHJ cells. We conclude that although both water ingress and the rear-cover glass factor in the degradation mechanism, preventing the module's water intake has more significant repercussions than curtailing the Na source.

Conversely, our G/T-BS scheme with the POE/EVA packaging configuration gathers all the

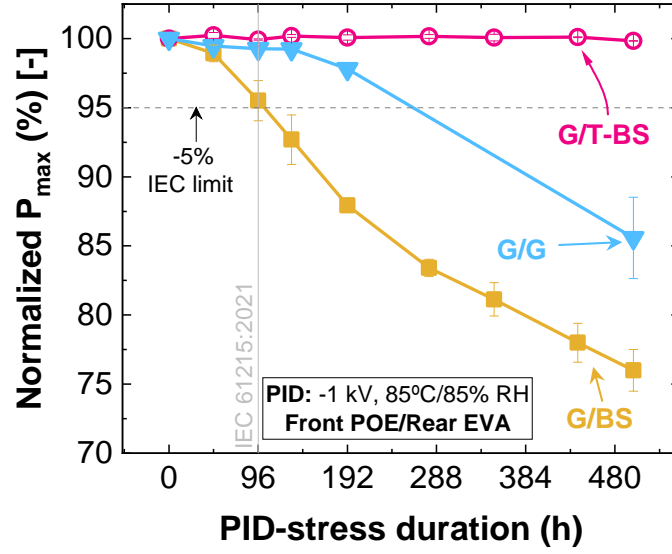


Figure 5.14: Normalized values of the maximum power SHJ 1-cell mini-modules in G/G (light blue), G/BS (mustard) and G/T-BS (magenta) structures, after an extended 500 hours of testing at 85°C/85% RH and -1 kV conditions. All module configurations had a front POE and rear EVA encapsulation scheme.

prerequisites listed above: moisture ingress is limited to the edges of the laminate and the rear-side T-BS lacks the Na reserve. The results presented in Figure 5.14 confirm that these mini-modules are not prone to PID (and DH), even when the test is extended to 500 hours.

5.6 Conclusions

In this chapter, we studied the PID mechanisms of bifacial rear-emitter SHJ solar cells encapsulated in a 1-cell G/G mini-module configuration with a high-quality EVA. We tested the mini-modules in a climatic chamber in DH conditions, and simulated the effect of PID by applying -1 kV and +1 kV to the solar cells with respect to the grounded frame (always keeping unbiased references). The results highlight the sensitivity of SHJ cells to moisture and high negative voltages. The mini-modules are prone to degradation in standard DH conditions, and experience an increased degradation when subjected to -1kV. Conversely, high positive biases prevent degradation from occurring. Although the extended 800 hours of testing reveals that SHJ mini-modules are sensitive to degradation, they pass the IEC standard 96-hour long PID test, and the results reveal that PID starts impacting the cell performance after approximately 192 hours of test exposure (i.e. twice the IEC standard). However, understanding the root cause of the degradation mechanism is key to identify potential weaknesses and to ensure the long-term reliability and the market acceptance of the SHJ technology. We therefore interpret the experimental findings presented in this chapter, and propose a microscopical model

Chapter 5. Degradation Model and Mitigation Strategies for PID in Bifacial SHJ Solar Cells and Modules

aimed at describing the PID phenomenon occurring in the SHJ cells used in this study.

We investigated the degradation mechanism at the front and rear sides of the solar cells. The I-V curves show that passivation was lost at both sides of the cell. We also observe losses in I_{SC} and FF at the front and rear sides, respectively. These results, along with the dark J-V measurements, indicate an increased recombination current at the p-n junction and at the bulk and/or interfaces. The EQE curves, both experimental and simulated, point to increased degradation at short wavelengths due to front-surface recombination.

We then analyzed by cross-sectional transmission electron microscopy G/G mini-module subjected to 800 hours of PID testing. EDX measurements revealed the presence of Na inside the TCO and its accumulation at the a-Si:H/ITO interface when applying -1 kV. The samples tested in DH conditions (no bias) and subjected to +1 kV did not exhibit any migration of Na.

Based on these findings, we developed a multi-factorial two-level degradation model (i.e. DH and PID) for SHJ solar cells: the combination of diffusion of NaOH molecules from the glass corrosion due to the high water content and the drift of Na^+ caused by the negative bias (i.e. -1 kV). We hypothesize that the positively charged Na^+ ions can further diffuse into both sides of the SHJ cells through the micro-cracks and grain boundaries of the TCO, reaching the a-Si:H/c-Si interface and creating recombination sites for charge carriers.

Several mitigation strategies to prevent PID at the module level are also developed. The first one is to substitute EVA with other encapsulants, such as ionomers or POE, which is a strategy already developed and implemented by the industry. These do not only present high-volume resistivities, but also lower WVTR values – with slower water diffusion, thus preventing PID caused by high voltages and moisture. The second suggestion is to directly prevent water from entering the module using of an edge sealant. This strategy allows the use of EVA to encapsulate SHJ solar cells in G/G module structures. The third is to encapsulate the SHJ cells in a G/T-BS configuration with a low permeability backsheets, using a POE encapsulant at the front side and an EVA one at the rear side. We thus prevent the drift of Na^+ towards the cell and the moisture ingress from the rear side. This module scheme not only would provide a good stability under DH-induced degradation and PID, but would also lower the costs of the PV modules by only using one layer of POE.

6 Development of PID-resistant SHJ Solar Cells

Summary

Developing technologies resistant to potential-induced degradation (PID) at the cell level is critical in reducing costs on module components and having more flexibility on the choice of the bill of materials (BOM). In this chapter, we focus on reinforcing silicon heterojunction (SHJ) solar cells against degradation mechanisms induced by moisture and high-negative voltages. In order to verify that, the solar cells are encapsulated in a glass/backsheet (G/BS) module scheme with a low-volume resistivity ethylene vinyl acetate (EVA) as an encapsulant. The aim of this module configuration is to accelerate degradation caused by PID. In the first part of this chapter, we investigate the role of the transparent conductive oxide (TCO) morphology, thickness, homogeneity and texturization on the degradation mechanism. The impact of the substrate layers on the growth of TCO layers and the consequent degradation rates is also studied. The second part of the chapter seeks to develop SHJ cells resistant to PID (and DH as a consequence) by the addition of capping layers on top of the TCO. The roles of the capping layer material, deposition process, density and thickness regarding their potentially beneficial impact on the degradation kinetics and rates are investigated.

6.1 Introduction

The cost of PV has reached an all-time low recently, with $\sim 0.3\$/W$ on average for modules. The module components, and the packaging materials, in particular, play a key role in the final cost. Solar-grade glass is one of the most costly components. It is however the encapsulating material that often allows for a higher degree of freedom. Most recently, some module manufacturers are adopting newer polyolefin-based formulations that reportedly have superior stability compared to ethylene vinyl acetate (EVA), due to the lower water diffusion properties (i.e. lower water vapor transmission rates (WVTR)) and the lack the vinyl acetate units that can later produce acetic acid. Nevertheless, due to the lower cost and easier processability of EVA, it is still an attractive material for manufacturers [195].

In Chapter 5 Section 5.5, we illustrated strategies to mitigate potential-induced degradation (PID) on silicon heterojunction (SHJ) technology at the module level. These strategies represent either higher costs due to more expensive materials or increased steps in module production lines. It would thus be relevant for the industry to manufacture technologies resistant to degradation at the cell level for increased safety (in terms of long-term performance) and for higher flexibility on the choice of bill of materials (BOM), so as to enable the use of encapsulating materials with lower cost and easier processing such as EVA.

In conventional crystalline silicon (c-Si) solar cells (i.e. aluminium back-surface field, Al-BSF), PID occurs as a consequence of the accumulation of positively charged sodium (Na^+) ions in the dielectric anti-reflective coating (ARC) (i.e. silicon nitride, SiN_x) that can further diffuse into the c-Si through stacking faults and create shunts (see Chapter 1 Section 1.4.1 for a detailed explanation). Initial investigations by Koch et al. demonstrated the significance of the SiN_x ARC in the degradation mechanism [80]. Indeed, the authors showed that SiN_x layers with higher refractive indexes could reduce the sensitivity of Al-BSF cells to PID by preventing/minimizing the diffusion of ions. Other strategies to produce "PID-free" cells involve surface treatments and changes in the emitter formation processes (e.g. ion implantation instead of a diffused emitter) [196]–[198]. Han et al. showed that the growth of a thin silicon oxide (SiO_2) layer between the c-Si and SiN_x AR layer during the ion implantation process provided better passivation and enhanced resistance to PID [197].

The cell structure and, consequently, degradation mechanism in SHJ solar cells is however different from conventional p-type technologies. Strategies to prevent PID should therefore consider the degradation mechanism and should be adapted to cater for the needs of our particular solar cell structure. In the degradation model presented in Chapters 4 and 5, we discuss how the transparent conductive oxide (TCO) layer is not an effective barrier against the transport of Na^+ ions and hydroxyl (OH^-) groups when SHJ solar cells are exposed to high-moisture contents and high-negative biases. Preventing damp heat (DH)-induced degradation and PID in SHJ cells should thus consider the role of the TCO in the degradation mechanisms.

Liu et al. also investigated DH-induced degradation in SHJ technology and proposed a strategy to mitigate it at the cell level [158]. The authors achieved the latter by adding a double capping layer - consisting of $\text{SiO}_x/\text{SiN}_x$ stack - on top of their TCO (i.e. indium tungsten oxide (IWO)). Although the results were promising, the tests were not performed on encapsulated cells. Considering the significant role of the cover glass in the degradation mechanism even in DH, as highlighted in this work, such cell structures with double capping layers should be encapsulated and tested following the standards adopted by the industry to validate whether modules would pass the DH testing and, potentially, the PID testing as well.

In this chapter, we investigate the role of the TCO and its substrate layer - with regards to morphology, structure, and electrical parameters - in the degradation mechanism and we aim at developing PID-resistant SHJ solar cells by adding different material stacks as capping layers.

6.2 Experimental methods

6.2.1 Sample design and fabrication

The experimental work in this chapter was carried out on $2 \times 2 \text{ cm}^2$ lab-scale SHJ solar cells (solar cell structure shown in Figure 6.1 (a)). The cells, manufactured at PV-Lab¹, had the standard monofacial front-emitter (i.e. p-n junction at the front side) structure. The hydrogenated intrinsic and doped amorphous Si layers (i.e. (i/p) a-Si:H and (i/n) a-Si:H layers at the front and rear sides, respectively) were deposited on both sides of the float zone (FZ) n-type c-Si wafer by plasma-enhanced vapour deposition (PECVD). These layers provide surface passivation and carrier selectivity. Then, the TCO was sputtered on both sides, followed by the rear Ag full-area metallization. The front-side Ag grids were finally screen-printed and the cells were annealed at 210°C for 30 minutes to cure damage from sputtering.

The development of SHJ cells resistant to DH-induced degradation and PID was performed by depositing capping layers on top of the cells, manufactured as described above. Depending on the capping layer, two different processes were employed: PECVD for SiO_x and $\text{SiN}-x$ films and atomic layer deposition (ALD) for aluminium oxide (Al_2O_3) films. The TCO and other capping layers and combinations employed for the SHJ cells investigated in each test will be defined in the corresponding subsections.

We anticipate observing some variation in the degradation rates of cells from different batches due to the in-house manufacturing of smaller-scale cells and potential issues with sample reproducibility.

We then encapsulated the SHJ solar cells in $6 \times 6 \text{ cm}^2$ 1-cell glass/backsheet (G/BS) mini-module configurations incorporating the $2 \times 2 \text{ cm}^2$ cells (see Figure 6.1 (b)). A 3.2 mm-thick solar-grade glass and a conventional permeable BS as front and rear covers, respectively, were used. We employed a low-volume resistivity EVA ($\rho \sim 6 \cdot 10^{14} \Omega \cdot \text{cm}$) as an encapsulant to promote a faster PID degradation. The soldering of cell interconnections was performed by using an electrically conductive adhesive (ECA) with a low-curing temperature. An Al tape was placed around the edges of the laminates to simulate the metallic frame in commercial-size modules. The laminates were subjected to -1 kV and 0 kV (as reference) in a climatic chamber at 85°C and 85% relative humidity (RH) for an extended PID testing of 500 hours. Two replicas were tested at each condition.

The selected BOM (encapsulant and module structure) provides on purpose a weak resistance against PID degradation. For this reason, we believe that a solar cell structure truly resistant to PID (and DH) with this combination of BOM, should provide effective resistance to overcome these failure modes.

Other samples that we manufactured to investigate the properties of the TCOs depending on

¹We gratefully acknowledge Vincent Paratte, Deniz Turkay, Joël Spitznagel and Sylvain Dunand (from PV-Lab) for assisting in the solar cell manufacturing processes.

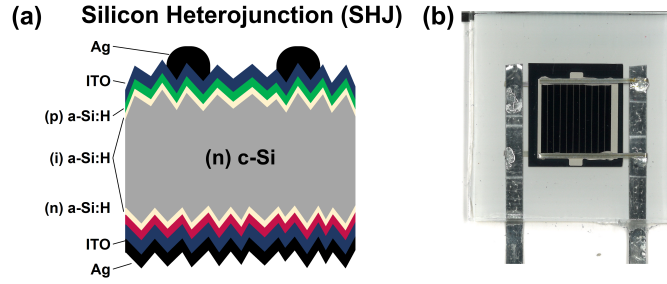


Figure 6.1: (a) Schematic of lab-scale front-emitter SHJ solar cell technology and (b) picture of the mini-modules employed in the experimental work of this chapter. The solar cell is not drawn to scale.

their sub-layers were the following (see Figure 6.2).

- (a) a-Si:H/TCO and nanocrystalline Si/TCO (nc-Si:H/TCO) layer stacks on textured wafers for atomic force microscopy (AFM) measurements to study TCO morphology and surface roughness.
- (b) a-Si:H/TCO and nc-Si:H/TCO layer stacks on flat wafers to perform X-ray diffraction (XRD) measurements to compare the crystallinity and grain size.
- (c) a-Si:H/TCO and nc-Si:H/TCO layer stacks on 2 x 4 cm² glass coupons to measure the Hall effect and extract mobility and bulk concentration parameters.

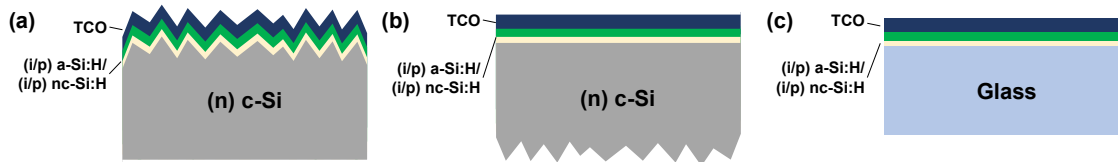


Figure 6.2: Schematic representation of the different a-Si:H/TCO and nc-Si:H/TCO layer stacks on textured and flat n-type c-Si wafers and on glass. The stacks are not drawn to scale.

6.2.2 Material and module characterization

The laminates were removed at regular intervals from the climatic chamber to keep track of their performance over the extended duration of the PID testing. We visually inspected the mini-modules and performed illuminated current-voltage (I-V) and electroluminescence (EL) measurements.

The morphologies of the different TCOs employed were initially studied by performing scanning electron microscopy (SEM) imaging on top view and cross-sections of unencapsulated SHJ solar cells. We then investigated the surface roughness of the cells through AFM measurements. The crystallinity - and grain size - were quantified by XRD measurements on the

(a/nc)-Si:H/TCO layer stacks on the wafers (flat and textured). We then compared the mobility and carrier concentration of the TCO layers via Hall effect measurement on the samples deposited on glass.

6.3 Improved PID and DH resistance: the role of different cell structures and TCOs

In this section, we investigate the impact of the different parameters of SHJ solar cells on DH-induced degradation and PID mechanisms. The aspects investigated in the next subsections are the following:

- the difference in performance between industrial-size cells manufactured in a production line and lab-scale cells manufactured at PV-Lab;
- the role of surface texturing;
- the composition, morphology and electrical parameters of the TCO and the substrate layers (i.e. passivating layers).

This study will provide a context and basis for the development of PID-resistant SHJ solar cells carried out in Sections 6.4 and 6.5.

6.3.1 Industrial- vs. lab-scale SHJ cells

In previous chapters, the impact of moisture and high voltages was investigated in commercial-size bifacial SHJ solar cells and modules. In this chapter, however, the development of "PID-resistant" SHJ cells is performed on small-scale cells manufactured at PV-Lab. Here, we perform a comparison between the two technologies as a benchmark to the cells tested in the previous chapters with respect to the ones in the present work. Besides, the manufacturer, the main differences between the two technologies are listed below.

- **Size of cell and module (large-area vs small-area cells).** Although the PID tests are carried out in a climatic chamber in DH conditions to ensure an equipotential over the surface of the glass, it is not an accurate representation of what occurs experimentally. The voltage difference between the grounded frame and the biased cell is generally larger at the edges of the solar cell, even in 1-cell mini-modules. In the case of the lab-scale cells, due to the reduction in the distance between the edge of the module and the middle of the cell (roughly by a third compared to the commercial-size cell, as shown in Figure 6.3), we expect not to observe such an "edge-effect" and the degradation to be more homogeneous and severe.

- Position of the emitter.** The large-area cells investigated in previous chapters had a rear-emitter structure. For simplicity, in the manufacturing processes and in the understanding of the degradation mechanism, we opted to investigate the performance of small-area monofacial front-emitter SHJ cells. Moreover, as seen in Appendix A.2, the position of the emitter does impact the degradation rates. When isolating both sides (i.e. applying the voltage difference only on one side and limiting the degradation on the other), front-emitter structures seem to be more sensitive to losses in maximum power (P_{max}) by 3%. Hence, we assume that preventing PID in front-emitter SHJ cells will likewise mitigate it in rear-emitter ones.

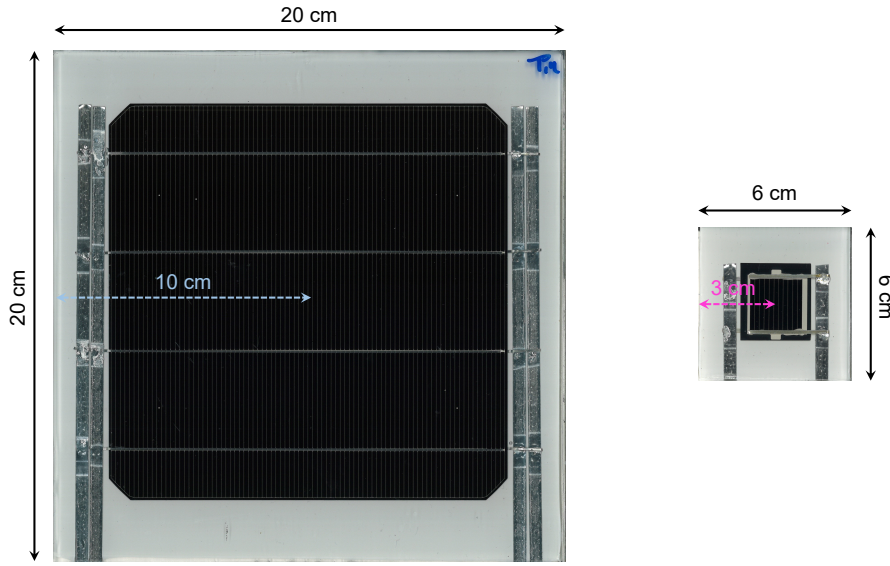


Figure 6.3: Comparison of dimensions between 1-cell commercial-size and lab-scale mini-modules.

Figure 6.4 (a) presents the comparison between these two technologies encapsulated in a G/BS module configuration and subjected to -1 kV and 0 kV (i.e. standard DH) for an extended PID duration of 500 hours. We note that the two technologies have a-Si:H/indium tin oxide (ITO) layer stacks on both sides. As noted in Chapter 5, the commercial-size SHJ technology exhibits 69% of P_{max} loss under negative PID after 500 hours of testing when encapsulated in a G/BS structure. We also remark on the sensitivity of the large-area technology to just moisture ingress by the 47% of loss in DH-like conditions. To our surprise, The lab-scale SHJ laminates show degradation rates of 51% and 29% for the samples subjected to -1 kV and 0 kV (i.e. DH) after 500 hours, respectively. Despite what we assume to be more severe stress on lab-scale cells, these seem to slightly saturate in their degradation kinetics after 132 hours of PID testing, while the industrial-size modules maintain a relatively linear degradation rate over time. Consequently, in spite of the lower size, the small-area cells turn out to be more resistant to PID and DH.

Similarly to what we observed in Chapter 5, the degradation of the lab-scale cells under

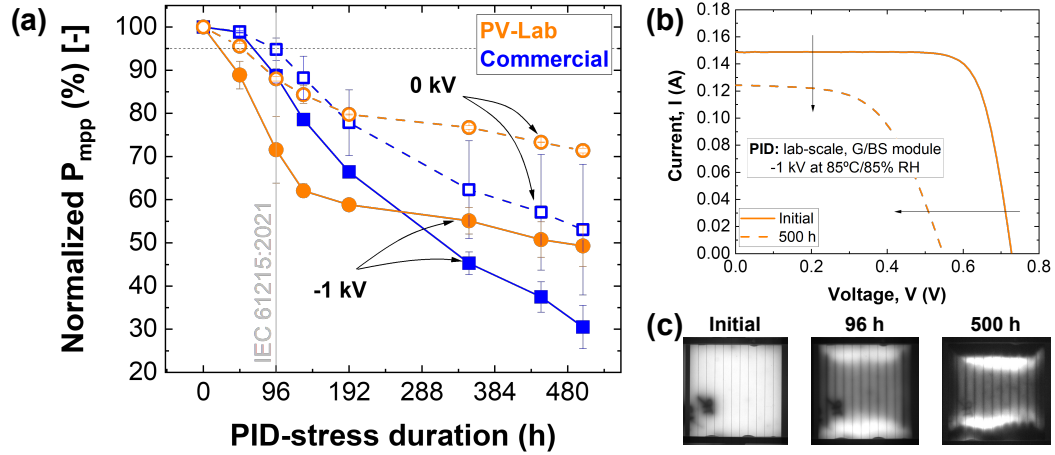


Figure 6.4: (a) Normalized values of P_{max} of 1-cell industrial-size (blue) and lab-scale (orange) G/BS mini-modules throughout the extended PID testing of 500 hours. The laminates were tested under -1 kV and 0 kV (corresponding to standard DH conditions). (b) Illuminated I-V curves and (c) EL images of the lab-scale module tested under negative PID (i.e. -1 kV) for 500 hours. I-V measurements show losses in V_{OC} , FF and I_{SC} , and an increased series resistance is observed.

negative PID is driven by losses in open-circuit voltage (V_{OC}) and fill factor (FF), and to a lower extent in short-circuit current (I_{SC}), as well as increased series resistance (R_s), as shown in Figure 6.4 (b), due to increased recombination rates at the p-n junction. The I-V measurements do not exhibit any shunting phenomena. As expected, Figure 6.4 demonstrates that the degradation is relatively homogeneous and no edge effect is observed.

In our microscopic model, we hypothesized that the TCO played a key role in the DH-induced and PID degradation mechanisms by enabling the transport of Na^+ ions and hydroxyl groups through the grain boundaries and "cracks". We assume that the rate at which the degradation occurs is affected by the quality of materials and the manufacturing processes (e.g. deposition parameters and material composition), particularly of the TCO. TCOs with more porosity, voids and grain boundaries are potentially more likely to facilitate the percolation of Na^+ and OH^- groups and, thus, exhibit more sensitivity to such types of degradation.

We also performed SEM measurements on the lab-scale solar cells before encapsulation in order to identify any potential distinction between the two 6.5. Unlike what was observed in the commercial-size ones, these did not portray any "wrinkles" or "nano-cracks" on the TCO. Indeed, the ITO seems to be homogeneously deposited throughout the surface of the solar cell. We thus assume that the differences in TCO morphology and density are the main reason for the difference in degradation.

In the next sections, we exclusively focus on the lab-scale front-emitter SHJ solar cells, thus we will not make more distinctions on the size of the cells/modules and the position of the emitter.

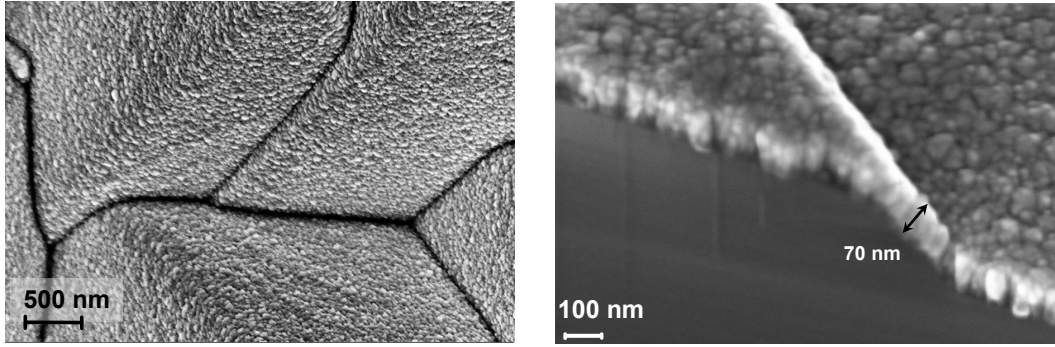


Figure 6.5: SEM images of the top view (left) and cross-section (right) of a lab-scale textured SHJ solar cell with ITO before encapsulation and testing. The measured ITO thickness is 70 nm.

6.3.2 The role of surface texturization

The next step in understanding the impact of the morphology of the TCO on the transport of ions - and consequent degradation - was investigating the role of surface texturization. In order to do that, we compared the degradation kinetics of flat SHJ cells (on double-side polished (DSP) wafers) to the baseline investigated in the previous section. The results shown in Figure 6.6 are quite encouraging. After 500 hours of PID testing, the losses in performance correspond to 49% and 74% for the flat and textured samples, respectively. Surprisingly, the flat samples remain stable in DH-like conditions (i.e. no bias). The degradation mechanism appears to be the same, but with minor losses in I_{SC} and V_{OC} and with slower kinetics (see EL image in Figure 6.6 (c)). The loss in FF is driven by an increased R_s and is not induced by shunting.

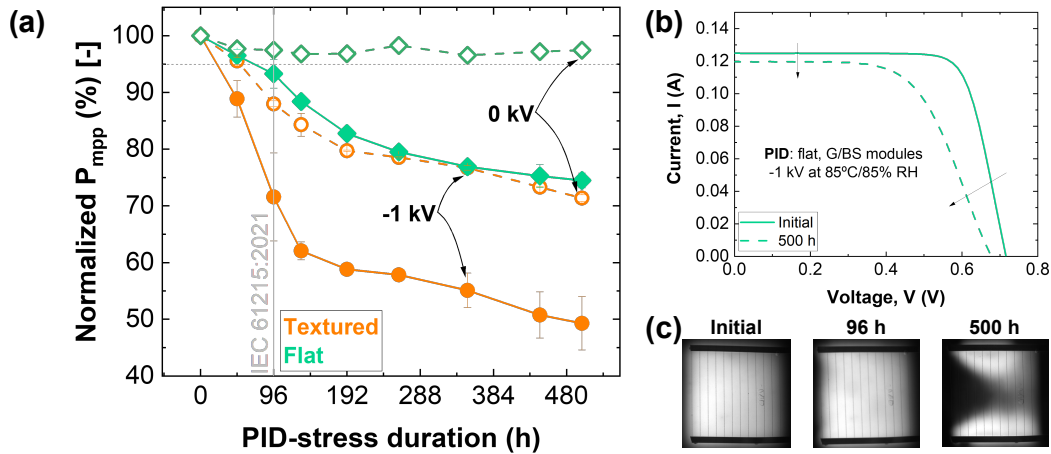


Figure 6.6: (a) Normalized values of P_{max} of 1-cell textured (orange) and flat (green) G/BS mini-modules throughout the extended PID testing of 500 hours. The laminates were tested under -1 kV and 0 kV (standard DH conditions). (b) Illuminated I-V curves and (c) EL images of a representative flat SHJ cell tested under -1 kV for 500 hours. I-V curves exhibit very little loss in I_{SC} and V_{OC} .

6.3. Improved PID and DH resistance: the role of different cell structures and TCOs

SEM measurements in Figure 6.7 show that the ITO is very homogeneous, both from the top view and cross-section images. Again, the TCO of the cells manufactured at PV-Lab does not display any type of voids or cracks and seems to be quite densely deposited. Additionally, the ARC of these particular cells is also thicker than in the previously analyzed ones: 110-120 nm thick compared to the 70 nm-thick ITO of textured cells. We expect that the gain in thickness is beneficial for the decrease of PID.

These results, although not completely unexpected, are very meaningful. We assume the difference in performance between the textured and untextured samples to be the TCO morphology. That is, TCOs on flat surfaces grow more conformal and usually have much fewer cracks, grain boundaries and voids. Our previous hypothesis on the role of TCO density and morphology is therefore partly confirmed.

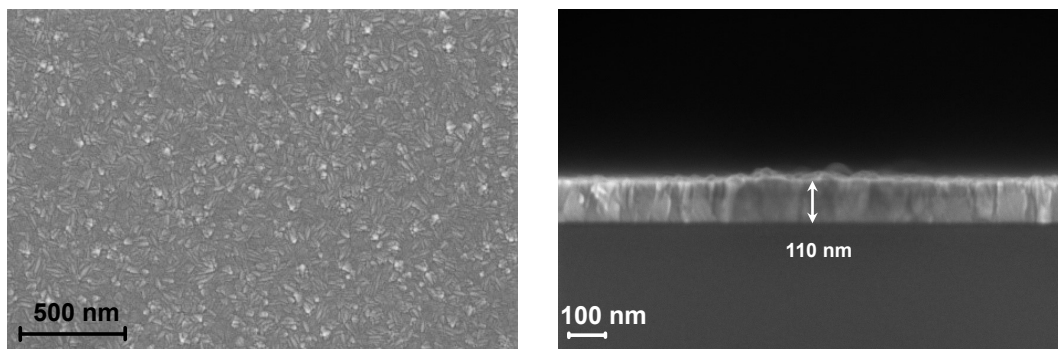


Figure 6.7: SEM images of the top view (left) and cross-section (right) of a flat SHJ solar cell before encapsulation and testing.

Taking into consideration the results in this subsection, there are two likely causes for the differences between the degradation kinetics:

1. **ITO thickness.** The thicker ITO in the flat cells (110 nm compared to the 70 nm-thick ITO on textured cells) may potentially present a better barrier against the transport of Na^+ ions and OH^- groups (see Figure 6.5 and Figure 6.7). These will require a longer time to diffuse through the TCO and, thus, lower the degradation kinetics in both DH and PID conditions, as demonstrated in Figure 6.6. Since the two types of cells were made using identical precursors and procedures, we rule out that the material quality is the cause of the varying performances.
2. **Surface availability.** As shown in Chapter 5, SHJ technology - like other high-efficiency technologies - relies significantly on good surface passivation. When this is minimally disrupted, the repercussions on the cell's performance are critical. In our case study, the textured cells have a 1.7 times larger surface area - due to the pyramidal structure - exposed to the transport of Na^+ than the flat ones. Therefore, a large surface is available to collect Na^+ ions and hence the probability for increased surface recombination - with the consequent loss in performance - is higher.

3. **ITO morphology.** TCO layers deposited on flat surfaces can grow more conformal and present fewer cracks, voids and vacancies than the ones deposited on textured surfaces. Therefore, they can also act as more effective barriers against the transport of ionic species and hydroxyl groups, as validated by our results.

However, since the use of textured cells is more or less an industry standard due to the increases in light absorption, the adoption of untextured cells by the industry is likely not going to happen. For this reason, despite the interesting results, from now on we are focusing our attention on how to make textured solar cells more robust to PID and DH-induced degradation.

6.3.3 The role of different TCO compositions and of substrate layers

In the previous sections, we worked on SHJ solar cells with an ITO as the TCO layer. Although it is the most widely adopted TCO in the industry, other materials can also yield good optical and electrical properties. IWO [199], [200] and zirconium-doped (Zr-doped) In_2O_3 (IZrO) [201], [202] are among the most promising TCO compositions. The latter, well developed and researched in our laboratory, has shown higher carrier mobility and better broadband transparency than ITO [201]. Nevertheless, one of the main concerns of employing the aforementioned TCOs for large-scale industrial applications is the use of In and its scarcity [115]. Therefore, the development of In-free TCOs such as aluminium-doped zinc oxide (AZO) is a topic of special interest [119], [120]. The sensitivity of pure AZO films to moisture is however well documented [203], [204] and our results on SHJ solar cells with such layer can be found in Appendix B.1. Owing to their instability in DH conditions (with and without an applied bias), we do not consider this cell configuration to be the most suitable for the development of PID-resistant SHJ solar cells. Consequently, hereafter, we investigate the behaviour of cells with ITO and IZrO films under PID conditions and study how their morphology and electrical parameters may impact their degradation rates.

However, several works have shown that the optoelectrical parameters of TCOs can also be influenced by the surface roughness of the substrate layers (i.e. passivating layers) they are deposited on [205], [206]. a-Si:H layers are the ones most commonly employed in SHJ technology to provide passivation and carrier selectivity [34]. The high parasitic absorption due to relatively low transparency [37] and charge transport losses [207] of a-Si:H films have nonetheless led to the development of other substrate layers that can display superior properties. nc-Si:H layers postulate as good candidates to improve the efficiency of SHJ solar cells due to their higher transparency and conductivity [208], [209]. Cruz et al. investigated the relation between substrate morphology and TCO properties and observed that the increased crystallinity and surface roughness of nc-Si:H layers can significantly impact ITO growth [205]. Furthermore, SHJ cells with nc-SiO_x:H films were reportedly more stable than those with a-Si:H when sprayed with a NaHCO₃ solution and exposed to DH for 3 hours [210]. Although the tests were performed on unencapsulated cells, they show promising results for this type of cell configuration. We thus assume that varying the passivating layer will influence our solar

cell behaviour under PID (and DH) testing.

In view of all the different factors potentially impacting the TCO morphology and electrical parameters, in this subsection, we study how the aforementioned two underlying Si layers (i.e. a-Si:H and nc-Si:H) can impact the cells' performance when subjected to high moisture and voltages. We also investigate the effect of the substrates on the morphology and electrical parameters of the TCOs under study (i.e. ITO and IZrO) and aim to elucidate the correlation between these properties with the observed performance loss.

Figure 6.8 (a) summarizes the loss in P_{max} after 500 hours of extended PID test for 1-cell textured SHJ G/BS mini-modules (encapsulated with EVA). Overall, SHJ cells with ITO as the TCO layer show better performance than the ones with IZrO. The cells with the a-Si:H/ITO layer stack show 3% lower losses in P_{max} than the ones with a-Si:H/IZrO films. The difference in performance loss is more significant when the nc-Si:H is used as the passivating layer. Indeed, in that scheme, cells with the ITO layer exhibit 21% less P_{max} loss than the ones with IZrO. Moreover, we remark that the laminates with IZrO exhibit highly unstable behaviours throughout the PID testing duration (see Figure 6.8 (b)). Additionally, the degradation trends with respect to the substrate layers are different: while nc-Si:H substrates show high stability for ITO films, the opposite occurs for the modules with IZrO. This lack of consistency could be due to the unpredictable behaviour mentioned previously^{II}. We nonetheless assume that the instability derives from this particular material composition, and not from a random manufacturing error. Moreover, we highlight that the cells with the nc-Si:H/ITO stacks also exhibit very good performance in standard DH conditions, in fact, they are barely above the 5% loss in P_{max} threshold after 500 hours of testing.

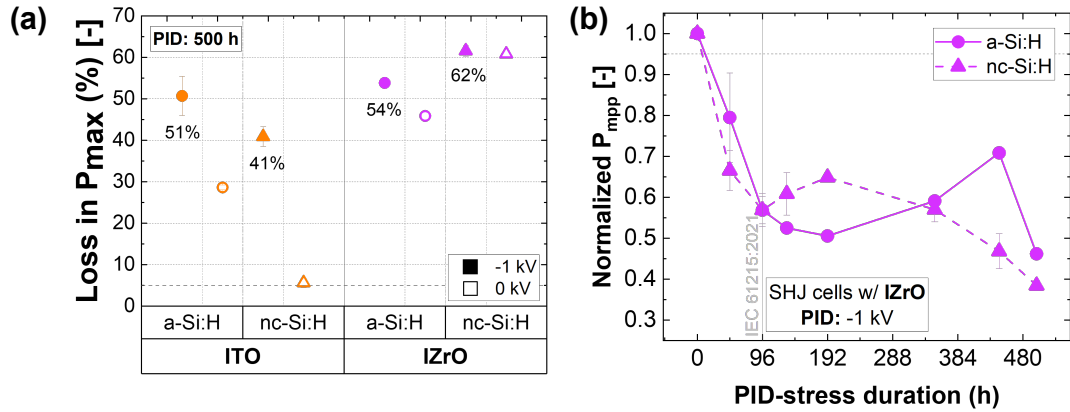


Figure 6.8: (a) Loss in P_{max} of the different substrate/TCO layer stacks on 1-cell textured SHJ cells, encapsulated in G/BS and EVA module schemes, after 500 hours of PID testing. (b) Normalized P_{mpp} of SHJ G/BS mini-modules with a-Si:H/IZrO and nc-Si:H/IZrO layer stacks subjected to -1 kV for 500 hours.

^{II}We note that the two SHJ cell configurations with IZrO were from different batches and tested in separate experiments. Other modules measured simultaneously with these samples did not exhibit this behaviour.

The analysis performed on the TCO and passivating layer stacks, presented in Figure 6.9, indicates the strong dependence of the TCO characteristics (i.e. the morphological and electrical parameters) on the substrate used. This dependence seems to be more critical for IZrO. Hall effect measurements show that carrier mobility and bulk concentration are consistently reduced when the TCO is deposited on top of a nc-Si:H layer (see Figure 6.9 (a)). The reduction in mobility is more significant for IZrO (from $67 \text{ m}^2/\text{Vs}$ to $31 \text{ m}^2/\text{Vs}$) than for the ITO film ($35 \text{ m}^2/\text{Vs}$ to $13 \text{ m}^2/\text{Vs}$). These results are in agreement with what was previously observed by Cruz and co-authors [205]. However, unlike what was reported, the bulk concentration in our TCO layers did experience a change depending on the layer: the concentration in the ITO and IZrO layers decreased from $6.7 \times 10^{19} \text{ cm}^{-3}$ to $5.8 \times 10^{19} \text{ cm}^{-3}$ and from $7.2 \times 10^{19} \text{ cm}^{-3}$ to $4.3 \times 10^{19} \text{ cm}^{-3}$, respectively.

Regarding the topography and morphology of the investigated ARCs, the RMS roughness and crystallite size also exhibit considerable variation depending on the substrate layer. Both parameters show the tendency to increase when the TCO is deposited on a nc-Si:H. Unlike the rest of the parameters in this study, the ITO surface roughness depends much more significantly on the substrate (it increases by a factor of 5) than IZrO. We assume that the surface roughness, besides being dependent on the sub-TCO layers, is an intrinsic characteristic of each TCO composition and does not have an impact on the degradation.

Grain sizes in the ITO layers display an increase of 2.1 nm whereas the ones in the IZrO layers grow significantly (i.e. by 19.7 nm). According to Li et al. [183], highly crystallized IWO films are more resistant to PID and DH due to a lower grain boundary density and, hence a reduced grain-boundary scattering. Indeed, our SHJ solar cells with ITO exhibit lower degradation rates - and a highly stable performance in DH - when nc-Si:H films are employed as the substrate. We assume that larger grain sizes induce fewer grain boundaries through which Na^+ ions and hydroxyl groups can migrate, consequently reducing the formation of recombination and scattering centres in the ITO. Additionally, these fewer grain boundaries would potentially hinder the transport of Na^+ ions towards the ITO/nc-Si:H interface, delaying the disruption of cell passivation. We assume that the role of the TCO morphology is much more significant than the surface roughness.

These results are however not consistent with the performance loss observed for the IZrO films. We speculate that this discrepancy is due to the lack of reproducibility of the IZrO layer deposition. We thus assume that the instability observed in Figure 6.8 (b) might be caused by, for instance, the presence of vacancies, lower layer density, etc. that can potentially enhance the migration of ions through the TCO layer.

In summary, this section has reviewed three key aspects of SHJ cells that can impact their behaviour when subjected to PID and DH testing: (1) the industrial-size cells investigated in previous chapters, with a less homogeneous TCO, are more sensitive to degradation than the lab-scale SHJ cells; (2) textured layers and surfaces are more sensitive to the transport of ions than flat ones; and (3) the conformity (and clean morphology of) the TCO layer seems to play

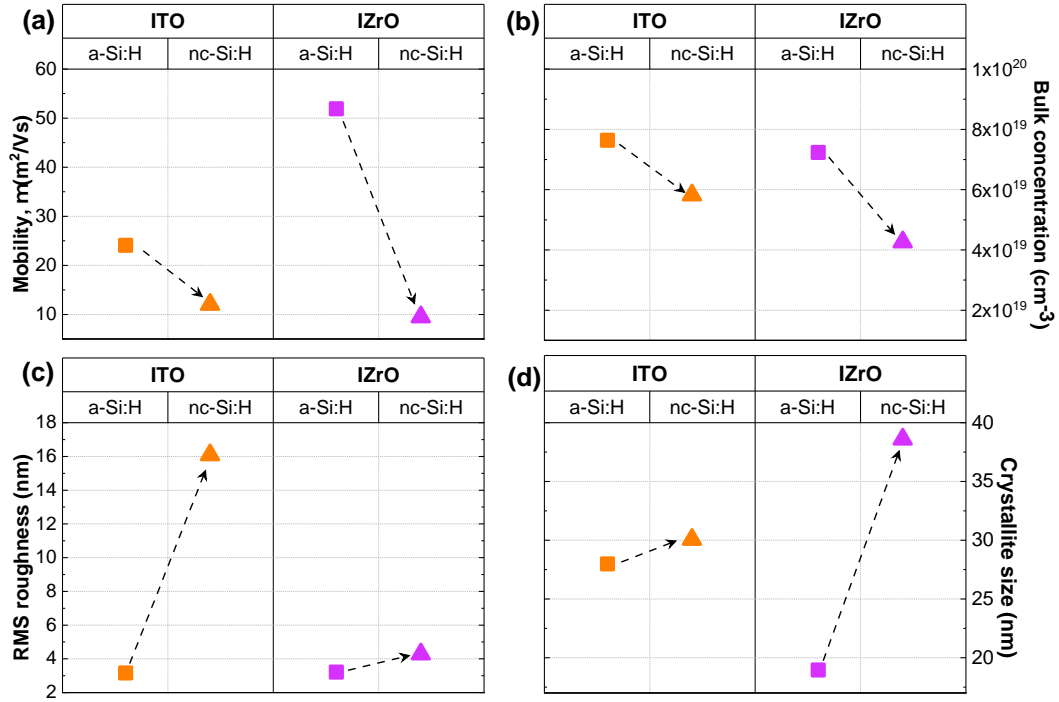


Figure 6.9: (a) Mobility (b) bulk concentration, (c) surface roughness and (d) crystallite size values of the different sub-TCO/TCO layer stacks. Measurements in (a) and (b) were performed on the layers deposited on glass substrates, while the ones in (c) and (d) were done on films deposited on c-Si wafers.

a considerable role to prevent DH-induced degradation and PID, while other parameters may also play a role, but with a second order effect.

6.4 The role of capping layers deposited by PECVD

In the previous section, we presented the beneficial impact of employing nc-Si:H/ITO layer stacks to improve the long-term stability of SHJ cells under DH and PID testing. Here, we focus on developing SHJ solar cells resistant to PID with the aforementioned cell structure by additionally reinforcing the cell structure using different capping layers. The role of such layers is to act as barriers against the migration of ionic species and hydroxyl groups to prevent these from reaching the TCO and the passivating layers of SHJ cells.

The optical parameters need to be considered when introducing additional layers at the surface of solar cells. Usually, the TCO layers - that act as ARC - have been optimized to enhance light absorption in the solar cells. Hence, depending on several parameters (e.g. material, refractive index and thickness), the capping layer(s) on top of the TCO might have either detrimental or beneficial repercussions on the optics of the solar cell. Although our goal is not to manufacture the best-performing SHJ cells efficiency-wise, we work with materials

that are known for their anti-reflective properties and are compatible with SHJ technology: SiO_x and SiN_x . Both materials are widely used in the industry as passivating layers and dielectric ARC, respectively, for other solar cell technologies and have also shown potential for mitigating degradation induced by moisture and high voltages.

These layers will be deposited by using a PECVD process. This deposition technique allows for the deposition of relatively conformal thin films at low temperatures, but the growth of such films is very complex to control.

6.4.1 Single capping layer

Besides proving the reliability of SHJ cells, the adoption of a double ARC (DARC) (i.e. deposition of a TCO with a subsequent dielectric layer such as SiO_x or SiN_x) layer may as well lead to a potential reduction of In consumption by reducing the TCO thickness [211]–[213]. It however remains the question of whether the reduction of the TCO (ITO in our case) has detrimental effects on the module's reliability. Initial tests were performed with varying thicknesses of ITO (i.e. 50 nm and the standard 70 nm) and a 70 nm-thick dielectric layer (i.e. SiO_x). The modules did not exhibit significant differences in their performance over the PID test duration (see Appendix B.2 for more details). Consequently, from this point forward, we employ SHJ cells with thinner ITO films (i.e. 50 nm thick).

In the following section, we investigate the impact of single SiO_x and SiN_x films on the PID and DH effects on textured front-emitter SHJ solar cells. We do so by increasing the thicknesses of the capping layers, with an ITO with a fixed thickness of 50 nm, and analysing their effect on the stability of the mini-modules.

SiO_x

SiO_x dielectric layers constitute as valid candidates to be used in combination with ITOs for the formation of DARC in SHJ solar cells. Besides increasing the light coupling by reducing reflection effects [212], [214], the addition of a SiO_x film has shown to boost the passivation and conductivity of SHJ cells [206], [215], [216]. The ARCs reduce reflection losses by bridging the gap between the refractive indexes of air ($n = 1$) and the nc-Si ($n = 4.5$ – 5). With a refractive index of around 1.45, SiO_x layers can further reduce the reflectance loss by covering the TCO layer, which has a higher refractive index ($n = 2$).

All the optical optimizations are usually done considering air as the first interface, but these become less critical when the cells are encapsulated due to the refractive index of encapsulants being very similar to that of SiO_x ($n = 1.49$ – 1.52) [214]. This is well represented in Figure 6.10, where we simulated how the varying thicknesses of SiO_x , combined with a 50 nm-thick ITO, can alter the absorption in the bulk [217]. Variations in the current density as a function of the SiO_x capping-layer thickness are negligible for the cell encapsulated with EVA (0.12%) but become more pronounced for the bare cell, in direct contact with air (1.23%).

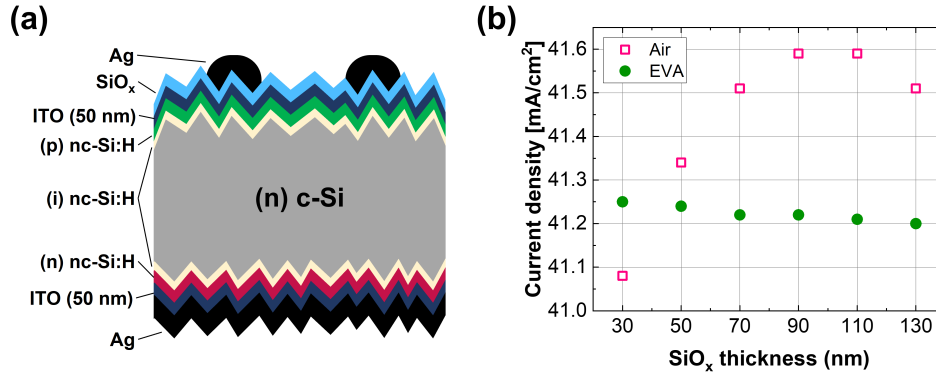


Figure 6.10: (a) Schematics of SHJ solar cell with a single SiO_x capping layer; (b) simulation of current density in the bulk with respect to an increasing thickness of SiO_x layer grown on a 50 nm-thick ITO, for unencapsulated (pink square) and cells encapsulated with EVA (green circles).

Besides gains in cell performance, Du et al. indicated that the SiO_x could enhance the adhesion strength between the polymeric encapsulant and the SHJ cell, potentially increasing the reliability of the latter [218]. The role of SiO_x as a capping layer to mitigate PID in SHJ solar cells is nonetheless still unclear. One of the few studies on SiO_x films regarding reliability was performed on ion-implanted Al-BSF cells. The cells with a 7 to 10 nm-thick SiO_x layer between the c-Si and the SiN_x exhibited high resistance to PID [197]. More recently, Zhang et al. demonstrated that introducing a SiO_x layer between the passivating SiN_x and AlO_x layers at the rear side of PERC cells mitigated PID [219]. We note however that the degradation mechanism in SHJ cells differs from that of conventional p-type c-Si technologies, and we assume that both the cell structure and testing conditions will have an impact on the observed stability.

Figure 6.11 presents the loss in P_{max} for 1-cell textured SHJ mini-modules, encapsulated in G/BS module schemes with EVA, subjected to PID for the standard and extended durations of 96 and 500 hours, with varying thicknesses of SiO_x capping layer (i.e. from 70 nm to 130 nm). These results provide some key information on the application of SiO_x on SHJ as barrier against degradation. First, we note that most of the mini-modules pass the IEC 61215:2021 PID standard, with a performance loss lower than 5% after 96 hours of testing. Second, we observe a clear trend between the loss in P_{max} and the thickness of the dielectric layer. Besides the outlying cells with a 70 nm-thick SiO_x showing a better performance than the thicker permutations of the same, the degradation decreases linearly with SiO_x thickness ($P_{loss} = -0.6 \cdot t_{SiO_x} + 88.8$). Considering this trend, we assume that we would be able to manufacture PID-resistant SHJ cells by depositing a minimum SiO_x thickness of 142 nm on a 50 nm-thick ITO.

It is worth noting that 350 hours of PID test is well beyond the standard protocol established in the IEC 61215:2021 [67], but still within the DH test duration of 1000 hours. The results presented in Figure 6.11 show that DH-induced degradation is mostly prevented, regardless of

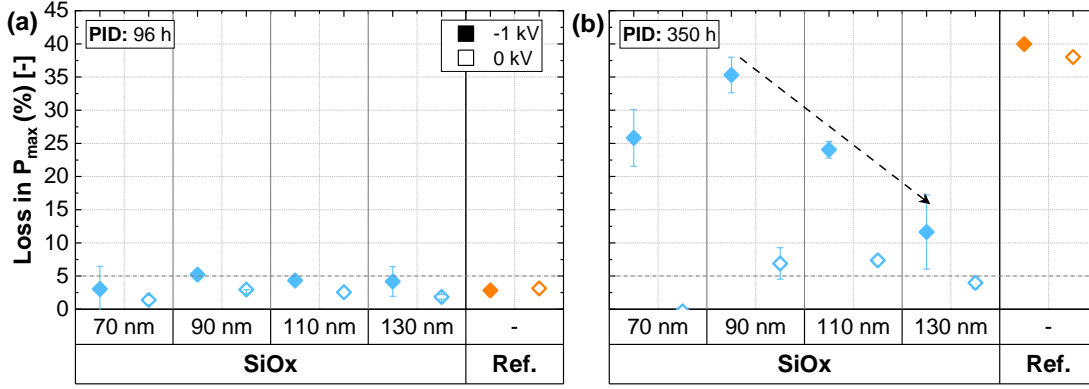


Figure 6.11: Loss in P_{max} for 1-cell textured SHJ cells encapsulated in G/BS mini-modules with EVA as an encapsulant, with varying thicknesses of a single SiO_x capping layer after (a) 96 hours and (b) 350 hours of PID testing. The reference sample is the cell without a capping layer, with a 50 nm-thick ITO layer only. The thickness of the ITO layer is the same for the capped and uncapped cells.

the capping layer thickness. Indeed, both laminates with 70 nm and 130 nm of SiO_x capping layer degrade less than 5%.

SiN_x

The application of SiN_x layers in combination with TCOs to form ARC is not as common, but can also yield interesting results with optimized light absorption. In fact, Batzner et al. reported the possibility of coupling SiN_x with a thinner ITO layer with the aim of reducing In consumptions and, hence, costs [220].

The simulation of the optics of the solar cells with a growing thickness of SiN_x is presented in Figure 6.12. The refractive index of this dielectric layer is close to 2, very similar to the TCO, so that the optimization of the DARC is more critical. However, we observe that the layer of EVA, with an intermediate refractive index, strongly reduces current losses, which are strong for the bare cell (in direct contact to air).

Figure 6.13 shows the loss in P_{max} of the mini-modules with different thicknesses of SiN_x at 96 hours and 350 hours of PID test. In addition to the layers deposited at PV-Lab, one set of SHJ cells had a SiN_x film with higher density and in the range of 70 nm to 90 nm of thickness, deposited by an external company, labelled as "other". In this case, the majority of the mini-modules do not pass the threshold of <5% after 96 hours of testing. We speculate that this might be due to the batch of cells employed, and inconsistencies in the manufacturing processes. Similarly to the results of the previous subsection, the laminates exhibit a linear trend between the thickness of the SiN_x layer and the degradation rate for those cells with capping layers with thicknesses in the range of 70 nm and 110 nm ($P_{loss} = -0.2 \cdot t_{SiN_x} + 57.0$). In this case, if we assume this trend to be consistent, we would need a SiN_x layer with a minimum

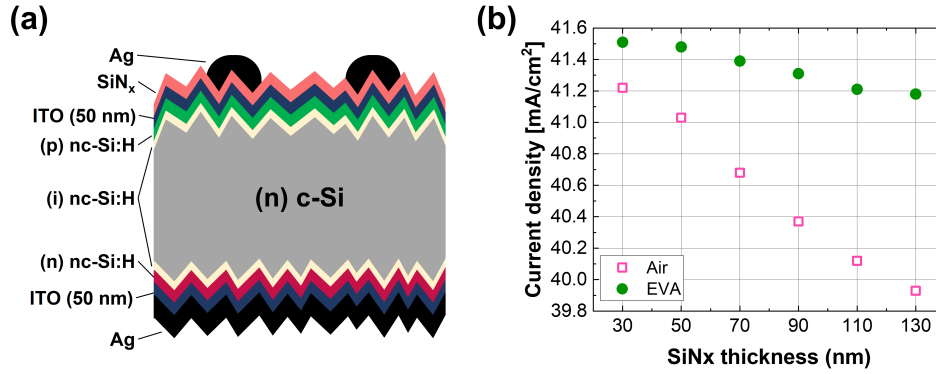


Figure 6.12: (a) Schematics of SHJ solar cell with a single SiN_x capping layer; (b) simulation of current density in the bulk with respect to an increasing thickness of SiN_x layer grown on a 50 nm-thick ITO, for unencapsulated (pink square) and encapsulated (green circles) cells.

thickness of 228 nm for the modules to pass the PID test. It would imply a significant reduction in light absorption at the cell level.

Conversely, the cells with a denser SiN_x exhibit more promising results than the permutations with the SiN_x deposited in our laboratory. These results are in accordance with the early investigations performed by Koch et al. [80], where SiN_x layers with higher refractive indexes (and higher densities, as a general rule) mitigated PID in Al-BSF solar cells. Consequently, we determine that two parameters are key in the development of capping layers to prevent degradation: thickness and layer density.

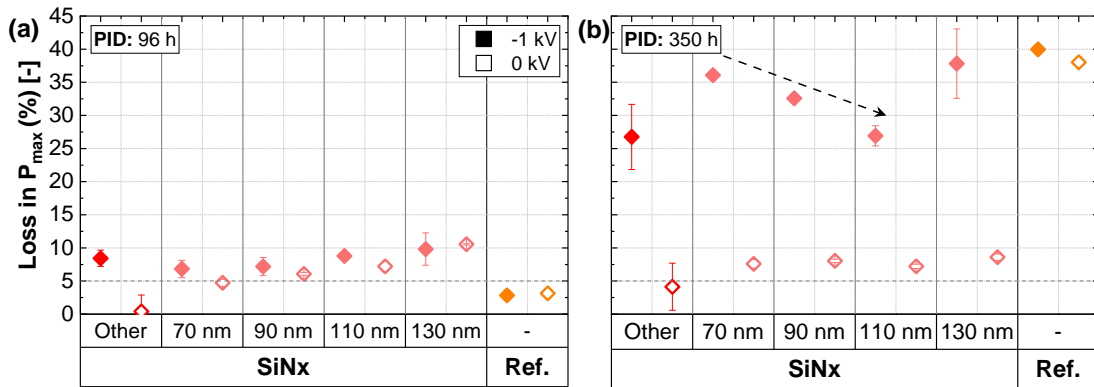


Figure 6.13: Loss in P_{max} for 1-cell textured SHJ cells encapsulated in G/BS mini-modules with EVA as an encapsulant, with varying thicknesses of a single SiN_x capping layer after (a) 96 hours and (b) 350 hours of PID testing. All laminates were tested under -1 kV (full symbol) and standard DH-testing conditions (empty symbol). The reference sample is the cell without a capping layer, with a 50 nm-thick ITO only. The samples labelled as "other" had a denser SiN_x capping layer with a thickness of around 80 nm, deposited by a third party. The thickness of the ITO layer is the same for the capped and uncapped cells.

The results with the SiN_x again demonstrate that sensitivity to DH can be significantly improved with a capping layer, regardless of thickness. In fact, all mini-modules with varying thicknesses of SiN_x exhibit approximately the same performance loss. Like the performance under PID conditions, the denser SiN_x layer seems to prevent DH more efficiently.

Table 6.1 summarizes and compares the results obtained in this section regarding the mitigation of PID by employing single capping layers deposited by PECVD. The presented strategies may not be a perfect solution because additional deposition processes and potentially, costs are added to the manufacturing of the solar cells, besides reducing the cell efficiency by increasing parasitic absorption. We are nonetheless proposing strategies to mitigate In consumption, which is an interesting aspect for the industry. Nevertheless, we demonstrate that a capping layer can lessen the degradation induced by moisture and high negative voltages in SHJ solar cells. Depending on the material used, raising the capping layer's thickness will have different effects. The effect of increasing thickness in SiO_x films has a more significant impact on the module performance ($\sim 29\%$ of P_{loss} difference after 350 hours of PID testing between the best-performing laminate and the reference) than doing so for SiN_x layers ($\sim 13\%$ variation in P_{loss} between the best-capped cell and the uncapped reference).

The difference in DH-induced degradation between the reference cell and the capped SHJ cells (regardless of the material used) is much more significant. The addition of a layer improves significantly the stability of the cells, reducing the degradation to below the 5% limit for some of them. We assume that the difference in results between the DH and PID tests, although correlated, is the considerably higher concentration of Na^+ ions drifting to the cell as a consequence of the electric field induced by the latter. Conversely, in standard DH conditions, the transport of Na^+ ions and hydroxyl groups occurs at a slower rate and is not forcefully driven by additional stressors, making them easier to be protected against.

In summary, SiO_x films seem to be the better option to develop SHJ cell structures more robust to degradation, especially PID. We assume that the difference between the two materials, deposited by the same process, is their density once deposited on ITO. We however note that this assumption applies to our particular case with the films developed in our laboratory and could otherwise depend on the stoichiometry, precursors and deposition parameters used for each individual layer (as demonstrated by the denser SiN_x deposited at an external company).

6.4.2 Double and triple capping layers

In the present section, we investigate the potential of manufacturing PID-resistant SHJ cells by combining the materials studied in the previous section and applying them in double and triple capping layer structures. Table 6.2 summarizes the structures tested here. For clarity, in the following, we refer to the samples with the label indicated in column ID of the table. As a trade-off between optics and stability, we established a thickness of 70 nm per film for these stacks, thus we deposited a total of 140 nm and 210 nm-thick double and triple capping layers, respectively.

6.4. The role of capping layers deposited by PECVD

Table 6.1: Comparison of P_{max} loss of the SHJ cells with single capping layers after 350 hours of PID and DH testing. The values are averages of two laminates. The reference cell (uncapped) and capped cells all have a 50 nm-thick ITO.

Material	Capping layer thickness (nm)	Loss in P_{max} (%)	
		Negative PID	DH
Reference	-	-40.0	-38.0
SiO_x	70	-25.8	-0.3
	90	-35.3	-6.9
	110	-24.1	-7.4
	130	-11.6	-4.0
SiN_x	Other (80)	-26.8	-4.1
	70	-36.1	-7.6
	90	-32.6	-8.0
	110	-26.9	-7.2
	130	-37.8	-8.6

Table 6.2: Double and triple capping-layer structures deposited on SHJ solar cells with a 50 nm-thick ITO encapsulated in G/BS module schemes with EVA for PID tests.

Capping layer	ITO/Capping layers	ID
Double	ITO/ SiO_x / SiN_x	O/N
	ITO/ SiN_x / SiO_x	N/O
Triple	ITO/ SiO_x / SiN_x / SiO_x	O/N/O
	ITO/ SiN_x / SiO_x / SiN_x	N/O/N

We speculate that having double and triple capping layer may potentially mitigate PID and, consequently DH, by:

1. increasing the total thickness and thus presenting a larger barrier for ionic species and hydroxyl groups to diffuse through;
2. adding interfaces between two materials with different refractive indexes and densities to act as traps for Na^+ ions and OH^- groups;
3. having a random distribution of in the different layers to deter the migration of ionic species and hydroxyl groups.

In a recent work, the authors investigated DH-induced degradation in SHJ technology and developed a strategy to mitigate it at the cell level [158]. The methodology employed was to deposit a double capping layer consisting of 40 nm-thick SiN_x and 85 nm-thick SiO_x films on the TCO (i.e. IWO) of their SHJ solar cells. The cells were then stored in a box in a desertic environment close to the Red Sea for a duration supposedly equivalent to 1000 hours in DH. Although this cell structure yielded good results, we note that it was not encapsulated. As previously mentioned, we determined that SHJ technology is sensitive to the transport of Na

and hydroxyl groups originating from the cover glass when exposed to DH conditions, and the phenomenon is further enhanced when the cells are negatively biased. Therefore, we assume a different behaviour might occur to this type of structure when first, the cells are encapsulated and second, when these are subjected to PID.

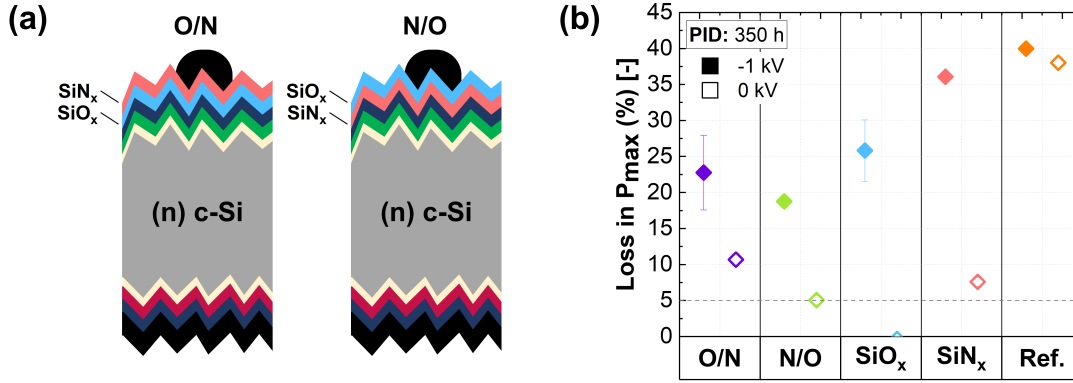


Figure 6.14: (a) Schematics of the SHJ solar cells with double capping layers; (b) loss in P_{max} for 1-cell textured SHJ cells encapsulated in G/BS mini-modules with EVA as an encapsulant, with the two structures with double capping layers after 350 hours of PID testing, compared to the results pertaining to the cells with single capping layers and the uncapped cell (reference). The reference has a 50 nm-thick ITO only. The thickness of the ITO layer is the same for all cells.

In order to verify whether a double capping layer can mitigate PID at the cell level, we manufacture SHJ cells with similar structures to the one used by Liu et al. [158], but with a fixed thickness of 70 nm per layer. We also investigate whether the position of each dielectric layer in the stack has an influence on the degradation rates (see Figure 6.14 (a)). Figure 6.14 (b) presents the losses in P_{max} for the cells with these double dielectric layers after 350 hours of PID test. The laminates with $\text{SiO}_x/\text{SiN}_x$ (i.e. O/N) and $\text{SiN}_x/\text{SiO}_x$ (i.e. N/O) stacks exhibit 23% and 19% performance loss after 350 hours of PID testing, respectively. Although degradation is partly mitigated with respect to the cells without a capping layer and the ones with a 70 nm-thick dielectric layer, the structures are not as effective as the 130 nm-thick SiO_x . We however note that the laminates exhibit a higher stability than when using cells with pure SiN_x layer, regardless of its density. Regarding the order of deposition of the two dielectric layers, the mini-modules with the $\text{SiN}_x/\text{SiO}_x$ stack - with better optical properties - remain slightly more stable under PID conditions. We however note that in the case of PID and considering the standard deviation, both performance losses fall in the same range of values.

Although the double capping layers seem to benefit the stability under PID conditions, we do not observe such an improvement for standard DH-testing conditions compared to the single capping layers. The laminates with double capping layers degrade similarly (or even more for the O/N modules) to the SHJ cells with single SiO_x and SiN_x films.

Triple capping layers have also shown the potential to mitigate PID at the cell level. Li et al. suggested that a multi-gradient triple-layer design can prevent PID in PERC solar cells

[221]. The authors developed a $\text{SiN}_x/\text{SiN}_x\text{O}_y/\text{SiO}_x$ stack that exhibited stability under PID conditions ($P_{\text{loss}} < 5\%$) for the standard and extended testing of 192 hours when encapsulated in a G/BS module configuration with EVA as an encapsulant. These multi-layer stacks were deposited by different processes and modified to achieve different densities to match both the performance and stability. We also note that the PID tests were performed on commercial-size PV modules, where the "edge effect" is more prominent than in 1-cell mini-modules and thus, cells at the center of the module can be less affected by the applied bias than those at the edges.

In order to introduce an additional interface into the previous multi-layer stack, we form a triple capping layer by adding another dielectric film as shown in Figure 6.15 (a). We again combine the two materials for a more abrupt interface between the layers. The performance loss for the cells with triple capping layers after 350 hours of DH and PID testing is shown in Figure 6.15 (b). Unfortunately, these structures do not mitigate PID either. The laminates with $\text{SiO}_x/\text{SiN}_x/\text{SiO}_x$ and $\text{SiN}_x/\text{SiO}_x/\text{SiN}_x$ portray losses of 32% and 25%, respectively, but the latter with a large deviation. The mitigation for DH-induced degradation is again not enhanced with respect to the samples with single capping layers.

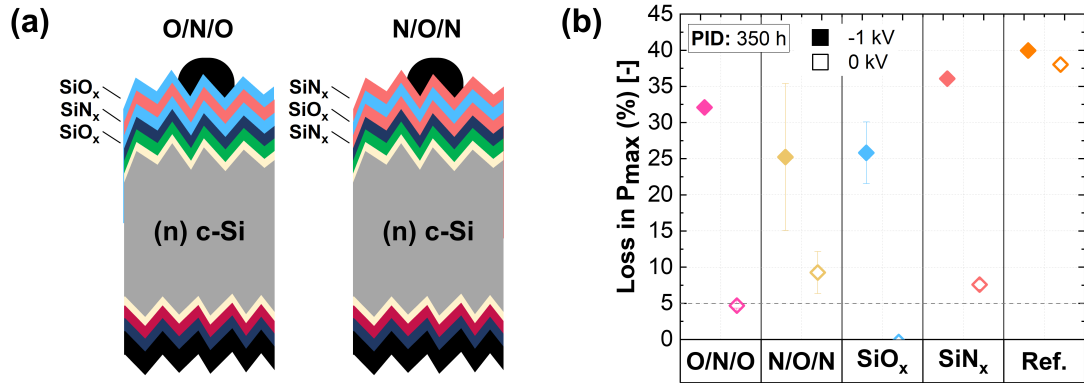


Figure 6.15: (a) Schematics of the SHJ solar cells with triple capping layers; (b) Loss in P_{max} for 1-cell textured SHJ cells encapsulated in G/BS mini-modules with EVA as an encapsulant, with the two structures with triple capping layers after 350 hours of PID testing, compared to the results pertaining to the cells with single capping layers and the uncapped cell (reference). The reference has a 50 nm-thick ITO only. The thickness of the ITO layer is the same for all cells.

This section has attempted to develop PID-resistant SHJ solar cells by depositing capping layers (i.e. single and multi-layer stacks) on top of 50 nm-thick ITO and nc-Si:H films (in conventional uncapped solar cells, the thickness of the TCO is usually 70 nm). In summary, we can highlight the following findings from the work in this section.

1. **Negative PID.** SiO_x layers can mitigate PID more effectively than SiN_x . In both cases, the thickness of the capping layers and for SiN_x , the density (not tested for SiO_x), improves PID resistance.

2. **DH-induced degradation.** In both cases (i.e. SiO_x and SiN_x), the presence of a single capping layer considerably improves resistance to DH-induced degradation. The thickness of the layer does not seem to play a role.
3. Multiple capping layers do not seem to bring any added value. We hypothesize that this can be due to increased mechanical stresses causing cracks and vacancies in the layers, hence enabling the transport of ionic species.
4. To avoid impacting excessively the manufacturing cost and time, and solar cell efficiency, the use of a thin capping layer of SiO_x - or SiN_x - seems to be a reasonable compromise, as it reinforces considerably DH resistance and slightly PID resistance. In the case of PID, the test durations are extended well beyond the duration foreseen by industry standards (IEC 61215:2021), thus higher degradation rates are expected.

6.5 The role of capping layers deposited by ALD

The capping layers in the previous section were deposited by PECVD. Although it is a process that enables the deposition of relatively conformal thin films, it does not provide perfect conformal coverage and can come with many different nano- and micro-structures. Considering that capping-layer density is a key parameter in mitigating degradation, we speculate that ALD can potentially be a suitable deposition method. This technique enables the control to deposit thin films uniformly and with high precision. In addition, it is an industrially compatible process, already employed in the manufacturing of aluminium oxide (Al_2O_3) layers for PERC and TOPCon technologies.

Similarly to SiO_x , Al_2O_3 films with a refractive index of ~ 1.67 - 1.69 can also be employed for the formation of DARC along with TCOs. Indeed, Lee et al. indicated that a 20 nm-thick Al_2O_3 can improve the light coupling in SHJ solar cells [222]. Additionally, other works demonstrated that the deposition of ultra-thin Al_2O_3 layers is compatible with SHJ technology to boost the passivation [223].

With regard to its role concerning reliability, depositing a film of Al_2O_3 between the front-cover glass and the encapsulant to prevent the migration of Na^+ is reportedly a good strategy to mitigate PID in PERC cells and modules [224]. Nevertheless, it is to be seen whether an Al_2O_3 film on top of ITO in SHJ cells can prevent PID. Hereafter, we study the impact of an ALD-grown 70 nm-thick Al_2O_3 layer on a 50 nm-thick ITO when exposed to -1 kV under DH-like conditions.

Figure 6.16 (a) presents the normalized values of P_{max} - with respect to the $P_{initial}$ - throughout the duration of the PID testing for the G/BS modules under -1 kV and 0 kV (i.e. standard DH conditions). Not only do these mini-modules pass the IEC 61215:2021 PID standard of 96 hours, but they also show a very stable behaviour after 192 hours (i.e. 2x IEC), more than their single capping layer counterparts. Although the laminates exhibit a P_{loss} of 6.6% after 192 hours of testing, we consider that this would fall in the measurement uncertainty. The

degradation however accelerates after 280 hours of PID testing, with the laminates exhibiting 14% and 27% performance loss after 350 hours and 500 hours of PID testing. As seen in Figure 6.16 (b), degradation in negative PID is driven by slight changes in I_{SC} and V_{OC} , with a significant impact on R_s .

Again, we highlight the fact that with the addition of a capping layer, DH-induced degradation is vastly improved, and almost deterred.

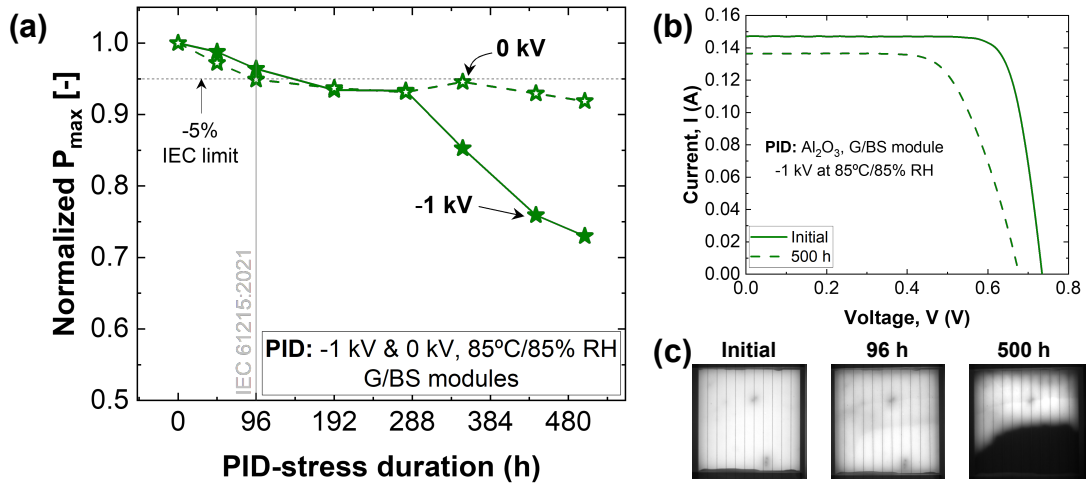


Figure 6.16: (a) Normalized values of P_{max} of 1-cell textured SHJ encapsulated in a G/BS module scheme with EVA, with a 70 nm-thick Al_2O_3 capping layer throughout the extended PID testing of 500 hours. The laminates were tested under -1 kV and 0 kV (standard DH conditions). (b) Illuminated I-V curves and (c) EL images of a representative module tested under -1 kV for 500 hours.

Figure 6.17 compares the loss in P_{max} of the SHJ cells with the Al_2O_3 capping layer to the ones capped with the previously studied layers deposited by PECVD (i.e. SiO_x and SiN_x) and the reference - uncapped - cells. The results indicate that for the same thickness, Al_2O_3 layers can mitigate PID 11% and 21% more effectively than the SiO_x and SiN_x films, respectively. This particular combination of layer composition and deposition process appears to be the most suitable to reduce PID mechanisms at the cell level.

To conclude this section, we note that despite Al_2O_3 /ITO layers appearing as promising candidates for the development of PID-resistant cells, the transport of ionic species is not completely deterred when the PID tests are extended. Nonetheless, it is worth mentioning that PID is mitigated by ~24% and ~18% in P_{loss} with respect to the SHJ solar cells with a 70 nm- and 50 nm-thick ITO layers, respectively, after 500 hours of PID testing. Moreover, the laminates remain stable (P_{loss} about 5%) for a longer testing duration than the capping layers tested in the previous section.

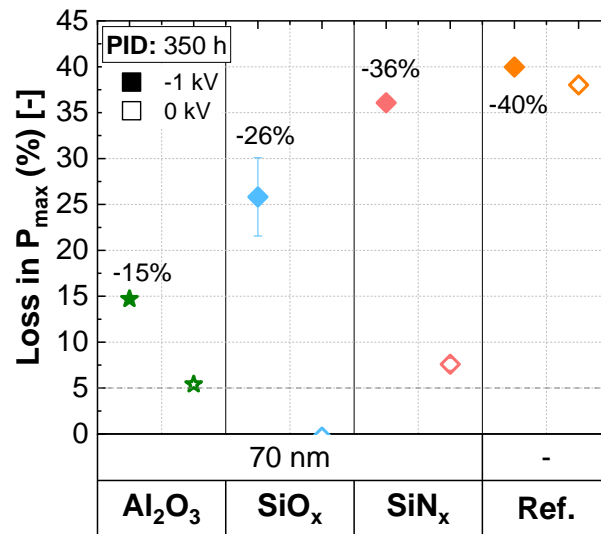


Figure 6.17: Loss in P_{max} for 1-cell textured SHJ cells encapsulated in G/BS mini-modules with EVA as an encapsulant, and the three single capping layers (Al_2O_3 , SiO_x and SiN_x) of 70 nm of thickness after 350 hours of PID testing, compared to the results pertaining to the uncapped cell (reference). The reference has a 50 nm-thick ITO only. The thickness of the ITO layer is the same for all cells.

6.6 Conclusions

In this chapter, we investigated the potential of developing SHJ technology resistant to PID at the cell level. This achievement would pose an interesting possibility for manufacturing PV modules with EVA with increased reliability, which would represent a reduction in cost and easier processability. In order to develop PID-resistant SHJ cells, we focused on two parts: first, we investigated the role of TCO and the passivating layer stacks on the degradation mechanism; and second, we aimed at mitigating PID by adding capping layers on top of the TCO.

We first focused on understanding the role of the TCO morphology and composition in DH and PID mechanisms, by analyzing different aspects of the cell layers. We initially compared the degradation rates between the industrial-size and lab-scale SHJ cells and modules. Despite what we assume to be harsher stress on lab-scale modules due to a smaller centre-to-edge ratio, these exhibit 16% less performance loss than commercial-size modules. We thus assume that the TCO - ITO in this case - is more relevant to degradation than the module dimensions and the difference in performance might be caused by the different ITO quality and densities. Nonetheless, we remark that the batch-to-batch reproducibility of cells and TCO layers are not easy to ensure due to the cells being manufactured on small-area wafers and not in an industrial production line.

We then studied the effect of texturization and determined that flat surfaces are more resistant to the transport of ionic species than textured ones. This could be due to either an increased

TCO thickness, a lower (by 1.7 times) surface availability for Na^+ ions to destroy the cell passivation or a higher layer conformity. The stability of SHJ cells with two different TCO materials (i.e. ITO and IZrO) and substrate layers (i.e. a-Si:H and nc-Si:H) was also investigated. We determined that the TCO substrate - in particular, its surface roughness - changes the growth and impacts the optoelectrical properties of the TCO, more so for IZrO layers. While cells with IZrO are more sensitive to degradation and exhibit inconsistent behaviour throughout the duration of the PID test, the DH-induced degradation and PID in textured SHJ cells ITO/nc-Si:H layers are lessened. We attribute this to a reduction of the grain boundaries where the Na^+ ions and hydroxyl groups can migrate through, thus decreasing the grain boundary scattering.

Next, we attempted to develop "PID-resistant" SHJ cells by depositing capping layers (i.e. SiO_x , SiN_x and Al_2O_3) on top of the front nc-Si:H/ITO stacks deposited on textured front-emitter cells. The goal of the dielectric films, compatible with solar cell manufacturing processes, is to act as barriers against the transport of ionic species and hydroxyl groups. Initially, cells with single layers of SiO_x and SiN_x , deposited by PECVD, with varying thicknesses were subjected to PID for extended durations. We found that degradation can be prevented more efficiently with SiO_x layers and by depositing capping layers with increasing thickness and higher density. Double and triple capping-layer stacks - formed with a combination of SiN_x and SiO_x films - did not deter PID significantly more than the single-layer counterparts. We hypothesize that the sequential deposition of layers can induce mechanical stresses and cause the formation of cracks that can enable the transport of Na^+ ions and hydroxyl groups. Although the addition of an ALD-grown 70 nm-thick Al_2O_3 showed initially higher stability than the other capping layers for longer durations (i.e. 280 hours of PID test), the laminates also degraded after 500 hours of testing. Conversely, DH-induced degradation was mitigated in all cases, regardless of the capping layer material, thickness and the number of layers.

Consequently, we determine that encapsulating SHJ solar cells in a G/BS module scheme and with EVA as an encapsulant would be possible, as long as the materials deposited as capping layers are thick and dense enough to prevent migration of ionic species. We consider the thickness of 70 nm of the capping layer in combination with a thinned-down ITO (from the conventional 70 nm to 50 nm) to be a reasonable compromise since PID is reduced and DH-induced degradation is mostly mitigated. We also believe that it would be an acceptable trade-off between the increased reliability and the cost (maybe higher due to the additional capping layer, but potentially compensated due to the reduced scaled-down consumption of In), the additional processing times in the production line and the potential loss in efficiency.

7 Sensitivity to Moisture and High Voltages of High-efficiency c-Si Technologies

Summary

Potential-induced degradation (PID) is known to vary between solar cell structures, and differences in degradation mechanisms can also be expected within the same technology. In this chapter, we investigate the sensitivity of two bifacial high-efficiency crystalline silicon (c-Si) technologies, passivated emitter and rear contact (PERC) and tunnel oxide passivating contact (TOPCon), and aim to understand their particular PID mechanisms. The PID (and damp heat (DH)) tests are performed by encapsulating the cells in glass/glass (G/G) module packaging with a low-volume resistivity ethylene vinyl acetate (EVA) encapsulant to enhance degradation. This provides a basis to compare the DH-induced degradation and PID mechanisms of silicon heterojunction (SHJ) modules, investigated in Chapters 4 and 5, to PERC and TOPCon technologies. Finally, we investigate the role of moisture ingress in the PID mechanisms of bifacial PERC and TOPCon solar cells by encapsulating them in different module configurations with respect to water permeability.

7.1 Introduction

In the last years, the photovoltaic (PV) industry has taken the leap towards crystalline silicon (c-Si) technologies, in particular, those characterized by high efficiencies and passivating contacts [15]. The reduction in manufacturing costs for c-Si-based cells worldwide and, specifically in China, has driven this transition even further. The PV industry is currently dominated by passivated emitter and rear contact (PERC) solar cells, but silicon heterojunction (SHJ) and tunnel oxide passivating contact (TOPCon) technologies are projected to increase their market shares in the near future [15].

Additional ways of increasing the energy yield - by 10 to 20% depending on several factors like ground albedo - of PV systems are to employ bifacial solar cells and modules. The current production costs for bifacial cells and modules are low enough for their manufacturing and

installation to be cost-competitive. By 2032, it is expected the manufacturing of bifacial modules to increase to 85% [15]. With bifaciality factors of over 90% [114], 80 to 85% [32] and 70% [114], this market trend represents added interest for SHJ, TOPCon and PERC technologies, respectively.

The long-term performance of these technologies is however a significant topic in the field. Moreover, as explained in Chapter 1, high-efficiency technologies are significantly more sensitive to variations in the solar cell parameters (e.g. surface recombination velocities), thus their susceptibility to degradation mechanisms caused by moisture and high-voltage differences might increase.

Reliability studies on PERC technology have been of interest in the last few years due to their rising presence in the market. Unlike SHJ technology, several studies performed on bifacial PERC cells have shown their stability under DH-testing conditions [101], [172]. Their behaviour, when subjected to potential-induced degradation (PID) testing, is however significantly different. A detailed account of the works investigating PID in PERC solar cells is performed in Chapter 1 Section 1.4.1. The predominant assumption is that PID occurs in PERC cells when these are negatively biased with respect to the grounded frame [97]–[99], although Sulas-Kern et al. also reported the occurrence of PID under high positive biases [101]. Most of the literature agrees on the fact that due to the similarity to aluminium back-surface field (Al-BSF) solar cells, the front side of PERC solar cells exhibits PID of the shunting type [97], [101]. The mechanism at the rear side seems to however experience a two-stage process: an initial degradation stage caused by a surface polarization effect [97], [98] (similar to that observed by Swanson et al. on n-type c-Si cells [77]), followed by the corrosion of the Si wafer when the modules are further stressed [99], [100].

The long-term performance of TOPCon solar cells is also highly relevant for their industrialization. However, presently studies on the topic are very limited, most probably due to their relative novelty in the market. In particular, Luo et al. investigated PID in n-type TOPCon solar cells, with a front boron-emitter structure [225]. The authors highlighted the fact that the rear-side n-type poly-Si was resilient to negative PID stresses. Conversely, the front-side emitter exhibited sensitivity to high-negative biases due to increased surface polarization (i.e. PID-p) causing losses in the field-effect passivation. Nevertheless, we also note that DH-induced degradation and/or PID mechanisms on TOPCon solar cells might vary depending on the particular cell structure and manufacturing processes.

It is always significant to put research topics and results into perspective. In this chapter, we aim at investigating and understanding the degradation mechanisms of bifacial PERC and TOPCon technologies under damp heat (DH) and PID testing and comparing the observed mechanisms with those found for our SHJ cells/modules. The mini-modules were manufactured with exactly the same materials as in previous chapters (i.e. glass/glass (G/G) module configuration with ethylene vinyl acetate (EVA)) and the accelerated ageing tests were performed at the same conditions and duration. Moreover, we also investigate the impact of

moisture ingress - or lack thereof - on the PID mechanisms of the two technologies.

7.2 Experimental methods

Mini-module preparation and testing

The solar cells employed for this chapter are all industrial-size bifacial technologies: rear-emitter n-type SHJ, standard p-type PERC and front-emitter n-type TOPCon (see Figure 7.1). The SHJ cells were manufactured in a pilot production line, and PERC and TOPCon cells are commercially available (see Chapter 2 for more details).

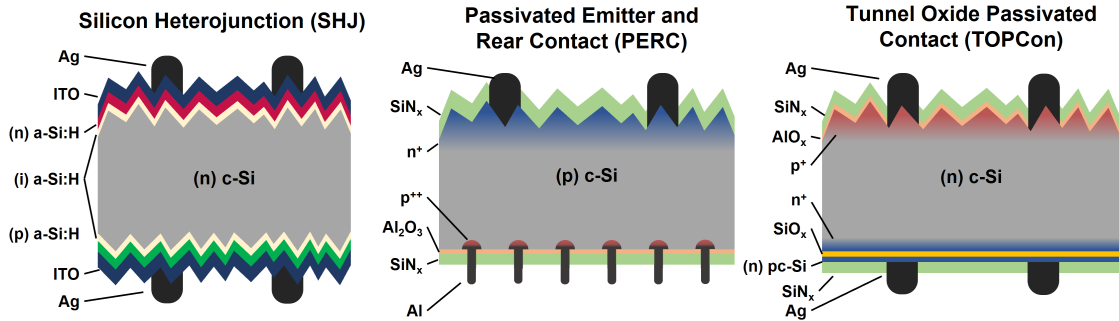


Figure 7.1: Schematics of bifacial solar cell technologies employed in the experimental work of this chapter: rear-emitter SHJ (left), standard p-type PERC (center) and front-emitter n-type TOPCon (right). The solar cells are not drawn to scale.

We manufactured six replicas of 20 x 20 cm² 1-cell G/G mini-module laminates per solar cell technology. The glass utilized as front and rear covers was standard 3.2 mm-thick soda-lime glass. The encapsulant employed was a low-volume resistivity EVA ($\rho \sim 6 \cdot 10^{14} \Omega \cdot \text{cm}$). As explained in previous chapters, the use of a low-resistivity EVA enables us to accelerate degradation, observe degradation modes and understand potential weaknesses. The cell interconnections for the SHJ solar cells were performed by a low-temperature process (i.e. using an ECA as a soldering agent), while the PERC and TOPCon cells were contacted on both sides by the conventional high-temperature (i.e. $\sim 370^\circ\text{C}$) process.

The PID testing was performed following the IEC 61215 standard [67], as seen in Chapter 2. We placed a conductive tape around the mini-modules to simulate the Al frame of commercial-scale modules and placed the samples in a climatic chamber in the conditions described in Table 7.1. The mini-modules were tested for 96 hours as stated in the IEC standard, and the testing was exacerbated by extending the testing duration to 500 hours (i.e. more than 5 times the duration of the standard).

Table 7.1: Experimental matrix employed in this chapter for PID (and DH) testing.

Temperature / Relative Humidity	Cell technology	Voltage
85°C / 85%	Rear-emitter n-type SHJ	-1 kV (x2)
		0 kV (x2) (DH)
		+1 kV (x2)
	p-type PERC	-1 kV (x2)
		0 kV (x2) (DH)
		+1 kV (x2)
	Front-emitter n-type TOPCon	-1 kV (x2)
		0 kV (x2) (DH)
		+1 kV (x2)

Electrical characterization

The mini-modules were tested at regular intervals to monitor their performance. The front and rear sides of the modules were visually inspected and then the 1-sun I-V characteristics were measured at standard test conditions (STC) (i.e. 25°C and irradiation of 1000 W/m²). Each side of the mini-modules was measured separately by covering the non-illuminated side with a black cover to avoid any type of undesired absorption. The electrical parameters were monitored at each measurement (i.e. maximum power (P_{max}), short-circuit current (I_{SC}), open-circuit voltage (V_{OC}) and fill factor (FF)) to assess the degradation rate and mechanism for each module configuration. Dark current density-voltage (J-V) and electroluminescence (EL) measurements were performed to assess the properties of the diode and to evaluate the state of electrical connections and current extraction, respectively. Finally, we performed photoluminescence (PL) imaging and external quantum efficiency (EQE) measurements at both the front and rear sides of the mini-modules.

We note that the results reported for SHJ technology pertain to the analysis performed in Chapter 5, and they provide a reference point to compare the sensitivity of other technologies to DH-induced degradation and PID.

7.3 Degradation mechanism on G/G module configuration

7.3.1 Comparison of cell technologies

Figure 7.2 summarizes the variation in P_{max} experienced for the mini-modules subjected to PID under -1 kV and +1 kV, in DH-like conditions (i.e. 85°C and 85% RH). At all times, modules tested in standard DH conditions were kept as a reference, and their performance was monitored throughout the test duration in parallel with the biased ones. These values were extracted from the illuminated I-V curve measurements.

We observe that for the 96-hour duration (the standard PID-testing protocol) and negative bias (i.e. -1 kV), only SHJ mini-modules pass the test (see Figure 7.2 (a)). Conversely, both

7.3. Degradation mechanism on G/G module configuration

PERC and TOPCon technologies already exhibit significant degradation rates: the former presents P_{max} losses of 51% and 55% and the latter 16% and 36% for the front and rear sides, respectively. The loss in P_{max} when measured at the rear side of PERC cells seems to be greater (albeit only by 4%) than at the front side. The difference in degradation between the two sides is instead more significant in TOPCon cells, with the rear side (i.e. tunnel oxide side) exhibiting 20% more P_{max} losses than the boron-emitter side. Conversely, the three technologies are not sensitive to degradation under high positive bias and, as expected, to the standard DH-like conditions for the duration time of 96 hours.

The results clearly vary - for all testing conditions and technologies - when the test is extended to 500 hours. The degradation mechanisms for SHJ technology under DH and PID testing conditions were explained in detail in Chapters 4 and 5. The investigated SHJ technology exhibits losses of 31% and 20% in P_{max} at the front and rear sides, respectively, under negative PID conditions. The degradation observed in DH-like conditions at the front side is more significant than the one at the rear side, by around 4%. We determined that the front side of our SHJ cells is very sensitive to variations in surface recombination. As explained in Section 7.1, positive biases prevented SHJ solar cells/modules from degrading.

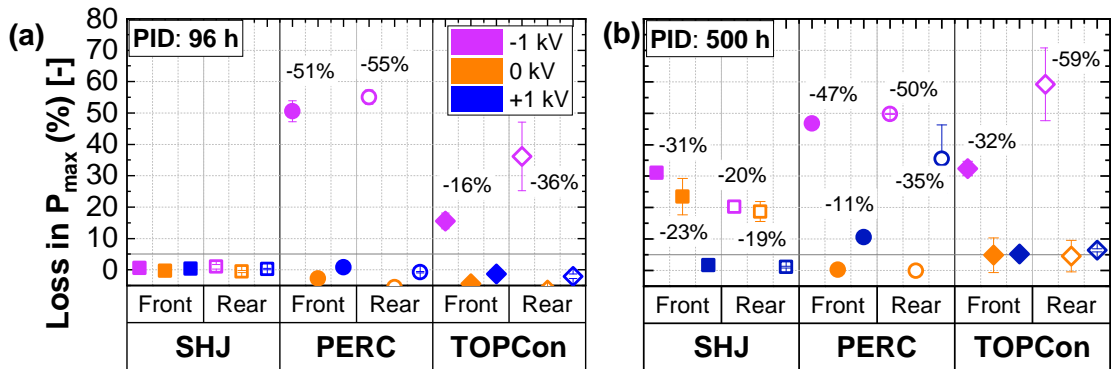


Figure 7.2: Loss in P_{max} of bifacial SHJ, PERC and TOPCon technologies encapsulated in a G/G module structure with EVA, for PID testing at 85°C/85% RH for (a) the IEC standard duration of 96 hours and (b) the extended duration of 500 hours. The mini-modules were subjected to -1 kV (pink), 0 kV (standard DH conditions) (orange), and +1 kV (blue).

Instead, as described in the literature, the PERC technology remains stable in standard DH-like conditions (i.e. 85°C and 85% RH only) throughout the extended PID testing. The behaviour under negative and positive biases is however significantly different. The degradation under -1 kV seems to stabilize over the extended testing at both the front and rear sides. Conversely, although initially unperturbed by a high-positive bias (i.e. +1 kV), PERC laminates exhibit degradation when tested for an extended duration - almost 5 times the standard, particularly at the rear side (i.e. 24% more P_{max} loss than at the front side).

By contrast, the bifacial n-type TOPCon technology investigated in this work continues de-

grading over time, and losses in P_{max} approximately double after 500 hours of PID testing. Regarding the behaviour under DH-like conditions and positive bias, TOPCon modules display similar degradation rates (i.e. $\sim 5\%$). We thus hypothesise that the loss observed in positive bias might as well be a consequence of just the DH-testing conditions and not of the voltage applied. We nevertheless extend the DH testing of our TOPCon modules (in parallel with SHJ and PERC technologies) to 1000 hours (i.e. the IEC 61215 standard protocol [67]) and 2000 hours to investigate their performance when exposed to high temperature and humidity conditions for a long duration (see Section 7.3.2).

A more detailed investigation of PID under high negative and positive biases is carried out in Sections 7.3.3 and 7.3.4 with the aim of understanding the degradation mechanism of our bifacial PERC and TOPCon cells/modules.

7.3.2 DH-induced degradation

Figure 7.3 shows the loss in P_{max} for the three technologies in the standard 1000 hours of the IEC 61215 DH test and for an extended duration of 2000 hours. As explained in the previous section, all three high-efficiency technologies portray different behaviours when exposed to high moisture content.

The bifacial rear-emitter SHJ cells/modules investigated in this work have shown degradation rates proportional to the rate of water ingress, exhibiting the highest degradation when moisture reaches a saturation point within the mini-module. Our microscopic model indicates that the underlying physical degradation mechanism (i.e. diffusion of sodium (Na^+) ions and hydroxyl (OH^-) groups through the grain boundaries of the indium tin oxide (ITO)) is particular to this cell technology due to its intrinsic cell structure. Conversely, PERC solar cells exhibit no degradation whatsoever even when DH testing is performed for an extended duration [172]. Here, our results with the commercially-available bifacial PERC cells confirm that these are stable in DH even when encapsulated with EVA.

We note that the results observed here are valid for the devices tested in this work only. The extrapolation of the results to cover the full cell technology is however somehow critical, as processes, coating thicknesses and compositions may vary from manufacturer to manufacturer, and even from batch to batch from a single manufacturer. Here, we focus on understanding the degradation particular to these bifacial n-type TOPCon solar cells.

Although they initially seem to withstand DH conditions (passing the IEC 61215 DH test, with P_{max} losses of 3% and 4% at the front and rear sides, respectively), the mini-modules exhibit 26% and 25% loss in performance at the front and rear sides after doubling the standard duration (see Figure 7.3 (b)). In opposition to the PID results displayed in Figure 7.2, no significant difference can be observed between the front and rear sides. The results are further confirmed by the illuminated I-V curves in Figure 7.4 (a), where no clear distinction is noted between the two sides. Both I_{SC} and V_{OC} remain stable throughout the test, the FF being

7.3. Degradation mechanism on G/G module configuration

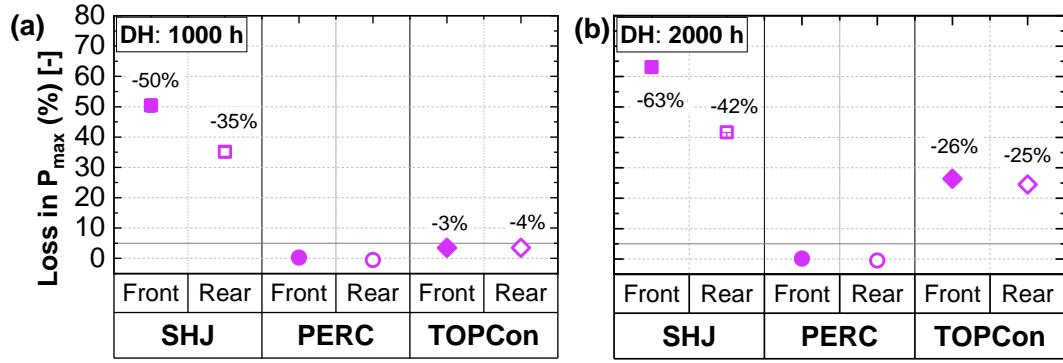


Figure 7.3: Loss in P_{max} of bifacial SHJ (square), PERC (circle) and TOPCon (diamond) technologies encapsulated in a G/G module structure with EVA, for DH testing at 85°C/85% RH for (a) the IEC standard duration of 1000 hours and (b) the extended duration of 2000 hours.

the only electrical parameter affected by the high humidity conditions. The fitting of the I-V curves indicates a certain rise in the series resistance, which might be the cause of the observed degradation.

The degradation is however significantly more evident in the EL images taken, as displayed in Figure 7.4 (b). Contrarily to what could be expected (and what we have observed in our SHJ modules), no edge effect is observed. The mini-modules show degradation in certain areas of the module (as darkened spots), but these do not follow any sort of pattern. The PL image shown in Figure 7.4 (c), performed on the laminates after 2000 hours of DH testing, however, does not display the same behaviour. In fact, despite a small decrease in brightness at the center of the laminate, the PL image does not completely overlap with the EL analysis. This indicates problems in the stability of the metallization, and not so much on the solar cell materials.

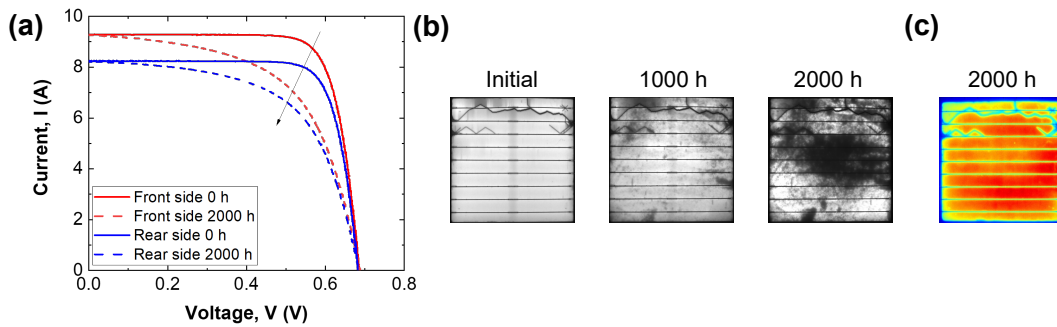


Figure 7.4: (a) Illuminated I-V curves of the front and rear sides; (b) EL images of a bifacial TOPCon cell encapsulated in a G/G mini-module configuration with EVA, before and after 1000 hours and 2000 hours of DH testing; and (c) PL image of the same sample after 2000 hours of DH.

Taking into consideration the reduction in FF and increase of series resistance, along with the EL and PL analyses, we speculate that the DH-induced degradation in the present TOPCon cells is linked to corrosion of the metallization, potentially to the degradation of the screen-printed contacts. Although the findings do not yet give us a full understanding of what occurs in TOPCon cells under high humidity conditions, they reveal that the mechanism is different to the one observed in SHJ solar cells. The difference in performance may be due to the difference in ARC materials. The AR layer in TOPCon cells, in a similar fashion to PERC technology, is silicon nitride (SiN_x), which has shown to be highly stable in DH conditions and when treated with a sodium hydroxide (NaOH) solution (see Chapter 4).

7.3.3 Negative PID

In the previous section, degradation rates and kinetics demonstrated to depend on the cell technology, which is in accordance with what has always been reported in the field. In the present section, we investigate the negative PID mechanisms pertaining to PERC and TOPCon technologies.

PERC technology

Figure 7.6 shows the variation in electrical parameters through the PID testing duration, extended to 500 hours, for the front and rear sides of bifacial PERC cells encapsulated in a G/G module scheme. The variation of P_{max} over time clearly indicates that PERC technology is extremely sensitive to negative PID (i.e. -1 kV), which abruptly degrades by 51% and 55% in the first 96 hours of testing at the front and rear sides, respectively. Taking into account the rapidness of the performance loss and the stability in standard DH conditions, we can assume that the degradation is strictly linked to the applied bias and not to the exposure to humidity. The I-V parameters indicate that the degradation is driven by substantial losses in FF on both sides (36% at the front vs. 38% at the rear after 500 hours of testing), followed by losses in V_{OC} (14% at the front vs. 16% at the rear). It is worth noting that the mechanism and kinetics on both sides are surprisingly similar, unlike what has been previously reported on bifacial PERC cells [98], [101], where the rear side exhibits significantly higher losses.

It is common knowledge that shunting caused by the diffusion of Na^+ ions results in reductions in FF at the front side of Al-BSF solar cells. PID-s is also believed to be the primary degradation mechanism at the front side of PERC solar cells given the similarity in their structures. The I-V curve in Figure 7.6 illustrates how the findings of this research are consistent with the front-side shunting hypothesis.

Conversely, the mechanism at the rear side is not fully understood. While studies performed by Luo and co-authors - among others - reported surface polarization (PID-p) to be the cause of degradation [97], [98], others have attributed it to the corrosion of the c-Si bulk at the rear side (PID-c) [99], [100]. These processes are nonetheless not mutually exclusive and, as reported

7.3. Degradation mechanism on G/G module configuration

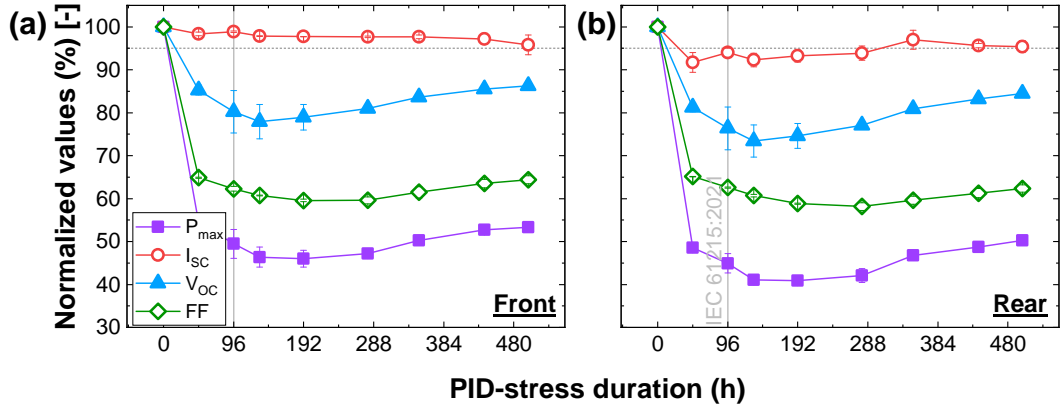


Figure 7.5: Normalized values of the electrical parameters of the (a) front and (b) rear sides of PERC 1-cell mini-modules encapsulated in a G/G structure with EVA, after an extended 500 hours of testing at 85°C/85% RH and -1 kV conditions.

by Ohdaira et al. [226] in n-type front-emitter c-Si solar cells, they can be mechanisms part of different degradation stages. Nevertheless, the aforementioned works described a degradation led by losses in FF and I_{sc} and enhanced rear-surface recombination. In our work, however, the rear side of the PERC cells exhibits exactly the same behavior as the front. The I-V and EQE curves (see Figure 7.6 (a) and (b)) exhibit increased shunting (i.e. reduction in shunt resistance) and a rise in series resistance, as well as a decrease in signal over all wavelengths (i.e. 350-1200 nm) on both sides. Consequently, we assume that the diffusion of Na^+ within the solar cell creates shunts and destroys the passivation of the solar cell.

We nonetheless do not exclude other mechanisms occurring simultaneously. Indeed, the EL images depicted in Figure 7.6 (c) exhibit regions with increased degradation at the edges after 500 hours of PID test, most probably as a consequence of water ingress (remember the water ingress model from Chapter 4, where the edges of the modules are saturated at 500 hours in DH) and the high voltage difference. Conversely, PL measurements (see Figure 7.6 (d)) do not display the same behaviour. In fact, while the signal at the center part of the cell is very low, it is less so at the edges, which indicates a lower material degradation. Thus, we assume that corrosion of the metallization takes place at the edges of the mini-modules when high moisture content and high negative voltage are combined.

Moreover, the mini-modules show a partial recovery (7% at the front and 9% at the rear sides) when the test is extended over the standard PID testing of 96 hours. This has been previously observed in PERC cells in which PID-p was ascribed as the root mechanism [97]. The recovery was attributed to the formation of an inversion layer at the rear side, pushing the majority carriers (i.e. holes) away, and leaving only the minority carriers (i.e. electrons). Considering however that we have not observed enhanced rear-surface recombination in our cells, the recovery mechanism may not be fully understood. We also note that we have not observed recovery when the mini-modules were stored in the dark in ambient conditions.

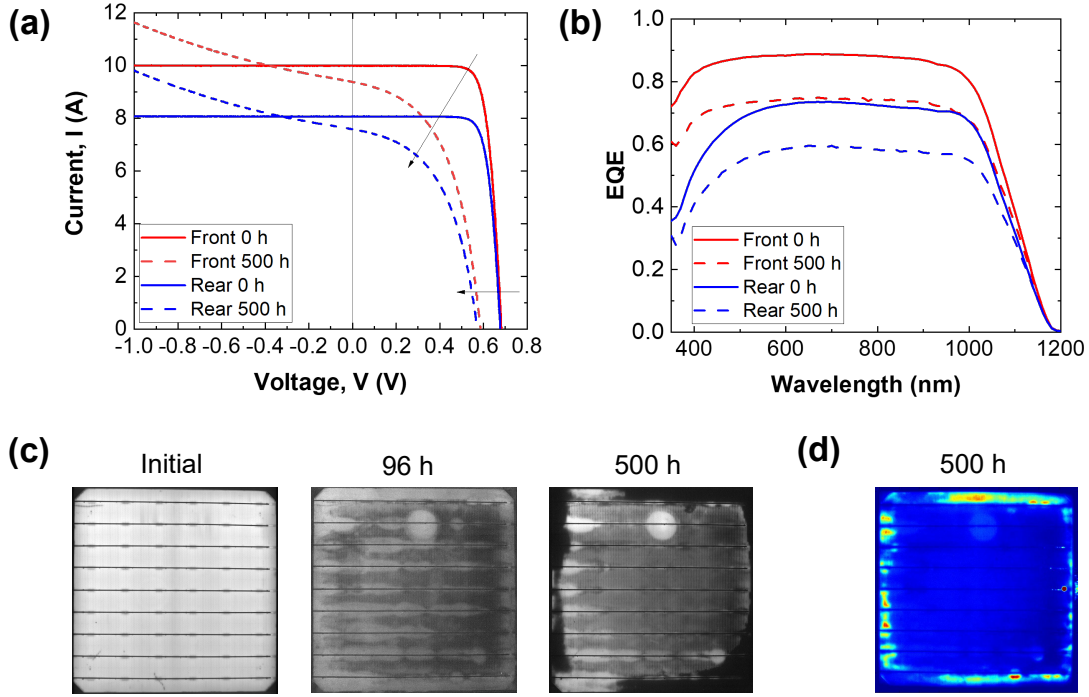


Figure 7.6: (a) Illuminated I-V curves, (b) EQE curves, (c) EL and (d) (PL) images of the PERC I-cell G/G mini-modules exposed to negative PID at 85°C/85% RH for 500 hours.

The discrepancy between the findings in this study with the previously published work [98], [99], [143] could be attributed to different manufacturing processes and material qualities, such as the $\text{AlO}_x/\text{SiN}_x$ layer stack at the rear side. Consequently, careful consideration needs to be given to products from different manufacturers and developing modules that cater to individual technologies.

TOPCon technology

The initial results on bifacial boron-emitter TOPCon cells/modules demonstrate to less sensitive to PID than PERC. Although the mini-modules exhibit lower performance loss during the standard test duration of 96 hours, Figure 7.7 shows how they progressively degrade as the test is extended to 500 hours (unlike PERC modules). In this case, the tunnel-oxide side (i.e. rear side) shows a higher sensitivity to PID than the front: the performance loss at the rear side is 59%, compared to the 32% at the front. From the I-V parameters, we also observe that the mechanism is different on both sides. The front side exhibits equal losses in I_{SC} , V_{OC} and FF (i.e. $\sim 12\%$), while the rear-side degradation is clearly driven by losses in I_{SC} . The similar losses in V_{OC} on both sides indicate a general loss of passivation in the solar cell.

The illuminated I-V and EQE curves in Figure 7.8 (a) and (b) provide more explicit information on the mechanism. As noted before, the loss experienced in V_{OC} is similar on both sides, whereas the loss in I_{SC} is more significant at the rear compared to the front side. The EQE

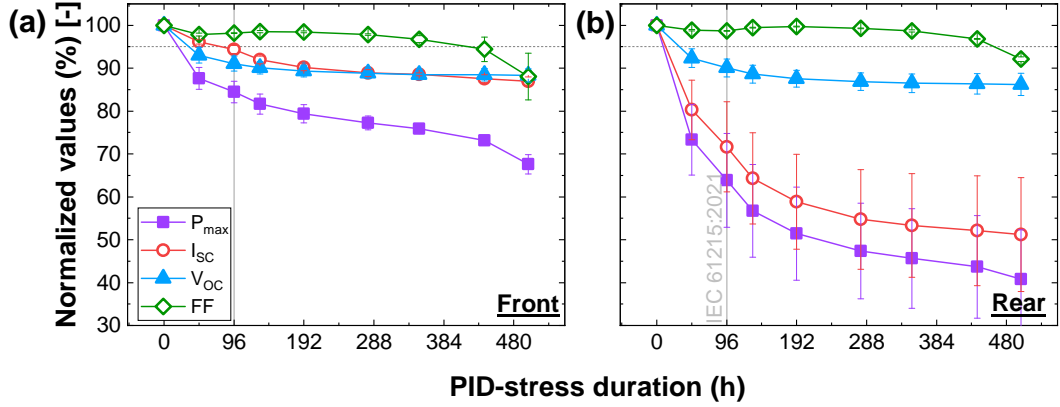


Figure 7.7: Normalized values of the electrical parameters of the (a) front and (b) rear sides of TOPCon 1-cell mini-modules encapsulated in a G/G structure with EVA, after an extended 500 hours of testing at 85° C/85% RH and -1 kV conditions.

curves measured on the most degraded areas of the mini-module complement the I-V parameters. The measurements exhibit a significant reduction at short wavelengths when the mini-module is measured at the rear side, thus indicating increased rear-surface recombination. We however also observe a certain loss in short wavelengths (i.e. photon absorption at the cell surface) when the module is measured at the front side. Similarly to the observations in our bifacial PERC cells, EL images show an edge effect after 500 hours of negative PID, when the moisture at the edges reaches the saturation point. In this case, however, the PL image after 500 hours of PID testing overlaps more consistently with the EL images. We thus assume that the potential corrosion at the edges is also affecting the solar cell material.

We hypothesize that bifacial n-type TOPCon solar cells/modules suffer from multiple degradation modes, occurring simultaneously when subjected to high moisture ingress and negative biases. The front side exhibits a certain loss in shunt resistance after extended PID testing, and increased recombination is observed from the EQE measurements. We ascribe this to the positively charged Na^+ ions being trapped in the SiN_x layer and disrupting the field passivation effect [95], [227], [228]. Another potential phenomenon happening simultaneously is the diffusion of Na^+ into the cell, creating shunts. This might be however less critical than in Al-BSF or PERC solar cells due to the AlO_x layer being a more effective barrier against the diffusion of ionic species than a bare SiN_x layer. On the other hand, we attribute the degradation at the rear side to increased recombination phenomena between the Na^+ ions accumulated in the SiN_x layer and the fixed negative charges of the tunnel oxide. The increased surface recombination rate at the rear side is probably more crucial than at the front. As it was explained in Chapter 5, charge carriers generated at the p-n junction side (the front boron-emitter in this case) are so close to the front metallization that holes can be easily collected as soon as they are generated, while the charge carriers generated near the rear surface depend more on the diffusion length and the surface passivation. In addition to these mechanisms, we speculate that the edge

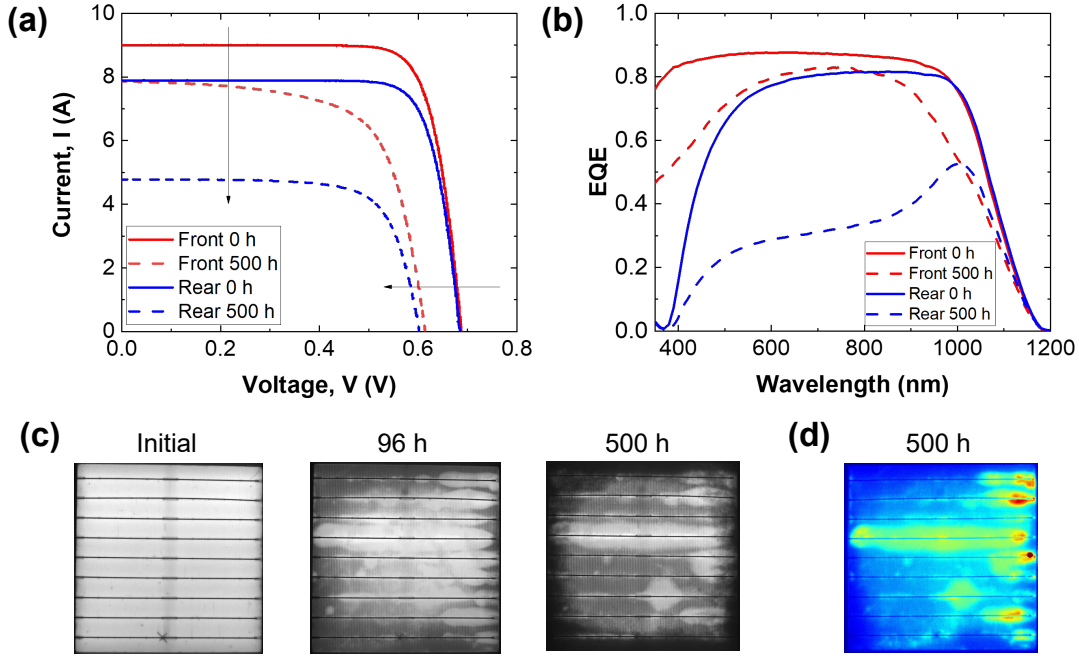


Figure 7.8: (a) Illuminated I-V curves, (b) EQE curves, (c) EL and (d) PL images of the TOPCon 1-cell G/G mini-modules exposed to negative PID at 85°C/85% RH for 500 hours.

effect observed in the EL images is due to corrosion caused by the -1 kV and high moisture contents damaging the cell layers (i.e. PID-c).

The results in the present work differ from the study published by Luo and co-authors, who reported high stability of the passivating contact at the rear side. Therefore, we note that the sensitivity to PID and the degradation mechanisms most probably depend on the particular TOPCon solar cell structure used (e.g. n-type vs. p-type wafers), the manufacturing processes and quality materials. Therefore, each structure should be evaluated individually.

7.3.4 Positive PID

Sunpower IBC is the main technology to exhibit sensitivity to positive PID. Conversely, conventional p-type c-Si (i.e. Al-BSF) are reportedly not affected by high positive biases. Additionally, our findings demonstrate +1 kV can prevent degradation from occurring in SHJ solar cells and modules. The TOPCon technology studied in this work has not exhibited significant performance losses under positive biases either (see Figure 7.2). Therefore, we only investigate the effect of +1 kV PID on our bifacial PERC solar cells/modules.

PERC technology

Although having a very similar structure to Al-BSF, our bifacial PERC solar cells exhibit significant performance loss when subjected to +1 kV in DH-like conditions for extended testing, as presented in Figure 7.9. The mini-modules pass the standard IEC 61215 PID test of 96 hours (i.e. loss in P_{max} lower than 5%), but the degradation increases after 192 hours of testing. In the present case, the rear side exhibits 35% of P_{max} loss compared to the 11% at the front, with an exponential decay on the former. The I-V parameters clearly indicate that the degradation is driven by losses in I_{SC} at the rear side.

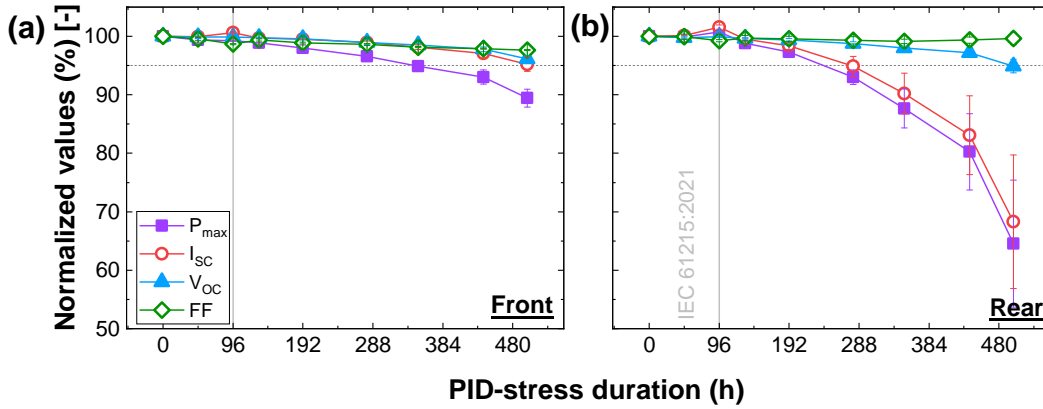


Figure 7.9: Normalized values of the electrical parameters of the (a) front and (b) rear sides of PERC 1-cell mini-modules encapsulated in a G/G structure with EVA, after an extended 500 hours of testing at 85°C/85% RH and +1 kV conditions.

The I-V curves in Figure 7.10 (a) confirm that the loss, mainly in current, at the rear side is much more dramatic than at the front side. The EQE measurements performed on very degraded areas of the modules display a decrease in signal at long wavelengths on the front side (inferring the rear side of the cell) and a significant decrease in short wavelengths when measured at the rear side (signal generated from photons absorbed at the cell surface). The results indicate that the degradation is caused by an increased rear-surface recombination rate. We ascribe this rear-surface behaviour to the 11% of performance loss observed at the front, where charge carriers generated at the rear side cannot be collected efficiently. Both EL and PL images (see Figure 7.10 (c) and (d)) exhibit an edge effect (i.e. display a stronger degradation at the edges) after 500 hours of testing, thus we assume that the effect of a positive bias in PERC cells is influenced by moisture ingress and this causes the cell materials to degrade.

The results investigated in this section are consistent with the published work of Sulas-Kern and co-authors [101]. The authors attributed the performance loss to enhanced corrosion on the metallization or Al pads at the rear side, due to electrochemical reactions between the c-Si and the passivation stacks. However, the exact chemical reactions are not well understood yet, so more detailed analytical work is required for the root mechanism to be properly identified.

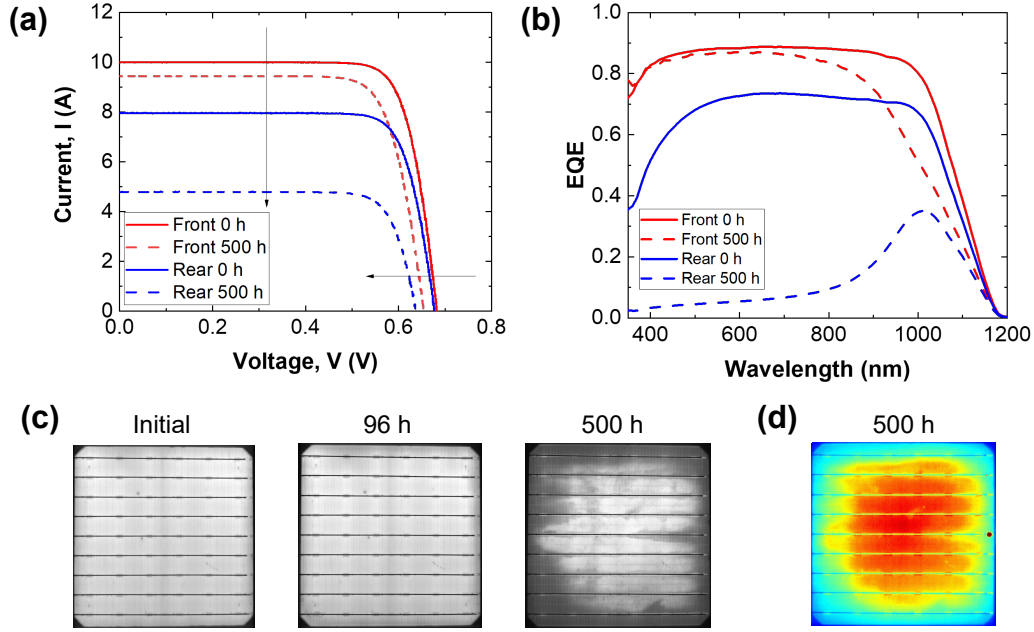


Figure 7.10: (a) Illuminated I-V curves, (b) EQE curves, (c) EL and (d) PL images of the PERC 1-cell G/G mini-modules exposed to positive PID at 85°C/85% RH for 500 hours.

7.4 Investigation of sensitivity to moisture

In Chapters 4 and 5 we discussed the role of moisture in the degradation of SHJ solar cells and modules and presented a detailed microscopic model that described the underlying physical degradation mechanism when these were subjected to DH and PID testing. In Chapter 5 Section 5.5 in particular, we demonstrated that SHJ cells can be encapsulated with EVA if moisture ingress is completely prevented by employing a G/G module structure with an edge seal.

In the next sections, we investigate the role of moisture on the PID mechanisms of PERC and TOPCon technologies and whether the lack of it has a positive impact on their stability. In order to do so, we perform PID testing under -1 kV, 0 kV (as reference) and +1 kV biases, on G/G with edge seal (G/G-ES) and glass/backsheet (G/BS) module schemes, and compare their stabilities to the previously reported configurations (i.e. G/G). In G/G-ES laminates all moisture ingress is prevented, while in a G/BS scheme water enters from the rear side and the edges. All mini-modules were laminated using the same low-volume resistivity EVA as the encapsulant.

7.4.1 PERC technology

In Section 7.3, the occurrence of PID in PERC technology in a G/G module packaging was investigated. One of the most significant discoveries is the rapidness of degradation. Indeed,

modules portray over 50% of performance loss just after 96 hours of PID testing in -1 kV, when moisture has not yet had the time to make an effect in the laminate. Thus, as a first approximation, we could conclude that water ingress does not play a key role in the degradation mechanism of PERC technology under high-negative bias. Conversely, the performance loss under positive bias, mainly at the rear side, takes place after extended PID testing and is potentially induced by corrosion effects. This mechanism could therefore be motivated by the water intake in the laminate.

The summary of the loss in P_{max} for PERC mini-modules after 96 hours and 500 hours of PID testing, presented in Figure 7.11, confirms our hypothesis. Not only do modules in G/G-ES configuration degrade after 96 hours of testing under -1 kV, but the degradation rates are higher than the ones from the G/G laminates (i.e. 75% and 78% of P_{max} loss for the front and rear sides, respectively). We speculate that this 20% difference is due to the high variability of the PID testing process and the sensitivity of PERC to it. Although the cells belong to the same batch and were produced with exactly the same materials, the manufacturing of the mini-modules was done at a different time. In this case, when the test is extended to 500 hours (see Figure 7.11 (b)), the laminates do not recover; on the contrary, the performance losses increase to 89% and 92% for the front and rear sides. Although the mechanism is not clear, the present results lead us to speculate that the recovery mechanism observed in G/G laminates is linked to the moisture content in the laminate.

Conversely, the cells encapsulated in a G/BS configuration exhibit 44% P_{max} loss after 96 hours when tested under high-negative bias. Since the modules were laminated with a conventional non-transparent permeable backsheet, only the front side of the cells was measured. The performance loss is, as expected, lessened in the present scheme compared to the other two. Since the PID mechanism in PERC technology is not affected by moisture ingress, the degradation is partially mitigated by removing the rear-cover glass that acts as a Na reservoir. When the PID test is extended to 500 hours, the P_{loss} increases by only 3%, most probably due to the continuous drift of Na^+ towards the solar cell.

These two module configurations' stability under high-positive bias (i.e. +1 kV) is different from the G/G laminates. As a reminder, the positive PID mechanism is driven by rear-surface recombination and we hypothesize it is aided by moisture ingress. The lack of degradation in G/G-ES mini-modules under positive PID confirms our supposition. In addition, the results indicate that the potential electrochemical reaction occurring at the rear side of bifacial PERC cells (i.e. corrosion of the c-Si rear surface) is assisted by the presence of moisture in the laminates. In the case of G/BS mini-modules, the lack of a rear glass prevents PID.

The results in this section highlight the difference in mechanisms between SHJ and PERC technologies. We have shown that PID in SHJ technology - under negative bias - is driven by high-water contents and can be mitigated in SHJ G/G mini-modules encapsulated with EVA by preventing moisture ingress, that is, by employing an edge seal. Conversely, negative PID in PERC solar cells is not impacted by moisture. In fact, the modules degrade equally (if not

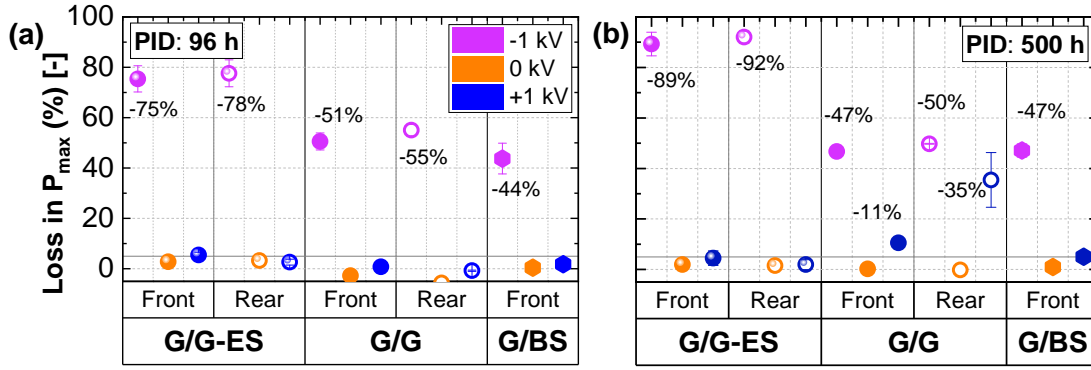


Figure 7.11: Loss in P_{max} of bifacial PERC cells encapsulated in G/G-ES (square), G/G (circle) and G/BS (diamond) module structures with EVA, for PID testing at 85°C/85% RH for (a) the IEC standard duration of 96 hours and (b) the extended duration of 500 hours. The mini-modules were subjected to -1 kV (pink), 0 kV (standard DH conditions) (orange), and +1 kV (blue).

more) when encapsulated in a G/G-ES packaging scheme. We speculate that the reduction in volume resistivity in hot dry conditions (see Figure 5.12 in Chapter 5) and the polarity of EVA are factors significant enough for the accumulation of Na^+ in the SiN_x layers and the ensuing degradation of PERC cells. By contrast, the degradation induced by high-positive voltages can be prevented by limiting moisture ingress in the module.

7.4.2 TOPCon technology

In the previous section, we established that TOPCon technology can be prone to negative PID when tested in -1 kV and DH-like conditions. With an increased sensitivity at the rear side driven by surface polarization phenomena (PID-p), it was supposed that degradation is exacerbated by moisture ingress.

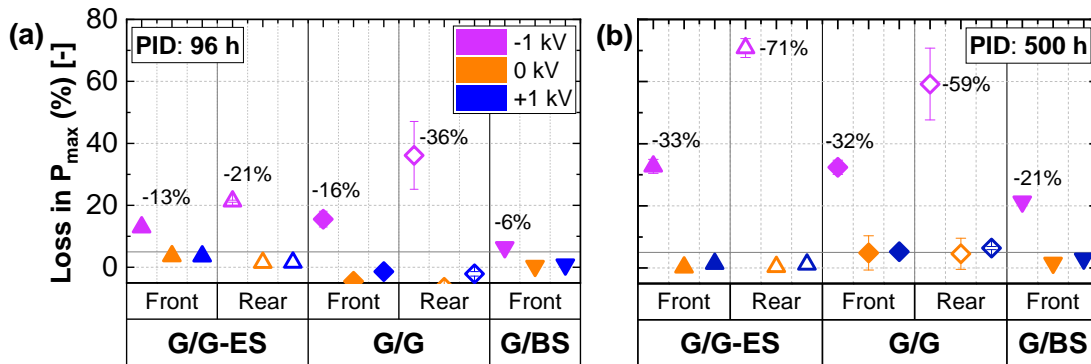


Figure 7.12: Loss in P_{max} of bifacial TOPCon cells encapsulated in G/G-ES (square), G/G (circle) and G/BS (diamond) module structures with EVA, for PID testing at 85°C/85% RH for (a) the IEC standard duration of 96 hours and (b) the extended duration of 500 hours. The mini-modules were subjected to -1 kV (pink), 0 kV (standard DH conditions) (orange), and +1 kV (blue).

7.4. Investigation of sensitivity to moisture

Losses in P_{max} of TOPCon solar cells packaged in different module configurations exposed to PID in DH-like conditions after 96 hours and 500 hours of testing are depicted in Figure 7.12. The results highlight that, like PERC technology, the occurrence of PID in our TOPCon solar cells does not depend on moisture ingress either. In fact, we observe that the progression of performance loss over time is remarkably similar between the G/G and G/G-ES mini-modules¹.

TOPCon cells exhibit increased stability when encapsulated in G/BS module configurations. In this particular case, we determine that the absence of a rear-cover glass prevents the surface polarization effect at the rear side, thus the degradation is mainly driven by increased charge recombination rates and potential shunting at the boron-emitter side - which has shown to be more stable. In this particular case, although the lack of rear-cover glass does not contribute to degradation by acting as a Na reservoir, we assume that the continuous exposure to high-negative biases increases the drift of Na^+ ions towards the solar cell and the accumulation of the same in the SiN_x layers, increasing the degradation from 6% after 96 hours to 21% after 500 hours of PID testing.

To conclude this section, PID tests performed on TOPCon cells encapsulated in varying module configurations with respect to moisture ingress show that the degradation mechanism is not impacted by it. G/G-ES mini-modules degrade as much as the G/G laminates, displaying the same behaviour over time. In accordance with these results, G/BS modules - with a large water intake - exhibit lower degradation rates due to the lack of a rear glass that can act as a Na reservoir. We thus derive that the surface polarization effect observed in these cells does not require the presence of moisture.

A summary of the present chapter is done in Table 7.2. The main takeaways are: i) PERC and TOPCon technologies are significantly more sensitive to PID than SHJ; ii) in contrast, SHJ technology is more sensitive to DH-induced degradation; and iii) negative PID mechanism in PERC and TOPCon technologies is not influenced by the moisture contents in the laminate.

Table 7.2: Summary of whether the technologies and module schemes investigated in this chapter exhibit P_{max} losses below the 5% threshold to pass the IEC 61215 tests, after the standard and extended negative PID and DH testings.

Cell technology	Standard IEC 61215: $P_{loss} < 5\%$						Extended IEC 61215: $P_{loss} < 5\%$					
	(-) PID test - 96 h			DH test - 1000 h			(-) PID test - 500 h			DH test - 2000 h		
	GG-ES	GG	G/BS	GG-ES	GG	G/BS	GG-ES	GG	G/BS	GG-ES	GG	G/BS
SHJ	Yes	Yes	No	Yes	No	No	Yes	No	No	Yes	No	No
PERC	No	No	No	Yes	Yes	Yes	No	No	No	Yes	Yes	Yes
TOPCon	No	No	No	Yes	Yes	Yes	No	No	No	Yes	No	N/A

¹We remark on the large variability in performance between different cells encapsulated in G/G module configurations exposed to -1 kV. Nonetheless, the standard deviation in P_{loss} between G/G laminates falls within the range of the G/G-ES ones.

7.5 Conclusions

The ever-increasing presence of bifacial high-efficiency c-Si technologies (i.e. PERC, TOPCon and SHJ) in the PV market requires guarantees for their long-term stability. In previous chapters, we investigated and proposed DH-induced degradation and PID models for bifacial SHJ technology. In this section, we complement these studies by researching and understanding the PID - and DH - mechanisms of bifacial PERC and TOPCon technologies. We note that the degradation mechanisms investigated in this chapter are particular to the tested cells and products from different manufacturers may experience varying degradation mechanisms due to, for instance, different cell structures, deposition processes and SiN_x stoichiometries.

Initial results on G/G mini-modules encapsulated with EVA showed that both technologies are more sensitive to PID than SHJ. Particularly, PERC cells exhibit a significant degradation (around 50% of P_{max} loss) after 96 hours of negative PID testing, with similar degradation kinetics and mechanisms at the front and rear sides. The results described in this section show reduced FF and V_{OC} values on both sides, in particular a reduced shunt resistance. EQE measurements displayed increased recombination over the spectrum (350 nm to 1200 nm) and along with EL and PL imaging, indicate an overall material degradation. Besides what we consider to be PID-s, the mini-modules also exhibit corrosion of metallization at the edges. As expected, the mechanism under positive PID conditions is different. The modules subjected to +1 kV are prone to degradation mainly at the rear side after 192 hours of PID testing. The electrical characteristics of the solar cells exhibit losses in I_{SC} and significant rear-surface recombination (especially at the edges), which we ascribe to a PID-corrosion (PID-c) phenomenon [101]. Despite their high sensitivity to negative and positive PID, PERC laminates are stable in standard DH conditions.

Laminates with TOPCon solar cells are also prone to degradation - with a P_{max} loss 16% and 36% at the front and rear sides, respectively - after 96 hours of negative PID test. The mini-modules however experience increased degradation when the tests are extended to 500 hours. We determined that several mechanisms occur simultaneously on the bifacial n-type TOPCon solar cells investigated in this thesis. We found that the degradation mechanism is driven by losses in I_{SC} at the rear side, followed by passivation losses. I-V and EQE measurements indicate that besides significant rear-surface recombination due to increased recombination of charge carriers, the front-side boron emitter also experiences some degradation, most probably caused by increased surface polarization effects. The laminates also exhibit corrosion at the edges of the module after the extended PID testing, probably due to the combination of high-moisture contents and high-negative bias. Moreover, we discovered that the mini-modules encapsulated with EVA are also prone to DH-induced degradation when the testing is extended over the standard protocol. We ascribe the loss in FF to degradation in the metallization of the screen-printed contacts. The laminates investigated here are not however prone to degradation in positive PID conditions.

We then studied the dependence of the PID kinetics on the moisture ingress in the laminates

for these two technologies. In opposition to what we have demonstrated for SHJ cells, negative PID occurs in PERC and TOPcon technologies even when moisture ingress is prevented. Conversely, positive PID, which is enhanced with high water contents in the laminate, is prevented in PERC mini-modules.

We hypothesize that the root cause of the different performance between SHJ cells and PERC and TOPCon technologies is the presence of the transparent conductive oxide (TCO) and SiN_x layers, respectively. In DH conditions, without an electric field, Na^+ ions and hydroxyl groups can diffuse through the grain boundaries of the crystalline TCO (ITO in our particular case) of SHJ cells. The SiN_x , lacking these grain boundaries, is a good barrier against the diffusion of such species. Conversely, when a high-voltage difference is applied, and an electric field is induced as a consequence of increased leakage currents, the roles of these layers change. The TCO layer, being a conductive film, avoids any charge accumulation and the increased amount of Na^+ ions originating from the glass follow the same diffusion process through the grain boundaries as in DH conditions. On the contrary, Na^+ ions can accumulate in the SiN_x ARC due to its dielectric properties and easily diffuse further into the solar cell, creating shunts, for instance. The results pertaining to PERC cells, in particular, show that the SiN_x layer saturates very rapidly.

Taking into consideration the results described in this chapter, we can conclude that PID in PERC and TOPCon technologies cannot be mitigated using a G/G-ES module scheme with purely EVA as an encapsulant. The industry is already taking steps towards increasing the implementation of PO-based encapsulants, or even EPE multi-layers for increased reliability of bifacial modules [46]. We also assume that the adoption of a front POE/rear EVA encapsulation scheme in a G/BS or G/T-BS module configuration, either with permeable or impermeable foils, is a potential strategy to mitigate PID.

8 Conclusions and Perspectives

8.1 Summary of the main results

The current energy crisis requires for an efficient transition to energy produced from renewable energy sources. Owing to its worldwide availability and cost competitiveness, photovoltaics (PV) is one of the most promising sustainable technologies. Reducing the cost of systems is key to ensuring continued investment in PV. This can be achieved in two ways: one, by increasing the efficiency of the PV cells and modules and, two, by providing reliable products with longer-service lifetimes. In this thesis, we focus on the latter topic and mostly investigate the **reliability** of a novel high-efficiency technology which is now entering the global PV market and has the possibility to gain a considerable market share in the coming decade: **silicon heterojunction (SHJ)**. We study the main weaknesses of SHJ technology to understand the root cause of different degradation modes and propose mitigation strategies at the module and cell levels. We finally compare the stability of SHJ to other predominant high-efficiency crystalline silicon (c-Si) technologies in the market: passivated emitter and rear contact (PERC) and tunnel oxide passivated contact (TOPCon) solar cells.

In **Chapter 3**, a meta-analysis was performed on the reliability of SHJ modules installed in the field. Despite the limited reports on outdoor monitoring data of SHJ technology, some initial conclusions were extracted. With median performance loss rates (PLR) of 0.56 %/year, the long-term performance of SHJ showed to be in line with conventional c-Si technologies. The reported works highlighted two main failure modes outdoors: losses in current due to encapsulant discoloration (not particular to the technology) and losses in passivation. The latter is not well understood yet. We however note that these reports are based on one particular SHJ technology belonging to Sanyo/Panasonic, and the state-of-the-art products may exhibit different behaviors. We then performed a review of the published indoor accelerated ageing tests and highlighted three main sensitivities of SHJ: exposure to humidity, high-voltage differences (potential-induced degradation (PID)) and UV. Nonetheless, we consider that with the appropriate module configuration, SHJ technology can achieve service lifetimes of 35+ years.

In **Chapters 4 and 5** we focused on two of the aforementioned weaknesses of SHJ: moisture-induced degradation and PID. Our tests, performed on bifacial rear-emitter SHJ cells encapsulated in glass/glass (G/G) module schemes with ethylene vinyl acetate (EVA) as the encapsulant material, demonstrated that the phenomena are interlinked. A multi-factorial microscopic model was proposed to explain the degradation mechanism. First, high-water contents induce the leaching of the inner surface of the glass, creating sodium hydroxide (NaOH) molecules that can diffuse through the EVA and into the SHJ solar cells. Sodium ions (Na^+) and the hydroxyl (OH^-) can then percolate through the grain boundaries of the transparent conductive oxide (TCO) layer, increasing grain-boundary scattering. The ionic species can potentially reach the hydrogenated amorphous Si (a-Si:H) passivating layers, damaging the passivation and, thus degrading the solar cell. Second, when a high-negative bias is applied to the solar cell, the previous phenomenon is enhanced and the additional drift of Na^+ ions originating from the glass (both at the front and rear sides) further destroys the passivation of the solar cell. High-positive biases prevent all degradation, confirming our hypothesis.

We then proposed different mitigation strategies for DH-induced degradation and PID at the module level: i) the use of high-volume resistivity and low water vapor transmission rate (WVTR) encapsulants; ii) the addition of an edge seal in G/G module scheme to prevent moisture ingress (the degradation is mitigated even with employing EVA); iii) the adoption of a front-polyolefin (PO) and rear-EVA encapsulant combination in a glass/transparent backsheets (G/T-BS) module scheme, with a low WVTR T-BS.

Chapter 6 was dedicated to understanding the role of the TCO and its substrate layers (i.e. passivating layers) in the DH-induced degradation and PID mechanisms and developing stable SHJ solar cells under those stressors. The three main parameters that a TCO should exhibit for improved stability are i) high density and homogeneity, ii) flat surface and iii) large crystal grain sizes (obtained by depositing nanocrystalline Si (nc-Si:H) layers as substrate instead of a-Si:H). Taking those results into consideration, the development of stable SHJ cells was done employing nc-Si:H/indium tin oxide (nc-Si:H/ITO) layer stacks with the addition of capping layers on top to act as barriers against the diffusion of ionic species. We demonstrated that silicon oxide (SiO_x), silicon nitride (SiN_x) and aluminium oxide (Al_2O_3) single capping layers can be promising candidates to partially mitigate PID and that increasing the thickness of such layers is more effective than depositing multiple stacks of them. Moreover, we note that DH-induced degradation is prevented regardless of the thickness of the capping layer.

Finally, in **Chapter 7** we compared the performance of PERC and TOPCon technologies to SHJ under DH and PID conditions. We highlight that despite being more stable than SHJ in DH-testing conditions, both PERC and TOPCon laminates exhibit significantly higher sensitivity to PID. Moreover, we demonstrate that the degradation is not linked to the water ingress in the modules, thus PID (i.e. at -1 kV) cannot be prevented by employing G/G-ES module schemes with EVA as an encapsulant like in SHJ solar cells. Therefore, the mitigation of these technologies is limited to the use of PO-based encapsulants.

8.2 Perspectives

8.2.1 Update on reliability of SHJ technology

The survey performed in Chapter 3 was based on a very limited amount of works for relatively short time frames and it corresponded mainly to the SHJ technology particular to Sanyo/-Panasonic. First, the survey will have to be complimented in the coming years to have a more statistically significant sample. Moreover, besides the presence of new manufacturers, we also have novel materials (e.g. encapsulants) and different glass structures. We have expectations to report lower degradation rates for the SHJ modules entering the market today and learn about the long-term behaviour of state-of-the-art SHJ technology.

8.2.2 Microscopic model on DH-induced degradation

Although in Chapter 4 we propose what we consider an accurate degradation model for SHJ laminates when exposed to high water contents, the exact mechanism is not completely understood. We do some assumptions which will have to be validated: i) the glass corrosion process; ii) the diffusion of NaOH molecules through the encapsulant; iii) the diffusion of ionic species through the TCO.

Moreover, we have not been able to identify the presence of Na and/or NaOH in the TCO at the microscopic level. Therefore, it is important to develop a testing and measurement procedure to identify ionic species at low concentrations. Potentially, developing a cell extraction procedure (without the encapsulant and glass) to perform secondary ion mass spectrometry (SIMS) measurements would be meaningful. Similarly, also the PID model for SHJ could be improved since it relies (as a first step) on the DH model.

8.2.3 Updates on PID with increased bias

Our PID tests were performed with an applied bias of ± 1 kV. Because of the recent trend of going towards larger system voltages (i.e. 1.5 kV), we may have to repeat our tests by applying higher biases. On the other hand, as PID tends to evolve linearly with applied bias (at least up to 1 kV), the degradation at higher voltages can be potentially modelled.

8.2.4 Improvements in the development of PID-free SHJ cells

In Chapter 6, two parameters were found to be key in mitigating PID (and DH-induced degradation) in SHJ cells: the TCO and the dielectric capping layers. The consistency and reproducibility of the TCO layer deposition have been limiting factors in developing PID-resistant solar cells. Seeing the significance of having a dense, conformal layer, strategies to improve the TCO films should be considered. Additionally, the performance under moisture and high-voltage conditions of other TCO materials besides the ones investigated in this thesis

(e.g. indium zinc oxide (IZO) or indium tungsten oxide (IWO)) should be investigated in parallel.

Regarding the capping layers, we have observed that density is also a key parameter. Seeing that SiO_x layers performed relatively well in PID conditions, developing such films with varying degrees of density should be investigated.

8.2.5 Understanding of PID mechanism in PERC and TOPCon technologies

We performed some preliminary PID tests on PERC and TOPCon technologies in Chapter 7. Despite PID in PERC cells being a topic of thorough research in recent years, the mechanism at the rear side is not well understood yet. Some researchers indicate surface polarization being the cause, while others assume it is induced by the corrosion of the bulk c-Si. Our results lead to a different mechanism. Therefore, investigating more deeply into the root cause is a crucial task to understand the mechanism so as to prevent it at the cell and module scales. For that, microscopy measurements (e.g. SEM, TEM and EDX) should be performed.

There is a very limited literature on the reliability of TOPCon cells/modules, and we are about the first ones to report on DH-induced degradation and PID in this technology. Again, in order to accurately assess the degradation mechanism, microscopic measurements would be the next steps to take.

Finally, for all cell technologies investigated, it is difficult to extrapolate our results and observations to cover the full technology, as there may be a lot of differences in the materials, solar cell structures and manufacturing processes used by different manufacturers. In particular, we note that the changes in the degradation phenomena in different TOPCon cells may be more critical than in other technologies. Therefore, testing other schemes would be crucial to correctly encapsulate them in robust module packagings.

A Appendix on PID in bifacial large-area SHJ cells and modules

A.1 Appendix on the front and rear-side contributions to PID in SHJ modules

The results of the present Appendix section were presented in an oral presentation and conference proceedings: O. Arriaga Arruti, L. Gnocchi, F. Lisco, A. Virtuani and C. Ballif, *The front- and rear-side contributions to the potential-induced degradation of bifacial silicon heterojunction solar modules*, oral presentation and proceedings at the 38th European PV Solar Energy Conference and Exhibition (EU PVSEC), online, 2021.

In the present section, we aim to give further insight into the potential-induced (PID) mechanism in bifacial silicon heterojunction (SHJ) solar cells, studying the contribution from both the front and rear sides. We do this by manufacturing bifacial SHJ one-cell mini-modules in a glass/glass (G/G) scheme. We compare the contribution of each of the sides by combining two different polymers, ethylene vinyl acetate (EVA) along with a high-resistivity encapsulant (POE) (see Table A.1). A voltage bias of -1 kV was applied to the short-circuited module leads with respect to the grounded frame and, at each testing condition, two samples were kept unbiased (i.e. standard damp heat (DH) conditions) as reference.

We aim to isolate the contribution of PID to one side of the module at a time, by using one layer of POE on one side, which has shown to be PID-resistant in SHJ solar cells, as seen in Chapter 5. We consider that the POE acts as a protective layer against degradation. In order to provide a point of reference, the modules were compared at all times to the EVA/EVA and POE/POE laminates.

The mini-modules were characterized during the PID testing by illuminated current-voltage (I-V) curves, and measured separately at the front and rear sides.

The comparison in the evolution of maximum power (P_{max}) loss of the front side of the laminates throughout the extended negative PID testing is summarized in Figure A.1. These modules were subjected to PID under a bias of -1 kV for 450 hours. All module structures

Table A.1: Encapsulant combinations on the G/G mini-modules using bifacial SHJ solar cells.

ID	Front encapsulant	Rear encapsulant
EVA/EVA	EVA	EVA
POE/POE	POE	POE
POE/EVA	POE	EVA
EVA/POE	EVA	POE

degrade less than 5% after 96 hours of testing, thus “passing” the IEC 61215 standard [67]. In fact, the kinetics for the different structures change after 192 hours (2 times the IEC TS), with very different evolutions.

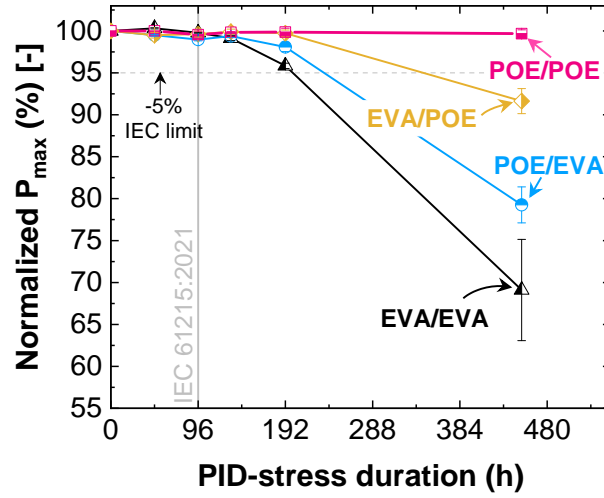


Figure A.1: Normalized P_{max} at the front-side of 1-cell SHJ G/G mini-modules with EVA/EVA, POE/POE, POE/EVA and EVA/POE structures, after an extended PID testing of 450 hours at 85°C/85% RH and -1 kV conditions. The values plotted in the chart are the averages of each type of sample.

As expected, we observe that having one POE layer on one of the sides of the cell already has an impact on the degradation of the mini-module. POE/EVA modules exhibit a power loss of 21% after the extended PID test, while the EVA/POE modules, with the POE layer at the rear side, show a P_{max} loss of 8%.

The relative variation of electrical parameters for the POE/EVA and EVA/POE module structures (along with the reference modules) is summarized in Figure A.2. The degradation in the former is dominated by a considerable loss in the fill factor (FF). Conversely, the degradation of the cells with an EVA/POE structure is less pronounced and driven equally by losses in the short-circuit current (I_{SC}) and FF.

As observed in the relative variation of the modules with the EVA/EVA scheme, the loss of P_{max} at the front side of these bifacial SHJ solar cells is 10% larger than at the rear side. Furthermore, the mechanism itself is different: the front side is characterized by a loss in I_{SC} , derived from

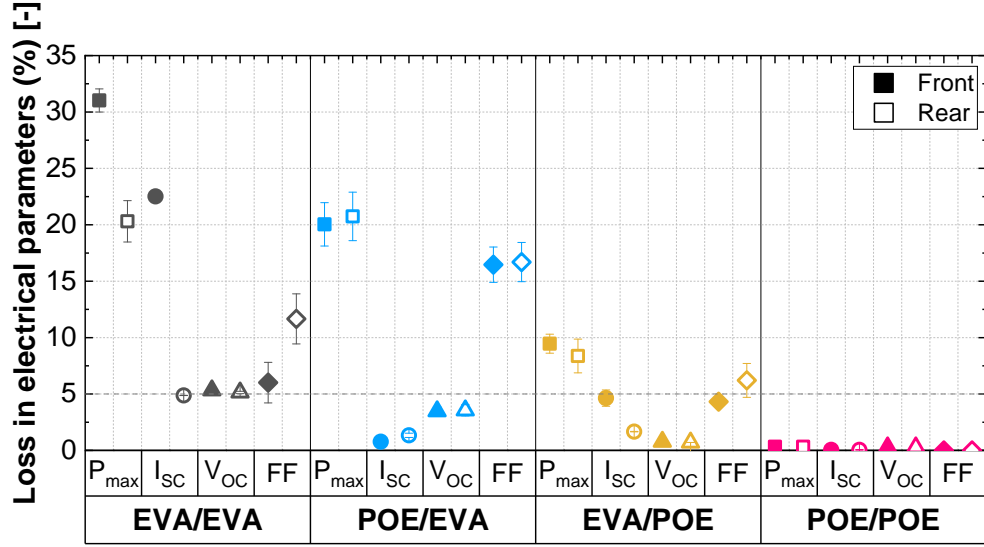


Figure A.2: Relative variation of electrical parameters at the front and rear sides of G/G mini-modules encapsulated in the EVA/EVA, POE/EVA, EVA/POE and POE/POE schemes, subjected to -1 kV for 450 hours.

increased front-surface recombination (see Chapter 5), whereas the degradation at the rear side is driven by FF losses, due to increased recombination at the p-n junction of the cell.

These findings led us to believe that protecting the front side would be more efficacious to reduce the effect of PID in these cells. Nonetheless, we observe the opposite effect. Indeed, protecting the rear side, where the p-n junction is located (i.e. EVA/POE scheme), improves the performance of the module by 10%, compared to the POE/EVA configuration. Therefore, using POE as the encapsulant to protect the rear side of a bifacial SHJ mini-module can have a very positive impact on decelerating degradation, albeit it does not completely prevent it.

The POE layer at the front side in the POE/EVA scheme does not have an effect on the rear side of the SHJ cell. Although, as expected, it does at the front side. Conversely, the module benefits in its entirety when this POE layer is placed at the rear side, that is, in the EVA/POE module structure. All electrical parameters display a lower degradation in this module scheme. In fact, the degradation of the V_{oc} in the SHJ cell is minimal, showing stable passivation throughout the extended PID test. Consequently, we can say that the front-surface recombination observed in EVA/EVA module schemes is caused by the contribution of issues generated at both the front and rear sides of the cell. Thus, these results confirm that the introduction of defects in the p-n junction will impact the collection of charge carriers at the front side. Therefore, if we prevent sodium (Na^+) ion diffusion with the use of POE at the rear side of the cell, we avoid the potential defects at the p-n junction, thus minimizing the recombination current and allowing a good carrier collection at both sides of the cell.

A.2 Appendix on the role of the emitter position on the PID mechanism

Complementary to the previous section, we investigated the role of the emitter position of SHJ cells on the PID (and DH-induced degradation) mechanisms. In order to do so, we used the bifacial rear-emitter SHJ cells investigated throughout this work, and flipped them to "make" them front-emitter cells. The cells were encapsulated in glass/aluminium foil (G/Al-BS) module schemes with the same low-volume resistivity EVA as before. We assume that the use of an Al-BS (with low water permeability) as the rear cover prevents water ingress and diffusion of Na^+ ions, so the degradation is decoupled (i.e. only at the front side).

The results, shown in Figure A.3, indicate that front-emitter structures are more sensitive to PID than rear-emitter ones. We hypothesize that this is due to the Na^+ ions directly attacking the p-n junction, increasing the recombination junction and hence, losses in FF.

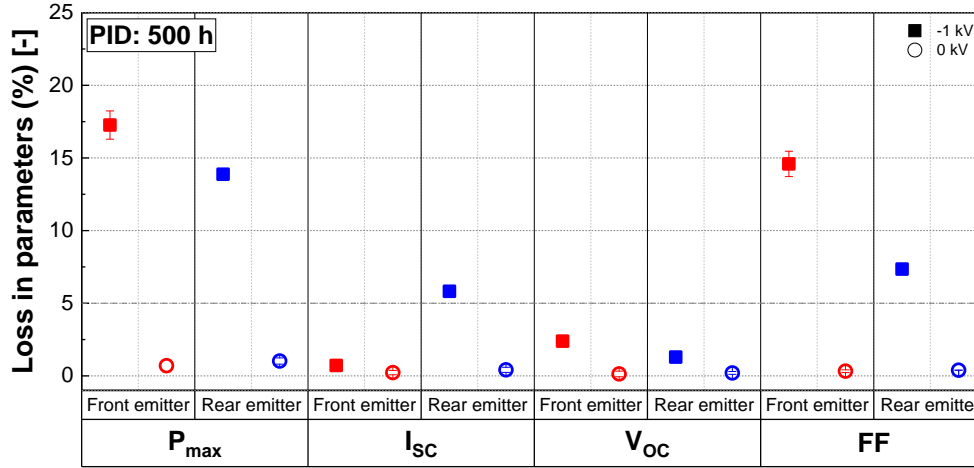


Figure A.3: Loss in electrical parameters for bifacial SHJ 1-cell G/Al-BS mini-modules encapsulated with a low-volume resistivity EVA, subjected to -1 kV and 0 kV for 500 hours. The same large-area rear-emitter bifacial SHJ cells as in the previous work were used, but the cells were flipped to consider them as "front emitter" for testing purposes.

B Appendix on development of PID-free SHJ cells

B.1 The role of AZO in the degradation mechanism

Initially, SHJ cells with AZO as the TCO material were also considered for the development of PID-resistant cells. The cells were encapsulated in G/BS module schemes, with a low-resistivity EVA to induce PID, and subjected to DH and PID testing for 500 hours. The results, depicted in Figure B.1, indicate this scheme to be much more sensitive to degradation, in both moisture and high-voltage conditions, than the conventional SHJ cells with the ITO layer.

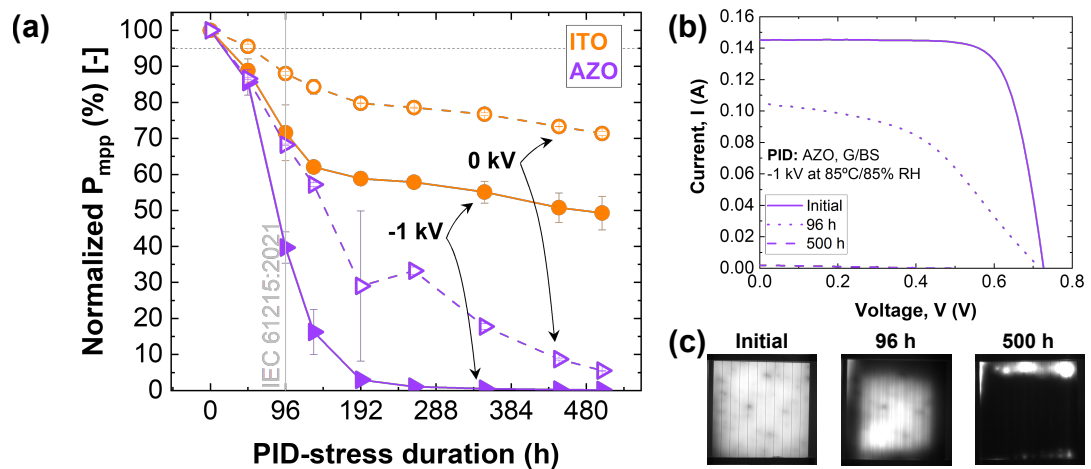


Figure B.1: (a) Normalized values of P_{max} of 1-cell textured SHJ encapsulated in a G/BS module scheme with EVA, with an AZO layer as the TCO, throughout the extended PID testing of 500 hours. The laminates were tested under -1 kV and 0 kV (standard DH conditions). (b) Illuminated I-V curves and (c) EL images of a representative module tested under -1 kV for 500 hours.

We hypothesize that this is related to the degradation of the AZO layer when exposed to high-humidity conditions. In Chapter 4, the effect of the diffusion of hydroxyl (OH^-) groups through the TCO layers was explained. These can increase grain-boundary scattering, reducing charge

carrier collection. Moreover, several research works on the stability of thin-film technologies have reported that water molecules and these OH^- can be chemisorbed in the grain boundaries of the AZO layers, inducing its degradation [177]–[180]. The latter phenomenon, which does not occur in ITO layers, could explained the enhanced DH-induced degradation and PID of SHJ cells with AZO films seen in Figure B.1.

B.2 The role of TCO thickness on degradation rates

The reduction of indium (In) consumption is a critical topic in the PV industry. The development of PID-resistant SHJ cells in Chapter 6 is done by depositing capping layers on top of the TCO film. The research work published by Cruz et al. [211] demonstrated that for good optical properties, a SiO_x layer should be combined with a thinner ITO layer. Here, we investigate whether thinner ITO and indium zirconium oxide (IZrO) films, below the SiO_x layer, can hinder the stability of the SHJ cells.

In order to test this, we encapsulated SHJ cells, with two different TCO materials (i.e. ITO and IZrO) and thicknesses of 50 nm and 70 nm with the additional 70 nm-thick SiO_x capping layer on top, in G/BS module configurations and EVA. We then subjected the mini-modules to DH and PID testing at -1 kV for 500 hours. The results, presented in Figure B.2 indicate that reducing the TCO by 20 nm does not significantly impact PID (DH is prevented in all cases). Therefore, a 50 nm-thick ITO was employed in the development of PID-free SHJ solar cells in Chapter 6.

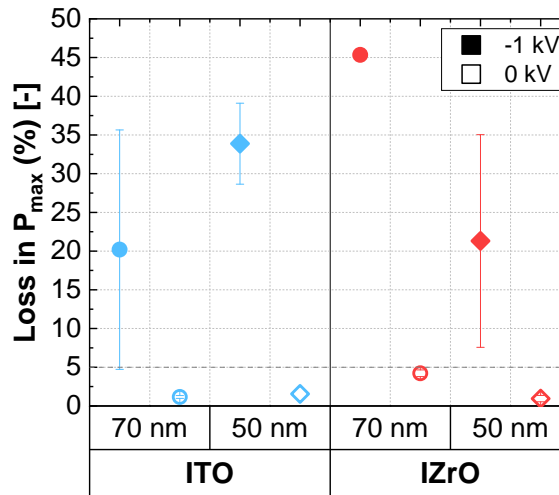


Figure B.2: Loss in P_{\max} of textured front-emitter SHJ cells encapsulated in G/BS module schemes with EVA as an encapsulant, after 500 hours of DH and PID testing. Two different TCO materials were tested, ITO and IZrO, each of them with thicknesses of 50 nm and 70 nm, with a 70 nm-thick SiO_x capping layer on top.

Bibliography

- [1] P. Pfleiderer, C.-F. Schleussner, M. Mengel, and J. Rogelj, “Global mean temperature indicators linked to warming levels avoiding climate risks”, *Environmental Research Letters*, vol. 13, no. 6, p. 064015, Jun. 2018, ISSN: 1748-9326. DOI: 10.1088/1748-9326/aac319. [Online]. Available: <https://iopscience.iop.org/article/10.1088/1748-9326/aac319> (visited on 11/13/2022).
- [2] “Adoption of the Paris Agreement”, UNFCCC, Tech. Rep.
- [3] I. E. Agency, “World Energy Outlook 2022”, IEA, Tech. Rep.
- [4] “State of the Global Climate Report 2022”, World Meteorological Organization, Tech. Rep., 2022.
- [5] S. Bouckaert, A. Pales Fernandez, C. McGlade, *et al.*, “Net Zero by 2050: A Roadmap for the Global Energy Sector”, 2021.
- [6] M. Roser, “The world’s energy problem”, *Our World in Data*, Dec. 2020.
- [7] IEA, “Global Energy Crisis”, *International Energy Agency*, 2022.
- [8] “Renewables 2022 Global Status Report”, *REN21*, 2022.
- [9] W. Hemetsberger, M. Schmela, and R. Lopes Sampaio, “Global Market Outlook for Solar Power 2022-2026”, *SolarPower Europe*, pp. 1–116, 2022.
- [10] IEA, “Solar PV”, *IEA*, 2022. [Online]. Available: <https://www.iea.org/reports/solar-pv>.
- [11] S. F. O. of Energy, “Solar Energy Statistics 2021”, *SFOE*, Jul. 2022.
- [12] S. F. O. of Energy, “Energy Strategy 2050. Monitoring-Report 2021. Abridged Version”, *SFOE*, 2021.
- [13] C. Ballif, F.-J. Haug, M. Boccia, P. J. Verlinden, and G. Hahn, “Status and perspectives of crystalline silicon photovoltaics in research and industry”, *en, Nature Reviews Materials*, vol. 7, no. 8, pp. 597–616, Mar. 2022, ISSN: 2058-8437. DOI: 10.1038/s41578-022-00423-2. [Online]. Available: <https://www.nature.com/articles/s41578-022-00423-2> (visited on 12/20/2022).
- [14] K. Branker, M. Pathak, and J. Pearce, “A review of solar photovoltaic levelized cost of electricity”, *en, Renewable and Sustainable Energy Reviews*, vol. 15, no. 9, pp. 4470–4482, Dec. 2011, ISSN: 13640321. DOI: 10.1016/j.rser.2011.07.104. [Online]. Available: <https://linkinghub.elsevier.com/retrieve/pii/S1364032111003492> (visited on 12/20/2022).

BIBLIOGRAPHY

- [15] ITRPV, “International Technology Roadmap for Photovoltaic - Results 2021”, ITRPV, Tech. Rep., 2022.
- [16] C. A. Wolden, J. Kurtin, J. B. Baxter, *et al.*, “Photovoltaic manufacturing: Present status, future prospects, and research needs”, en, *Journal of Vacuum Science & Technology A: Vacuum, Surfaces, and Films*, vol. 29, no. 3, p. 030 801, May 2011, ISSN: 0734-2101, 1520-8559. DOI: 10.1116/1.3569757. [Online]. Available: <http://avs.scitation.org/doi/10.1116/1.3569757> (visited on 12/06/2022).
- [17] E ISE, “Photovoltaics Report”, Fraunhofer ISE, Tech. Rep., Dec. 2022.
- [18] S. Sadhukhan, S. Acharya, T. Panda, *et al.*, “Evolution of high efficiency passivated emitter and rear contact (PERC) solar cells”, en, in *Sustainable Developments by Artificial Intelligence and Machine Learning for Renewable Energies*, Elsevier, 2022, pp. 63–129, ISBN: 978-0-323-91228-0. DOI: 10.1016/B978-0-323-91228-0.00007-0. [Online]. Available: <https://linkinghub.elsevier.com/retrieve/pii/B9780323912280000070> (visited on 12/06/2022).
- [19] J. del Alamo, J. Eguren, and A. Luque, “Operating limits of Al-alloyed high-low junctions for BSF solar cells”, en, *Solid-State Electronics*, vol. 24, no. 5, pp. 415–420, May 1981, ISSN: 00381101. DOI: 10.1016/0038-1101(81)90038-1. [Online]. Available: <https://linkinghub.elsevier.com/retrieve/pii/0038110181900381> (visited on 12/06/2022).
- [20] A. W. Blakers, A. Wang, A. M. Milne, J. Zhao, and M. A. Green, “22.8% efficient silicon solar cell”, en, *Applied Physics Letters*, vol. 55, no. 13, pp. 1363–1365, Sep. 1989, ISSN: 0003-6951, 1077-3118. DOI: 10.1063/1.101596. [Online]. Available: <http://aip.scitation.org/doi/10.1063/1.101596> (visited on 12/06/2022).
- [21] T. Dullweber and J. Schmidt, “Industrial Silicon Solar Cells Applying the Passivated Emitter and Rear Cell (PERC) Concept—A Review”, *IEEE Journal of Photovoltaics*, vol. 6, no. 5, pp. 1366–1381, Sep. 2016, ISSN: 2156-3381, 2156-3403. DOI: 10.1109/JPHOTOV.2016.2571627. [Online]. Available: <http://ieeexplore.ieee.org/document/7493618/> (visited on 12/06/2022).
- [22] M. A. Green, A. W. Blakers, J. Shi, E. M. Keller, and S. R. Wenham, “19.1% efficient silicon solar cell”, en, *Applied Physics Letters*, vol. 44, no. 12, pp. 1163–1164, Jun. 1984, ISSN: 0003-6951, 1077-3118. DOI: 10.1063/1.94678. [Online]. Available: <http://aip.scitation.org/doi/10.1063/1.94678> (visited on 12/06/2022).
- [23] M. A. Green, “The Passivated Emitter and Rear Cell (PERC): From conception to mass production”, en, *Solar Energy Materials and Solar Cells*, vol. 143, pp. 190–197, Dec. 2015, ISSN: 09270248. DOI: 10.1016/j.solmat.2015.06.055. [Online]. Available: <https://linkinghub.elsevier.com/retrieve/pii/S0927024815003244> (visited on 12/06/2022).
- [24] D. Kray, M. Hermle, and S. W. Glunz, “Theory and experiments on the back side reflectance of silicon wafer solar cells”, en, *Progress in Photovoltaics: Research and Applications*, vol. 16, no. 1, pp. 1–15, Jan. 2008, ISSN: 10627995, 1099159X. DOI: 10.1002/pip.769. [Online]. Available: <https://onlinelibrary.wiley.com/doi/10.1002/pip.769> (visited on 12/06/2022).

- [25] F. Feldmann, M. Bivour, C. Reichel, M. Hermle, and S. Glunz, "A Passivated Rear Contact for High-Efficiency n-Type Si Solar Cells Enabling High Voc's and FF>82 %", en, *28th European Photovoltaic Solar Energy Conference and Exhibition*; 988-992, 5 pages, 4939 kb, 2013, Artwork Size: 5 pages, 4939 kb Medium: application/pdf Publisher: WIP. DOI: 10.4229/28THEUPVSEC2013-2CO.4.4. [Online]. Available: <http://www.eupvsec-proceedings.com/proceedings?paper=21651> (visited on 12/06/2022).
- [26] F. Feldmann, M. Bivour, C. Reichel, M. Hermle, and S. W. Glunz, "Passivated rear contacts for high-efficiency n-type Si solar cells providing high interface passivation quality and excellent transport characteristics", en, *Solar Energy Materials and Solar Cells*, vol. 120, pp. 270–274, Jan. 2014, ISSN: 09270248. DOI: 10.1016/j.solmat.2013.09.017. [Online]. Available: <https://linkinghub.elsevier.com/retrieve/pii/S0927024813004868> (visited on 12/06/2022).
- [27] Z. Rui, Y. Zeng, X. Guo, *et al.*, "On the passivation mechanism of poly-silicon and thin silicon oxide on crystal silicon wafers", en, *Solar Energy*, vol. 194, pp. 18–26, Dec. 2019, ISSN: 0038092X. DOI: 10.1016/j.solener.2019.10.064. [Online]. Available: <https://linkinghub.elsevier.com/retrieve/pii/S0038092X19310606> (visited on 12/06/2022).
- [28] A. Morisset, R. Cabal, B. Grange, *et al.*, "Conductivity and Surface Passivation Properties of Boron-Doped Poly-Silicon Passivated Contacts for c-Si Solar Cells", en, *physica status solidi (a)*, vol. 216, no. 10, p. 1 800 603, May 2019, ISSN: 1862-6300, 1862-6319. DOI: 10.1002/pssa.201800603. [Online]. Available: <https://onlinelibrary.wiley.com/doi/10.1002/pssa.201800603> (visited on 12/06/2022).
- [29] M. Hermle, F. Feldmann, M. Bivour, J. C. Goldschmidt, and S. W. Glunz, "Passivating contacts and tandem concepts: Approaches for the highest silicon-based solar cell efficiencies", en, *Applied Physics Reviews*, vol. 7, no. 2, p. 021 305, Jun. 2020, ISSN: 1931-9401. DOI: 10.1063/1.5139202. [Online]. Available: <http://aip.scitation.org/doi/10.1063/1.5139202> (visited on 12/06/2022).
- [30] F. Meyer, A. Ingenito, J. J. Diaz Leon, *et al.*, "Localisation of front side passivating contacts for direct metallisation of high-efficiency c-Si solar cells", en, *Solar Energy Materials and Solar Cells*, vol. 235, p. 111 455, Jan. 2022, ISSN: 09270248. DOI: 10.1016/j.solmat.2021.111455. [Online]. Available: <https://linkinghub.elsevier.com/retrieve/pii/S0927024821004955> (visited on 12/06/2022).
- [31] S. Choi, O. Kwon, K. H. Min, *et al.*, "Formation and suppression of hydrogen blisters in tunnelling oxide passivating contact for crystalline silicon solar cells", en, *Scientific Reports*, vol. 10, no. 1, p. 9672, Jun. 2020, ISSN: 2045-2322. DOI: 10.1038/s41598-020-66801-4. [Online]. Available: <https://www.nature.com/articles/s41598-020-66801-4> (visited on 12/06/2022).
- [32] Y. Chen, D. Chen, C. Liu, *et al.*, "Mass production of industrial tunnel oxide passivated contacts (i-TOPCon) silicon solar cells with average efficiency over 23% and modules over 345 W", en, *Progress in Photovoltaics: Research and Applications*, vol. 27, no. 10, pp. 827–834, Oct. 2019, ISSN: 1062-7995, 1099-159X. DOI: 10.1002/pip.3180.

BIBLIOGRAPHY

- [Online]. Available: <https://onlinelibrary.wiley.com/doi/10.1002/pip.3180> (visited on 12/06/2022).
- [33] Panasonic, *Panasonic HIT Sanyo history*. [Online]. Available: <https://eu-solar.panasonic.net/en/panasonic-hit-sanyo-history.htm>.
- [34] S. D. Wolf, A. Descoeudres, Z. C. Holman, and C. Ballif, “High-efficiency silicon heterojunction solar cells: A review”, *Green*, vol. 2, no. 1, pp. 7–24, 2012.
- [35] T. G. Allen, J. Bullock, X. Yang, A. Javey, and S. De Wolf, “Passivating contacts for crystalline silicon solar cells”, en, *Nature Energy*, vol. 4, no. 11, pp. 914–928, Nov. 2019, ISSN: 2058-7546. DOI: 10.1038/s41560-019-0463-6. [Online]. Available: <http://www.nature.com/articles/s41560-019-0463-6> (visited on 12/08/2022).
- [36] LONGi, *At 26.81%, LONGi sets a new world record efficiency for silicon solar cells*, Nov. 2022. [Online]. Available: <https://www.longi.com/en/news/propelling-the-transformation/>.
- [37] Z. C. Holman, A. Descoeudres, L. Barraud, *et al.*, “Current Losses at the Front of Silicon Heterojunction Solar Cells”, *IEEE Journal of Photovoltaics*, vol. 2, no. 1, pp. 7–15, Jan. 2012, ISSN: 2156-3381, 2156-3403. DOI: 10.1109/JPHOTOV.2011.2174967. [Online]. Available: <http://ieeexplore.ieee.org/document/6129468/> (visited on 12/09/2022).
- [38] Z. C. Holman, M. Filipič, A. Descoeudres, *et al.*, “Infrared light management in high-efficiency silicon heterojunction and rear-passivated solar cells”, en, *Journal of Applied Physics*, vol. 113, no. 1, p. 013 107, Jan. 2013, ISSN: 0021-8979, 1089-7550. DOI: 10.1063/1.4772975. [Online]. Available: <http://aip.scitation.org/doi/10.1063/1.4772975> (visited on 12/09/2022).
- [39] K. Yoshikawa, H. Kawasaki, W. Yoshida, *et al.*, “Silicon heterojunction solar cell with interdigitated back contacts for a photoconversion efficiency over 26%”, en, *Nature Energy*, vol. 2, no. 5, p. 17 032, May 2017, ISSN: 2058-7546. DOI: 10.1038/nenergy.2017.32. [Online]. Available: <http://www.nature.com/articles/nenergy201732> (visited on 12/09/2022).
- [40] B. Ehrler, E. Alarcón-Lladó, S. W. Tabernig, T. Veeken, E. C. Garnett, and A. Polman, “Photovoltaics Reaching for the Shockley–Queisser Limit”, en, *ACS Energy Letters*, vol. 5, no. 9, pp. 3029–3033, Sep. 2020, ISSN: 2380-8195, 2380-8195. DOI: 10.1021/acsenenergylett.0c01790. [Online]. Available: <https://pubs.acs.org/doi/10.1021/acsenenergylett.0c01790> (visited on 03/09/2023).
- [41] A. Shah, Ed., *Solar Cells and Modules* (Springer Series in Materials Science), en. Cham: Springer International Publishing, 2020, vol. 301, ISBN: 978-3-030-46485-1 978-3-030-46487-5. DOI: 10.1007/978-3-030-46487-5. [Online]. Available: <http://link.springer.com/10.1007/978-3-030-46487-5> (visited on 03/09/2023).

- [42] A. De Rose, D. Erath, T. Geipel, A. Kraft, and U. Eitner, "Low-Temperature Soldering for the Interconnection of Silicon Heterojunction Solar Cells", en, *33rd European Photovoltaic Solar Energy Conference and Exhibition*; 710-714, 5 pages, 7827 kb, 2017, Artwork Size: 5 pages, 7827 kb Medium: application/pdf Publisher: WIP. DOI: 10.4229/EUPVSEC20172017-2AV.3.1. [Online]. Available: <http://www.eupvsec-proceedings.com/proceedings?paper=41280> (visited on 03/09/2023).
- [43] A. Virtuani, H. Müllejans, and E. D. Dunlop, "Comparison of indoor and outdoor performance measurements of recent commercially available solar modules", en, *Progress in Photovoltaics: Research and Applications*, vol. 19, no. 1, pp. 11–20, Jan. 2011, ISSN: 10627995. DOI: 10.1002/pip.977. [Online]. Available: <https://onlinelibrary.wiley.com/doi/10.1002/pip.977> (visited on 03/09/2023).
- [44] A. Lachowicz, P. Wyss, J. Geissbühler, *et al.*, "Review on plating processes for silicon heterojunction cells", Constance, 2019.
- [45] C. Peike, I. Hädrich, K.-A. Weiss, I. Dürr, and F. ISE, "Overview of PV module encapsulation materials", *Photovoltaics International*, vol. 19, no. 22, p. 85, 2013.
- [46] S. Chunduri, "Combining The Best Of Two – EVA And POE – Encapsulation Materials Suppliers Have Developed A Co-Extruded Multilayer Structure EVA-POE-EVA For Bifacial Modules", *Taiyang News*, May 2022.
- [47] W. Muehleisen, L. Neumaier, C. Hirschl, *et al.*, "Comparison of output power for solar cells with standard and structured ribbons", *EPJ Photovoltaics*, vol. 7, p. 70 701, 2016, ISSN: 2105-0716. DOI: 10.1051/epjpv/2016003. [Online]. Available: <http://www.epjpv.org/10.1051/epjpv/2016003> (visited on 03/09/2023).
- [48] A. Faes, M. Despeisse, J. Levrat, *et al.*, "SmartWire Solar Cell Interconnection Technology", en, *29th European Photovoltaic Solar Energy Conference and Exhibition*; 2555-2561, 7 pages, 10258 kb, 2014, Artwork Size: 7 pages, 10258 kb Medium: application/pdf Publisher: WIP. DOI: 10.4229/EUPVSEC20142014-5DO.16.3. [Online]. Available: <http://www.eupvsec-proceedings.com/proceedings?paper=29604> (visited on 03/09/2023).
- [49] European Commission. Joint Research Centre. Institute for Energy, *Guidelines for PV power measurement in industry*, eng. LU: Publications Office, 2010. [Online]. Available: <https://data.europa.eu/doi/10.2788/90247> (visited on 03/09/2023).
- [50] H. P. Yin, Y. F. Zhou, S. L. Sun, *et al.*, "Optical enhanced effects on the electrical performance and energy yield of bifacial PV modules", *Solar Energy*, vol. 217, pp. 245–252, 2021.
- [51] L. Wang, Y. Tang, S. Zhang, F. Wang, and J. Wang, "Energy yield analysis of different bifacial PV (photovoltaic) technologies: TOPCon, HJT, PERC in Hainan", en, *Solar Energy*, vol. 238, pp. 258–263, May 2022, ISSN: 0038092X. DOI: 10.1016/j.solener.2022.03.038. [Online]. Available: <https://linkinghub.elsevier.com/retrieve/pii/S0038092X22002043> (visited on 07/12/2022).

BIBLIOGRAPHY

- [52] D. C. Jordan, T. J. Silverman, J. H. Wohlgemuth, S. R. Kurtz, and K. T. VanSant, “Photovoltaic failure and degradation modes”, en, *Progress in Photovoltaics: Research and Applications*, vol. 25, no. 4, pp. 318–326, Apr. 2017, ISSN: 1062-7995, 1099-159X. DOI: 10.1002/pip.2866. [Online]. Available: <https://onlinelibrary.wiley.com/doi/10.1002/pip.2866> (visited on 07/12/2022).
- [53] I. E. Commission, “IEC 60050 (191): International Electrotechnical Vocabulary, Chapter 191: Dependability and quality of service”, 1990.
- [54] A. Zielnik, “Validating photovoltaic module durability tests”, *Solar America Board for Codes and Standards*, 2013.
- [55] D. Kececioğlu, *Reliability engineering handbook. 1*, eng. Lancaster, Penn: DEStech Publ, 2002, ISBN: 978-1-932078-00-8.
- [56] P. D. T. O’Connor and A. Kleyner, *Practical reliability engineering*, eng, 5. ed. Chichester: Wiley, 2012, ISBN: 978-0-470-97981-5 978-0-470-97982-2.
- [57] D. DeGraaff, R. Lacerda, Z. Campeau, and C. Sunpower, “Degradation mechanisms in si module technologies observed in the field; their analysis and statistics”, in *NREL 2011 Photovoltaic Module Reliability Workshop*, 2011.
- [58] IEA, “Review of failures of photovoltaic modules—report IEA-PVPS T13-01: 2014”, Tech. Rep., 2014.
- [59] S. Kurtz, J. Wohlgemuth, M. Yamamichi, *et al.*, “A framework for a comparative accelerated testing standard for PV modules”, in *2013 IEEE 39th Photovoltaic Specialists Conference (PVSC)*, Tampa, FL, USA: IEEE, Jun. 2013, pp. 0132–0138, ISBN: 978-1-4799-3299-3 978-1-4799-3298-6. DOI: 10.1109/PVSC.2013.6744114. [Online]. Available: <http://ieeexplore.ieee.org/document/6744114/> (visited on 03/09/2023).
- [60] D. C. Miller, E. Annigoni, A. Ballion, *et al.*, “Degradation in PV encapsulant strength of attachment: An interlaboratory study towards a climate-specific test”, in *2016 IEEE 43rd Photovoltaic Specialists Conference (PVSC)*, Portland, OR, USA: IEEE, Jun. 2016, pp. 0095–0100, ISBN: 978-1-5090-2724-8. DOI: 10.1109/PVSC.2016.7749556. [Online]. Available: <https://ieeexplore.ieee.org/document/7749556/> (visited on 03/09/2023).
- [61] A. Virtuani, E. Annigoni, and C. Ballif, “One-type-fits-all-systems: Strategies for preventing potential-induced degradation in crystalline silicon solar photovoltaic modules”, en, *Progress in Photovoltaics: Research and Applications*, vol. 27, no. 1, pp. 13–21, Jan. 2019, ISSN: 10627995. DOI: 10.1002/pip.3066. [Online]. Available: <https://onlinelibrary.wiley.com/doi/10.1002/pip.3066> (visited on 07/12/2022).
- [62] T. Ishii and A. Masuda, “Annual degradation rates of recent crystalline silicon photovoltaic modules: Annual degradation rates of recent c-Si PV modules”, en, *Progress in Photovoltaics: Research and Applications*, vol. 25, no. 12, pp. 953–967, Dec. 2017, ISSN: 10627995. DOI: 10.1002/pip.2903. [Online]. Available: <https://onlinelibrary.wiley.com/doi/10.1002/pip.2903> (visited on 01/23/2023).

- [63] H. Han, X. Dong, H. Lai, *et al.*, “Analysis of the Degradation of Monocrystalline Silicon Photovoltaic Modules After Long-Term Exposure for 18 Years in a Hot-Humid Climate in China”, *IEEE Journal of Photovoltaics*, pp. 1–7, 2018, ISSN: 2156-3381, 2156-3403. DOI: 10.1109/JPHOTOV.2018.2819803. [Online]. Available: <http://ieeexplore.ieee.org/document/8338398/> (visited on 01/23/2023).
- [64] A. Virtuani, M. Caccivio, E. Annigoni, *et al.*, “35 years of photovoltaics: Analysis of the TISO-10-kW solar plant, lessons learnt in safety and performance—Part 1”, en, *Progress in Photovoltaics: Research and Applications*, vol. 27, no. 4, pp. 328–339, Apr. 2019, ISSN: 1062-7995, 1099-159X. DOI: 10.1002/pip.3104. [Online]. Available: <https://onlinelibrary.wiley.com/doi/10.1002/pip.3104> (visited on 07/12/2022).
- [65] E. Annigoni, A. Virtuani, M. Caccivio, G. Friesen, D. Chianese, and C. Ballif, “35 years of photovoltaics: Analysis of the TISO-10-kW solar plant, lessons learnt in safety and performance—Part 2”, en, *Progress in Photovoltaics: Research and Applications*, vol. 27, no. 9, pp. 760–778, Sep. 2019, ISSN: 1062-7995, 1099-159X. DOI: 10.1002/pip.3146. [Online]. Available: <https://onlinelibrary.wiley.com/doi/10.1002/pip.3146> (visited on 07/12/2022).
- [66] M. Quintana, D. King, T. McMahon, and C. Osterwald, “Commonly observed degradation in field-aged photovoltaic modules”, in *Conference Record of the Twenty-Ninth IEEE Photovoltaic Specialists Conference, 2002.*, New Orleans, LA, USA: IEEE, 2002, pp. 1436–1439, ISBN: 978-0-7803-7471-3. DOI: 10.1109/PVSC.2002.1190879. [Online]. Available: <http://ieeexplore.ieee.org/document/1190879/> (visited on 01/23/2023).
- [67] I. E. Commission, “IEC 61215-2: Terrestrial photovoltaic (PV) modules - Design qualification and type approval - Part 2: Test procedures”, *International Electrotechnical Commission (IEC), International Standard*, 2021.
- [68] M. Knausz, G. Oreski, G. C. Eder, *et al.*, “Degradation of photovoltaic backsheets: Comparison of the aging induced changes on module and component level”, en, *Journal of Applied Polymer Science*, vol. 132, no. 24, n/a–n/a, Jun. 2015, ISSN: 00218995. DOI: 10.1002/app.42093. [Online]. Available: <https://onlinelibrary.wiley.com/doi/10.1002/app.42093> (visited on 05/31/2023).
- [69] B. Ottersböck, G. Oreski, and G. Pinter, “Correlation study of damp heat and pressure cooker testing on backsheets”, en, *Journal of Applied Polymer Science*, vol. 133, no. 47, Dec. 2016, ISSN: 00218995. DOI: 10.1002/app.44230. [Online]. Available: <https://onlinelibrary.wiley.com/doi/10.1002/app.44230> (visited on 05/31/2023).
- [70] W. Gambogi, T. Felder, S. MacMaster, *et al.*, “Sequential Stress Testing to Predict Photovoltaic Module Durability”, in *2018 IEEE 7th World Conference on Photovoltaic Energy Conversion (WCPEC) (A Joint Conference of 45th IEEE PVSC, 28th PVSEC & 34th EU PVSEC)*, Waikoloa Village, HI: IEEE, Jun. 2018, pp. 1593–1596, ISBN: 978-1-5386-8529-7. DOI: 10.1109/PVSC.2018.8547260. [Online]. Available: <https://ieeexplore.ieee.org/document/8547260/> (visited on 03/09/2023).

BIBLIOGRAPHY

- [71] M. Owen-Bellini, S. L. Moffitt, A. Sinha, *et al.*, “Towards validation of combined-accelerated stress testing through failure analysis of polyamide-based photovoltaic backsheets”, en, *Scientific Reports*, vol. 11, no. 1, p. 2019, Jan. 2021, ISSN: 2045-2322. DOI: 10.1038/s41598-021-81381-7. [Online]. Available: <https://www.nature.com/articles/s41598-021-81381-7> (visited on 03/09/2023).
- [72] M. Owen-Bellini, P. Hacke, D. C. Miller, *et al.*, “Advancing reliability assessments of photovoltaic modules and materials using combined-accelerated stress testing”, en, *Progress in Photovoltaics: Research and Applications*, vol. 29, no. 1, pp. 64–82, Jan. 2021, ISSN: 1062-7995, 1099-159X. DOI: 10.1002/pip.3342. [Online]. Available: <https://onlinelibrary.wiley.com/doi/10.1002/pip.3342> (visited on 03/09/2023).
- [73] R. Ross, G. Mon, L. Wen, and R. Sugimura, “Measurement and characterization of voltage- and current-induced degradation of thin-film photovoltaic modules”, en, *Solar Cells*, vol. 27, no. 1-4, pp. 289–298, Oct. 1989, ISSN: 03796787. DOI: 10.1016/0379-6787(89)90037-9. [Online]. Available: <https://linkinghub.elsevier.com/retrieve/pii/0379678789900379> (visited on 02/06/2023).
- [74] J. A. del Cueto and T. J. McMahon, “Analysis of leakage currents in photovoltaic modules under high-voltage bias in the field”, en, *Progress in Photovoltaics: Research and Applications*, vol. 10, no. 1, pp. 15–28, Jan. 2002, ISSN: 1062-7995, 1099-159X. DOI: 10.1002/pip.401. [Online]. Available: <https://onlinelibrary.wiley.com/doi/10.1002/pip.401> (visited on 02/05/2023).
- [75] D. E. Carlson, R. Romero, F. Willing, *et al.*, “Corrosion effects in thin-film photovoltaic modules”, en, *Progress in Photovoltaics: Research and Applications*, vol. 11, no. 6, pp. 377–386, Sep. 2003, ISSN: 1062-7995, 1099-159X. DOI: 10.1002/pip.500. [Online]. Available: <https://onlinelibrary.wiley.com/doi/10.1002/pip.500> (visited on 02/06/2023).
- [76] C. Osterwald, T. McMahon, and J. del Cueto, “Electrochemical corrosion of SnO₂:F transparent conducting layers in thin-film photovoltaic modules”, en, *Solar Energy Materials and Solar Cells*, vol. 79, no. 1, pp. 21–33, Aug. 2003, ISSN: 09270248. DOI: 10.1016/S0927-0248(02)00363-X. [Online]. Available: <https://linkinghub.elsevier.com/retrieve/pii/S092702480200363X> (visited on 02/06/2023).
- [77] R. Swanson, M. Cudzinovic, D. DeCeuster, *et al.*, “The surface polarization effect in high-efficiency silicon solar cells”, in *15th PVSEC*, Shanghai, China, 2005.
- [78] S. Pingel, O. Frank, M. Winkler, *et al.*, “Potential Induced Degradation of solar cells and panels”, in *2010 35th IEEE Photovoltaic Specialists Conference*, Honolulu, HI, USA: IEEE, Jun. 2010, pp. 002 817–002 822, ISBN: 978-1-4244-5890-5. DOI: 10.1109/PVSC.2010.5616823. [Online]. Available: <http://ieeexplore.ieee.org/document/5616823/> (visited on 02/05/2023).

- [79] P. Hacke, M. Kempe, K. Terwilliger, *et al.*, “Characterization of Multicrystalline Silicon Modules with System Bias Voltage Applied in Damp Heat”, en, *25th European Photovoltaic Solar Energy Conference and Exhibition / 5th World Conference on Photovoltaic Energy Conversion*, vol. 6-10 September 2010, 6 pages, 12339 kb, 2010, Artwork Size: 6 pages, 12339 kb Medium: application/pdf Publisher: WIP-Munich. DOI: 10.4229/25THEUPVSEC2010-4BO.9.6. [Online]. Available: <http://www.eupvsec-proceedings.com/proceedings?paper=8802> (visited on 02/05/2023).
- [80] S. Koch, D. Nieschalk, J. Berghold, S. Wendlandt, S. Krauter, and P. Grunow, “Potential Induced Degradation Effects on Crystalline Silicon Cells with Various Antireflective Coatings”, en, *27th European Photovoltaic Solar Energy Conference and Exhibition; 1985-1990*, 6 pages, 7096 kb, 2012, Artwork Size: 6 pages, 7096 kb Medium: application/pdf Publisher: WIP. DOI: 10.4229/27THEUPVSEC2012-2CV.7.3. [Online]. Available: <http://www.eupvsec-proceedings.com/proceedings?paper=19410> (visited on 02/07/2023).
- [81] A. Núñez Jiménez and R. Bkayrat, “Utility scale 1,500 VDC PV power plant architecture evolution: advantages and challenges”, *Integration of Renewable Energy into High and Medium Voltage Systems Conference & Exhibition*, Jul. 2015.
- [82] R. Malachi, S. Schönberger, J. Mayer, and M. Kasemann, “Techno-Economic Analysis of Utility Scale PV Power Plants with Up to +/-1500 VDC”, en, *29th European Photovoltaic Solar Energy Conference and Exhibition; 2323-2326*, 4 pages, 5195 kb, 2014, Artwork Size: 4 pages, 5195 kb Medium: application/pdf Publisher: WIP. DOI: 10.4229/EUPVSEC20142014-5CO.12.5. [Online]. Available: <http://www.eupvsec-proceedings.com/proceedings?paper=28233> (visited on 02/07/2023).
- [83] J. Berghold, S. Koch, A. Bötcher, A. Ukar, M. Leers, and P. Grunow, “Potential-induced degradation (PID) and its correlation with experience in the field”, *Photovoltaics International*, vol. 19, no. 7, pp. 82–93, 2013.
- [84] J. Berghold, S. Koch, S. Pingel, *et al.*, “PID: from material properties to outdoor performance and quality control counter measures”, N. G. Dhere, J. H. Wohlgemuth, and R. Jones-Albertus, Eds., San Diego, California, United States, Sep. 2015, 95630A. DOI: 10.1117/12.2188464. [Online]. Available: <http://proceedings.spiedigitallibrary.org/proceeding.aspx?doi=10.1117/12.2188464> (visited on 02/07/2023).
- [85] E. Annigoni, “Reliability of photovoltaic modules: from indoor testing to long-term performance prediction”, en, May 2018, Publisher: Lausanne, EPFL. DOI: 10.5075/EPFL-THESIS-8672. [Online]. Available: https://infoscience.epfl.ch/record/255400/files/EPFL_TH8672.pdf (visited on 02/07/2023).
- [86] W. Luo, Y. S. Khoo, P. Hacke, *et al.*, “Potential-induced degradation in photovoltaic modules: a critical review”, en, *Energy & Environmental Science*, vol. 10, no. 1, pp. 43–68, 2017, ISSN: 1754-5692, 1754-5706. DOI: 10.1039/C6EE02271E. [Online]. Available: <http://xlink.rsc.org/?DOI=C6EE02271E> (visited on 07/12/2022).

BIBLIOGRAPHY

- [87] P. Hacke, R. Smith, K. Terwilliger, G. Perrin, B. Sekulic, and S. Kurtz, "Development of an IEC test for crystalline silicon modules to qualify their resistance to system voltage stress: IEC test for c-Si modules", en, *Progress in Photovoltaics: Research and Applications*, vol. 22, no. 7, pp. 775–783, Jul. 2014, ISSN: 10627995. DOI: 10.1002/pip.2434. [Online]. Available: <https://onlinelibrary.wiley.com/doi/10.1002/pip.2434> (visited on 02/07/2023).
- [88] P. Hacke, K. Terwilliger, R. Smith, *et al.*, "System voltage potential-induced degradation mechanisms in PV modules and methods for test", in *2011 37th IEEE Photovoltaic Specialists Conference*, Seattle, WA, USA: IEEE, Jun. 2011, pp. 000 814–000 820, ISBN: 978-1-4244-9965-6 978-1-4244-9966-3 978-1-4244-9964-9. DOI: 10.1109/PVSC.2011.6186079. [Online]. Available: <http://ieeexplore.ieee.org/document/6186079/> (visited on 02/09/2023).
- [89] J. Bauer, V. Naumann, S. Großer, C. Hagendorf, M. Schütze, and O. Breitenstein, "On the mechanism of potential-induced degradation in crystalline silicon solar cells: On the mechanism of potential-induced degradation in crystalline silicon solar cells", en, *physica status solidi (RRL) - Rapid Research Letters*, vol. 6, no. 8, pp. 331–333, Aug. 2012, ISSN: 18626254. DOI: 10.1002/pssr.201206276. [Online]. Available: <https://onlinelibrary.wiley.com/doi/10.1002/pssr.201206276> (visited on 02/05/2023).
- [90] V. Naumann, C. Hagendorf, S. Grosser, M. Werner, and J. Bagdahn, "Micro Structural Root Cause Analysis of Potential Induced Degradation in c-Si Solar Cells", en, *Energy Procedia*, vol. 27, pp. 1–6, 2012, ISSN: 18766102. DOI: 10.1016/j.egypro.2012.07.020. [Online]. Available: <https://linkinghub.elsevier.com/retrieve/pii/S1876610212012337> (visited on 10/27/2022).
- [91] V. Naumann, D. Lausch, A. Graff, *et al.*, "The role of stacking faults for the formation of shunts during potential-induced degradation of crystalline Si solar cells: The role of stacking faults for the formation of shunts during potential-induced degradation of crystalline Si solar cells", en, *physica status solidi (RRL) - Rapid Research Letters*, vol. 7, no. 5, pp. 315–318, May 2013, ISSN: 18626254. DOI: 10.1002/pssr.201307090. [Online]. Available: <https://onlinelibrary.wiley.com/doi/10.1002/pssr.201307090> (visited on 02/09/2023).
- [92] V. Naumann, D. Lausch, A. Hähnel, *et al.*, "Explanation of potential-induced degradation of the shunting type by Na decoration of stacking faults in Si solar cells", en, *Solar Energy Materials and Solar Cells*, vol. 120, pp. 383–389, Jan. 2014, ISSN: 09270248. DOI: 10.1016/j.solmat.2013.06.015. [Online]. Available: <https://linkinghub.elsevier.com/retrieve/pii/S0927024813003000> (visited on 02/09/2023).
- [93] D. Lausch, V. Naumann, A. Graff, *et al.*, "Sodium Outdiffusion from Stacking Faults as Root Cause for the Recovery Process of Potential-induced Degradation (PID)", en, *Energy Procedia*, vol. 55, pp. 486–493, 2014, ISSN: 18766102. DOI: 10.1016/j.egypro.2014.08.013. [Online]. Available: <https://linkinghub.elsevier.com/retrieve/pii/S1876610214012375> (visited on 02/09/2023).

-
- [94] V. Naumann, T. Geppert, S. Großer, *et al.*, “Potential-induced Degradation at Interdigitated Back Contact Solar Cells”, en, *Energy Procedia*, vol. 55, pp. 498–503, 2014, ISSN: 18766102. DOI: 10.1016/j.egypro.2014.08.015. [Online]. Available: <https://linkinghub.elsevier.com/retrieve/pii/S1876610214012399> (visited on 02/10/2023).
 - [95] K. Hara, S. Jonai, and A. Masuda, “Potential-induced degradation in photovoltaic modules based on n-type single crystalline Si solar cells”, en, *Solar Energy Materials and Solar Cells*, vol. 140, pp. 361–365, Sep. 2015, ISSN: 09270248. DOI: 10.1016/j.solmat.2015.04.037. [Online]. Available: <https://linkinghub.elsevier.com/retrieve/pii/S0927024815001981> (visited on 02/10/2023).
 - [96] S. Yamaguchi, A. Masuda, and K. Ohdaira, “Changes in the current density–voltage and external quantum efficiency characteristics of n-type single-crystalline silicon photovoltaic modules with a rear-side emitter undergoing potential-induced degradation”, en, *Solar Energy Materials and Solar Cells*, vol. 151, pp. 113–119, Jul. 2016, ISSN: 09270248. DOI: 10.1016/j.solmat.2016.03.003. [Online]. Available: <https://linkinghub.elsevier.com/retrieve/pii/S0927024816000994> (visited on 02/10/2023).
 - [97] W. Luo, P. Hacke, K. Terwilliger, *et al.*, “Elucidating potential-induced degradation in bifacial PERC silicon photovoltaic modules”, en, *Progress in Photovoltaics: Research and Applications*, vol. 26, no. 10, pp. 859–867, Oct. 2018, ISSN: 1062-7995, 1099-159X. DOI: 10.1002/pip.3028. [Online]. Available: <https://onlinelibrary.wiley.com/doi/10.1002/pip.3028> (visited on 02/09/2023).
 - [98] J. Carolus, J. A. Tsanakas, A. van der Heide, E. Voroshazi, W. De Ceuninck, and M. Daenen, “Physics of potential-induced degradation in bifacial p-PERC solar cells”, en, *Solar Energy Materials and Solar Cells*, vol. 200, p. 109 950, Sep. 2019, ISSN: 09270248. DOI: 10.1016/j.solmat.2019.109950. [Online]. Available: <https://linkinghub.elsevier.com/retrieve/pii/S092702481930279X> (visited on 02/05/2023).
 - [99] K. Sporleder, V. Naumann, J. Bauer, *et al.*, “Root cause analysis on corrosive potential-induced degradation effects at the rear side of bifacial silicon PERC solar cells”, en, *Solar Energy Materials and Solar Cells*, vol. 201, p. 110 062, Oct. 2019, ISSN: 09270248. DOI: 10.1016/j.solmat.2019.110062. [Online]. Available: <https://linkinghub.elsevier.com/retrieve/pii/S0927024819303915> (visited on 02/05/2023).
 - [100] K. Sporleder, V. Naumann, J. Bauer, *et al.*, “Microstructural Analysis of Local Silicon Corrosion of Bifacial Solar Cells as Root Cause of Potential-Induced Degradation at the Rear Side”, en, *physica status solidi (a)*, vol. 216, no. 17, p. 1 900 334, Sep. 2019, ISSN: 1862-6300, 1862-6319. DOI: 10.1002/pssa.201900334. [Online]. Available: <https://onlinelibrary.wiley.com/doi/10.1002/pssa.201900334> (visited on 02/05/2023).
 - [101] D. B. Sulas-Kern, M. Owen-Bellini, P. Ndione, *et al.*, “Electrochemical degradation modes in bifacial silicon photovoltaic modules”, en, *Progress in Photovoltaics: Research and Applications*, vol. 30, no. 8, pp. 948–958, Aug. 2022, ISSN: 1062-7995, 1099-159X. DOI: 10.1002/pip.3530. [Online]. Available: <https://onlinelibrary.wiley.com/doi/10.1002/pip.3530> (visited on 02/14/2023).

BIBLIOGRAPHY

- [102] T. Ishiguro, H. Kanno, M. Taguchi, and S. Okamoto, "Study on PID resistance of HIT PV modules", 2013.
- [103] S. Yamaguchi, C. Yamamoto, K. Ohdaira, and A. Masuda, "Comprehensive study of potential-induced degradation in silicon heterojunction photovoltaic cell modules", en, *Progress in Photovoltaics: Research and Applications*, vol. 26, no. 9, pp. 697–708, Sep. 2018, ISSN: 10627995. DOI: 10.1002/pip.3006. [Online]. Available: <https://onlinelibrary.wiley.com/doi/10.1002/pip.3006> (visited on 10/27/2022).
- [104] S. Yamaguchi, C. Yamamoto, Y. Ohshita, K. Ohdaira, and A. Masuda, "Influence of emitter position of silicon heterojunction photovoltaic solar cell modules on their potential-induced degradation behaviors", en, *Solar Energy Materials and Solar Cells*, vol. 216, p. 110716, Oct. 2020, ISSN: 09270248. DOI: 10.1016/j.solmat.2020.110716. [Online]. Available: <https://linkinghub.elsevier.com/retrieve/pii/S0927024820303159> (visited on 07/12/2022).
- [105] V. Naumann, D. Lausch, and C. Hagendorf, "Sodium Decoration of PID-s Crystal Defects after Corona Induced Degradation of Bare Silicon Solar Cells", en, *Energy Procedia*, vol. 77, pp. 397–401, Aug. 2015, ISSN: 18766102. DOI: 10.1016/j.egypro.2015.07.055. [Online]. Available: <https://linkinghub.elsevier.com/retrieve/pii/S1876610215008231> (visited on 02/11/2023).
- [106] J. Berghold, S. Koch, B. Frohmann, P. Hacke, and P. Grunow, "Properties of encapsulation materials and their relevance for recent field failures", in *2014 IEEE 40th Photovoltaic Specialist Conference (PVSC)*, Denver, CO, USA: IEEE, Jun. 2014, pp. 1987–1992, ISBN: 978-1-4799-4398-2 978-1-4799-4399-9. DOI: 10.1109/PVSC.2014.6925315. [Online]. Available: <http://ieeexplore.ieee.org/document/6925315/> (visited on 10/27/2022).
- [107] Y.-H. Lee, M.-A. Tsai, K.-W. Lu, *et al.*, "Potential Induced Degradation Experiments on Different Encapsulated Silicon Mini-Solar Modules", en, *29th European Photovoltaic Solar Energy Conference and Exhibition*; 3357-3359, 3 pages, 2069 kb, 2014, Artwork Size: 3 pages, 2069 kb Medium: application/pdf Publisher: WIP. DOI: 10.4229/EUPVSEC20142014-5DV.3.10. [Online]. Available: <http://www.eupvsec-proceedings.com/proceedings?paper=27855> (visited on 02/11/2023).
- [108] O. Arriaga Arruti, A. Virtuani, and C. Ballif, "Long-term performance and reliability of silicon heterojunction solar modules", *Progress in Photovoltaics: Research and Applications*, pip.3688, Mar. 2023, ISSN: 1062-7995, 1099-159X. DOI: 10.1002/pip.3688. [Online]. Available: <https://onlinelibrary.wiley.com/doi/10.1002/pip.3688> (visited on 03/07/2023).
- [109] L. Gnocchi, A. Virtuani, O. Arriaga Arruti, and C. Ballif, "Insights into the sensitivity of Silicon Heterojunction (SHJ) solar photovoltaic modules to water ingress: a detailed microscopic model", *Submitted to Cell Reports*, 2023.

-
- [110] O. Arriaga Arruti, L. Gnocchi, Q. Jeangros, A. Virtuani, and C. Ballif, "Potential-Induced Degradation in Bifacial Silicon Heterojunction Solar Modules: Insights and Mitigation Strategies", *Submitted to Progress in Photovoltaics: Research and Applications*, 2023.
 - [111] I. E. Commission, "IEC 60904-3:2021: Photovoltaic devices - Part 3: Measurement principles for terrestrial photovoltaic (PV) solar devices with reference spectral irradiance data", 2016.
 - [112] J. F. Weaver, "World has installed 1TW of solar capacity", *PV Magazine*, Mar. 2022. [Online]. Available: <https://www.pv-magazine.com/2022/03/15/humans-have-installed-1-terawatt-of-solar-capacity/#:~:text=The%20world%20has%20very%20recently,at%20the%20end%20of%202020..>
 - [113] M. A. Green, E. D. Dunlop, J. Hohl-Ebinger, M. Yoshita, N. Kopidakis, and X. Hao, "Solar cell efficiency tables (Version 58)", en, *Progress in Photovoltaics: Research and Applications*, vol. 29, no. 7, pp. 657–667, Jul. 2021, ISSN: 1062-7995, 1099-159X. DOI: 10.1002/pip.3444. [Online]. Available: <https://onlinelibrary.wiley.com/doi/10.1002/pip.3444> (visited on 07/12/2022).
 - [114] C. Deline, S. Ayala Peláez, B. Marion, B. Sekulic, and J. Stein, "Understanding Bifacial Photovoltaic Potential: Field Performance", Dec. 2019.
 - [115] "Mineral Commodity Summaries 2022", en, *US Geological Survey: Reston, VA*, vol. 2022, 2022. DOI: 10.3133/mcs2022.
 - [116] Z. Wu, W. Duan, A. Lambertz, *et al.*, "Low-resistivity p-type a-Si:H/AZO hole contact in high-efficiency silicon heterojunction solar cells", en, *Applied Surface Science*, vol. 542, p. 148 749, Mar. 2021, ISSN: 01694332. DOI: 10.1016/j.apsusc.2020.148749. [Online]. Available: <https://linkinghub.elsevier.com/retrieve/pii/S016943322033508X> (visited on 07/12/2022).
 - [117] Y. Won, A. Kim, D. Lee, *et al.*, "Annealing-free fabrication of highly oxidation-resistive copper nanowire composite conductors for photovoltaics", en, *NPG Asia Materials*, vol. 6, no. 6, e105–e105, Jun. 2014, ISSN: 1884-4049, 1884-4057. DOI: 10.1038/am.2014.36. [Online]. Available: <http://www.nature.com/articles/am201436> (visited on 07/12/2022).
 - [118] D. D. Tune, N. Mallik, H. Fornasier, and B. S. Flavel, "Breakthrough Carbon Nanotube–Silicon Heterojunction Solar Cells", en, *Advanced Energy Materials*, vol. 10, no. 1, p. 1 903 261, Jan. 2020, ISSN: 1614-6832, 1614-6840. DOI: 10.1002/aenm.201903261. [Online]. Available: <https://onlinelibrary.wiley.com/doi/10.1002/aenm.201903261> (visited on 07/12/2022).
 - [119] A. B. Morales-Vilches, A. Cruz, S. Pingel, *et al.*, "ITO-Free Silicon Heterojunction Solar Cells With ZnO:Al/SiO₂ Front Electrodes Reaching a Conversion Efficiency of 23%", *IEEE Journal of Photovoltaics*, vol. 9, no. 1, pp. 34–39, Jan. 2019, ISSN: 2156-3381, 2156-3403. DOI: 10.1109/JPHOTOV.2018.2873307. [Online]. Available: <https://ieeexplore.ieee.org/document/8493365/> (visited on 07/12/2022).

BIBLIOGRAPHY

- [120] J.-P. Niemelä, B. Macco, L. Barraud, *et al.*, “Rear-emitter silicon heterojunction solar cells with atomic layer deposited ZnO:Al serving as an alternative transparent conducting oxide to In₂O₃:Sn”, en, *Solar Energy Materials and Solar Cells*, vol. 200, p. 109 953, Sep. 2019, ISSN: 09270248. DOI: 10.1016/j.solmat.2019.109953. [Online]. Available: <https://linkinghub.elsevier.com/retrieve/pii/S092702481930282X> (visited on 07/12/2022).
- [121] J. Scully, “REC Group scaling up HJT module production in Singapore with new launch”, *PV Tech*, Aug. 2022.
- [122] E. Bellini, “Hevel Solar unveils 22.3%-efficient heterojunction BIPV module”, *PV Magazine*, Apr. 2022.
- [123] J. T. Jacobo, “Meyer Burger optimising production expansion to 1.4 GW in Germany to cater for European demand”, *PV Tech*, Apr. 2022.
- [124] E. Bellini, “Enel, European Commission sign grant agreement for 3 GW Italian module factory”, *PV Magazine*, Apr. 2022.
- [125] M. Nair, “GS-Solar To Build 10 GW HJT Production Line; 2nd Phase Of JA Solar 20 GW Monocrystal Production Line Begins; DZS & Trina Win China Energy 250 MW PV Modules Bid; Solar, Wind And Hydro Power Increase Significantly In Oct: NDRC”, *Taiyang News*, Nov. 2020.
- [126] E. Bellini, “Huasun achieves 25.26% efficiency for heterojunction solar cell”, *PV Magazine*, Jul. 2021.
- [127] V. Shaw, “Chinese PV Industry Brief: Talesun plans 5GW heterojunction PV module factory”, *PV Magazine*, Mar. 2022.
- [128] V. Shaw and M. Hall, “Chinese PV Industry Brief: China’s NEA predicts 108 GW of solar in 2022”, *PV Magazine*, Apr. 2022.
- [129] A. Skoczek, T. Sample, and E. D. Dunlop, “The results of performance measurements of field-aged crystalline silicon photovoltaic modules”, en, *Progress in Photovoltaics: Research and Applications*, vol. 17, no. 4, pp. 227–240, Jun. 2009, ISSN: 10627995. DOI: 10.1002/pip.874. [Online]. Available: <https://onlinelibrary.wiley.com/doi/10.1002/pip.874> (visited on 07/12/2022).
- [130] D. C. Jordan and S. R. Kurtz, “Photovoltaic Degradation Rates-an Analytical Review”, en, *Progress in Photovoltaics: Research and Applications*, vol. 21, no. 1, pp. 12–29, Jan. 2013, ISSN: 10627995. DOI: 10.1002/pip.1182. [Online]. Available: <https://onlinelibrary.wiley.com/doi/10.1002/pip.1182> (visited on 07/12/2022).
- [131] D. C. Jordan, S. R. Kurtz, K. VanSant, and J. Newmiller, “Compendium of photovoltaic degradation rates”, en, *Progress in Photovoltaics: Research and Applications*, vol. 24, no. 7, pp. 978–989, Jul. 2016, ISSN: 1062-7995, 1099-159X. DOI: 10.1002 / pip .2744. [Online]. Available: <https://onlinelibrary.wiley.com/doi/10.1002/pip.2744> (visited on 07/12/2022).

-
- [132] D. C. Jordan, T. J. Silverman, B. Sekulic, and S. R. Kurtz, "PV degradation curves: non-linearities and failure modes", en, *Progress in Photovoltaics: Research and Applications*, vol. 25, no. 7, pp. 583–591, Jul. 2017, ISSN: 1062-7995, 1099-159X. DOI: 10.1002/pip.2835. [Online]. Available: <https://onlinelibrary.wiley.com/doi/10.1002/pip.2835> (visited on 07/12/2022).
 - [133] J. Lopez-Garcia and T. Sample, "Evolution of measured module characteristics versus labelled module characteristics of crystalline silicon based PV modules", en, *Solar Energy*, vol. 160, pp. 252–259, Jan. 2018, ISSN: 0038092X. DOI: 10.1016/j.solener.2017.12.018. [Online]. Available: <https://linkinghub.elsevier.com/retrieve/pii/S0038092X17311015> (visited on 07/12/2022).
 - [134] T. Ishii, T. Takashima, and K. Otani, "Long-term performance degradation of various kinds of photovoltaic modules under moderate climatic conditions", en, *Progress in Photovoltaics: Research and Applications*, vol. 19, no. 2, pp. 170–179, Mar. 2011, ISSN: 10627995. DOI: 10.1002/pip.1005. [Online]. Available: <https://onlinelibrary.wiley.com/doi/10.1002/pip.1005> (visited on 07/12/2022).
 - [135] T. Ishii, S. Choi, R. Sato, Y. Chiba, and A. Masuda, "Annual Degradation Rates of Recent c-Si PV Modules under Subtropical Coastal Climate Conditions", in *2018 IEEE 7th World Conference on Photovoltaic Energy Conversion (WCPEC) (A Joint Conference of 45th IEEE PVSC, 28th PVSEC & 34th EU PVSEC)*, Waikoloa Village, HI: IEEE, Jun. 2018, pp. 705–708, ISBN: 978-1-5386-8529-7. DOI: 10.1109/PVSC.2018.8548088. [Online]. Available: <https://ieeexplore.ieee.org/document/8548088/> (visited on 07/12/2022).
 - [136] C. Raupp, C. Libby, S. Tatapudi, *et al.*, "Degradation rate evaluation of multiple PV technologies from 59,000 modules representing 252,000 modules in four climatic regions of the United States", in *2016 IEEE 43rd Photovoltaic Specialists Conference (PVSC)*, Portland, OR, USA: IEEE, Jun. 2016, pp. 0255–0260, ISBN: 978-1-5090-2724-8. DOI: 10.1109/PVSC.2016.7749590. [Online]. Available: <http://ieeexplore.ieee.org/document/7749590/> (visited on 07/12/2022).
 - [137] P. Ingenhoven, G. Belluardo, G. Makrides, *et al.*, "Analysis of Photovoltaic Performance Loss Rates of Six Module Types in Five Geographical Locations", *IEEE Journal of Photovoltaics*, vol. 9, no. 4, pp. 1091–1096, Jul. 2019, ISSN: 2156-3381, 2156-3403. DOI: 10.1109/JPHOTOV.2019.2913342. [Online]. Available: <https://ieeexplore.ieee.org/document/8720235/> (visited on 07/12/2022).
 - [138] H. Solar, "Silicon heterojunction solar modules - field performance and long-term reliability testing", 2021.
 - [139] V. Sharma, O. Sastry, A. Kumar, B. Bora, and S. Chandel, "Degradation analysis of a-Si, (HIT) hetro-junction intrinsic thin layer silicon and m-C-Si solar photovoltaic technologies under outdoor conditions", en, *Energy*, vol. 72, pp. 536–546, Aug. 2014, ISSN: 03605442. DOI: 10.1016/j.energy.2014.05.078. [Online]. Available: <https://linkinghub.elsevier.com/retrieve/pii/S0360544214006458> (visited on 07/12/2022).

BIBLIOGRAPHY

- [140] N. I. of Solar Energy (NISE), “All-India Survey of Photovoltaic Module Reliability: 2018”, National Centre for Photovoltaic Research and Education (NCPRE), Tech. Rep., 2019.
- [141] D. C. Jordan, C. Deline, S. Johnston, *et al.*, “Silicon Heterojunction System Field Performance”, *IEEE Journal of Photovoltaics*, vol. 8, no. 1, pp. 177–182, Jan. 2018, ISSN: 2156-3381, 2156-3403. DOI: 10.1109/JPHOTOV.2017.2765680. [Online]. Available: <http://ieeexplore.ieee.org/document/8114171/> (visited on 07/12/2022).
- [142] D. Jordan, D. Sulas-Kern, S. Johnston, *et al.*, “High Efficiency Module Degradation – from Atoms to Systems”, en, *37th European Photovoltaic Solar Energy Conference and Exhibition*; 828–833, 6 pages, 9000 kb, 2020, Artwork Size: 6 pages, 9000 kb Medium: application/pdf Publisher: WIP. DOI: 10.4229/EUPVSEC20202020-4BO.14.2. [Online]. Available: <https://www.eupvsec-proceedings.com/proceedings?paper=49122> (visited on 07/12/2022).
- [143] W. Luo, Y. S. Khoo, P. Hacke, *et al.*, “Analysis of the Long-Term Performance Degradation of Crystalline Silicon Photovoltaic Modules in Tropical Climates”, *IEEE Journal of Photovoltaics*, vol. 9, no. 1, pp. 266–271, Jan. 2019, ISSN: 2156-3381, 2156-3403. DOI: 10.1109/JPHOTOV.2018.2877007. [Online]. Available: <https://ieeexplore.ieee.org/document/8520911/> (visited on 07/12/2022).
- [144] A. Limmanee, S. Songtra, N. Udomdachanut, *et al.*, “Degradation analysis of photovoltaic modules under tropical climatic conditions and its impacts on LCOE”, en, *Renewable Energy*, vol. 102, pp. 199–204, Mar. 2017, ISSN: 09601481. DOI: 10.1016/j.renene.2016.10.052. [Online]. Available: <https://linkinghub.elsevier.com/retrieve/pii/S096014811630917X> (visited on 07/12/2022).
- [145] E. Ozkalay, G. Friesen, M. Caccivio, *et al.*, “Operating Temperatures and Diurnal Temperature Variations of Modules Installed in Open-Rack and Typical BIPV Configurations”, *IEEE Journal of Photovoltaics*, vol. 12, no. 1, pp. 133–140, Jan. 2022, ISSN: 2156-3381, 2156-3403. DOI: 10.1109/JPHOTOV.2021.3114988. [Online]. Available: <https://ieeexplore.ieee.org/document/9576676/> (visited on 07/12/2022).
- [146] M. Schweiger, J. Bonilla, W. Herrmann, A. Gerber, and U. Rau, “Performance stability of photovoltaic modules in different climates”, en, *Progress in Photovoltaics: Research and Applications*, vol. 25, no. 12, pp. 968–981, Dec. 2017, ISSN: 10627995. DOI: 10.1002/pip.2904. [Online]. Available: <https://onlinelibrary.wiley.com/doi/10.1002/pip.2904> (visited on 07/12/2022).
- [147] E. Carigiet, C. J. Brabec, and F. P. Baumgartner, “Long-term power degradation analysis of crystalline silicon PV modules using indoor and outdoor measurement techniques”, en, *Renewable and Sustainable Energy Reviews*, vol. 144, p. 111 005, Jul. 2021, ISSN: 13640321. DOI: 10.1016/j.rser.2021.111005. [Online]. Available: <https://linkinghub.elsevier.com/retrieve/pii/S1364032121002951> (visited on 07/12/2022).
- [148] M. Taguchi, J. Irikawa, M. Iwata, H. Kannou, Y. Murakami, and S. Okamoto, “Approaches to the long-term stability of silicon heterojunction modules”, 2021.

- [149] J. H. Wohlgemuth, P. Hacke, N. Bosco, D. C. Miller, M. D. Kempe, and S. R. Kurtz, "Assessing the causes of encapsulant delamination in PV modules", in *2016 IEEE 43rd Photovoltaic Specialists Conference (PVSC)*, Portland, OR, USA: IEEE, Jun. 2016, pp. 0248–0254, ISBN: 978-1-5090-2724-8. DOI: 10.1109/PVSC.2016.7749589. [Online]. Available: <http://ieeexplore.ieee.org/document/7749589/> (visited on 11/26/2022).
- [150] S. M. Zhang, D. B. Sulas-Kern, R. L. Chin, *et al.*, "Investigation of SHJ Module Degradation: A Post- Mortem Approach", in *2020 47th IEEE Photovoltaic Specialists Conference (PVSC)*, Calgary, AB, Canada: IEEE, Jun. 2020, pp. 0814–0817, ISBN: 978-1-72816-115-0. DOI: 10.1109/PVSC45281.2020.9300728. [Online]. Available: <https://ieeexplore.ieee.org/document/9300728/> (visited on 07/12/2022).
- [151] J. Cattin, L.-L. Senaud, J. Haschke, *et al.*, "Influence of Light Soaking on Silicon Heterojunction Solar Cells With Various Architectures", *IEEE Journal of Photovoltaics*, vol. 11, no. 3, pp. 575–583, May 2021, ISSN: 2156-3381, 2156-3403. DOI: 10.1109/JPHOTOV.2021.3065537. [Online]. Available: <https://ieeexplore.ieee.org/document/9393795/> (visited on 07/12/2022).
- [152] H. Park, J. Jeong, E. Shin, S. Kim, and J. Yi, "A reliability study of silicon heterojunction photovoltaic modules exposed to damp heat testing", in *Microelectronic Engineering*, vol. 216, p. 111081, Aug. 2019, ISSN: 01679317. DOI: 10.1016/j.mee.2019.111081. [Online]. Available: <https://linkinghub.elsevier.com/retrieve/pii/S0167931718303447> (visited on 07/12/2022).
- [153] J. H. Wohlgemuth and M. D. Kempe, "Equating damp heat testing with field failures of PV modules", in *2013 IEEE 39th Photovoltaic Specialists Conference (PVSC)*, Tampa, FL, USA: IEEE, Jun. 2013, pp. 0126–0131, ISBN: 978-1-4799-3299-3 978-1-4799-3298-6. DOI: 10.1109/PVSC.2013.6744113. [Online]. Available: <http://ieeexplore.ieee.org/document/6744113/> (visited on 07/12/2022).
- [154] J. Zhu, M. Koehl, S. Hoffmann, *et al.*, "Changes of solar cell parameters during damp-heat exposure", in *Progress in Photovoltaics: Research and Applications*, vol. 24, no. 10, pp. 1346–1358, Oct. 2016, ISSN: 10627995. DOI: 10.1002/pip.2793. [Online]. Available: <https://onlinelibrary.wiley.com/doi/10.1002/pip.2793> (visited on 07/12/2022).
- [155] J. Zhu, D. Montiel-Chicharro, T. Betts, and R. Gottschalg, "Correlation of Degree of EVA Crosslinking with Formation and Discharge of Acetic Acid in PV Modules", in *33rd European Photovoltaic Solar Energy Conference and Exhibition; 1795-1798*, 4 pages, 3660 kb, 2017, Artwork Size: 4 pages, 3660 kb Medium: application/pdf Publisher: WIP. DOI: 10.4229/EUPVSEC20172017-5DV.3.21. [Online]. Available: <http://www.eupvsec-proceedings.com/proceedings?paper=44217> (visited on 07/12/2022).
- [156] A. Masuda, N. Uchiyama, and Y. Hara, "Degradation by acetic acid for crystalline Si photovoltaic modules", *Japanese Journal of Applied Physics*, vol. 54, no. 4S, 04DR04, Mar. 2015, Publisher: IOP Publishing. DOI: 10.7567/jjap.54.04dr04. [Online]. Available: <https://doi.org/10.7567/jjap.54.04dr04>.

BIBLIOGRAPHY

- [157] J. Karas, A. Sinha, V. S. P. Buddha, *et al.*, “Damp Heat Induced Degradation of Silicon Heterojunction Solar Cells With Cu-Plated Contacts”, *IEEE Journal of Photovoltaics*, vol. 10, no. 1, pp. 153–158, Jan. 2020, ISSN: 2156-3381, 2156-3403. DOI: 10.1109/JPHOTOV.2019.2941693. [Online]. Available: <https://ieeexplore.ieee.org/document/8878168/> (visited on 07/12/2022).
- [158] W. Liu, L. Zhang, X. Yang, *et al.*, “Damp-Heat-Stable, High-Efficiency, Industrial-Size Silicon Heterojunction Solar Cells”, en, *Joule*, vol. 4, no. 4, pp. 913–927, Apr. 2020, ISSN: 25424351. DOI: 10.1016/j.joule.2020.03.003. [Online]. Available: <https://linkinghub.elsevier.com/retrieve/pii/S2542435120300957> (visited on 07/12/2022).
- [159] C. Barretta, G. Oreski, S. Feldbacher, K. Resch-Fauster, and R. Pantani, “Comparison of Degradation Behavior of Newly Developed Encapsulation Materials for Photovoltaic Applications under Different Artificial Ageing Tests”, en, *Polymers*, vol. 13, no. 2, p. 271, Jan. 2021, ISSN: 2073-4360. DOI: 10.3390/polym13020271. [Online]. Available: <https://www.mdpi.com/2073-4360/13/2/271> (visited on 07/12/2022).
- [160] B. K. Sharma, U. Desai, A. Singh, and A. Singh, “Effect of vinyl acetate content on the photovoltaic-encapsulation performance of ethylene vinyl acetate under accelerated ultra-violet aging”, en, *Journal of Applied Polymer Science*, vol. 137, no. 2, p. 48 268, Jan. 2020, ISSN: 0021-8995, 1097-4628. DOI: 10.1002/app.48268. [Online]. Available: <https://onlinelibrary.wiley.com/doi/10.1002/app.48268> (visited on 07/12/2022).
- [161] A. Jentsch, K.-J. Eichhorn, and B. Voit, “Influence of typical stabilizers on the aging behavior of EVA foils for photovoltaic applications during artificial UV-weathering”, en, *Polymer Testing*, vol. 44, pp. 242–247, Jul. 2015, ISSN: 01429418. DOI: 10.1016/j.polymertesting.2015.03.022. [Online]. Available: <https://linkinghub.elsevier.com/retrieve/pii/S0142941815000768> (visited on 07/12/2022).
- [162] A. Sinha, J. Qian, K. Hurst, *et al.*, “UV-Induced Degradation of High-Efficiency Solar Cells with Different Architectures”, in *2020 47th IEEE Photovoltaic Specialists Conference (PVSC)*, Calgary, AB, Canada: IEEE, Jun. 2020, pp. 1990–1991, ISBN: 978-1-72816-115-0. DOI: 10.1109/PVSC45281.2020.9300993. [Online]. Available: <https://ieeexplore.ieee.org/document/9300993/> (visited on 07/12/2022).
- [163] A. Sinha, K. Hurst, S. Ulicna, L. T. Schelhas, D. C. Miller, and P. Hacke, “Assessing UV-Induced Degradation in Bifacial Modules of Different Cell Technologies”, in *2021 IEEE 48th Photovoltaic Specialists Conference (PVSC)*, Fort Lauderdale, FL, USA: IEEE, Jun. 2021, pp. 0767–0770, ISBN: 978-1-66541-922-2. DOI: 10.1109/PVSC43889.2021.9518728. [Online]. Available: <https://ieeexplore.ieee.org/document/9518728/> (visited on 07/12/2022).
- [164] R. Witteck, B. Veith-Wolf, H. Schulte-Huxel, *et al.*, “UV-induced degradation of PERC solar modules with UV-transparent encapsulation materials”, en, *Progress in Photovoltaics: Research and Applications*, vol. 25, no. 6, pp. 409–416, Jun. 2017, ISSN: 10627995. DOI: 10.1002/pip.2861. [Online]. Available: <https://onlinelibrary.wiley.com/doi/10.1002/pip.2861> (visited on 07/12/2022).

-
- [165] J. Scully, “Maxwell, Cybrid use light conversion film to boost HJT module power output”, *PV Tech*, Apr. 2022.
 - [166] O. Arriaga Arruti, L. Gnocchi, Q. Jeangros, A. Virtuani, and C. Ballif, “Potential Induced Degradation Mechanism in Rear-Emitter Bifacial Silicon Heterojunction Solar Cells Encapsulated in Different Module Structures”, in *2021 IEEE 48th Photovoltaic Specialists Conference (PVSC)*, Fort Lauderdale, FL, USA: IEEE, Jun. 2021, pp. 2032–2036, ISBN: 978-1-66541-922-2. DOI: 10.1109/PVSC43889.2021.9518967. [Online]. Available: <https://ieeexplore.ieee.org/document/9518967/> (visited on 07/12/2022).
 - [167] M. A. Green, E. D. Dunlop, G. Siefer, *et al.*, “Solar cell efficiency tables (Version 61)”, en, *Progress in Photovoltaics: Research and Applications*, vol. 31, no. 1, pp. 3–16, Jan. 2023, ISSN: 1062-7995, 1099-159X. DOI: 10.1002/pip.3646. [Online]. Available: <https://onlinelibrary.wiley.com/doi/10.1002/pip.3646> (visited on 04/11/2023).
 - [168] J. Haschke, O. Dupré, M. Boccard, and C. Ballif, “Silicon heterojunction solar cells: Recent technological development and practical aspects - from lab to industry”, en, *Solar Energy Materials and Solar Cells*, vol. 187, pp. 140–153, Dec. 2018, ISSN: 09270248. DOI: 10.1016/j.solmat.2018.07.018. [Online]. Available: <https://linkinghub.elsevier.com/retrieve/pii/S0927024818303805> (visited on 04/11/2023).
 - [169] D. Andronikov, A. Abramov, S. Abolmasov, *et al.*, “A Successful Conversion of Silicon Thin-Film Solar Module Production to High Efficiency Heterojunction Technology”, en, *33rd European Photovoltaic Solar Energy Conference and Exhibition; 732-735*, 4 pages, 6013 kb, 2017, Artwork Size: 4 pages, 6013 kb Medium: application/pdf Publisher: WIP. DOI: 10.4229/EUPVSEC20172017-2AV.3.12. [Online]. Available: <http://www.eupvsec-proceedings.com/proceedings?paper=42720> (visited on 04/11/2023).
 - [170] W. Favre, G. Condorelli, A.-S. Ozanne, *et al.*, “From Advanced Thin-Films Modules to High Efficiency Silicon Heterojunction Technology at 3SUN”, en, *33rd European Photovoltaic Solar Energy Conference and Exhibition; 437-440*, 4 pages, 7588 kb, 2017, Artwork Size: 4 pages, 7588 kb Medium: application/pdf Publisher: WIP. DOI: 10.4229/EUPVSEC20172017-2DO.1.2. [Online]. Available: <http://www.eupvsec-proceedings.com/proceedings?paper=42816> (visited on 04/11/2023).
 - [171] G. Cattaneo, J. Levrat, H. Li, *et al.*, “Encapsulant Materials for High Reliable Bifacial Heterojunction Glass/Glass Photovoltaic Modules”, in *2020 47th IEEE Photovoltaic Specialists Conference (PVSC)*, Calgary, AB, Canada: IEEE, Jun. 2020, pp. 1056–1061, ISBN: 978-1-72816-115-0. DOI: 10.1109/PVSC45281.2020.9300702. [Online]. Available: <https://ieeexplore.ieee.org/document/9300702/> (visited on 04/11/2023).
 - [172] L. Gnocchi, “The role of Encapsulants in the long-term performance of advanced Crystalline Silicon Glass-Glass PV modules”, en, Jun. 2022, Publisher: Lausanne, EPFL. DOI: 10.5075/EPFL-THESIS-9385. [Online]. Available: https://infoscience.epfl.ch/record/294600/files/EPFL_TH9385.pdf (visited on 02/14/2023).

BIBLIOGRAPHY

- [173] M. Kempe, "Modeling of rates of moisture ingress into photovoltaic modules", en, *Solar Energy Materials and Solar Cells*, vol. 90, no. 16, pp. 2720–2738, Oct. 2006, ISSN: 09270248. DOI: 10.1016/j.solmat.2006.04.002. [Online]. Available: <https://linkinghub.elsevier.com/retrieve/pii/S0927024806001632> (visited on 04/11/2023).
- [174] M. Mittag, U. Eitner, and T. Neff, "TPedge: Progress on Cost-Efficient and Durable Edge-Sealed PV Modules", en, *33rd European Photovoltaic Solar Energy Conference and Exhibition; 48-54*, 7 pages, 8203 kb, 2017, Artwork Size: 7 pages, 8203 kb Medium: application/pdf Publisher: WIP. DOI: 10.4229/EUPVSEC20172017-1CO.1.4. [Online]. Available: <http://www.eupvsec-proceedings.com/proceedings?paper=40935> (visited on 04/11/2023).
- [175] S. Hava, J. Ivri, and M. Auslender, "Wavenumber-modulated patterns of transmission through one- and two-dimensional gratings on a silicon substrate", *Journal of Optics A: Pure and Applied Optics*, vol. 3, no. 6, S190–S195, Nov. 2001, ISSN: 1464-4258, 1741-3567. DOI: 10.1088/1464-4258/3/6/370. [Online]. Available: <https://iopscience.iop.org/article/10.1088/1464-4258/3/6/370> (visited on 04/11/2023).
- [176] Y. Sun, P. Gao, J. He, *et al.*, "Rear-Sided Passivation by SiNx:H Dielectric Layer for Improved Si/PEDOT:PSS Hybrid Heterojunction Solar Cells", en, *Nanoscale Research Letters*, vol. 11, no. 1, p. 310, Dec. 2016, ISSN: 1931-7573, 1556-276X. DOI: 10.1186/s11671-016-1505-7. [Online]. Available: <https://link.springer.com/10.1186/s11671-016-1505-7> (visited on 04/11/2023).
- [177] W. Shi, M. Theelen, V. Gevaerts, *et al.*, "Positron Annihilation Studies on the Damp Heat Degradation of ZnO:Al Transparent Conductive Oxide Layers for CIGS Solar Cells", *IEEE Journal of Photovoltaics*, vol. 8, no. 6, pp. 1847–1851, Nov. 2018, ISSN: 2156-3381, 2156-3403. DOI: 10.1109/JPHOTOV.2018.2863788. [Online]. Available: <https://ieeexplore.ieee.org/document/8437251/> (visited on 04/17/2023).
- [178] T. Tohsophon, J. Hüpkens, S. Calnan, *et al.*, "Damp heat stability and annealing behavior of aluminum doped zinc oxide films prepared by magnetron sputtering", en, *Thin Solid Films*, vol. 511-512, pp. 673–677, Jul. 2006, ISSN: 00406090. DOI: 10.1016/j.tsf.2005.12.130. [Online]. Available: <https://linkinghub.elsevier.com/retrieve/pii/S0040609005024685> (visited on 04/17/2023).
- [179] J. I. Kim, W. Lee, T. Hwang, *et al.*, "Quantitative analyses of damp-heat-induced degradation in transparent conducting oxides", en, *Solar Energy Materials and Solar Cells*, vol. 122, pp. 282–286, Mar. 2014, ISSN: 09270248. DOI: 10.1016/j.solmat.2013.12.014. [Online]. Available: <https://linkinghub.elsevier.com/retrieve/pii/S0927024813006478> (visited on 04/17/2023).
- [180] M. Theelen, T. Boumans, F. Stegeman, *et al.*, "Physical and chemical degradation behavior of sputtered aluminum doped zinc oxide layers for Cu(In,Ga)Se₂ solar cells", en, *Thin Solid Films*, vol. 550, pp. 530–540, Jan. 2014, ISSN: 00406090. DOI: 10.1016/j.tsf.2013.10.149. [Online]. Available: <https://linkinghub.elsevier.com/retrieve/pii/S0040609013017823> (visited on 04/17/2023).

- [181] M. D. Kempe, G. J. Jorgensen, K. M. Terwilliger, T. J. McMahon, C. E. Kennedy, and T. T. Borek, "Acetic acid production and glass transition concerns with ethylene-vinyl acetate used in photovoltaic devices", en, *Solar Energy Materials and Solar Cells*, vol. 91, no. 4, pp. 315–329, Feb. 2007, ISSN: 09270248. DOI: 10.1016/j.solmat.2006.10.009. [Online]. Available: <https://linkinghub.elsevier.com/retrieve/pii/S0927024806004107> (visited on 04/11/2023).
- [182] B. Ketola and A. Norris, "Degradation Mechanism Investigation of Extended Damp Heat Aged PV Modules", en, *26th European Photovoltaic Solar Energy Conference and Exhibition; 3523-3528*, 6 pages, 5395 kb, 2011, Artwork Size: 6 pages, 5395 kb Medium: application/pdf Publisher: WIP. DOI: 10.4229/26THEUPVSEC2011-4AV.2.14. [Online]. Available: <http://www.eupvsec-proceedings.com/proceedings?paper=13545> (visited on 04/11/2023).
- [183] X. Li, W. Liu, W. Zhao, *et al.*, "Highly crystallized tungsten doped indium oxide film stabilizes silicon heterojunction solar cells in sodium environment", en, *Solar Energy Materials and Solar Cells*, vol. 233, p. 111 387, Dec. 2021, ISSN: 09270248. DOI: 10.1016/j.solmat.2021.111387. [Online]. Available: <https://linkinghub.elsevier.com/retrieve/pii/S0927024821004293> (visited on 03/30/2023).
- [184] V. Guiheneuf, F. Delaleux, O. Riou, P.-O. Logerais, and J.-F. Durastanti, "Investigation of damp heat effects on glass properties for photovoltaic applications", en, *Corrosion Engineering, Science and Technology*, vol. 52, no. 3, pp. 170–177, Apr. 2017, ISSN: 1478-422X, 1743-2782. DOI: 10.1080/1478422X.2016.1234803. [Online]. Available: <https://www.tandfonline.com/doi/full/10.1080/1478422X.2016.1234803> (visited on 10/27/2022).
- [185] D. Adachi, T. Terashita, T. Uto, J. L. Hernández, and K. Yamamoto, "Effects of SiO_x barrier layer prepared by plasma-enhanced chemical vapor deposition on improvement of long-term reliability and production cost for Cu-plated amorphous Si/crystalline Si heterojunction solar cells", en, *Solar Energy Materials and Solar Cells*, vol. 163, pp. 204–209, Apr. 2017, ISSN: 09270248. DOI: 10.1016/j.solmat.2016.12.029. [Online]. Available: <https://linkinghub.elsevier.com/retrieve/pii/S0927024816305505> (visited on 04/11/2023).
- [186] K. Ohdaira, M. Akitomi, Y. Chiba, and A. Masuda, "Potential-induced degradation of n-type front-emitter crystalline silicon photovoltaic modules — Comparison between indoor and outdoor test results", en, *Solar Energy Materials and Solar Cells*, vol. 249, p. 112 038, Jan. 2023, ISSN: 09270248. DOI: 10.1016/j.solmat.2022.112038. [Online]. Available: <https://linkinghub.elsevier.com/retrieve/pii/S092702482200455X> (visited on 04/11/2023).
- [187] D. Chen, P. G. Hamer, M. Kim, *et al.*, "Hydrogen induced degradation: A possible mechanism for light- and elevated temperature- induced degradation in n-type silicon", en, *Solar Energy Materials and Solar Cells*, vol. 185, pp. 174–182, Oct. 2018, ISSN: 09270248. DOI: 10.1016/j.solmat.2018.05.034. [Online]. Available: <https://linkinghub.elsevier.com/retrieve/pii/S0927024818302617> (visited on 02/05/2023).

BIBLIOGRAPHY

- [188] H. C. Sio, H. Wang, Q. Wang, *et al.*, “Light and elevated temperature induced degradation in p-type and n-type cast-grown multicrystalline and mono-like silicon”, en, *Solar Energy Materials and Solar Cells*, vol. 182, pp. 98–104, Aug. 2018, ISSN: 09270248. DOI: 10.1016/j.solmat.2018.03.002. [Online]. Available: <https://linkinghub.elsevier.com/retrieve/pii/S0927024818301053> (visited on 02/05/2023).
- [189] S. V. Spataru, D. Sera, P. Hacke, T. Kerekes, and R. Teodorescu, “Fault identification in crystalline silicon PV modules by complementary analysis of the light and dark current–voltage characteristics”, en, *Progress in Photovoltaics: Research and Applications*, vol. 24, no. 4, pp. 517–532, Apr. 2016, ISSN: 1062-7995, 1099-159X. DOI: 10.1002/pip.2571. [Online]. Available: <https://onlinelibrary.wiley.com/doi/10.1002/pip.2571> (visited on 04/08/2023).
- [190] P. Procel, H. Xu, A. Saez, *et al.*, “The role of heterointerfaces and subgap energy states on transport mechanisms in silicon heterojunction solar cells”, en, *Progress in Photovoltaics: Research and Applications*, vol. 28, no. 9, pp. 935–945, Sep. 2020, ISSN: 1062-7995, 1099-159X. DOI: 10.1002/pip.3300. [Online]. Available: <https://onlinelibrary.wiley.com/doi/10.1002/pip.3300> (visited on 10/27/2022).
- [191] P. Hacke, M. D. Kempe, J. H. Wohlgemuth, J. Li, and Y.-C. Shen, “Potential-Induced Degradation-Delamination Mode in Crystalline Silicon Modules”, 2018.
- [192] O. K. Segbefia, A. G. Imenes, and T. O. Sætre, “Moisture ingress in photovoltaic modules: A review”, en, *Solar Energy*, vol. 224, pp. 889–906, Aug. 2021, ISSN: 0038092X. DOI: 10.1016/j.solener.2021.06.055. [Online]. Available: <https://linkinghub.elsevier.com/retrieve/pii/S0038092X21005375> (visited on 10/27/2022).
- [193] S. L. Moffitt, B. H. Hamadani, and X. Gu, “Characterizing Solar Panel Encapsulants during Potential Induced Degradation”, in *2021 IEEE 48th Photovoltaic Specialists Conference (PVSC)*, Fort Lauderdale, FL, USA: IEEE, Jun. 2021, pp. 1556–1559, ISBN: 978-1-66541-922-2. DOI: 10.1109/PVSC43889.2021.9518811. [Online]. Available: <https://ieeexplore.ieee.org/document/9518811/> (visited on 03/15/2023).
- [194] B. M. Habersberger, P. Hacke, and L. S. Madenjian, “Evaluation of the PID-s susceptibility of modules encapsulated in materials of varying resistivity”, in *2018 IEEE 7th World Conference on Photovoltaic Energy Conversion (WCPEC) (A Joint Conference of 45th IEEE PVSC, 28th PVSEC & 34th EU PVSEC)*, Waikoloa Village, HI: IEEE, Jun. 2018, pp. 3807–3809, ISBN: 978-1-5386-8529-7. DOI: 10.1109/PVSC.2018.8548117. [Online]. Available: <https://ieeexplore.ieee.org/document/8548117/> (visited on 03/15/2023).
- [195] T. Solar, *The Duomax plus+ dual glass 60-cell module*. [Online]. Available: https://static.trinasolar.com/sites/default/files/PS-M-0472%20B%20Datasheet_Duomax%20M%20Plus_DEG5.XX%28II%29_US_Jan2018_TS4_0.pdf.
- [196] B. Braisaz, B. Commault, N. Le Quang, *et al.*, “Improved 1500V PID Resistance: Encapsulants, Cover Glass and Ion Implanted Cells”, en, *32nd European Photovoltaic Solar Energy Conference and Exhibition; 1874-1878*, 5 pages, 5087 kb, 2016, Artwork Size: 5 pages, 5087 kb Medium: application/pdf Publisher: WIP. DOI: 10.4229/EUPVSEC20162016-

- 5BV.1.25. [Online]. Available: <http://www.eupvsec-proceedings.com/proceedings?paper=37158> (visited on 03/22/2023).
- [197] W. Han, W. Shan, X. Niu, *et al.*, “Ion Implantation- An Effective Solution to Prevent C-Si PV Module PID”, en, *28th European Photovoltaic Solar Energy Conference and Exhibition*; 3309-3312, 4 pages, 4654 kb, 2013, Artwork Size: 4 pages, 4654 kb Medium: application/pdf Publisher: WIP. DOI: 10.4229/28THEUPVSEC2013-4AV.5.40. [Online]. Available: <http://www.eupvsec-proceedings.com/proceedings?paper=22029> (visited on 03/22/2023).
- [198] S. Basame, Q. Zhai, T. Thanigaivelan, Y. Maruyama, and H. Naritomi, “Ion Implanted High Efficiency PID Free Cells for Today’s Solar Market”, en, *28th European Photovoltaic Solar Energy Conference and Exhibition*; 1197-1200, 4 pages, 6787 kb, 2013, Artwork Size: 4 pages, 6787 kb Medium: application/pdf Publisher: WIP. DOI: 10.4229/28THEUPVSEC2013-2BV.1.48. [Online]. Available: <http://www.eupvsec-proceedings.com/proceedings?paper=23505> (visited on 03/22/2023).
- [199] F. Meng, J. Shi, Z. Liu, Y. Cui, Z. Lu, and Z. Feng, “High mobility transparent conductive W-doped In₂O₃ thin films prepared at low substrate temperature and its application to solar cells”, en, *Solar Energy Materials and Solar Cells*, vol. 122, pp. 70–74, Mar. 2014, ISSN: 09270248. DOI: 10.1016/j.solmat.2013.11.030. [Online]. Available: <https://linkinghub.elsevier.com/retrieve/pii/S0927024813006144> (visited on 03/30/2023).
- [200] C. Han, Y. Zhao, L. Mazzarella, *et al.*, “Room-temperature sputtered tungsten-doped indium oxide for improved current in silicon heterojunction solar cells”, en, *Solar Energy Materials and Solar Cells*, vol. 227, p. 111 082, Aug. 2021, ISSN: 09270248. DOI: 10.1016/j.solmat.2021.111082. [Online]. Available: <https://linkinghub.elsevier.com/retrieve/pii/S0927024821001239> (visited on 03/30/2023).
- [201] M. Morales-Masis, E. Rucavado, R. Monnard, *et al.*, “Highly Conductive and Broadband Transparent Zr-Doped In₂O₃ as Front Electrode for Solar Cells”, *IEEE Journal of Photovoltaics*, vol. 8, no. 5, pp. 1202–1207, Sep. 2018, ISSN: 2156-3381, 2156-3403. DOI: 10.1109/JPHOTOV.2018.2851306. [Online]. Available: <https://ieeexplore.ieee.org/document/8410059/> (visited on 03/28/2023).
- [202] S. Calnan and A. Tiwari, “High mobility transparent conducting oxides for thin film solar cells”, en, *Thin Solid Films*, vol. 518, no. 7, pp. 1839–1849, Jan. 2010, ISSN: 00406090. DOI: 10.1016/j.tsf.2009.09.044. [Online]. Available: <https://linkinghub.elsevier.com/retrieve/pii/S0040609009014916> (visited on 03/30/2023).
- [203] V. H. Nguyen, D. Bellet, B. Masenelli, and D. Muñoz-Rojas, “Increasing the Electron Mobility of ZnO-Based Transparent Conductive Films Deposited by Open-Air Methods for Enhanced Sensing Performance”, en, *ACS Applied Nano Materials*, vol. 1, no. 12, pp. 6922–6931, Dec. 2018, ISSN: 2574-0970, 2574-0970. DOI: 10.1021/acsanm.8b01745. [Online]. Available: <https://pubs.acs.org/doi/10.1021/acsanm.8b01745> (visited on 03/30/2023).

BIBLIOGRAPHY

- [204] Y.-S. Liu, C.-Y. Hsieh, Y.-J. Wu, *et al.*, “Mechanism of conductivity degradation of AZO thin film in high humidity ambient”, en, *Applied Surface Science*, vol. 282, pp. 32–37, Oct. 2013, ISSN: 01694332. DOI: 10.1016/j.apsusc.2013.04.167. [Online]. Available: <https://linkinghub.elsevier.com/retrieve/pii/S0169433213008891> (visited on 03/30/2023).
- [205] A. Cruz, F. Ruske, A. Eljarrat, *et al.*, “Influence of Silicon Layers on the Growth of ITO and AZO in Silicon Heterojunction Solar Cells”, *IEEE Journal of Photovoltaics*, vol. 10, no. 2, pp. 703–709, Mar. 2020, ISSN: 2156-3381, 2156-3403. DOI: 10.1109/JPHOTOV.2019.2957665. [Online]. Available: <https://ieeexplore.ieee.org/document/8944078/> (visited on 03/30/2023).
- [206] L. M. Antognini, “Contact Design for Silicon Heterojunction Solar Cells”, en, Jun. 2022, Publisher: Lausanne, EPFL. DOI: 10.5075/EPFL-THESIS-9477. [Online]. Available: <http://infoscience.epfl.ch/record/294790> (visited on 03/30/2023).
- [207] M. Bivour, S. Schröer, and M. Hermle, “Numerical Analysis of Electrical TCO / a-Si:H(p) Contact Properties for Silicon Heterojunction Solar Cells”, en, *Energy Procedia*, vol. 38, pp. 658–669, 2013, ISSN: 18766102. DOI: 10.1016/j.egypro.2013.07.330. [Online]. Available: <https://linkinghub.elsevier.com/retrieve/pii/S1876610213014161> (visited on 03/30/2023).
- [208] J. P. Seif, A. Descoeudres, G. Nogay, *et al.*, “Strategies for Doped Nanocrystalline Silicon Integration in Silicon Heterojunction Solar Cells”, *IEEE Journal of Photovoltaics*, vol. 6, no. 5, pp. 1132–1140, Sep. 2016, ISSN: 2156-3381, 2156-3403. DOI: 10.1109/JPHOTOV.2016.2571619. [Online]. Available: <http://ieeexplore.ieee.org/document/7494651/> (visited on 03/30/2023).
- [209] J. Haschke, G. Christmann, C. Messmer, M. Bivour, M. Boccard, and C. Ballif, “Lateral transport in silicon solar cells”, en, *Journal of Applied Physics*, vol. 127, no. 11, p. 114 501, Mar. 2020, ISSN: 0021-8979, 1089-7550. DOI: 10.1063/1.5139416. [Online]. Available: <http://aip.scitation.org/doi/10.1063/1.5139416> (visited on 03/30/2023).
- [210] Y. Yang, W. Liu, L. Zhang, *et al.*, “N-type nc-SiO_x:H film enables efficient and stable silicon heterojunction solar cells in sodium environment”, en, *Materials Letters*, vol. 309, p. 131 360, Feb. 2022, ISSN: 0167577X. DOI: 10.1016/j.matlet.2021.131360. [Online]. Available: <https://linkinghub.elsevier.com/retrieve/pii/S0167577X21020589> (visited on 04/03/2023).
- [211] A. Cruz, E.-C. Wang, A. B. Morales-Vilches, *et al.*, “Effect of front TCO on the performance of rear-junction silicon heterojunction solar cells: Insights from simulations and experiments”, en, *Solar Energy Materials and Solar Cells*, vol. 195, pp. 339–345, Jun. 2019, ISSN: 09270248. DOI: 10.1016/j.solmat.2019.01.047. [Online]. Available: <https://linkinghub.elsevier.com/retrieve/pii/S0927024819300388> (visited on 04/01/2023).
- [212] A. Cruz, D. Erfurt, P. Wagner, *et al.*, “Optoelectrical analysis of TCO+Silicon oxide double layers at the front and rear side of silicon heterojunction solar cells”, en, *Solar Energy Materials and Solar Cells*, vol. 236, p. 111 493, Mar. 2022, ISSN: 09270248. DOI:

- 10.1016/j.solmat.2021.111493. [Online]. Available: <https://linkinghub.elsevier.com/retrieve/pii/S0927024821005328> (visited on 04/01/2023).
- [213] D. Zhang, I. Digdaya, R. Santbergen, *et al.*, “Design and fabrication of a SiO_x/ITO double-layer anti-reflective coating for heterojunction silicon solar cells”, en, *Solar Energy Materials and Solar Cells*, vol. 117, pp. 132–138, Oct. 2013, ISSN: 09270248. DOI: 10.1016/j.solmat.2013.05.044. [Online]. Available: <https://linkinghub.elsevier.com/retrieve/pii/S0927024813002675> (visited on 04/01/2023).
- [214] M. Boccard, V. Paratte, E. Rucavado, *et al.*, “Paths for maximal light incoupling and excellent electrical performances in silicon heterojunction solar cells”, in *2019 IEEE 46th Photovoltaic Specialists Conference (PVSC)*, Chicago, IL, USA: IEEE, Jun. 2019, pp. 2541–2545, ISBN: 978-1-72810-494-2. DOI: 10.1109/PVSC40753.2019.8980543. [Online]. Available: <https://ieeexplore.ieee.org/document/8980543/> (visited on 04/01/2023).
- [215] S. Y. Herasimenka, W. J. Dauksher, M. Boccard, and S. Bowden, “ITO/SiO_x:H stacks for silicon heterojunction solar cells”, en, *Solar Energy Materials and Solar Cells*, vol. 158, pp. 98–101, Dec. 2016, ISSN: 09270248. DOI: 10.1016/j.solmat.2016.05.024. [Online]. Available: <https://linkinghub.elsevier.com/retrieve/pii/S0927024816301258> (visited on 04/01/2023).
- [216] M. Boccard, L. Antognini, V. Paratte, *et al.*, “Hole-Selective Front Contact Stack Enabling 24.1%-Efficient Silicon Heterojunction Solar Cells”, *IEEE Journal of Photovoltaics*, vol. 11, no. 1, pp. 9–15, Jan. 2021, ISSN: 2156-3381, 2156-3403. DOI: 10.1109/JPHOTOV.2020.3028262. [Online]. Available: <https://ieeexplore.ieee.org/document/9223729/> (visited on 04/01/2023).
- [217] K. R. McIntosh and S. C. Baker-Finch, “OPAL 2: Rapid optical simulation of silicon solar cells”, in *2012 38th IEEE Photovoltaic Specialists Conference*, Austin, TX, USA: IEEE, Jun. 2012, pp. 000 265–000 271, ISBN: 978-1-4673-0066-7 978-1-4673-0064-3 978-1-4673-0065-0. DOI: 10.1109/PVSC.2012.6317616. [Online]. Available: <http://ieeexplore.ieee.org/document/6317616/> (visited on 04/03/2023).
- [218] G. Du, Y. Bai, J. Huang, *et al.*, “Surface Passivation of ITO on Heterojunction Solar Cells with Enhanced Cell Performance and Module Reliability”, *ECS Journal of Solid State Science and Technology*, vol. 10, no. 3, p. 035 008, Mar. 2021, ISSN: 2162-8769, 2162-8777. DOI: 10.1149/2162-8777/abeece. [Online]. Available: <https://iopscience.iop.org/article/10.1149/2162-8777/abeece> (visited on 04/03/2023).
- [219] S. Zhang, Y. Kuang, B. Zhao, W. Lian, Y. Liu, and Z. Ni, “Improvement of the PID problem of bifacial PERC solar modules based on rear passivation coating optimization”, Hamelin, Germany / Online, 2022, p. 100 004. DOI: 10.1063/5.0096663. [Online]. Available: <http://aip.scitation.org/doi/abs/10.1063/5.0096663> (visited on 04/03/2023).

BIBLIOGRAPHY

- [220] D. L. Batzner, J. P. Cardoso, C. Aeby, *et al.*, “Alleviating performance and cost constraints in silicon heterojunction cells with HJT 2.0”, in *2019 IEEE 46th Photovoltaic Specialists Conference (PVSC)*, Chicago, IL, USA: IEEE, Jun. 2019, pp. 1471–1474, ISBN: 978-1-72810-494-2. DOI: 10.1109 / PVSC40753.2019.8980666. [Online]. Available: <https://ieeexplore.ieee.org/document/8980666/> (visited on 04/02/2023).
- [221] B. Li, J. Yu, P. Wang, *et al.*, “Suppression of potential-induced degradation in monofacial PERC solar cells with gradient-designed capping layer”, en, *Solar Energy*, vol. 225, pp. 634–642, Sep. 2021, ISSN: 0038092X. DOI: 10.1016/j.solener.2021.07.067. [Online]. Available: <https://linkinghub.elsevier.com/retrieve/pii/S0038092X21006435> (visited on 04/03/2023).
- [222] D. Lee, M. Chae, J.-R. Kim, and H.-D. Kim, “Effects of Al₂O₃ Thickness in Silicon Heterojunction Solar Cells”, en, *Inorganics*, vol. 11, no. 3, p. 106, Mar. 2023, ISSN: 2304-6740. DOI: 10.3390/inorganics11030106. [Online]. Available: <https://www.mdpi.com/2304-6740/11/3/106> (visited on 04/03/2023).
- [223] S. Kim, P. Balaji, A. Augusto, S. Bowden, and C. B. Honsberg, “Ultra thin Al₂O₃ passivation for hetero-junction Si solar cell”, in *2019 IEEE 46th Photovoltaic Specialists Conference (PVSC)*, Chicago, IL, USA: IEEE, Jun. 2019, pp. 2684–2687, ISBN: 978-1-72810-494-2. DOI: 10.1109 / PVSC40753.2019.8980907. [Online]. Available: <https://ieeexplore.ieee.org/document/8980907/> (visited on 04/03/2023).
- [224] E. Jang, K.-s. Oh, and S. Ryu, “Reduction of Potential-Induced-Degradation of p-Type PERC Solar Cell Modules by an Ion-Diffusion Barrier Layer Underneath the Front Glass”, en, *Processes*, vol. 10, no. 2, p. 334, Feb. 2022, ISSN: 2227-9717. DOI: 10.3390/pr10020334. [Online]. Available: <https://www.mdpi.com/2227-9717/10/2/334> (visited on 04/03/2023).
- [225] W. Luo, N. Chen, C. Ke, *et al.*, “Investigation of polysilicon passivated contact’s resilience to potential-induced degradation”, en, *Solar Energy Materials and Solar Cells*, vol. 195, pp. 168–173, Jun. 2019, ISSN: 09270248. DOI: 10.1016/j.solmat.2019.02.038. [Online]. Available: <https://linkinghub.elsevier.com/retrieve/pii/S0927024819301047> (visited on 06/01/2023).
- [226] K. Ohdaira, Y. Komatsu, T. Suzuki, S. Yamaguchi, and A. Masuda, “Potential-Induced Degradation of n-Type Front-Emitter Crystalline Silicon Photovoltaic Modules with Different Degradation Stages”, en, *36th European Photovoltaic Solar Energy Conference and Exhibition; 822-824*, 3 pages, 5930 kb, 2019, Artwork Size: 3 pages, 5930 kb Medium: application/pdf Publisher: WIP. DOI: 10.4229/EUPVSEC20192019-4BO.12.5. [Online]. Available: <https://www.eupvsec-proceedings.com/proceedings?paper=48609> (visited on 06/01/2023).
- [227] S. Yamaguchi, A. Masuda, K. Marumoto, and K. Ohdaira, “Mechanistic Understanding of Polarization-Type Potential-Induced Degradation in Crystalline-Silicon Photovoltaic Cell Modules”, en, *Advanced Energy and Sustainability Research*, vol. 4, no. 4, p. 2 200 167, Apr. 2023, ISSN: 2699-9412, 2699-9412. DOI: 10.1002 / aesr.202200167.

- [Online]. Available: <https://onlinelibrary.wiley.com/doi/10.1002/aesr.202200167> (visited on 06/01/2023).
- [228] W. Luo, Y. S. Khoo, J. P. Singh, *et al.*, “Investigation of Potential-Induced Degradation in n-PERT Bifacial Silicon Photovoltaic Modules with a Glass/Glass Structure”, *IEEE Journal of Photovoltaics*, vol. 8, no. 1, pp. 16–22, Jan. 2018, ISSN: 2156-3381, 2156-3403. DOI: 10.1109/JPHOTOV.2017.2762587. [Online]. Available: <http://ieeexplore.ieee.org/document/8089707/> (visited on 06/01/2023).

Publication list

Updated: 19.06.2023

Publications as first author

1. O. Arriaga Arruti, A. Virtuani and C. Ballif, *Long-term Performance and Reliability of Silicon Heterojunction Solar Modules*, Progress in Photovoltaics: Research and Applications, pages 1-14, 2023.
2. O. Arriaga Arruti, A. Virtuani, L. Gnocchi, Q. Jeangros and C. Ballif, *Potential-Induced Degradation in Bifacial Silicon Heterojunction Solar Modules: Insights and Mitigation Strategies*, manuscript in preparation, 2023.
3. O. Arriaga Arruti, L. Gnocchi, F. Lisco, A. Virtuani and C. Ballif, *Optimized Module Packaging for Silicon Heterojunction Solar Cells and Increased PID Resistance*, 37th European PV Solar Energy Conference and Exhibition (EU PVSEC) Proceedings, 2020.
4. O. Arriaga Arruti, L. Gnocchi, A. Virtuani and C. Ballif, *Encapsulant Selection for Increased PID Resistance in Modules made with Silicon Heterojunction Solar Cells*, 37th European PV Solar Energy Conference and Exhibition (EU PVSEC) Proceedings, 2020.
5. O. Arriaga Arruti, L. Gnocchi, Q. Jeangros, A. Virtuani and C. Ballif, *Potential-Induced Degradation Mechanism in Rear-Emitter Bifacial Silicon Heterojunction Solar Cells Encapsulated in Different Module Structures*, 48th IEEE Photovoltaic Specialists Conference (IEEE PVSC) Proceedings, 2021.
6. O. Arriaga Arruti, L. Gnocchi, F. Lisco, A. Virtuani and C. Ballif, *The front- and rear-side contributions to the potential-induced degradation of bifacial silicon heterojunction solar modules*, oral presentation at the 38th European PV Solar Energy Conference and Exhibition (EU PVSEC) Proceedings, 2021.

Publications as co-author

1. L. Gnocchi, O. Arriaga Arruti, A. Virtuani, and C. Ballif, *Insights into the sensitivity of SHJ modules to Damp Heat: a microscopic model*, submitted to Cell Reports, 2023.

Conference and Workshop Presentations

1. O. Arriaga Arruti, L. Gnocchi, A. Virtuani, C. Ballif, *Encapsulant Selection for PID Resistant Modules made with Silicon Heterojunction Solar Cells*, visual presentation at the 37th European Photovoltaic Solar Energy Conference, online, 2020.
2. O. Arriaga Arruti, L. Gnocchi, F. Lisco, A. Virtuani, C. Ballif, *Optimized Module Packaging for Silicon Heterojunction Solar Cells and Increased PID Resistance*, oral presentation at the 37th European Photovoltaic Solar Energy Conference, online, 2020.
3. O. Arriaga Arruti, L. Gnocchi, F. Lisco, A. Virtuani, C. Ballif, *Increased PID Resistance of Silicon Heterojunction Solar Cells via Optimized Module Packaging*, oral presentation at the 3rd International Workshop on Silicon Heterojunction Solar Cells.
4. O. Arriaga Arruti, L. Gnocchi, Q. Jeangros, A. Virtuani, C. Ballif, *Potential Induced Degradation Mechanism in Rear-Emitter Bifacial Silicon Heterojunction Solar Cells Encapsulated in Different Module Structures*, oral presentation at the 48th IEEE Conference on Photovoltaic Specialists (IEEE PVSC), online, 2021.
5. O. Arriaga Arruti, L. Gnocchi, F. Lisco, A. Virtuani and C. Ballif, *The front- and rear-side contributions to the potential-induced degradation of bifacial silicon heterojunction solar modules*, oral presentation at the 38th European PV Solar Energy Conference and Exhibition (EU PVSEC), online, 2021.
6. O. Arriaga Arruti, A. Virtuani and C. Ballif, *Silicon Heterojunction Solar Technology at the Gate of the Giga-Watt-Age: Reliability and Long-term Performance*, oral presentation at the 8th World Conference on Photovoltaic Energy Conversion (WCPEC), Milan, Italy, 2022.

OLATZ ARRIAGA ARRUTI

Address: Rue des Fahys 129, Neuchâtel, Switzerland

Phone: +41 76 402 49 32

Email: ir.olatz.arriaga.arruti@gmail.com



After completing a European Master in Renewable Energy, I joined the Photovoltaics and Thin-Films Laboratory (PV-Lab) for a Ph.D degree. My research interests included the reliability analysis of silicon heterojunction and other high-efficiency technologies. Special attention was given to understanding unique degradation mechanisms of each technology and in the development of durable PV modules. I am pursuing a position as an R&D engineer in the field PV module reliability, with the goal of developing reliable products for industrial applications and finding novel solutions.

EDUCATION

École Polytechnique Fédérale de Lausanne (EPFL) | 2019 - 2023

Ph.D student in Photovoltaics and Thin-Films Laboratory (PV-Lab)

Thesis title: Investigation and Mitigation of Moisture- and Potential-Induced Degradation Mechanisms in Silicon Heterojunction Solar Cells and Modules

EUREC/Universidad de Zaragoza, Spain | 2017 - 2018

EUREC's European Master in Renewable Energy, Specialisation: Photovoltaics - Northumbria University, UK

Universitat Autònoma de Barcelona | 2013 - 2017

Bachelor's Degree in Nanoscience and Nanotechnology

WORK EXPERIENCE

RESEARCH SCIENTIST - EPFL — PV-Lab; Neuchâtel, Switzerland | April 2019 - May 2023

Topic: research on the reliability of high-efficiency crystalline Silicon (c-Si) technologies, with particular focus on SHJ.

ASSISTANT RESEARCHER, INTERN - EPFL — PV-Lab; Neuchâtel, Switzerland | Jun 2018 - Dec 2018

Project: *Potential-Induced Degradation in Silicon Heterojunction Solar Cells*

ASSISTANT RESEARCHER, INTERN - ICMAB — CSIC; Barcelona, Spain | Feb 2017 - Jul 2017

Project: *Synthesis of nanoparticles by microwave-assisted routes.*

ASSISTANT RESEARCHER, INTERN - CIC biomaGUNE; Donostia - San Sebastián, Spain | Jul 2016 - Sep 2016

Project: *Novel 3D structures based on carbon material nano composites for electroresponsive cell cultures.*

SKILLS & EXPERTISE

- **Project Management:** project planning, scientific writing and oral communication, analytical and creative thinking, team work.
- PV module manufacturing and characterization, performing accelerated ageing tests (IEC 61215) and material micro-structural characterization.
- **Data analysis tools:** Excel, Origin, CasaXPS, ImageJ, Zetasizer, Latex, Word

195

LANGUAGES

Basque: native **Spanish:** native **English:** C2 **Catalan:** B2 **French:** B1/B2 **Italian:** B1/B2